Doctoral theses at NTNU, 2022:309

Cristobal Javier Manquehual Mery

# Durability of rock support in Norwegian road tunnels

Doctoral thesis

NTNU
Norwegian University of Science and Technology
Thesis for the Degree of Philosophiae Doctor
Faculty of Engineering
Department of Civil and Environmental Engineering

NTNU
Norwegian University of Science and Technology

Cristobal Javier Manquehual Mery

# Durability of rock support in Norwegian road tunnels

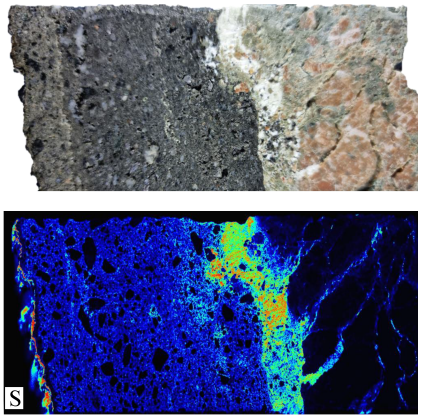


Thesis for the Degree of Philosophiae Doctor

Trondheim, October 2022

Norwegian University of Science and Technology
Faculty of Engineering
Department of Civil and Environmental Engineering

NTNU
Norwegian University of
Science and Technology

**NTNU**
Norwegian University of Science and Technology

Thesis for the Degree of Philosophiae Doctor

Faculty of Engineering
Department of Civil and Environmental Engineering



ISBN 978-82-326-5976-0 (printed ver.)
ISBN 978-82-326-6243-2 (electronic ver.)
ISSN 1503-8181 (printed ver.)
ISSN 2703-8084 (online ver.)

Doctoral theses at NTNU, 2022:309

Printed by NTNU Grafisk senter

**Abstract**

The durability of the rock support in road tunnels is relevant from the point of view of safety, life cycle cost and the impact on the environment. A better understanding of the rock support degradation in road tunnels is crucial to prevent accidents, that may involve road users. It would also allow the optimization of maintenance and rehabilitation strategies, define the budget needed in advance for those activities and properly perform life cycle impact assessment of the rock support from raw material extraction until the end of the lifespan of the tunnel.

This thesis focuses on the durability of rock bolts and steel fiber-reinforced shotcrete used as rock support in Norwegian road tunnels. These tunnels stand out as they use the initial rock support as part of the final support. Unlike many other road tunnels elsewhere, a typical Norwegian road tunnel does not include a waterproof membrane followed by a thick layer of cast-in-place concrete lining, leading to greater responsibility for the rock support installed and greater exposure to the surrounding environment.

Regarding rock bolts, the identification of aggressive environments, and the collection of corrosion kinetics in carbon steel used in underground works were obtained from a literature review. Based on the information collected, a probability distribution for the steel rebar was deduced for 25, 50 and 100 years of exposure time. The lifespan extension given by the hot-dip galvanizing, the duplex protection system and cement mortar to the steel rebar were obtained also from different observations reported in the literature, which allowed median values to be estimated for each corrosion protection element.

To address the durability of steel fiber-reinforced shotcrete is more complex since there is no direct link between a chemical attack identified in the field and its physical and mechanical consequences. In addition, little is known about the condition of singularities in the shotcrete layer, such as its contact with the rock, the boundary between two adjacent shotcrete layers and the shotcrete surface exposed to the traffic room. Based on this background, field and laboratory investigations were performed in shotcrete.

Subsea road tunnels are an interesting field to be inspected. Here, shotcrete of the same age and technology is exposed to fresh groundwater near the portals and saline groundwater containing sulfates, magnesium carbonates and chlorides in the rest of the tunnel.

The technological change in Norway from water-glass accelerator to alkali-free accelerator in the mid-1990s is also addressed in this research due to the concern that the sulfur content in the latter accelerator could become a detrimental factor for the cement paste in the shotcrete. In total, the shotcrete conditions in four tunnels constructed in the 1990s were inspected, three of them being subsea tunnels. In these four tunnels, 11 investigated locations were selected, leading to the drilling of 56 shotcrete cores. In all these locations, groundwater pH and electrical conductivity were also measured. The following investigations were performed in the laboratory:

- 102 samples for shotcrete density and suction porosity tests
- 36 samples for uniaxial compressive strength (UCS) test
- 28 samples for powder X-ray diffraction (XRD) analysis
- 8 mappings of micro X-ray fluorescence (μ-XRF) analysis
- 8 samples for pH indicator thymolphthalein tests
- 14 samples for thermogravimetric analysis (TGA) in two core profiles
- 1 polished section for scanning electron microscopy with energy dispersive spectroscopy (SEM/EDS)

In fresh groundwater, it is expected that both rock bolts and shotcrete should experience very limited degradation. In case of improper handling during construction, it is envisaged that rock bolts are more sensitive.

In subsea road tunnels constructed in the 1990s, it is expected that the condition of shotcrete could become worse than rock bolts. In this regard, the estimated lifespan extension of a rock bolt coated with the duplex protection system installed in subsea tunnels is, on average 45 years. In principle, during this time period, the

steel rebar will still be uncorroded. In contrast, in half that time, the condition of shotcrete investigated in this research has been seriously degraded in several cases.

**Preface**

This doctoral thesis is submitted in partial fulfilment of the requirements for the degree of philosophiae doctor (PhD) at the Norwegian University of Science and Technology (NTNU). In particular, this research has been performed at the Department of Civil and Environmental Engineering at NTNU, in Trondheim. The main supervisor is PhD Pål Drevland Jakobsen (NTNU and NGI) and the co-supervisors have been Professor Amund Bruland (NTNU) and Associate Professor Karl Gunnar Holter (NTNU and NGI).

The PhD project was mainly financed by the Faculty of Engineering at NTNU. However, a part of the PhD project related to the field work in the Hitra and Frøya subsea tunnels also received fundings from the Trøndelag county authority (*Trøndelag fylkeskommune*).

**Acknowledgements**

I am grateful for the support given from the first day by my main supervisor PhD Pål Drevland Jakobsen. I appreciate his orientation in academia, being always accessible to answer questions and give guidance, and was always concerned about me and my family.

I would like to thank the guidance of Professor Amund Bruland, especially in key moments of this research where his experience and wisdom allowed this investigation to proceed without setbacks. He was always available for questions and guidance when required.

I am grateful of the guidance given by Associate Professor Karl Gunnar Holter in the field, in the laboratory and in his reviews. I am convinced that his expertise and logistic help in the field allowed this thesis to have a higher quality and impact.

I am grateful for the support given by Professor Klaartje De Weerdt, who is the unofficial co-supervisor of this research. She did not only introduce me with several investigation techniques such as μ-XRF, TGA and SEM/EDS, but she always had time to clarify my inquiries and provide suggestions for improvement.

I appreciate the unselfish support of Mr. Johnny Johansen (Vianova), who showed interest of my work from the very beginning. I learned most of what I know about maintenance and rehabilitation activities in Norwegian road tunnels from him. With all the experience he has, amazed me with his willingness to listen and collaborate with the research of others.

Especial gratitude goes to Tobias Danner (SINTEF). His help with μ-XRF, XRD and his exhaustive reviews with suggestions for improvement were relevant to present clear results.

I am grateful for the wise feedback from professor Bjørn Nilsen and his support with key Norwegian references at the beginning of this research.

I want to thank senior engineer Per Øystein Nordtug, who helped me with patience in several tasks performed in the concrete laboratory. He was always very attentive and flexible to achieve the goals.

I also want to highlight the help given by the senior engineer Laurentius Tijhuis, who taught and guided me about XRD in the laboratory.

I appreciate the trust, logistic help and financial aid given by Bjørn Erik Andersson and Christian Baug (Trøndelag County Authority), who made the field investigations in the Hitra and Frøya tunnels possible.

I appreciate the rigorous work of senior engineer Jon Runar Drotninghaug, where I received insightful feedback from him as the various UCS tests were performed in the laboratory.

I do not forget the help provided in the field by John Lau (in the Frøya tunnel) and Erlend Norby (in the Frøya and Hitra tunnels), doing night shifts for several days. With their help, the drilling core performance improved considerably.

I extend my thanks to the first orientations about Norwegian tunnels given by Daniel Gunther and Trine Bye Sagen at Banenor.

Finally, I want to highlight the support of my wife Vanessa and my three children José, Pedro and Cristóbal. They followed and supported me once again, leaving behind their relatives in our home country.

**Table of Contents**


1 Introduction ..... 1
1.1. Background ..... 1
1.2 About Norwegian road tunnels ..... 2
1.3 Objectives and research questions ..... 3
1.4 Scope and research method ..... 3
1.4.1 Field and laboratory investigations in steel fiber-reinforced shotcrete ..... 4
1.5 Limitations ..... 9
1.6 Outline of thesis ..... 10
1.7 Publications: ..... 10
1.7.1 Core publications ..... 10
1.7.2 Supplemental publications ..... 12
2 Results of the literature review ..... 13
2.1 Evolution on durability aspects of rock bolts ..... 13
2.2 Evolution of durability aspects of steel fiber-reinforced shotcrete ..... 13
2.3 Degradation mechanisms in rock bolts ..... 16
2.3.1 Fundamentals of corrosion in fresh groundwater (Poorly ionic wet corrosion) ..... 16
2.3.2 Acidic environment ..... 17
2.3.3 Saline groundwater ..... 19
2.3.4 Flowing groundwater with dissolved oxygen ..... 23
2.4 Degradation kinetics in rock bolts ..... 25
2.4.1 Carbon steel rebar ..... 25
2.4.2 Cement grout ..... 25
2.4.3 Hot-dip galvanizing ..... 26
2.4.4 Duplex protection system ..... 28
2.4.5 Summary ..... 28
2.5 Degradation mechanisms in steel fiber-reinforced shotcrete ..... 29
2.5.1 Carbonation ..... 29
2.5.2 Leaching ..... 29
2.5.3 Sulfate attack ..... 31
2.5.4 Magnesium attack ..... 32
2.5.5 Corrosion of steel fibers ..... 32
2.6 Degradation kinetics in concrete ..... 33
2.6.1 Carbonation ..... 33
2.6.2 Leaching ..... 33

3 Field and laboratory results in steel fiber-reinforced shotcrete ..... 34
3.1 Carbonation ..... 34
3.2 Leaching ..... 35
3.3 Sulfate attack ..... 41
3.3.1 Gypsum ..... 41
3.3.2 Ettringite formation ..... 43
3.3.3 Thaumasite formation ..... 43
3.4 Magnesium attack ..... 47
3.5 Corrosion of steel fibers ..... 49
4 Prognosis of degradation kinetics in steel fiber-reinforced shotcrete used in Norwegian road tunnels ..... 50
4.1 Carbonation ..... 50
4.2 Corrosion of steel fibers ..... 51
4.3 Leaching interacting with carbonation, chlorides and sulfur ingress ..... 51
4.4 Sulfate and magnesium attack ..... 52
5 Discussion ..... 53
5.1 Sampling for UCS tests in shotcrete used as rock support ..... 53
5.2 The role of alkali-free accelerator in shotcrete ..... 54
5.3 Sulfur dioxide emitted by vehicles as an additional source of sulfur ..... 54
5.4 Corrosion of steel fibers in shotcrete installed in subsea tunnels ..... 55
5.5 Alkali-silica reaction ..... 55
5.6 Durability enhancement in rock bolts ..... 56
5.7 Durability enhancement in steel fiber-reinforced shotcrete ..... 56
5.7.1 Prevent shotcrete joints ..... 56
5.7.2 Quality control in shotcrete near the contact with the rock ..... 59
5.8 Useful life and tolerable degradation ..... 65
6 Conclusions ..... 68
7 Further work ..... 70
8 References ..... 71
Appendix A Laboratory research planning of shotcrete cores ..... 77
Appendix B Shotcrete density and uniaxial compressive strength results ..... 81
Appendix C Shotcrete density and suction porosity results ..... 83

# Chapter 1

## 1 Introduction

### 1.1. Background

The structural integrity of tunnels relies on the rock mass properties and the installed rock support. Over time materials degrade, and this includes the rock support exposed to the tunnel environment. Traditionally, the concern about degradation of rock support in road tunnels arises from a safety and cost perspective [1,2]. Regarding costs, the Norwegian Public Roads Administration (NPRA) undertook a survey in 2012 to estimate the cost of eliminating the maintenance backlog in the national road network [3] (this network is apart from other Norwegian road tunnels belonging to different counties). At that time, the number of tunnels in the national road network was 481, representing 4.6% of the length of the network. The resulting upgrading cost amounts to approximately 4 billion euro (2012), where approximately half of it corresponds to the upgrading of tunnels. The distribution of the needed investment in the existing road tunnels by 2012 is given in Fig. 1.

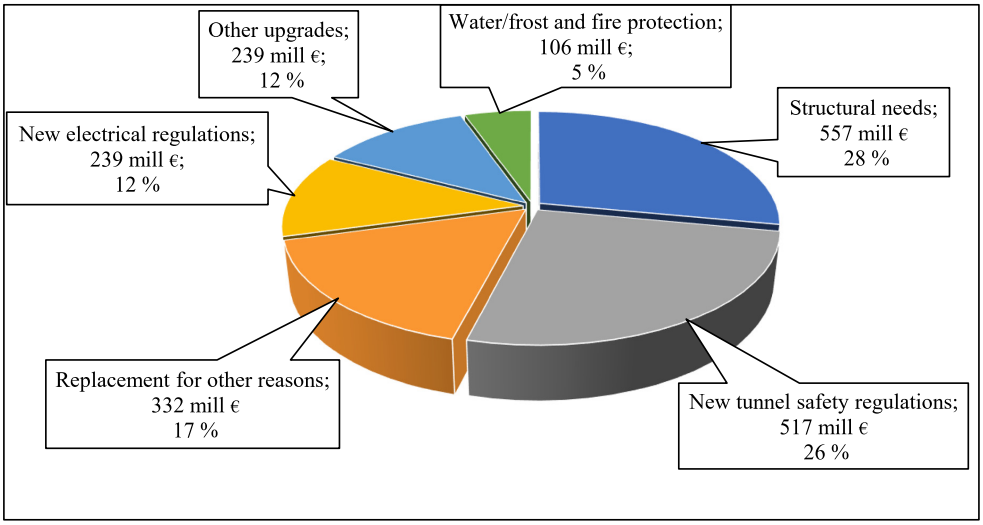


**Fig. 1:** Estimated distribution of upgrading costs in the 481 tunnels belonging to national road network in Norway by 2012 [3]. Costs are given in euro (2012).

As shown in Fig. 1, the largest portion of the upgrading costs in Norwegian road tunnels corresponds to structural needs, a concept which includes rock support, structure in tunnel portals, enlargement of the tunnel cross section for extra emergency lay-bays, niches, technical rooms, etc. The financial challenge is enormous.

While the new tunnels under construction are to be operated and maintained in the future, there is ongoing degradation of the existing ones.

In addition, an increasing concern about sustainability demands a more in-depth knowledge regarding the carbon footprint of the construction sector, where tunnels have a significant contribution in many countries' infrastructure [4–6]. In one meter of a Norwegian tunnel excavated in hard rock, the carbon footprint of the rock support is of a similar magnitude to that emitted by drill and blast tunnelling excavation with conventional equipment [7]. So far, the environmental life cycle assessment in tunnels has mainly been estimated from raw material extraction until the end of the construction period [6,8]. This research is designed to investigate the actual condition of rock support elements during the tunnel operation and anticipate the eventual need to replace or repair them at some point in the future.

In Norwegian road tunnels, rock bolts and shotcrete are the most common rock support elements [9]. Fig. 2 shows the proportion of carbon footprint between rock bolts and shotcrete for a typical Norwegian road tunnel in rock support class C (moderately fractured rock mass with a joint spacing between 0.3 m and 1.0 m) and tunnel size T 9.5 ( Cross sectional area = 66.7 $m^2$, arc length which includes tunnel walls and roof = 21 m) [10].

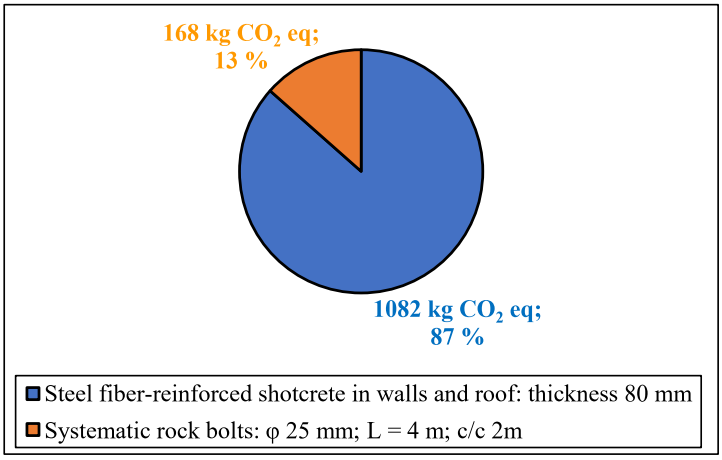


**Fig. 2:** Distribution of Global Warming Potential (GWP) between steel fiber-reinforced shotcrete and rock bolts in one meter of road tunnel in Norway in rock support class C and tunnel size T 9.5. Modified from [10].

Fig. 2 clearly shows that the contribution of shotcrete to the carbon footprint is higher than that of rock bolts for one meter in a typical Norwegian road tunnel. However, a wider assessment, until the end of the useful life of the tunnel might change this figure. This research concentrates on the durability of these rock support elements under different environmental conditions.

## 1.2 About Norwegian road tunnels

Norway has an uneven mountainous topography and cold climate, making tunnels a suitable alternative for road infrastructure in many cases [11]. Underground solutions have protected infrastructure from areas with the potential of snow avalanches and rock falls on numerous routes [12]. Furthermore, subsea tunnels have

improved the connection of several islands to the mainland where ferries were the only alternative [13]. In total, there are more than 1200 road tunnels in Norway in the National and county road networks as of 2019. The cumulative road tunnel length exceeds 1100 km [14].

The experience gained over the years in the rock support of Norwegian road tunnels is valuable since these tunnels have commonly been designed as drained structures with a single shell rock support [9]. This means that the typical waterproof lining followed by a second inner lining of cast-in-place concrete, used in many other countries, are avoided in Norway whenever possible. This Norwegian approach involves greater responsibility for the rock support installed and greater exposure to the surrounding environment than in many other countries. In case water and frost protection are needed, the Norwegian approach incorporates a slender inner lining detached from the rock support fastened with radial rock bolts [9].

## 1.3 Objectives and research questions

This PhD research has four main objectives:

1. To identify the most aggressive environmental conditions and the associated degradations which limit the lifespan of rock bolts and steel fiber-reinforced shotcrete.
2. In those identified degradations where the literature offers proposals for their degradation kinetics, predict the level of degradation expected in the future.
3. To quantify physically and mechanically the different degradation mechanisms in steel fiber-reinforced shotcrete.
4. Based on the experience gained and observations collected, make suggestions that contribute to the durability enhancement of rock bolts and steel fiber-reinforced shotcrete.

In order to meet these objectives, the following research questions have been addressed:

Q1. Have the rock bolts and steel fiber-reinforced shotcrete experienced technological changes motivated by durability concerns?
Q2. What are the aggressive environmental conditions and associated degradation mechanisms reported in the literature for rock bolts and steel fiber-reinforced shotcrete in the Norwegian road tunnels?
Q3. What is the state-of-the-art knowledge about the degradation mechanisms identified?
Q4. In which cases does the available literature offer proposals to predict the kinetics of these degradations in rock bolts and steel fiber-reinforced shotcrete?
Q5. What are the physical and mechanical consequences of the degradation mechanisms identified?
Q6. What are the measures that could mitigate or prevent the degradations in the future?

## 1.4 Scope and research method

To meet objective 1, Q1 must be answered so that the target objects to be investigated are clearly identified. In practice, it is necessary to know the evolution on durability aspects in the Norwegian regulations for rock bolts and steel fiber-reinforced shotcrete. Apart from the regulations, there might be technological milestones in the Norwegian tunnelling industry that influenced the durability of these rock support elements. All this information is obtained from Norwegian handbooks, guidelines and published papers.

In addition, objective 1 demands an answer to Q2. A literature review is performed to identify the environmental conditions which have triggered the main degradation mechanisms observed in rock bolts and steel fiber-reinforced shotcrete installed in Norwegian road tunnels. This task aims to address objective 1, but also contributes to objective 4 since the identification of relevant environmental conditions is the detection of the sources causing the degradations which could eventually be prevented or mitigated.

Questions Q3 and Q4 address objective 2. In both questions, a literature review is needed to investigate if the degradations observed in the field have a theoretical understanding that allows the prediction of the evolution of degradation over time. Applied to the rock bolts, Q4 will be addressed from the literature review by collecting corrosion rates observed in rock bolts installed in Norwegian road tunnels. The results will be contrasted with international standards and findings obtained in the literature review in order to explore the possibility to predict the corrosion kinetics of rock bolts.

Question Q5 aims to fulfill objective 3. In this regard, it is important to highlight that the mechanical changes caused by chemical degradations are easier to quantify in rock bolts than in shotcrete. In the former case, there is a good enough correlation between strength loss and mass loss due to the corrosion in the steel rebar [15].

In the case of steel fiber-reinforced shotcrete, the identification of a chemical attack in the shotcrete layer does not necessarily give a reliable prognosis of its physical and mechanical changes. The physical and mechanical consequences are needed to quantify the severity of different degradation mechanisms. In addition, it is foreseen that the field-defined shotcrete properties will result in a less homogeneous material than a steel rebar manufactured in a plant. Furthermore, little is known about the condition of singularities in the shotcrete layer, such as the contact with the rock, the boundary between adjacent shotcrete layers and the shotcrete surface exposed to the tunnel room. Thus, Q5 applied to shotcrete will be addressed from field and laboratory investigations.

Objective 4 in rock bolts and shotcrete will be addressed by question Q6. In turn, the answers to questions Q1, Q2, Q3 and Q4 will be assessed to answer Q6.

### 1.4.1 Field and laboratory investigations in steel fiber-reinforced shotcrete

The in-situ investigations performed in existing road tunnels are considered necessary to try to connect the chemical changes identified in the shotcrete layer with their physical and mechanical consequences. In this regard, a subsea road tunnel is an interesting field to be inspected, providing shotcrete of same age and technology exposed to fresh groundwater near the portals and saline groundwater in the rest of the tunnel. Saline groundwater usually has high concentrations of sulfate, magnesium, carbonate and chloride which might chemically react with the cement paste in the shotcrete. Thus, the inspection of subsea tunnels might allow to identify different degradation mechanisms and quantify their consequences.

Regarding the selection of the tunnels to be inspected, a compromise had to be made between not choosing old tunnels which are far from the current technology used in shotcrete and avoiding selecting recently commissioned road tunnels where the years of exposure for shotcrete are limited. Thus, the understanding of the evolution on durability aspects of shotcrete in Norwegian practice is crucial. In this regard, one of the technological changes was to start using alkali-free instead of water-glass accelerators in the mid-1990s. The main durability concern of alkali-free accelerators, widely used these days, is its sulfur content [16]. The impact of this technological change on the durability of shotcrete is also investigated in this research.

Subsea road tunnels constructed in the early and late 1990s provide shotcrete samples exposed to fresh and saline groundwater with water-glass and alkali-free accelerators. Three out of the four tunnels selected are subsea road tunnels. Among them, The Nordkapp tunnel is highlighted, which is the first subsea tunnel in Norway where alkali-free accelerator was used. The fourth tunnel called Honningsvåg lies on-shore, where the shotcrete is exposed to fresh groundwater. The tunnel is near the Nordkapp tunnel and has a similar age and technology to the shotcrete used in the Nordkapp tunnel.

Table 1 summarizes the groundwater conditions and accelerator types from where the shotcrete samples will be extracted in the tunnels investigated.

**Table 1:** Road tunnels where the in-service condition of steel fiber-reinforced shotcrete was investigated

| Tunnel | Start of construction | Completion | Type | Condition of groundwater exposure investigated | Accelerator type used in shotcrete |
|---|---|---|---|---|---|
| Hitra | 1992 | 1994 | Subsea | Fresh and saline | Water glass |
| Nordkapp | 1995 | 1999 | Subsea | Saline | Water glass / alkali-free |
| Honningsvåg | 1995 | 1999 | On-shore | Fresh | Water glass |
| Frøya | 1998 | 2000 | Subsea | Fresh and saline | Alkali-free |

In the case of the Nordkapp tunnel, the objective was to contrast the shotcrete conditions in different tunnel locations with a saline environment where different accelerators (water-glass and alkali-free) were used in the shotcrete installed.

In the case of the Frøya and Hitra subsea road tunnels, the main objective is to investigate the possible difference in the condition of the shotcrete exposed to fresh groundwater and exposed to saline groundwater. This means in practice drilling shotcrete near portal areas, and in the middle of these subsea tunnels.

In all the tunnels inspected, three criteria were considered when drilling in the shotcrete layer:

- To drill at least three shotcrete cores next to each other in order to have a good representation of the location with the availability of shotcrete samples for different chemical, physical and mechanical tests.
- To drill in thick shotcrete layers whenever possible. A thicker shotcrete layer may allow changes along the shotcrete layer to be visualized and also discover the condition at the boundary of two adjacent shotcrete layers (shotcrete joints). In practice, this was generally achieved by drilling shotcrete lying adjacent to tunnel stretches where cast-in-place concrete lining had been installed.
- To cross the shotcrete layer and drill a couple of centimeters in rock, so that the condition at the contact between shotcrete and rock can also be assessed.

According to the standard EN 12390-1:2012 [17] for testing hardened concrete, the minimum diameter of a cylindrical concrete sample is to be 3.5 times the diameter of the aggregates, so that the aggregate size has a limited influence on the concrete performance. On the other hand, the Norwegian guidelines for sprayed concrete in 1993 [18], which is relevant for the tunnels inspected, establishes the maximum allowable aggregate diameter to be 16 mm. This would lead to a minimum shotcrete sample diameter of 56 mm. Nevertheless, the shotcrete specification in the Nordkapp tunnel stated a maximum aggregate size of 8 mm, while in the Frøya tunnel was 10 mm. Based on this information, the core bit diameter selected was 62 mm in all the tunnels. With this core bit diameter, it was expected to obtain shotcrete core diameters of approximately 56 mm. In the specific case of the Frøya and Hitra tunnels, some core drillings were also performed with a core bit of 92 mm. This was done to investigate if a larger diameter could have an impact on the uniaxial compressive strength (UCS) test results. In addition, for UCS tests, the consequences of choosing shorter samples with a height-to-diameter ratio (h/D) equal to 1.0 is explored instead of the traditional h/D equal to 2.0. This reduction in sample height aimed to increase the number of samples along a core and increase the possibilities to identify strength variations in the case of a local degradation.

Figs. 3-4 show two investigated locations in the Hitra and Frøya tunnels respectively.

**Fig. 3:** Six shotcrete cores extracted in the Hitra tunnel at chainage 3+090 (approximately in the middle of the tunnel). The extracted cores are shown in Fig. 33.

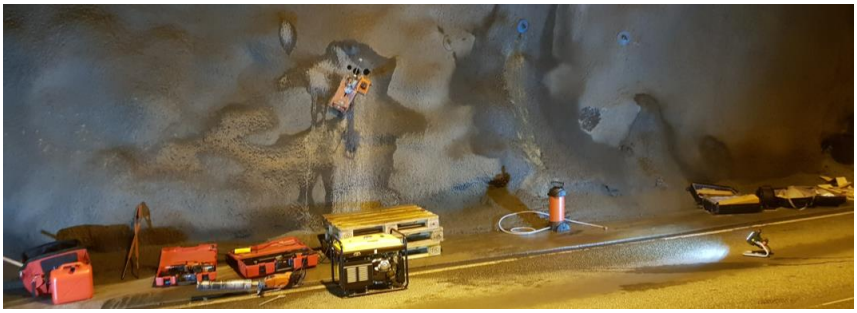

**Fig. 4:** Three shotcrete cores already extracted in the Frøya tunnel at chainage 8+070 near the north portal. The corresponding extracted cores are shown in paper 3, Fig. 5.

In all the investigated locations, after core extraction, the cores were marked, photographed, and wrapped with stretch plastic film to prevent corrosion of steel fibers and further carbonation [19]. On top of the plastic film, bubble wrap was used for transportation. The marking included the number assigned to the core and the orientation.

The electrical conductivity and pH of groundwater seepage from the tunnel roof was measured in all the investigated locations. The measurement of electrical conductivity was performed to distinguish between saline and fresh groundwater exposures. The pH was measured to discard an unforeseen acidic source. In addition, the calcium ion concentration was measured in the Frøya and Hitra tunnels, as part of the leaching investigations in the shotcrete. Fig. 5 illustrates the technique employed and the instruments used.


**Fig. 5:** Groundwater seepage from the tunnel roof collected in a plastic cup for different chemical measurements performed in the field. (a) water sample extraction with a syringe, and (b) instruments for electrical conductivity, pH and calcium ion concentration measurements in water.

Several laboratory investigations were performed to assess the conditions of the shotcrete cores that were extracted. Carbonation was systematically investigated by the pH indicator thymolphthalein (where a bluish color after application is related to non-carbonated concrete), by the identification of calcite via powder X-ray diffraction (XRD) and through an eventual local reduction in suction porosity in profiles constructed along a shotcrete core. The details concerning the procedures are given in paper 2. Additionally, in some shotcrete cores, carbonation was also investigated through the identification of carbonates in the shotcrete through thermogravimetric analysis (TGA). The details about the procedure of the latter investigation technique is given in paper 3.

Possible sulfur, chlorine and magnesium enrichments along the different cores were investigated by μ-XRF. This investigation technique is described in paper 2 and paper 3. The identification of deleterious minerals was undertaken by XRD.

In case a higher resolution than μ-XRF is needed to identify different elements in the cement paste, scanning electron microscopy (SEM) with energy dispersive spectroscopy SEM/EDS will be performed to obtain a higher resolution of the cement paste. A thin polished section cast in epoxy is needed for this specific test. Further details about SEM/EDS are given in Section 3.3.1.

Leaching was chemically investigated by potassium maps via μ-XRF and profiles of portlandite content via TGA. The physical tests performed to investigate leaching indications were suction porosity and shotcrete density along the cores. The mechanical test performed is the uniaxial compressive strength (UCS) with axial strain measurements to observe post-peak behaviors of the UCS test results.

The distribution of tests for each investigated location is given in Appendix A. In order to have a logging of the different cores, the shotcrete was photographed before and after being sliced in the concrete saw. The sequence in the laboratory is shown in Fig. 6.

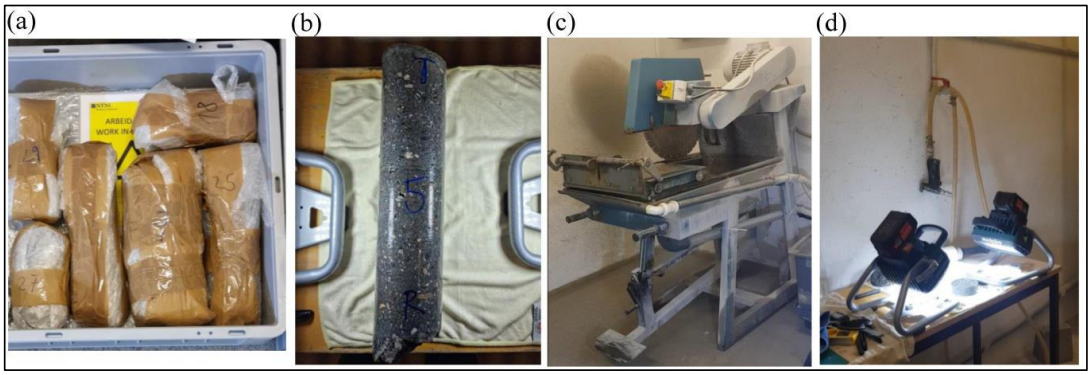


**Fig. 6:** Shotcrete images before and after being sliced in the concrete saw. (a) shotcrete cores received in the laboratory, (b) shotcrete core photographed, (c) concrete saw, and (d) shotcrete sample marked and photographed.

Shotcrete cores sliced crosswise are done in suction porosity, shotcrete density and UCS tests. In these tests, special care is taken to distinguish between the samples that have shotcrete joints and those that do not. Shotcrete cores sliced lengthwise are performed for pH indicator thymolphthalein, μ-XRF and TGA. In the latter case, after the lengthwise slicing, one of the resulting half-cores is systematically sliced crosswise to create a profile of small shotcrete samples that will be later milled. With regard to XRD tests, special slices were performed to focus on specific targets of the shotcrete core. Some sample preparation illustrations are given in Fig. 7.

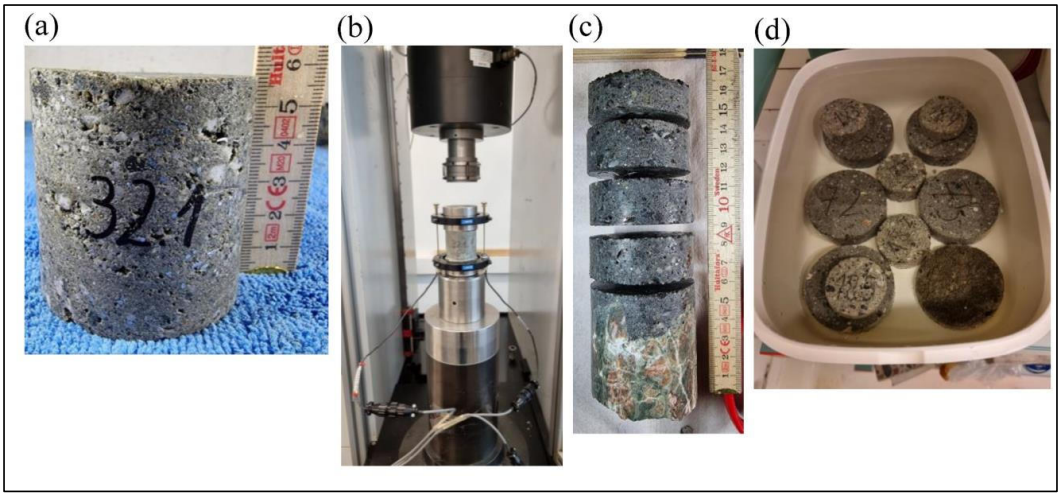


**Fig. 7**: Examples for sample preparation for different tests in the laboratory. (a) Shotcrete core sliced for the UCS test, (b) sample placed in the triaxial testing systems GCTS RTRX-140CL9 for the UCS test with axial strain measurement, (c) shotcrete core sliced crosswise prepared for the suction porosity and density tests, and (d) samples immersed in water during the suction porosity and density tests.

The investigation of steel fiber corrosion will consist basically of visual inspection in search of corrosion products on top of the steel fibers. If there is suspicion of corrosion products with a brownish color in areas where there are no traces of steel, the μ-XRF technique is used to see if there is iron in those brownish stains. A positive result would strongly suggest that corrosion of steel fibers was found.

## 1.5 Limitations

- This research does not include the structural assessment of steel fiber-reinforced shotcrete or rock bolts and the measurement of external load and internal stresses.
- This research mainly investigates chemical/electrochemical degradation mechanisms in steel fiber-reinforced shotcrete. Biological degradations such as bacterial attack observed in some subsea tunnels and physical degradations such as freeze-thaw cycles are not addressed in this research.
- The field investigations performed for the condition assessment of steel fiber-reinforced shotcrete only cover two environmental conditions: saline and fresh groundwater. In addition, the representativity of the results in the tunnels inspected is limited.
- The present research does not perform field investigations for rock bolts. The prognosis of the corrosion rate for longer exposure times is based on collected experience from literature.

## 1.6 Outline of thesis

This thesis has seven chapters which are described below:

- Chapter 1: Introduction with background, objectives, the scope and research method, the limitations and outline of thesis.
- Chapter 2: Results from the literature review: Evolution on durability aspects, understanding of degradation mechanisms and corrosion kinetics for rock bolts and steel fiber-reinforced shotcrete.
- Chapter 3: Description of degradation mechanisms in steel fiber-reinforced shotcrete found from field and laboratory investigations performed in this research.
- Chapter 4: Prognosis of the kinetics of different degradation mechanisms in shotcrete in different environments.
- Chapter 5: Lessons learnt from sampling in this research, extent of the new findings obtained in this research and suggestions for durability enhancement of steel fiber-reinforced shotcrete and rock bolts.
- Chapter 6: Conclusions
- Chapter 7: Further work

## 1.7 Publications:

### 1.7.1 Core publications

The core papers connected to this PhD research are in short described below:

**Paper 1: Corrosion Level of Rock Bolts Exposed to Aggressive Environments in Nordic Road Tunnels**

C.J. Manquehual, P.D. Jakobsen, and A. Bruland,. Published in Rock Mechanics and Rock Engineering journal (2021).

This paper presents a summary of aggressive environmental conditions reported for rock bolts in Nordic Road tunnels. It also gives a prognosis of the corrosion kinetics of carbon steel used in Nordic underground works for 25, 50 and 100 years along with a discussion regarding the lifespan extension provided by cement mortar, hot-dip galvanizing and the duplex system in those environments.

This paper gives the basis for the prognosis of rock bolt corrosion in the relevant environments for Norwegian road tunnels.

*Contribution of main author:* Conceptualization, methodology, data curation and elaboration of original draft.

**Paper 2: Comparison of the condition of steel fiber-reinforced shotcrete with water-glass and alkali-free activators after more than 20 years of service in a subsea road tunnel**

C.J. Manquehual, P.D. Jakobsen, K.G. Holter, K.D. Weerdt, T. Danner, and A. Bruland. Published in Construction and Building Materials journal (2022).

This paper presents field and laboratory investigations of steel fiber-reinforced shotcrete installed in the Nordkapp subsea road tunnel. This paper focuses on the durability comparison of shotcrete using water-glass and alkali-free accelerators after more than 20 years of exposure to saline groundwater.

*Contribution of main author:* Given in the paper.

**Paper 3: Investigation of leaching in steel fiber-reinforced shotcrete exposed to fresh and saline groundwater in a subsea road tunnel**

C.J. Manquehual, P.D. Jakobsen, K.G. Holter, K.D. Weerdt, and A. Bruland. Under review in Cement and Concrete research journal.

This paper presents field and laboratory investigations of steel-fiber reinforced shotcrete in a subsea road tunnel constructed between 1998 and 2000 exposed to fresh and saline groundwater. This paper is relevant for this research because it compares the condition of shotcrete of the same age and technology exposed to different environments.

*Contribution of main author:* Given in the manuscript.

Figs. 8-9 aim to put in context the three core publications, the objectives of this research, the research method and the structure of thesis for rock bolts and steel fiber-reinforced shotcrete respectively.

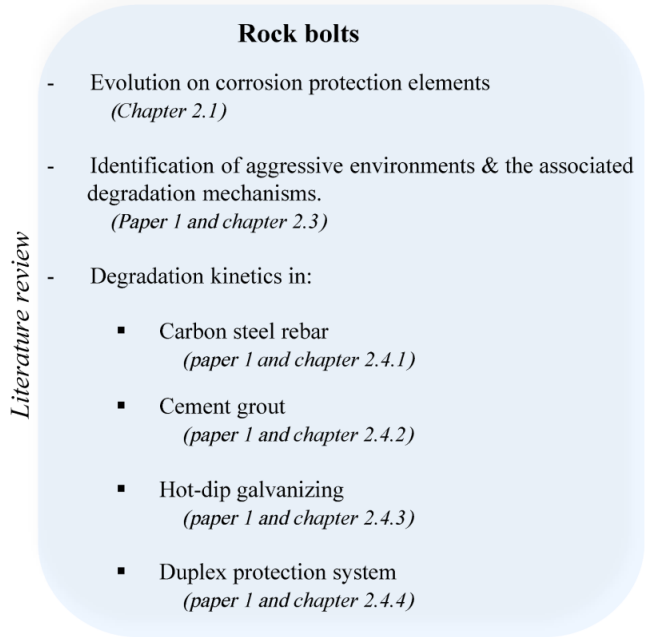


**Fig. 8:** Objectives, research method and structure of the thesis for rock bolts.

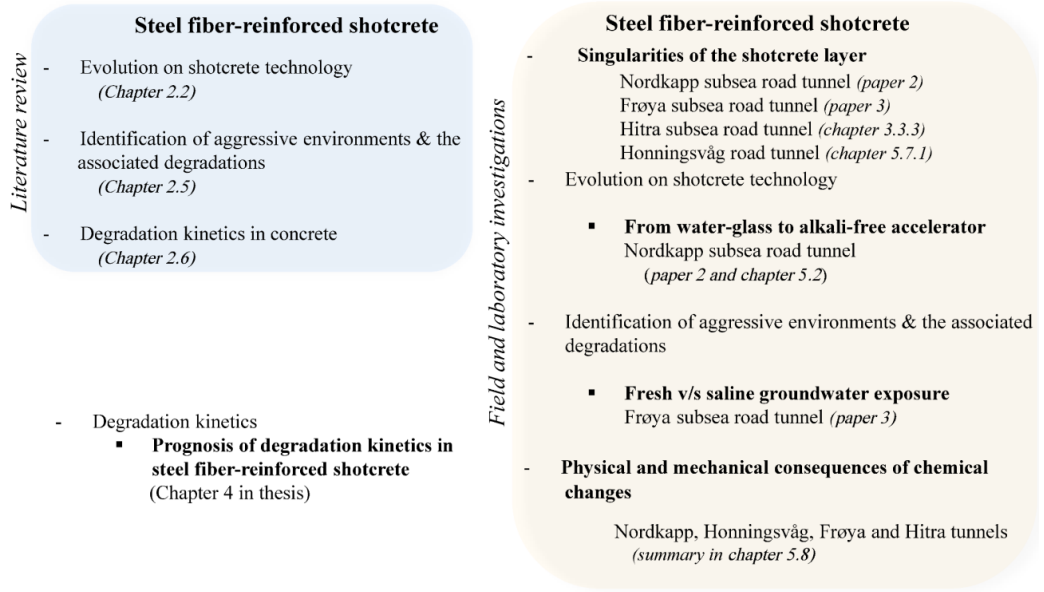


**Fig. 9:** Objectives, research method and structure of the thesis for steel fiber-reinforced shotcrete.

In Figs. 8-9, only objective 4 is not described. This latter objective encompasses an analysis of the main results of this research.

In Fig. 9, singularities of the shotcrete layer refer to the contact between the shotcrete layer and the rock, the contact between two adjacent shotcrete layers and the shotcrete surface exposed to the traffic room. As already mentioned in section 1.4.1, all the drillings extracted from the field tried to cross the shotcrete layer and reach the rock in order to recover the whole layer of shotcrete.

### 1.7.2 Supplemental publications

**Paper 4: Operation & Maintenance Costs of Subsea Road Tunnels in Norway**

C. Manquehual, J. Johansen, P.D. Jakobsen, and B. Nilsen. ITA-AITES World Tunnel Congress, WTC 2020.

This paper presents the annual Operation & Maintenance (O&M) cost of subsea road tunnels based on the raw data obtained from the program MOTIV developed by the NPRA.

This paper explored the role of rock support costs in relation to other O&M costs in subsea road tunnels.

*Contribution of main author:* Data processing, methodology and elaboration of original draft.

# Chapter 2

## 2 Results of the literature review

### 2.1 Evolution on durability aspects of rock bolts

The corrosion protection of rock bolts has evolved over the last decades as shown in Fig. 10. Both, the durability of the steel rebar and the lifespan extension given by cement mortar, hot-dip galvanizing and epoxy coating are addressed in this research.

### 2.2 Evolution of durability aspects of steel fiber-reinforced shotcrete

Fig. 11 shows the evolution of the shotcrete specifications in the Norwegian regulations over the years. It is important to highlight that the water-binder ratio (w/b) and the minimum shotcrete thickness variations were motivated by durability issues. Other technological changes motivated by other purposes, but with durability consequences are the introduction of silica fume more than 40 years ago, the introduction of blended cement with fly ash less than 20 years ago and the start of the use of alkali-free accelerator in the mid-1990s. Finally, the concern about the corrosion of steel fibers led to allowing the use of plastic fibers as shotcrete reinforcement in 2007. However, it was banned some years later due to environmental issues.

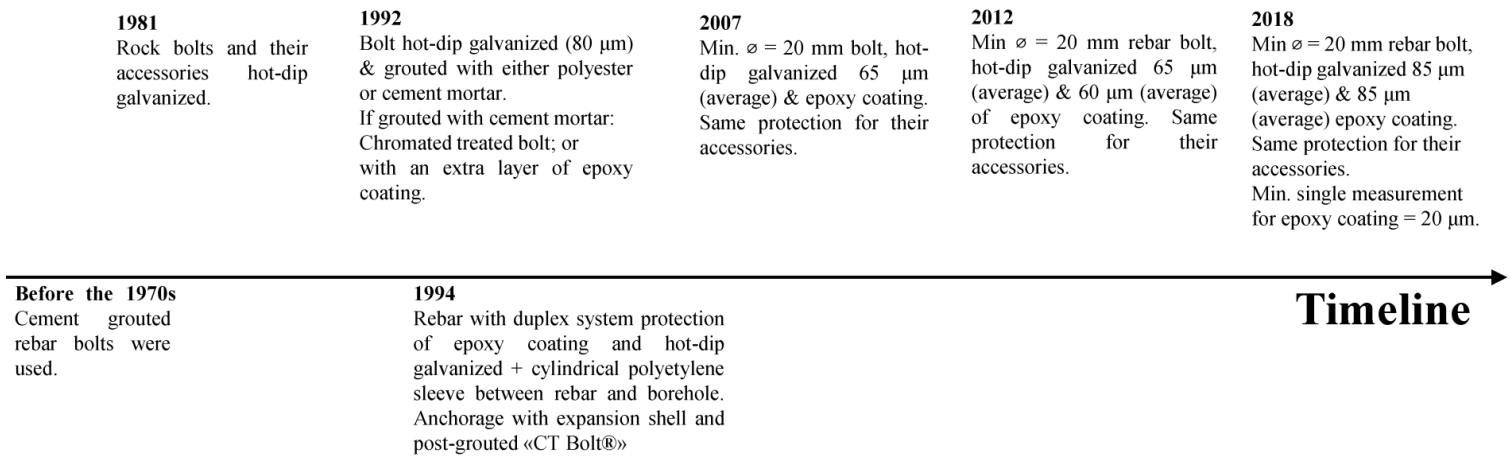


**Fig. 10:** Evolution on durability aspects of rock bolts in Norwegian road tunnels [20–26]. Above the timeline, evolution on Norwegian regulations. Below the timeline, common practice and milestones in the Norwegian tunnel industry.

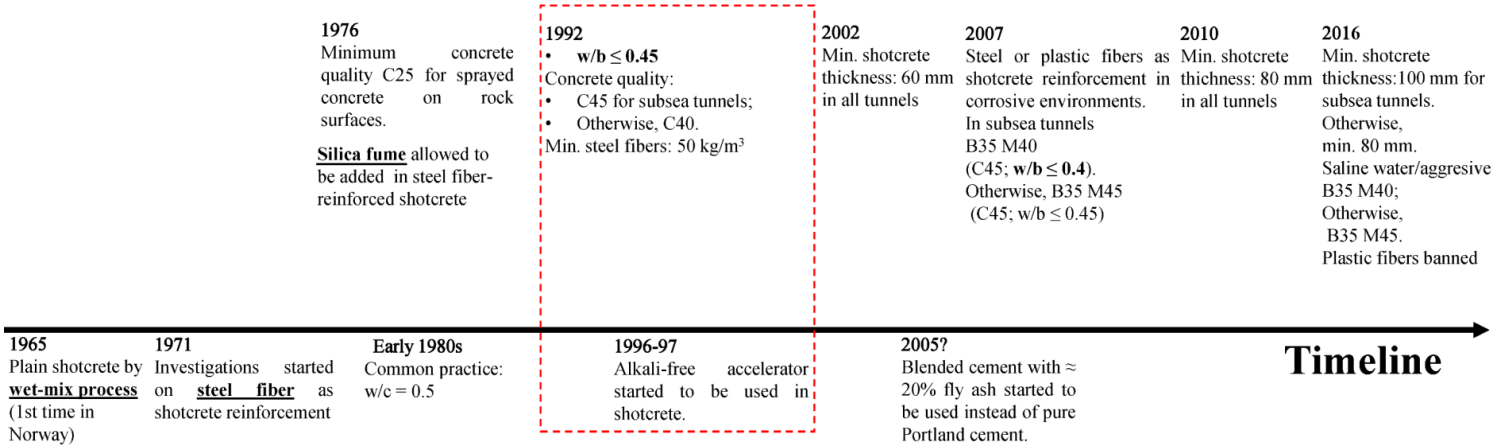


**Fig. 11:** Evolution on durability aspects of shotcrete in Norwegian road tunnels [23,24,27–33]. Above the timeline, evolution on Norwegian regulations. Below the timeline, common practice and milestones in the Norwegian tunnel industry.

In Fig. 11, a rectangle highlights the Norwegian regulations applicable to the tunnels described in Table 1.

## 2.3 Degradation mechanisms in rock bolts

The rock bolt consists mainly of carbon steel. As shown in Fig. 10, the rock bolt protection against corrosion of the steel rebar evolved in Norway. From the cement grout protecting the rebar before 1970, a galvanized layer on top of the rebar was added in practice in the early 1970's. Approximately two decades later, a layer of epoxy coating was added on top of the galvanized rebar fully grouted with cement. The combined protection of hot-dip galvanizing and epoxy coating is also known as the duplex protection system. This section addresses the degradation of the steel rebar, the zinc coating, the epoxy coating, and the cement grout in the context of rock bolts.

In paper 1 [34], a description of the conditions of rock bolts in several environments found in Nordic road tunnels is provided. This section provides a theoretical background to complement those findings from the literature and observations.

### 2.3.1 Fundamentals of corrosion in fresh groundwater (Poorly ionic wet corrosion)

The corrosion of unprotected steel is inevitable if it is in contact with water containing dissolved oxygen. The electrochemical process involved in the corrosion of steel can be split in two half-cell reactions which interact with each other. These two half-cell reactions are located in the anodic and cathodic regions (See Fig. 12). In this figure, the steel is represented by iron. The dissolution of iron at the surface occurs in the anodic region. In the process, iron also releases electrons which travel through this metal towards the cathodic region. Eq. 1 represents this reaction in the anodic region.

$$F_e \rightarrow F_e^{2+} + 2e^- \tag{1}$$

In the cathodic region, the electrons received from the anodic region react with water and oxygen to produce hydroxide ions ($OH^-$). Eq. 2 represents the reaction in the cathodic region in neutral and alkaline aqueous solution (reduction of oxygen):

$$\frac{1}{2} \cdot O_2 + H_20 \ + 2e^- \rightarrow 2OH^- \tag{2}$$

Water is the medium (electrolyte) in which electric current is transported by ions [35]. In the reactions described in Eq. 1 and Eq. 2, iron ions are transported from the anodic to the cathodic regions, while hydroxide ions are transported in the opposite direction.

Eq. 1 and Eq. 2 are summarized by Eq. 3 as follows:

$$F_e + \frac{1}{2} \cdot O_2 + H_2O \rightarrow F_e^{2+} + 2OH^- \tag{3}$$

Iron and hydroxide ions will react and form ferrous hydroxide ($F_e(OH)_2$) as a corrosion product. The corresponding chemical reactions in the anodic and cathodic regions described in Eq. 3 are shown in Fig. 12:

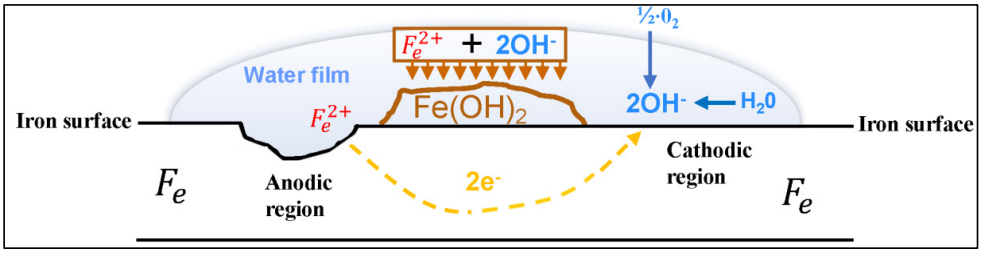


**Fig. 12:** Illustration of wet corrosion for steel in a neutral or alkaline aqueous solution. Modified from [36].

It is important to mention that after the formation of $(F_e(OH)_2)$, the corrosion product will probably experience further reactions depending on factors such as the temperature, pH, and the availability of dissolved oxygen. Further chemical reactions could be ferric oxide ($Fe_2O_3$), magnetite ($Fe_3O_4$), ferric hydroxide ($Fe(OH)_3$), and hydrated iron oxide ($Fe_2O_3{\cdot}3H_2O$).

It should also be emphasized that for the conditions described in Eq. 3, the corrosion should be uniform since anodic and cathodic regions will shift on the steel surface over time.

Regarding hot-dip galvanizing, it is important to point out that Fig. 12 might represent the corrosion process of zinc as well, releasing two electrons during the dissolution of zinc in the anodic region and the same process in the cathodic region [37].

### 2.3.2 Acidic environment

In an acidic environment, the cathodic reaction is governed by the hydrogen evolution reaction described in Eq. 4 [38].

$$2H^+ + 2e^- \rightarrow H_2 \tag{4}$$

The oxygen reduction reaction described in Eq. 2 (and other intermediate cathodic reactions) can also occur in the cathodic region depending on the amount of dissolved oxygen available and the pH of the electrolyte [39]. However, the lower the pH in the medium, the greater the role played by the hydrogen evolution reaction in the cathodic region. Note that the latter statement is valid for steel and zinc as well.

To put in context the corrosion rate of steel and zinc in acidic environments, Fig. 13 was constructed to illustrate their corrosion rate as a function of pH.

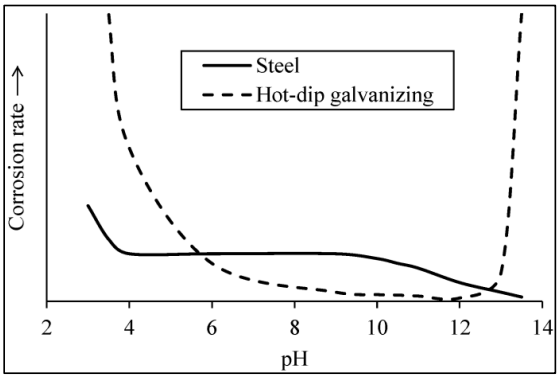


**Fig. 13:** Conceptual scheme of the corrosion rate of steel and hot-dip galvanizing as a function of the pH of the solution. Modified from [40,41].

Fig. 13 is only a conceptual illustration since the curves are the results of different authors studying the corrosion rate of steel and zinc in different environments. Nevertheless, Fig. 13 exemplifies several observations described in the literature:

- Zinc is sensitive to acidic and alkaline environments (amphoteric) [42].
- Steel is only sensitive to an acidic environment (pH < 4) [43].
- The corrosion rate of steel exposed to a pH environment between four and ten is approximately constant [36].
- The corrosion rate of zinc exposed to a near-neutral pH environment (low corrosivity level) is significantly lower than the corrosion rate of steel in the same environment [44].

Fig. 13 shows qualitatively that the hot-dip galvanized protection is poor in acidic environments and performs even worse than steel in that specific condition.

The durability of the epoxy coating is complex to analyze because there are many variables involved during its manufacture, transportation and environmental conditions after installation that will affect its performance once in service. Regarding manufacturing, the type of binder, the type of solvent, the additives, pigments and fillers used, and the pre-treatments undertaken before the application of the epoxy coating make the crosslinking density of the epoxy coating unique [45]. It is well known that the epoxy coating is sensitive to mechanical damage [46], and therefore, careful transportation and installation of rock bolts with the duplex protection system is critical. Once in service, other variables might influence the durability of the epoxy coating, such as external elements trying to diffuse through the epoxy coating, making the different observations difficult to generalize [47]. Nevertheless, laboratory experiments have shown that epoxy coating is an excellent corrosion protection to carbon steel in an acidic environment [34]. This is probably related to the fact that the diffusion rate of hydrogen ions through the epoxy coating is low [48].

The environment that a non-degraded cement grout can provide to the steel rock bolt exceeds a pH of 12.6 [42]. On the other hand, when the pH near the steel is above 11, a stable oxide film is formed on the steel surface by the precipitation of corrosion products on it, limiting the corrosion rate of the steel rock bolt (steel is passivated) [49]. Thus, the pH environment provided by cement grout is high enough to secure this stable film on the steel surface. However, the protection by cement grout in acidic groundwater is quite limited due to the thin annulus grout thickness surrounding the steel rebar. This was illustrated in paper 1 by extrapolating laboratory results [34]. Moreover, if a fully grouted rock bolt starts to be subjected to loads exerted by the rock

mass in hard rock tunnels, the grout will preferentially crack as an extension of the rock discontinuity [50], as shown in Fig. 14. The crack in the cement grout will occur since its tensile capacity is limited. Once created, the crack in the grout will facilitate the access of aggressive ions conveyed by the groundwater through the rock discontinuities to the rock bolt. This means that if the cement grout rock bolt is subjected to loads over time, at some point the grout will crack and its protection will decrease.

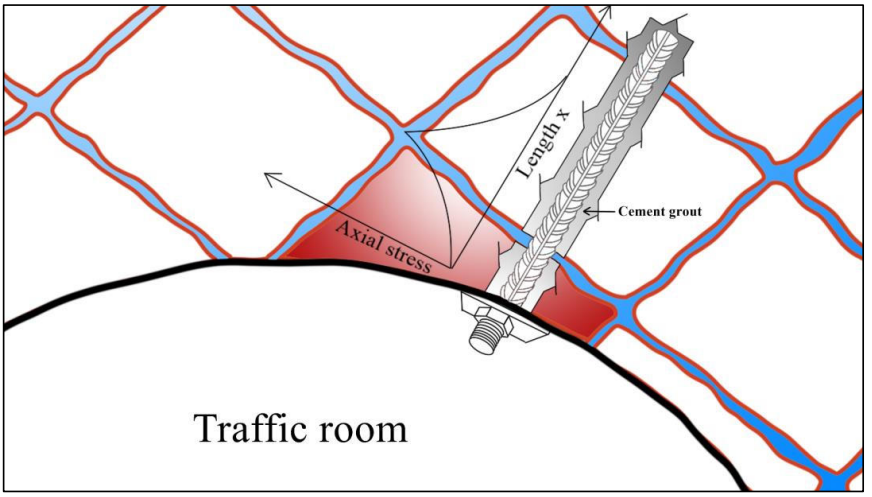


**Fig. 14:** Illustration of a crack in the cement grout surrounding the rock bolt triggered by an underground wedge about to fall. Modified from [50].

Furthermore, the highest axial stress along the rock bolt will occur exactly at the crack of the cement grout [51], where the aggressive groundwater will reach the rock bolt.

#### *2.3.2.1 Acidic environment in Norway*

In Norway, acidic water with a pH value below four has been measured in tunnels excavated in alum-shale rock mass [52]. This rock mass contains pyrite ($F_eS_2$), a mineral which undergoes oxidation in the presence of water and oxygen. Eq. 5 describes this reaction [53]:

$$F_eS_2 + \frac{7}{2} \cdot O_2 + H_2O \rightarrow F_e^{2+} + 2SO_4^{2-} + 2H^+ \quad (5)$$

As described in Eq. 5, the formation of hydrogen ions will acidify the water (electrolyte) involved in the reaction.

### 2.3.3 Saline groundwater

The attack of chloride ions on steel is pitting corrosion, a type of localized corrosion [54]. In general, chlorides ions have the tendency to be adsorbed by the passive film of metals [55]. Even though a stable oxide film can

exist on the steel surface, chloride ions present in the electrolyte start to compete with hydroxide ions at the film-electrolyte interface to form part of the oxide film [54,56]. If the concentration is high enough, chloride ions can break down the passive layer locally, start the dissolution of the steel, and acidify the anodic region.

Apart from the dissolution of iron ions described in Eq. 1, the reactions described in Eq. 6 and Eq. 7 are also expected in the anodic region when chloride ions attack the steel [57]:

$$F_e^{2+} + 2Cl^- \rightarrow F_eCl_2 \tag{6}$$

$$F_eCl_2 + 2H_2O \rightarrow F_e(OH)_2 + 2H^+ + 2Cl^- \tag{7}$$

As described by Eq. 7, chloride ions are not consumed in the reaction which promote further corrosion. Moreover, the more acidic environment (shown in Eq. 7 with the formation of hydrogen ions) fosters the hydrogen evolution reaction (Eq. 4) as an additional cathodic reaction. Fig. 15 illustrates the localized corrosion caused by chloride attack on passivated steel.

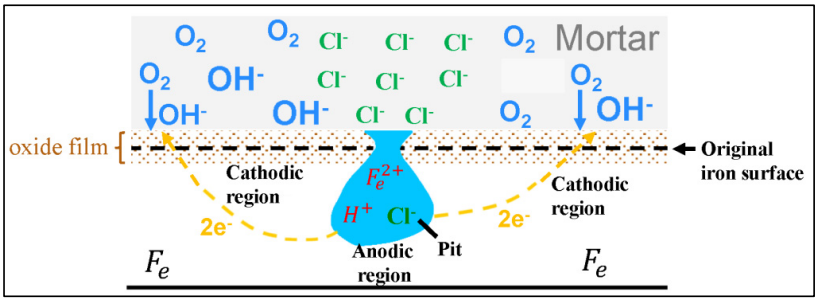


**Fig. 15:** Schematic representation of chloride-induced corrosion of passivated steel. Modified from [57]

The localized corrosion of chlorides and the rest of the rebar still passivated makes the chloride attack even more severe [36].

With regard to the attack of chloride ions on zinc, it is important to mention that the critical chloride concentration to initiate corrosion in zinc has been measured to be at least twice that of steel [42]. In addition, hot-dip galvanizing provides protection to the steel rebar even if the zinc coating has already disappeared. A representation of the cathodic protection of zinc to steel is given in Fig. 16.

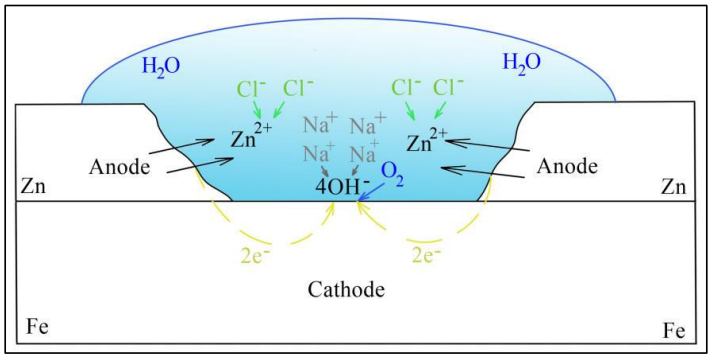


**Fig. 16:** Representation of the cathodic protection of hot-dip galvanizing to the steel rebar in saline environment. Modified from [58].

Fig. 16 shows that the exposed steel becomes the cathode, a region that consumes the electrons released when the zinc is dissolved in the anodic region. In saline groundwater, the sodium ions will tend to go to the cathodic region where negatively charged hydroxide ions are formed. The sodium and hydroxide ions will form sodium hydroxide ($NaOH$), which will probably alkalize the cathodic region even more. As shown in Fig. 13, a more alkaline environment near the steel surface reduces its corrosion rate. On the other hand, chloride ions in the electrolyte will tend to go towards the anodic region, where positively charged zinc ions are formed. Nevertheless, unlike steel, zinc chloride does not acidify the anodic region [58]. However, the cathodic protection of hot-dip galvanizing to an exposed steel surface is limited because zinc will not be able to polarize a large, exposed steel surface area. The extent of the cathodic protection on steel will depend on the resistivity of the electrolyte.

Regarding the degradation that the duplex protection system can experience in saline environment, Fig. 17 aims to harmonize the most widely agreed theories regarding the mechanism developed when a blister is formed [47,58,59].

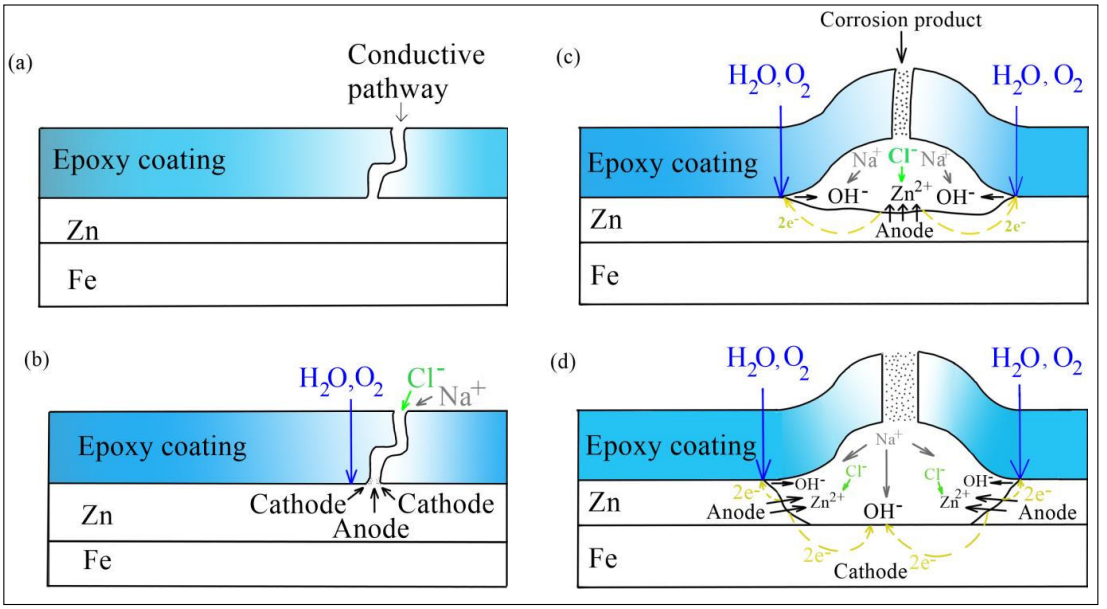


**Fig. 17:** Schematic diagram of the formation of a blister in the duplex protection system exposed to a saline environment. a) Defect in the epoxy coating, (b) formation of cathodic and anodic regions at the bottom of the conductive pathway, (c) blister formation and corrosion of the zinc coating, and (d) cathodic protection of zinc to exposed steel. Modified from [47,58,59].

It is important to highlight that the origin of the degradation represented in Fig. 17a is not an external damage, but rather zones in the epoxy coating with higher affinity to water (hydrophilic regions) or regions with lower cross-linking density where ions can have an easier access to the substrate [47].

Fig. 17b shows that water and oxygen will diffuse through the epoxy coating to the disbonding front underneath the epoxy layer where the cathodic region occurs with the formation of hydroxide ions (Eq. 2). This is the zone where loss of adhesion takes place at the periphery of the conductive pathway (cathodic disbonding). The dissolution of zinc ions (anodic region) takes place at the center of the conductive pathway. Chloride and sodium ions will reach the substrate through the existing conductive pathway attracted by the formation of ions of opposite charges.

Fig. 17c shows the formation of a blister due to the hygroscopic property of the corrosion products, bringing more water underneath the epoxy coating (osmosis) [47]. This figure also shows certain progression of the zinc corrosion. In principle, the cathodic region occurs at the epoxy coating-zinc interface (disbonding front), while the anodic region takes place on the zinc surface at the center of the blister, releasing zinc ions to the electrolyte. However, as shown in Fig. 13, zinc also corrodes at high pH. This creates a second anodic region near the cathodic disbonding forming corrosion products just behind the disbonding front. It is claimed that this corrosion product can act as a wedge to the adherence of the epoxy coating and zinc, contributing mechanically to the disbonding of the epoxy coating [60]. On the other hand, when it comes to the corrosion rate of zinc, the possibility of two different anodic areas will probably make the corrosion of zinc more uniform, and therefore, less aggressive [58].

Finally, Fig. 17d presents further zinc corrosion, exposing a portion of the steel underneath the blister. Two cathodic areas are represented in this figure by the formation of hydroxide ions. One of these areas is the disbonding front of the epoxy coating. The other cathodic region is on the steel surface underneath the blister, which is cathodically protected by the dissolution of zinc. Note that in all the processes described in Fig. 17, the steel rebar is still uncorroded. Of course, over time the zinc will disappear and the steel rebar will undergo corrosion as described in Fig. 15.

It is worth noting that the degradation of the duplex system shown in Fig. 17 did not need any mechanical damage to develop. If external damage occurs during the transportation of rock bolts, and the metal is exposed, the ingress of ions reaching the substrate will be easier and degradation will be faster.

Fig. 18 shows an example from the field where blisters in the duplex protection system were observed in a rock bolt plate.

**Fig. 18:** Blisters observed in a rock bolt plate in the Oslofjord subsea road tunnel after 10 years of exposure [61].

When it comes to cement grout, its protection to rock bolts in saline environment is limited by the same reasons as described in the acidic environment. That is to say: a thin annulus grout thickness will be penetrated by chloride ions, reaching the rock bolt after a short period of time [34], and the low tensile capacity of the cement grout that will lead it to crack in the event that the rock bolt starts to be subjected to loads.

#### *2.3.3.1 Saline groundwater in Norway:*

In Norwegian road tunnels, rock bolts installed in subsea tunnels are exposed to a high content of chlorides. Chemical analyses of dripping groundwater in these tunnels give chloride concentrations in the order of 19,000 mg/l [62]. Another source of chlorides might come from the traffic room, where sodium chloride is usually used as de-icing salts in road tunnels during winter.

### 2.3.4 Flowing groundwater with dissolved oxygen

Fig. 12 and Eq. 3 show the important role of dissolved oxygen in the corrosion of steel. On the other hand, the motion of the electrolyte can affect the corrosion rate of steel by preventing the deposition of the corrosion product on the steel surface or eroding the corrosion product [63]. Fig. 19 describes the corrosion rate of small steel plates, also known as coupons, as a function of dissolved oxygen and flow condition measured in eight

Australian hard rock underground mines [64]. In these mines, the groundwater was either brackish ( 3,000 mg/l < total dissolved solids < 10,000 mg/l) or saline (total dissolved solids > 10,000 mg/l).

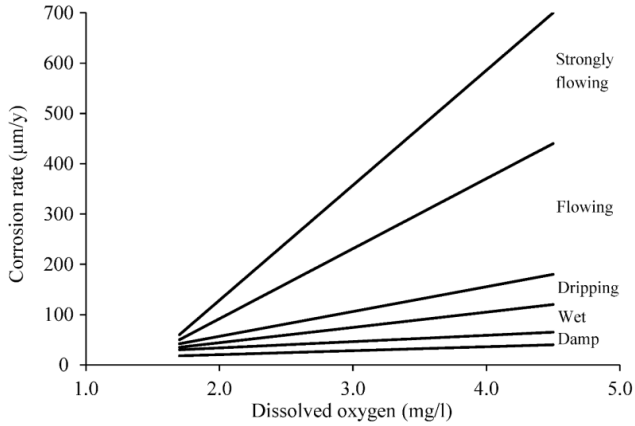


**Fig. 19:** Corrosion rate of steel plates measured in Australian underground mines as a function of dissolved oxygen and flow condition. Modified from [64].

In the case of zinc exposed to the motion of the electrolyte, it is expected that there is a similar behavior as shown for steel in Fig. 19. In fact, it has been stated that a flow velocity higher than 0.5 m/s on zinc is enough to prevent the formation of the corrosion product on the zinc surface [65].

With regard to epoxy coating, it has been described that a higher fluid velocity results in a higher flow shear stress at the contact with the epoxy coating which increases the corrosion rate [66]. Specifically, this reference states that a higher flow velocity decreases the coating thickness, reduces the electrical resistivity, accelerates the water uptake and the diffusion of oxygen.

Flowing water can also be a problem for the cement grout, especially during the installation of the rock bolts when the grout is still in its plastic stage by either increasing the water-cement ratio of the grout or creating voids [20]. During operation, flowing water percolating the cement grout can promote the decalcification of the cement grout.

#### *2.3.4.1 Flowing groundwater with dissolved oxygen in Norway*

Dripping/flowing groundwater with dissolved oxygen can occur in any tunnel excavated in a permeable rock. Higher concentrations of dissolved oxygen are found where the water temperature is low [67], which is the case for groundwater in Nordic countries, with average temperatures below 7° C [68]. In general, the dissolved oxygen concentration in groundwater decreases at higher depths [69]. Thus, it follows that sections of tunnels near portals with dripping/flowing water are of particular concern.

## 2.4 Degradation kinetics in rock bolts

### 2.4.1 Carbon steel rebar

In paper 1 [34], a corrosion level prognosis for 25, 50 and 100 years was obtained for unprotected carbon steel in Nordic underground structures in specific aggressive environments. These environments were saline groundwater, acidic groundwater and fresh groundwater with dripping/flowing conditions. Specifically, the prognosis is given in Fig. 8 of that paper [34]. From this figure, the following results are highlighted:

- For 25 years of exposure, the middle depth of corrosion in unprotected carbon steel would be 1.90 mm. Assuming a uniform corrosion around a rebar of 20 mm, this is equivalent to approximately 34% of loss in its cross-sectional area.
- For 50 years of exposure, the middle depth of corrosion in unprotected carbon steel would be 2.70 mm. Assuming a uniform corrosion around a rebar of 20 mm, this is equivalent to approximately 46% of loss in its cross-sectional area.
- For 100 years of exposure, the middle depth of corrosion in unprotected carbon steel would be 3.90 mm. Assuming a uniform corrosion around a rebar of 20 mm, this is equivalent to approximately 63% of loss in its cross-sectional area.

It has been shown in the literature that the loss in cross-sectional area of the rebar due to corrosion is approximately linear to the loss of tensile capacity [70]. Then, as a first approach, the loss of cross section area given above can be interpreted as the loss in its tensile capacity.

### 2.4.2 Cement grout

As already discussed, the cement grout provides protection to the rebar with an alkaline environment which secure a stable oxide film on the rebar surface. However, as described in Fig. 14, its contribution in case the rock bolt actually is subjected to loads is limited since it has a low tensile capacity. In this research, the contribution of cement grout is considered negligible.

### 2.4.3 Hot-dip galvanizing

In saline environments, the collection of corrosion rates of hot-dip galvanizing in Nordic underground structures was summarized in paper 1 [34], Table 2. A chart from that table is shown in Fig. 20.

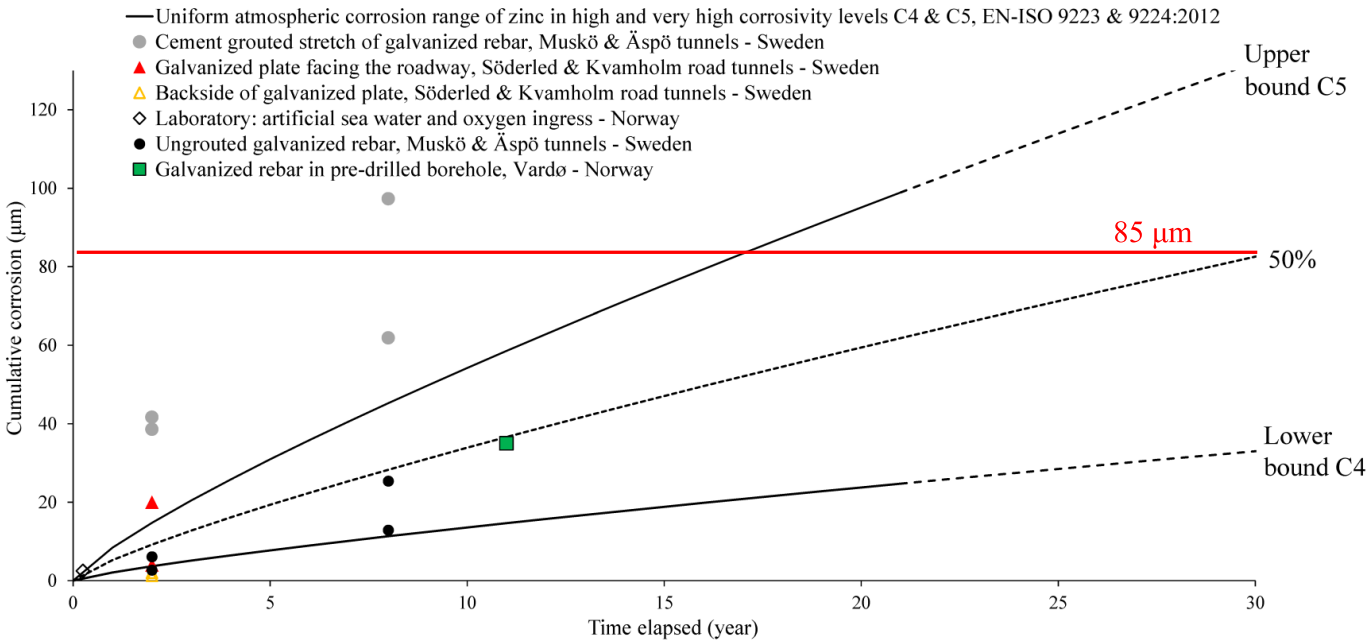


**Fig. 20:** Corrosion rates of hot-dip galvanizing exposed to saline environment collected from the Norwegian and Swedish literature. Modified from [34].

The confidence band proposed for hot-dip galvanizing exposed to saline environments in Fig. 20 comes from the corrosivity levels C4 and C5 in international standard EN-ISO 9223 &9224:2012 [44,71]. In this standard, C4 and C5 corrosivity levels are described as atmospheric environments affected by chlorides, de-icing salts and polluted industrial areas.

Fig. 20 shows that the dispersion of corrosivity levels undergone by hot-dip galvanizing is high. Some differences can be explained by the environment where the corrosion depth of hot-dip galvanizing was measured.

- In the case of Söderled and Kvamholm road tunnels, the main difference is the traffic density, being much higher in the first one. In general, a higher traffic density leads to a higher pollution and dispersion of de-icing salts all over the tunnel contour [52].
- A case with corrosion rates exceeding the upper bound C5 occurred in Muskö and Äspö tunnels. Apart from the saline environment, in these tunnels the rebars were fully grouted with cement (alkaline environment, see Fig. 13).
- The results in ungrouted galvanized rebars in Muskö and Äspö tunnels along with the results in the Vardø tunnel are considered reliable representations of saline groundwater, without any additional aggressive factor acting simultaneously with this environment.

Based on the confidence band proposed in Fig. 20, for 30 years of exposure in saline groundwater, the middle depth of corrosion in hot-dip galvanizing would be 85 µm. The latter value is the minimum average thickness of galvanizing in current Norwegian regulations (see Fig. 10).

It is interesting to highlight that previously in the literature, a lifespan extension of 30 years had already been described in average for an 85 µm thickness layer of hot-dip galvanizing exposed to a marine atmosphere [72]. Fig 21 shows this result:

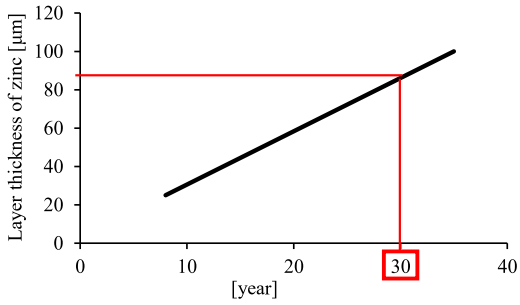


**Fig. 21:** Useful life extension given by a layer of zinc in marine atmosphere modified from [72]

As discussed in paper 1 [34], in acidic environments, especially with a pH < 4, the contribution of 85 µm thickness of hot-dip galvanizing is negligible.

### 2.4.4 Duplex protection system

As discussed in Section 2.3.3, there is a synergy of protection in the steel rebar by an epoxy coating layer on top of a galvanizing one compared to the case where galvanizing and the epoxy coating layers act independently and directly on the steel rebar. The two key differences can be synthesized as follows:

- When zinc corrodes, the zinc corrosion products do not acidify the anodic region in contrast to steel [58].
- The corrosion of zinc leads to a more uniform zinc corrosion behind the epoxy layer, preventing a more localized corrosion which is more aggressive.

It is claimed that this synergistic factor is 1.5 for aggressive environments [72]. Considering this synergistic factor and the 30 years of life extension given by 85 μm thickness of hot-dip galvanizing in a saline environment, it is expected that there will be a useful life extension by the duplex protection system of 45 years on average. In this time period, the carbon steel rebar is still uncorroded. After this time period, the corrosion rate prognosis of unprotected steel described in paper 1, Fig. 8 could be considered. By combining all of the above, it is possible to state that for a rebar of 20 mm, approximately half of the rock bolts with the duplex protection system in a saline environment will experience a reduction of approximately 34% in their cross-sectional area in 70 years, and approximately 46% reduction in 95 years.

In an acidic environment, the epoxy coating provides an extremely good protection. Laboratory measurements in acidic environments give corrosion depth reductions in the order of 90% for epoxy-coated carbon steel compared to unprotected steel [34]. By using Fig. 8 in paper 1 for 100 years of exposure time, the middle depth of corrosion in carbon steel would be 3.9 mm. Theoretically, by extrapolating the 90% efficiency given by the epoxy coating in acidic environment and neglecting the protection of hot-dip galvanizing, the middle depth of corrosion would be 0.39 mm for a carbon steel rebar with the duplex protection system. Following this reasoning, it could be stated that for a rebar of 20 mm, about half of the rock bolts with the duplex protection system in acidic environment would experience a reduction of approximately 8% in cross-sectional area in 100 years.

The corrosion protection figures given by the duplex system exposed to saline and acidic environments are theoretical approximations to the real problem. Nevertheless, it is clear that the protection performance in acidic environments is better than in saline environments with the duplex system. However, a mechanical defect in the epoxy coating will probably cause a higher corrosion rate in an acidic environment.

### 2.4.5 Summary

Table 2 provides the predicted median values of loss of cross-sectional area for a given exposure time in different environments for hot-dip galvanizing and the duplex protection system.

**Table 2:** Predicted median value of loss of cross-sectional area for a steel rebar (φ = 20 mm) as a function of exposure time and the environment.

| Loss of cross-sectional area in % (exposure time) | Hot-dip galvanizing | Duplex protection system |
|---|---|---|
| Saline groundwater | 34% (55 years) | 34% (70 years) |
| Acidic groundwater | 34% (25 years) | 8% (100 years) |

## 2.5 Degradation mechanisms in steel fiber-reinforced shotcrete

### 2.5.1 Carbonation

Carbonation occurs due to the ingress of atmospheric carbon dioxide ($CO_2$) in the pore solution of the cement paste. Once in solution, $CO_2$ reacts with water forming carbonate and hydrogen ions as described in Eq. 8.

$$CO_2 + H_2O \rightarrow CO_3^{2-} + 2H^+ \tag{8}$$

The formation of hydrogen ions will reduce the pH of the pore fluid to less than 9 if the concrete is fully carbonated [73]. On the other hand, the carbonate ions will react with calcium ions to form solid calcite as shown in Eq. 9.

$$Ca^{2+} + CO_3^{2-} \rightarrow CaCO_3 \tag{9}$$

In Eq. 9, the calcium ions will initially come from the pore solution. However, a gradual depletion of calcium ions in the pore solution will create a calcium concentration gradient between the hydrated cement paste and the pore solution that will stimulate the decalcification of the cement paste [74]. Primarily portlandite, but also calcium-silicate-hydrates, or in short C-S-H, will provide the calcium ions needed to continue the calcite formation [75]. Apart from calcite formation in the carbonated region, the decalcification of the C-S-H will form hydrated silica gel.

### 2.5.2 Leaching

Leaching is the process where ions such as hydroxide and calcium leave the concrete layer [76]. It is traditionally linked to concrete exposed to poorly ionic water in neutral or acidic environments [74]. This is probably because in these environments decalcification of concrete is more severe and the leaching process becomes more evident.

Leaching can also occur because of water permeation through the pores of the cement paste in the concrete. If the groundwater level is above the tunnel alignment, there will be a hydraulic gradient towards the traffic room that will promote the percolation of the shotcrete layer [19]. In the process, water might carry alkali-metals such as potassium and sodium, but also calcium and hydroxide ions that will reduce the calcium concentration and pH of the pore solution, and therefore, will contribute to further decalcification. In turn, decalcification leads to increased porosity of the cement paste, facilitating leaching [76]. Fig. 22 illustrates this process.

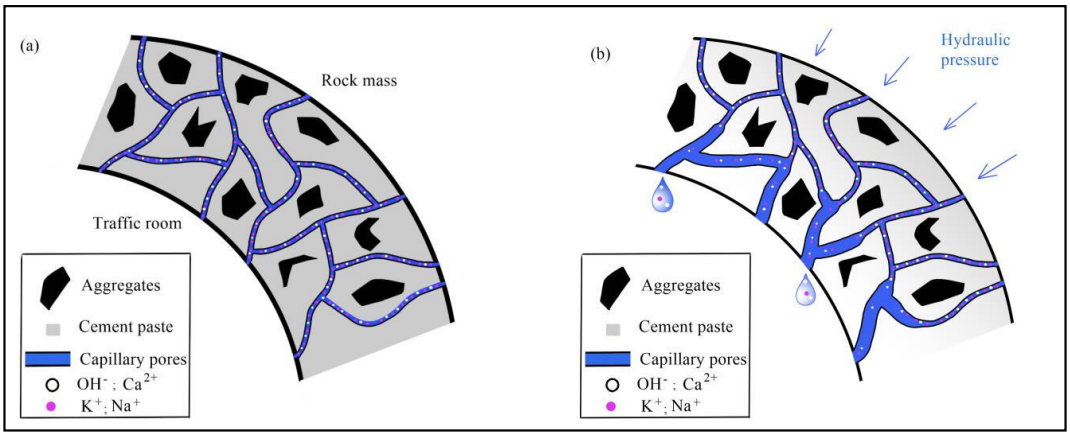


**Fig. 22:** Schematic representation of leaching in shotcrete caused by a unilateral hydraulic pressure triggered by groundwater. (a) Initial state of non-degraded shotcrete, and (b) leached shotcrete after some time exposed to a unilateral hydraulic pressure Modified from [76],[19].

In Fig. 22, steel fibers and gel/macro pores are not represented. Fig. 22b represents an increase in capillary pores, a reduction of alkali-metals and pH along with the decalcification of the cement paste propagating from the downstream end of the percolated water.

Apart from leaching by water permeation, the shotcrete surface exposed to the traffic room is the starting location of other degradation mechanisms such as carbonation, which also promotes a reduction in pH and decalcification. Furthermore, aggressive ions entering the shotcrete layer from its surface exposed to the traffic room may promote the dissolution of the cement paste. Sulfur-bearing compounds such as sulfur dioxide emitted by vehicles [77] or sulfates contained in saline groundwater are chemical elements that might exacerbate the shotcrete decalcification from this shotcrete location [78].

Chlorine present in de-icing salts used during winter or chlorides coming from saline groundwater might also promote the dissolution of the cement paste [79].

The interaction of the different degradation mechanisms just described is schematically represented in Fig. 23.

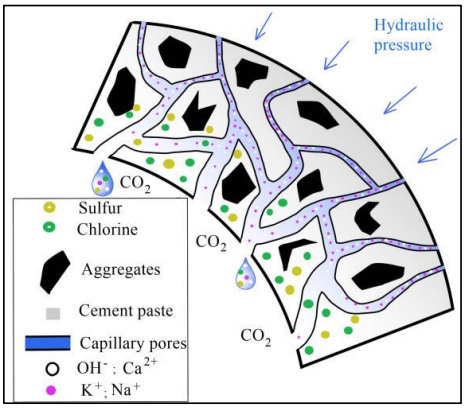


**Fig. 23:** Schematic representation of different mechanisms promoting leaching in steel fiber-reinforced shotcrete from the shotcrete surface exposed to the traffic room. Modified from [78].

### 2.5.3 Sulfate attack

In Norway, high concentrations of sulfate ions have been found in subsea tunnels and in tunnels excavated in alum-shale rock mass [80]. In groundwater seepage of subsea tunnels, concentration measurements have varied between 500 and 3,300 mg/l. In the case of tunnels excavated in alum-shale rock mass, the sulfate concentration measured has varied approximately between 500 and 2,000 mg/l [62]. These ranges overlap between slightly aggressive and highly aggressive chemical environments for concrete in the international standard EN 206:2013 [81].

The ingress of sulfur in hardened shotcrete might promote the formation of several minerals within the cement paste which might cause microstructural and mechanical damage [82]. The formation of gypsum, ettringite and thaumasite is described in this section along with the role of alkali-free accelerators as an additional source of sulfur to the cement paste.

#### *2.5.3.1 Gypsum formation*

The formation of solid secondary gypsum ($CaSO_4 \cdot 2H_2O$) can occur once external sulfate ions have entered the concrete, reacting with portlandite and water as shown in Eq. 10 [83].

$$SO_4^{2-} + Ca(OH)_2 + 2H_2O \rightarrow CaSO_4 \cdot 2H_2O + 2OH^- \quad (10)$$

There is volume expansion by the gypsum formation, but there are discrepancies in the literature regarding the destructive capacity of gypsum to the cement paste [82].

#### *2.5.3.2 Ettringite formation*

Ettringite formation ($3CaO \cdot Al_2O_3 \cdot 3CaSO_4 \cdot 32H_2O$) during the early age of hydration of cement is expected as gypsum is added to the clinker in order to prevent the fast hydration rate of the $C_3A$ phase. However, due to the depletion of sulfates in the process, most of the ettringite converts to monosulfate (AFm).

With the formation of secondary gypsum (Eq. 10), ettringite might form again from the AFm phase in the cement paste and water as shown in Eq. 11 [83]:

$$2 \cdot [CaSO_4 \cdot 2H_2O] + 4CaO \cdot Al_2O_3 \cdot SO_3 \cdot 12H_2O + 16H_2O \rightarrow 3CaO \cdot Al_2O_3 \cdot 3CaSO_4 \cdot 32H_2O \quad (11)$$

As with gypsum, ettringite formation might lead to swelling and possible shotcrete cracking.

#### *2.5.3.3 Thaumasite formation*

Sulfur compounds, carbonates and water are needed for thaumasite ($Ca_3Si \cdot OH_6 \cdot CO_3 \cdot SO_4 \cdot 12H_2O$) to form which interact with the C-S-H phase in the cement paste [75]. There is no consensus in the literature about the origin of the thaumasite formation [74]. One possible explanation is that it comes directly from ettringite, substituting $Al^{3+}$ by $Si^{4+}$ in the presence of carbonates. Other researchers postulate that thaumasite is the direct result of C-S-H reacting with sulfates and carbonates. There is consensus, nevertheless, that thaumasite is more favorable at low temperatures below 10 °C [82], which is usually the case of groundwater in the Nordic countries [68].

Once thaumasite is formed, it causes the concrete to crumble, i.e., losing the binding capacity of the cement [75].

#### *2.5.3.4 Internal sulfate attack: Alkali-free accelerator*

Alkali-free accelerators are widely used these days as admixtures in shotcrete to increase its early age hydration rate. In Norway, the use of alkali-free accelerators in shotcrete started in the 1990s as a technological change that allowed to spray concrete in thicker layers [19]. Alkali-free accelerators allowed faster tunnel excavations and the replacement in some cases of cast-in-place concrete linings. In addition, its low pH [84] reduces the risk of an alkali-silica reaction. When it comes to working safety, an alkali-free accelerator is desired rather than an alkali-rich accelerator, since the latter is caustic [85].

However, there are durability concerns on shotcrete when using the alkali-free accelerator in sulfate-bearing environments as its main component is aluminum sulfate [16]. A concrete with alkali-free accelerator is more susceptible to sulfate attack and has more AFm and ettringite than concrete without an alkali-free accelerator [86].

### 2.5.4 Magnesium attack

The presence of magnesium ions in groundwater might lead to brucite ($Mg(OH)_2$) and M-S-H formations as a replacement of portlandite and C-S-H respectively. M-S-H formation might be very aggressive leading to the total disintegration of the cement paste [74].

### 2.5.5 Corrosion of steel fibers

Uncoated steel fibers are protected by the alkaline environment given by the cement paste in the shotcrete. The reduction of the pH in the pore solution of the cement paste is a relevant factor that can foster the corrosion of the steel fibers [87]. Thus, degradation mechanisms such as carbonation, leaching and any other degradation that can lead to a pH reduction in the cement paste can promote corrosion.

Alike, chloride ingress into the shotcrete layer either from de-icing salts or saline groundwater might also lead to the corrosion of steel fibers. If the pH reduction in the pore solution of the cement paste interacts with chlorides, the corrosion kinetics are exacerbated [88].

The processes in which these factors affect steel fibers are in principle the same as in the corrosion of steel rebars used in rock bolts explained in Section 2.3. However, the anodic-cathodic surface area ratio between 3-4 cm long steel fibers and 4 m long steel rebars exposed to the same aggressive chemical element might be quite different. That is to say, exposed to an aggressive attack (in the anodic region), the cathodic surface area in the steel rebar will be significantly larger than that formed in a steel fiber, promoting a higher corrosion kinetics in the former. Additionally, it is claimed that there is a more homogeneous steel surface and more homogeneous fiber-matrix interface in the case of steel fibers in comparison with steel rebars [87].

## 2.6 Degradation kinetics in concrete

### 2.6.1 Carbonation

Once the carbon dioxide is dissolved in the pore solution of the cement paste, carbon dioxide will have to travel longer distances to reach the non-carbonated zone as carbonation progresses. Furthermore, to reach the carbonation front, carbon dioxide in the pore solution must diffuse through the carbonated area where calcite has already been formed, hindering the access of further carbon dioxide [89]. Thus, it is expected that the penetration of the carbonation front into the shotcrete layer slows down over time.

Experimental data has demonstrated that the carbonation depth $d$ measured from the concrete surface is proportional to the square root of time as shown in Eq. (12).

$$d = K \cdot \sqrt{t} \tag{12}$$

Some relevant variables affecting the proportionality factor $K$ are:

- Total porosity and pore size distribution of the concrete [73]
- Relative humidity and wetting and drying cycles [89]
- Temperature [89]
- Carbon dioxide concentration (higher in road tunnels) [56]

### 2.6.2 Leaching

The progress of the leaching front is governed by diffusion, suggesting that it is proportional to the square root of the time [90–92]. Eq. 13 shows this relation as follows:

$$x = a \cdot \sqrt{t} \tag{13}$$

Where $x$ is the leached depth in mm and $t$ is time in days. Some reference values for the proportionality factor $a$ are given as follows [90]:

- $a$ = 0.14 for a cement paste with a water-to-cement ratio equal to 0.4 exposed to deionized water with a pH equal to 7.
- $a$ = 2.0 for the same cement paste exposed to ammonium nitrate solution at 6 mol/l.

# Chapter 3

## 3 Field and laboratory results in steel fiber-reinforced shotcrete

This chapter is based on field and laboratory results from this PhD research.

### 3.1 Carbonation

Carbonation was systematically investigated with the pH indicator thymolphthalein. This pH indicator is sprayed on a fresh shotcrete surface to see if this surface becomes bluish or not. A bluish color is related to a pH of the concrete surface greater than 10.5. In turn, a pH value exceeding 10.5 in concrete is an indication of a non-carbonated zone.

The pH indicator results of different investigated locations exposed to fresh and saline groundwater are given in Fig. 24 and Fig. 25 respectively.

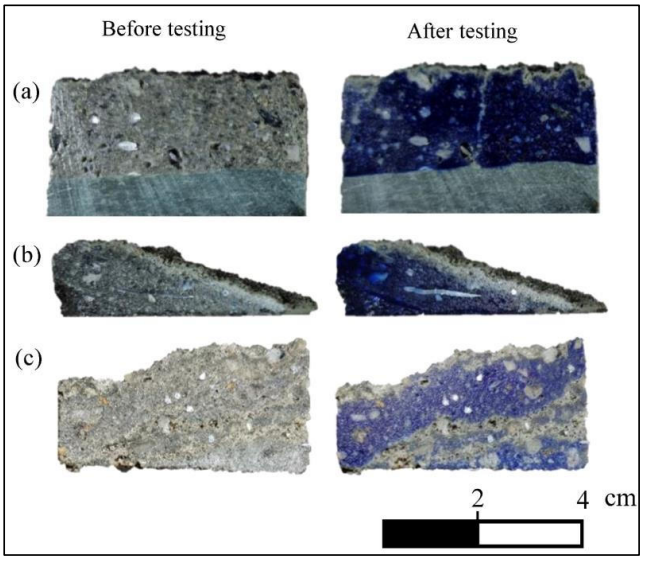


**Fig. 24:** Carbonation depth measured with pH indicator thymolphthalein in shotcrete exposed to fresh groundwater. (a) Hitra subsea road tunnel near the north portal, (b) Frøya subsea road tunnel near the north portal, and (c) Honningsvåg road tunnel at chainage 0+560.

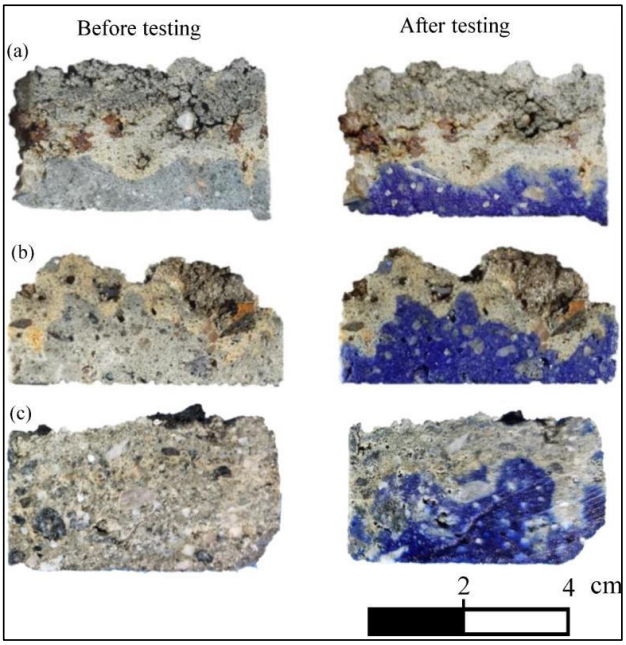


**Fig. 25:** Carbonation depth measured with pH indicator thymolphthalein in shotcrete exposed to saline groundwater. (a) Nordkapp subsea road tunnel at chainage 3+220, (b) Nordkapp subsea road tunnel at chainage 4+920, and (c) Hitra tunnel near the pump station.

The pH indicator results show that the carbonation depth is only a few mm when shotcrete is exposed to fresh groundwater, while in a saline environment the carbonation depth in shotcrete exceeds 1 cm. In the specific case of Fig. 25c, it suggests that a shotcrete joint lying close to the shotcrete surface was carbonated. Something similar was reported in Fig. 7, paper 3, where a shotcrete joint 7 cm away from the shotcrete surface was carbonated.

XRD analyses systematically found a higher content of calcite in the shotcrete sample exposed to the traffic room (see Fig. 15 in paper 2 and Fig. 12b and Fig. 13b in paper 3). In addition, the indication of carbonation by the pH indicator in shotcrete joints was always confirmed by a higher calcite content (see in paper 3, Fig. 12c with XRD analysis and Fig. 15b with TGA analysis).

Finally, carbonation was also identified in some cases by a local reduction in suction porosity compared to the trend values in the same core. See for example Figs. 20-23 in paper 2 [19].

## 3.2 Leaching

Figs. 26-27 provide real cases from the field of how serious leaching can be for the cement paste in shotcrete installed in subsea road tunnels. Leaching was observed in the Frøya tunnel at chainage 5+590 and in the Nordkapp tunnel at chainage 4+920.

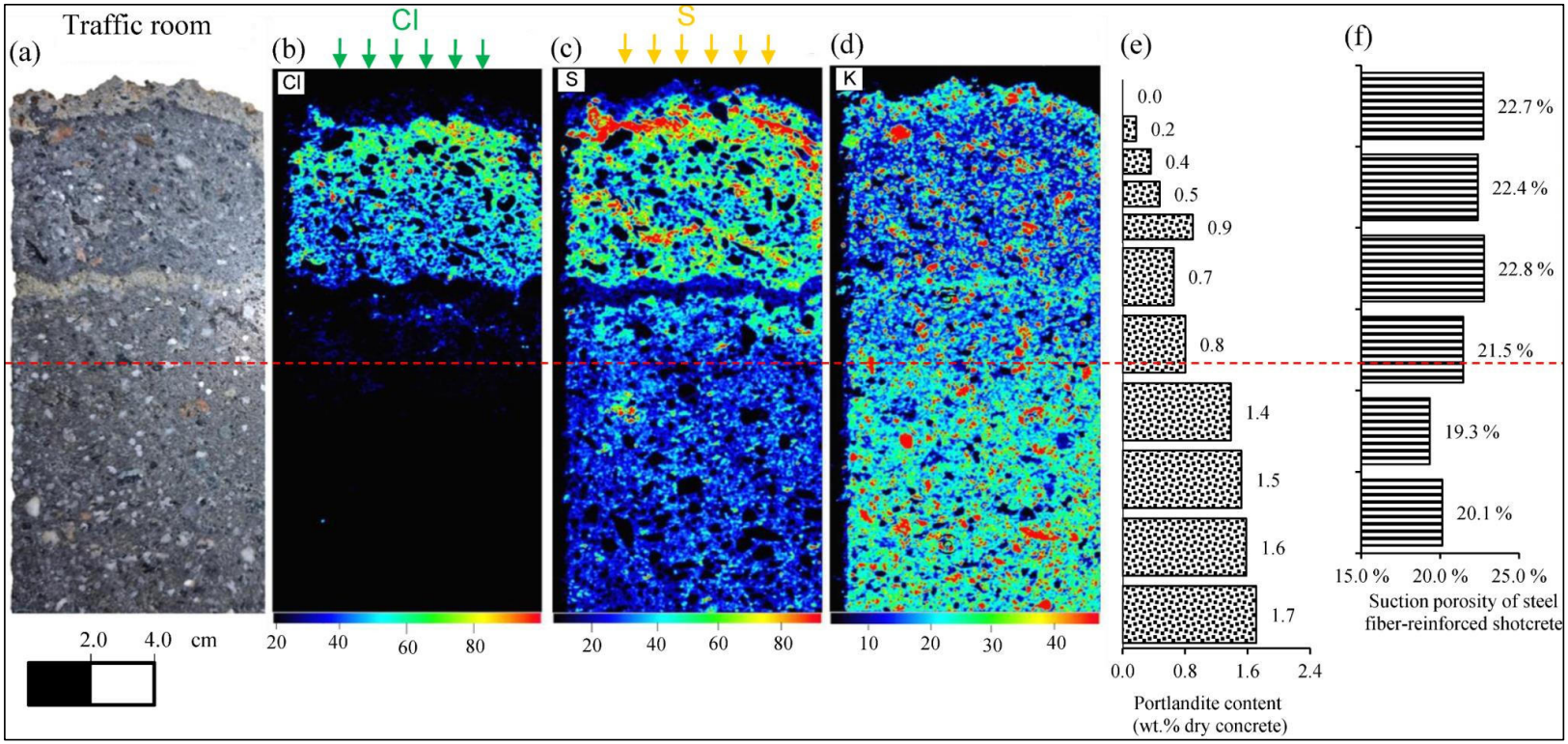


**Fig. 26:** Summary of investigations performed to estimate the leached depth and potential influential variables in the shotcrete layer near the traffic room in the Frøya tunnel at chainage 5+590. (a) One half of a shotcrete core split lengthwise, (b) chloride map via µ-XRF, (c) sulfur map via µ-XRF, (d) potassium map via µ-XRF, (e) portlandite content through TGA, and (f) suction porosity

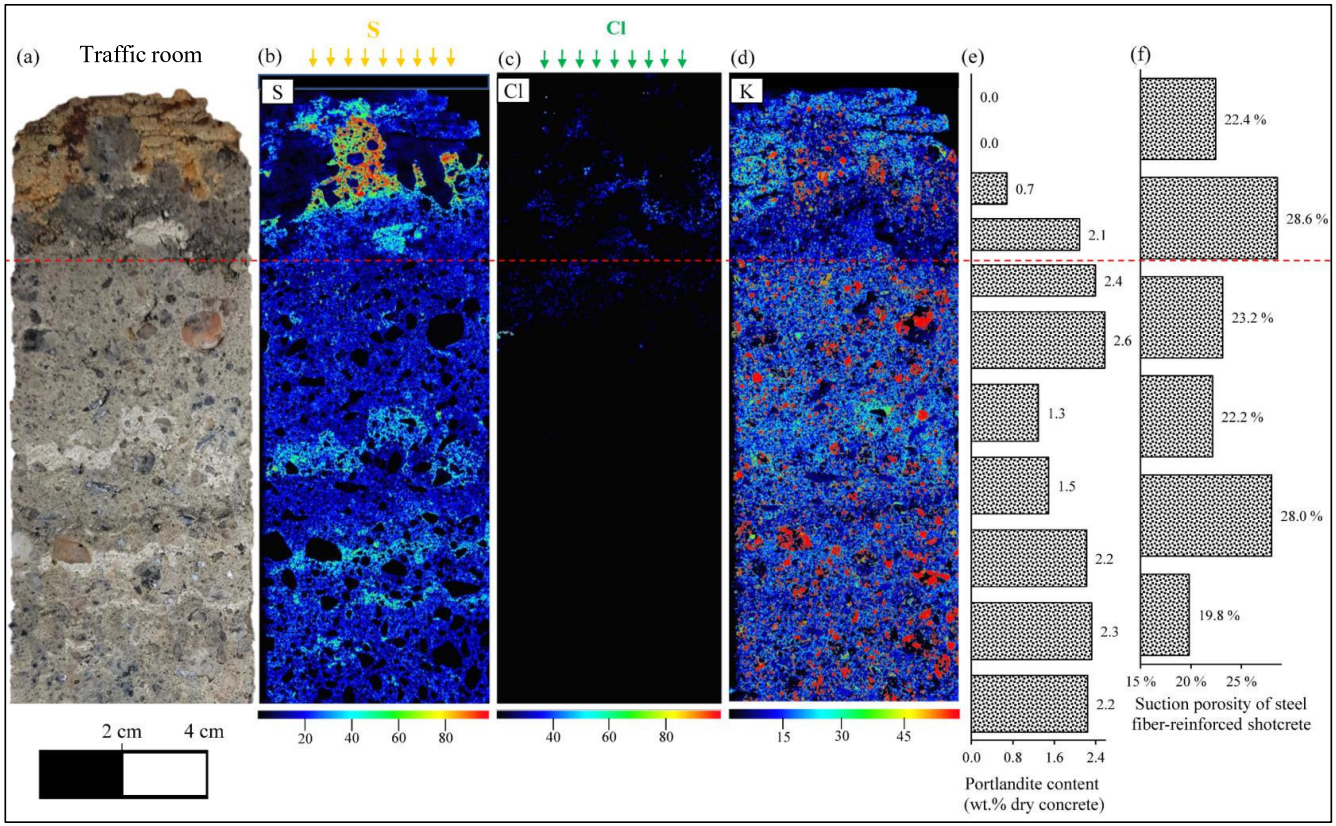


**Fig. 27:** Summary of investigations performed to estimate the leached depth and potential influential variables in the shotcrete layer near the traffic room in the Nordkapp tunnel at chainage 4+920. (a) One half of a shotcrete core split lengthwise, (b) sulfur map via μ-XRF, (c) chloride map via μ-XRF, (d) potassium map via μ-XRF, (e) portlandite content through TGA, and (f) suction porosity

In. Figs 26-27, the leached depth is assessed by considering the following observations:

- The portlandite content near the shotcrete surface is significantly reduced.
- The potassium content near the shotcrete surface is evidently lower than the rest of the shotcrete layer.
- There is no further penetration of chloride or sulfur from the shotcrete surface.
- There is an increase in suction porosity towards the traffic room.

Based on Fig. 26, the leaching front in the Frøya tunnel at chainage 5+590 lies approximately 90 mm away from the shotcrete surface after 22 years of exposure. On the other hand, the leaching front in the Nordkapp tunnel at chainage 4+920 is approximately 35 mm away from the shotcrete surface after 23 years of exposure (Fig. 27).

This degradation might cause mechanical strength reduction in the shotcrete towards the traffic room after 22-23 years of exposure. The mechanical strength loss towards the traffic room in the shotcrete installed in the Nordkapp tunnel shown in Fig. 16, paper 2, and the mechanical strength loss in the shotcrete installed in the Frøya tunnel shown in Fig. 23, paper 3 are repeated in Fig. 28 and Fig. 29 respectively in this thesis.

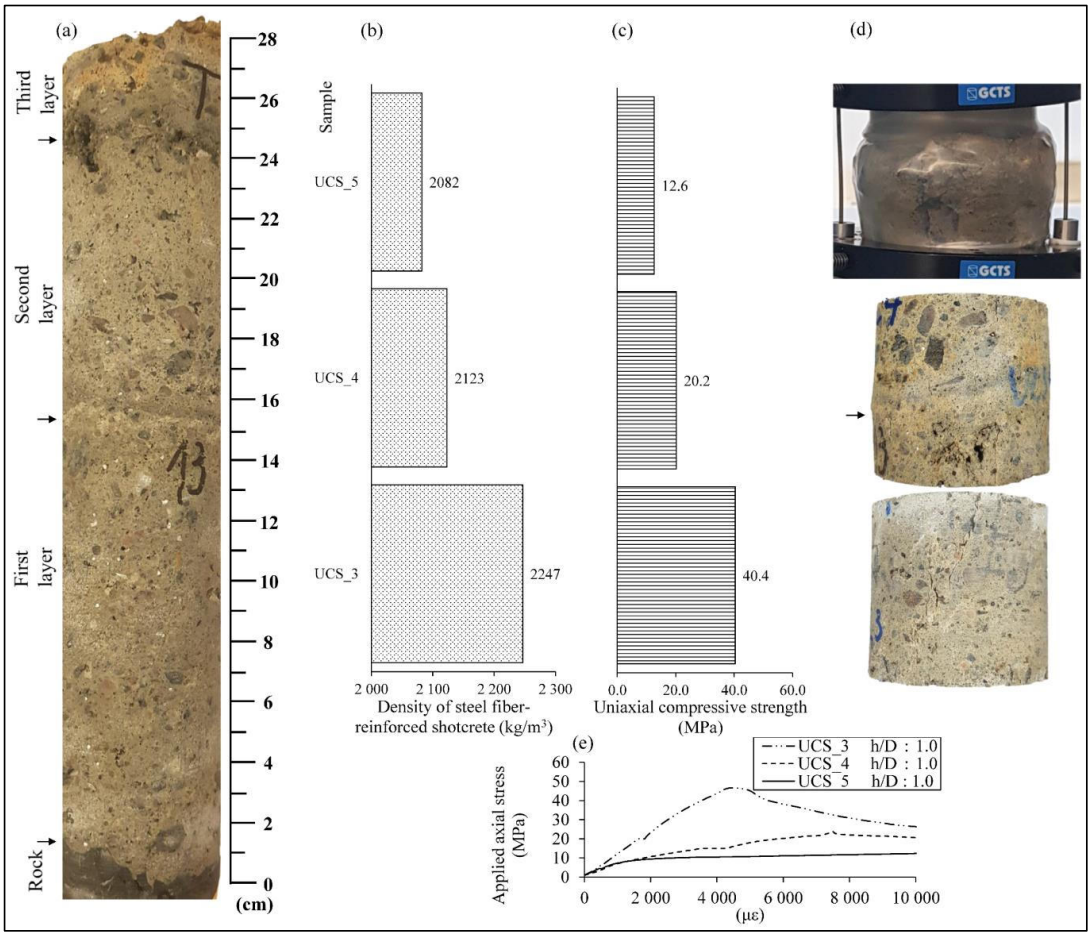


**Fig. 28:** Core 13 from the Nordkapp subsea road tunnel at chainage 4+920 where alkali-free accelerator was used: (a) Whole shotcrete core, (b) shotcrete density, (c) equivalent UCS test results for a h/D equal to 2.0, (d) shotcrete sample images after being tested for UCS strength, and (e) stress−strain curve.

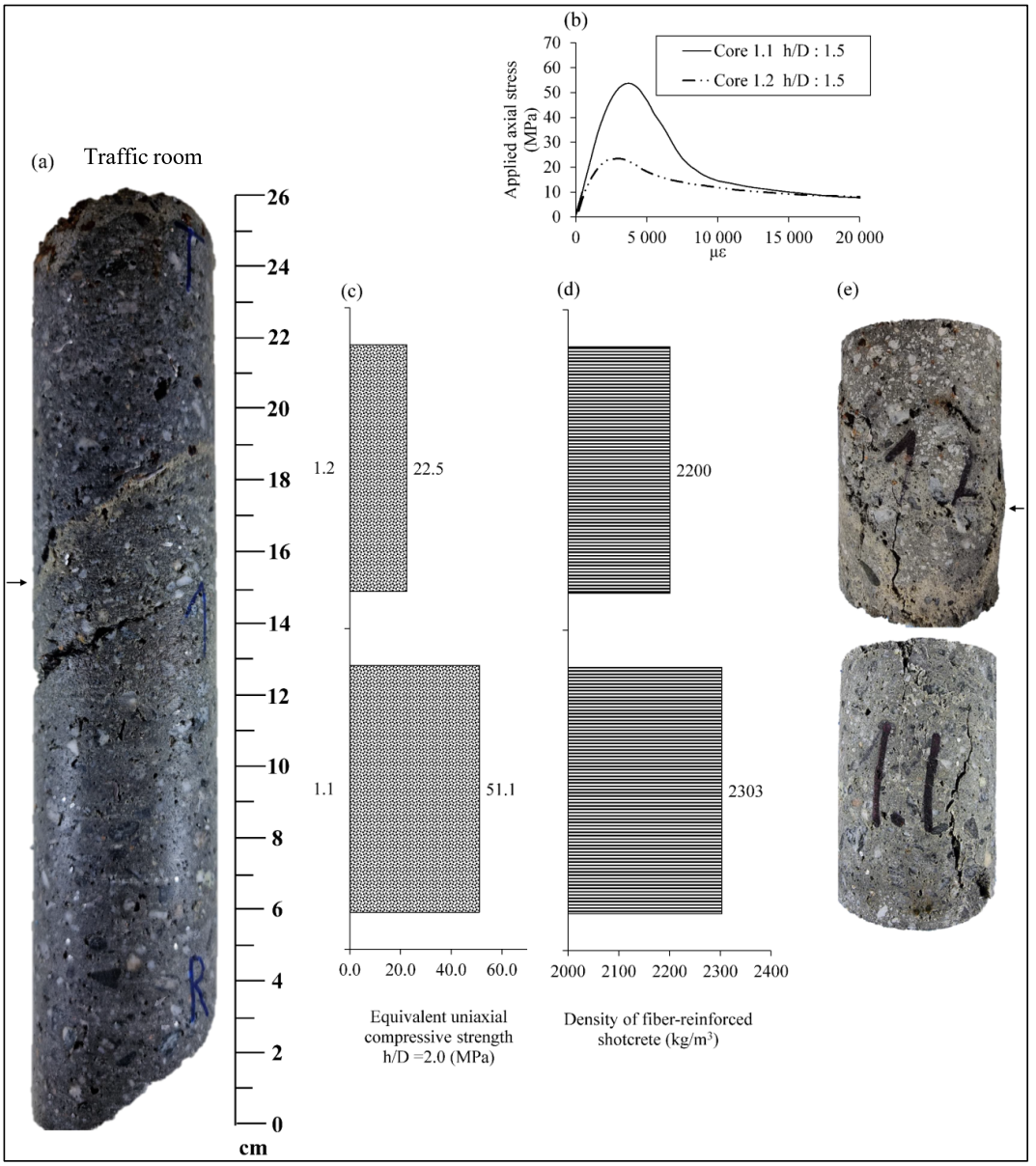


**Fig. 29:** Core 1 extracted from the Frøya subsea road tunnel at chainage 5+590 (approximately in the middle of the tunnel). (a) Shotcrete core, (b) stress-strain curve during UCS test, (c) equivalent uniaxial compressive test results for a h/D equal to 2.0 (d) shotcrete density results, and (e) shotcrete sample images after being tested for UCS strength.

Figs. 28-29 show evident compressive strength reduction and lower shotcrete density towards the traffic room. In addition, the stress-strain curves depict a completely different behavior depending on how far the UCS sample lies from the shotcrete surface. Finally, it is important to highlight that the shotcretes analyzed in Figs. 26-29 used alkali-free accelerators.

## 3.3 Sulfate attack

### 3.3.1 Gypsum

Sulfur-enrichment was found in several shotcrete cores extracted by μ-XRF mapping. In the specific case of the shotcrete installed in the Nordkapp tunnel, where alkali-free accelerator was used, μ-XRF detected higher sulfur concentrations near the shotcrete surface (Fig. 10b in paper 2 [19]). SEM/EDS is performed in that particular zone as an additional investigation technique to identify different chemical elements with a higher resolution than μ-XRF. The instrument used was the Hitachi S-3400 N. The selected sample was polished and cast in epoxy. Figs. 30-32 present the SEM/EDS results of elemental maps and point analyses in a shotcrete zone located approximately 2.0 cm away from the shotcrete surface.

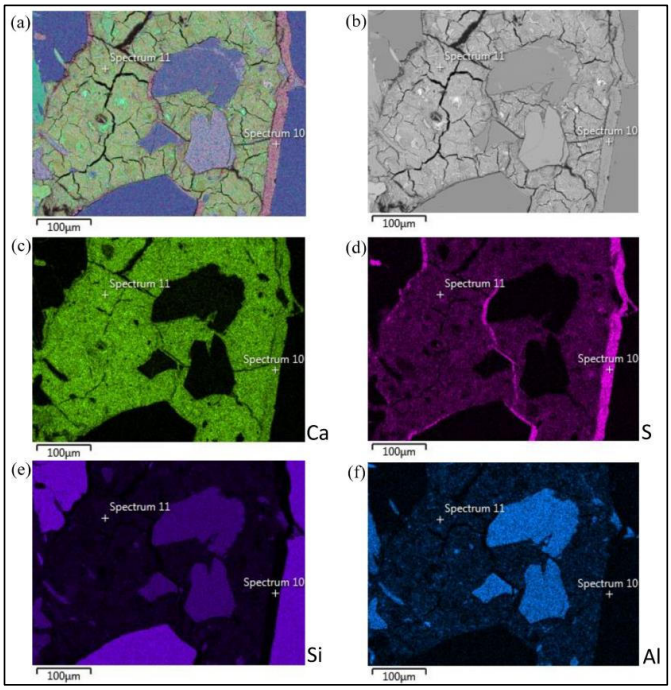


**Fig. 30:** Scanning electron microscopy (SEM) images of polished section taken from a shotcrete core extracted from the Nordkapp tunnel where alkali-free accelerator was used approximately 2 cm away from the shotcrete surface. (a) fused elemental map for several elements, (b) backscatter electron image, (c) calcium, (d) sulfur, (e) silicon, and (f) aluminum elemental map. Note that EDS spectra 10 and 11 are indicated in the figures.

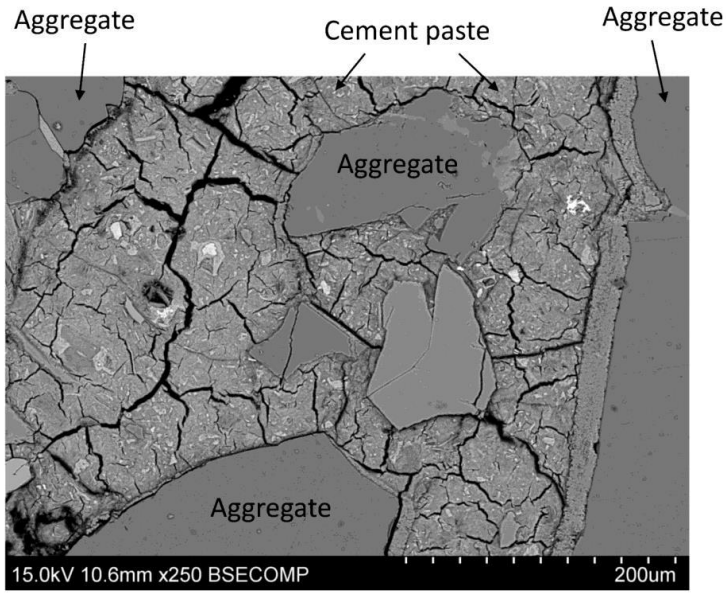


**Fig. 31:** Back-scattered electron (BSE) image obtained with SEM.

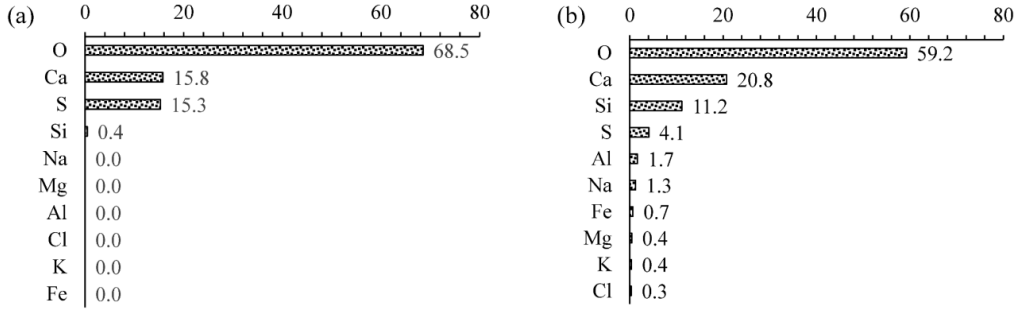


**Fig. 32:** Point analysis results in (a) atomic % for spectrum 10, and (b) atomic % for spectrum 11, both indicated in Fig. 30.

The elemental map of Ca usually represents the cement paste satisfactorily (shown in Fig. 30c). Fig. 30a and Fig. 30b reveal that the cement paste in the area has cracks all over. Fig. 30d illustrates sulfur-enrichment at the contact between the cement paste and the aggregates (at the interfacial transition zone, or in short ITZ).

Fig. 32a suggests that spectrum 10 detected gypsum, as the content of calcium and sulfur are similar, and the rest of the elements are barely present or not present at all. This implies that gypsum was formed at the ITZ.

Fig. 32b suggests that spectrum 11 detected an intermixing between decalcified C-S-H and thaumasite. It is very likely that the gypsum formation is responsible for the cracks in the cement paste shown in Fig. 31.

### 3.3.2 Ettringite formation

In paper 2 [19], ettringite enrichment was identified by μ-XRF and XRD analyses at the boundary of two adjacent shotcrete layers (shotcrete joints). Furthermore, a suction porosity sample containing one of these shotcrete joints showed macro-cracks after the drying and wetting cycle needed for the execution of the test (Sample 17 in Fig. 22, paper 2 [19]), suggesting that sulfate attack is latent due to ettringite enrichment.

### 3.3.3 Thaumasite formation

Thaumasite was found in this research in the Hitra subsea tunnel at the contact between the shotcrete layer and the rock. All the work performed in the Hitra tunnel has not been published. Fig. 33 shows a set of six shotcrete cores extracted very close to each other approximately in the middle of the Hitra tunnel (exposed to saline groundwater).

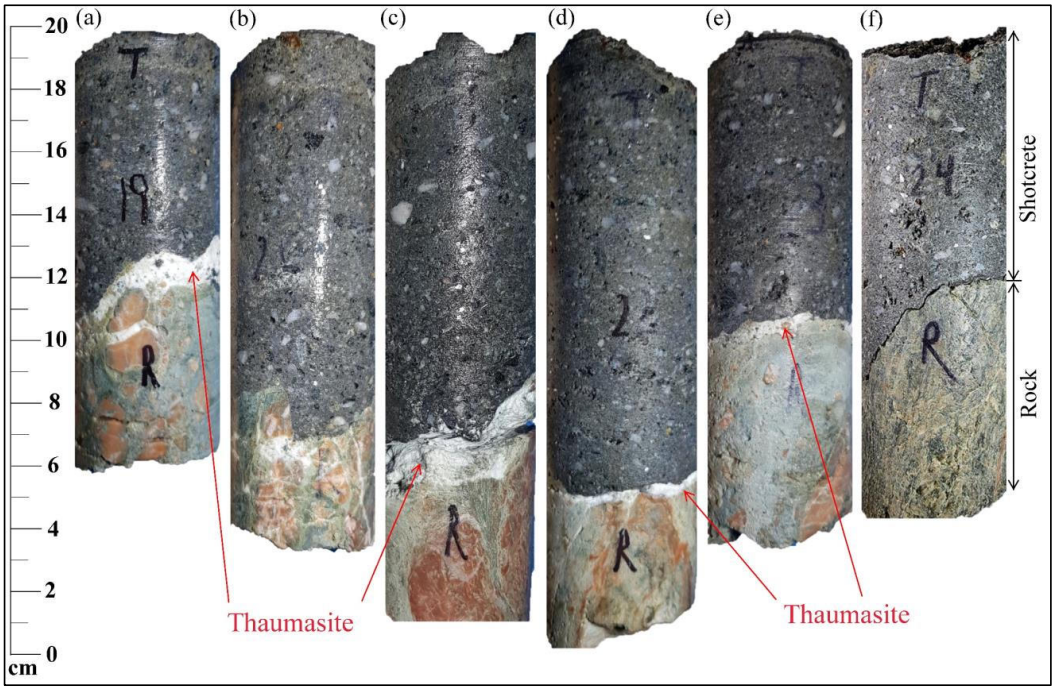


**Fig. 33:** Set of shotcrete cores of 55 mm in diameter extracted from the Hitra subsea tunnel at chainage 3+090 (approximately in the middle of the tunnel). From left to right: (a) Core 19, (b) core 20, (c) core 21, (d) core 22, (e) core 23, and (f) core 24.

Note in Fig. 33 that the "*white powder*" observed at the contact between shotcrete and rock is not seen in all the cores. Core 19, shown in Fig. 33a, was analyzed by µ-XRF. The results are given in Fig. 34.

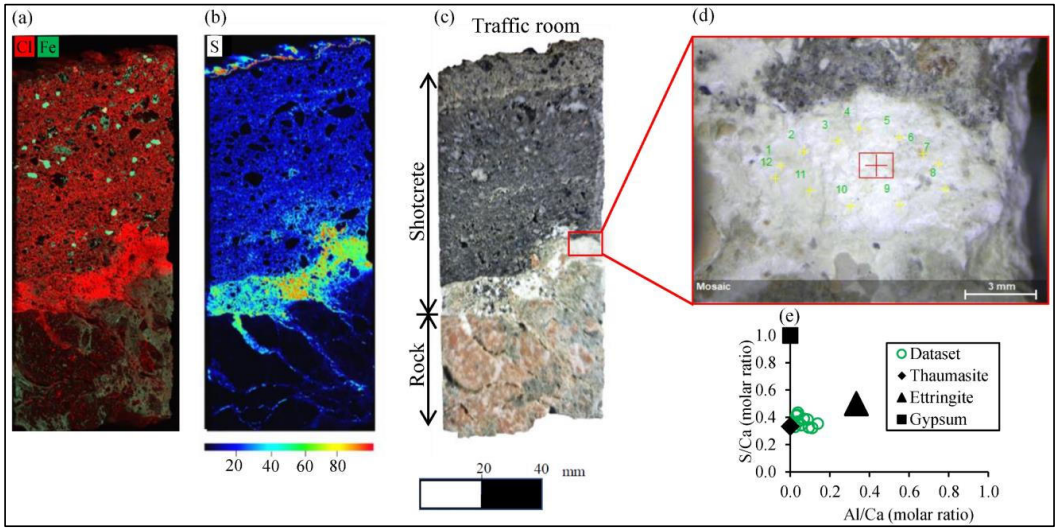


**Fig. 34:** µ-XRF results in shotcrete core 19 extracted from the Hitra subsea road tunnel at chainage 3+090. (a) Chlorine and iron maps along the core, (b) sulfur map along the core, (c) one half of the shotcrete core split lengthwise, (d) close-up image where 12 points were analyzed with µ-XRF, (e) atomic molar ratio analysis in points described in Fig. 34d.

Fig. 34b indicates that the white powder observed at the contact with the rock in Fig. 34c is rich in sulfur. In this zone, point analysis was also performed through µ-XRF. The results shown in Fig. 34e indicate that the atomic molar ratio between calcium, aluminum and sulfur of this white powder is very close to that of thaumasite.

XRD analysis was also performed in this white powder. The results obtained from core 21 (see Fig. 33c) are shown in Fig. 35.

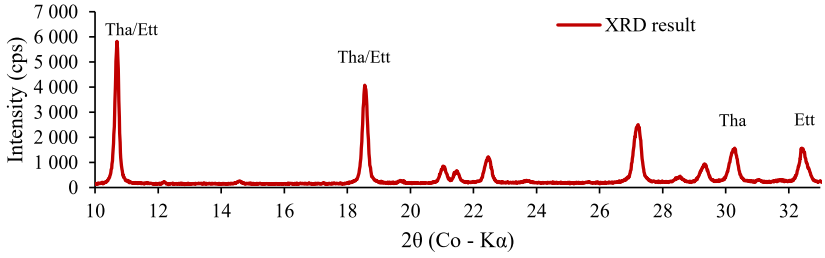


**Fig. 35:** XRD results in white powder observed at the contact between shotcrete and rock obtained from core 21 (shown in Fig. 33c). (Tha = *Thaumasite*; Ett = *Ettringite*).

Fig. 35 indicates that both thaumasite and ettringite are present in this white powder. The latter result does not contradict Fig.34e, where some point analyses actually contain some aluminum. Nevertheless, it is believed that thaumasite predominates because of the general absence of aluminum in this white powder as shown in Fig. 36.

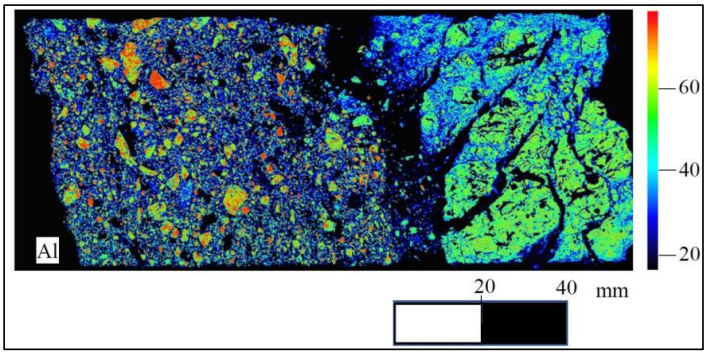


**Fig. 36:** Aluminum map through μ-XRF in core 19 (real image shown in Fig. 34c).

Figs 37 illustrates how serious this thaumasite attack can be for shotcrete.

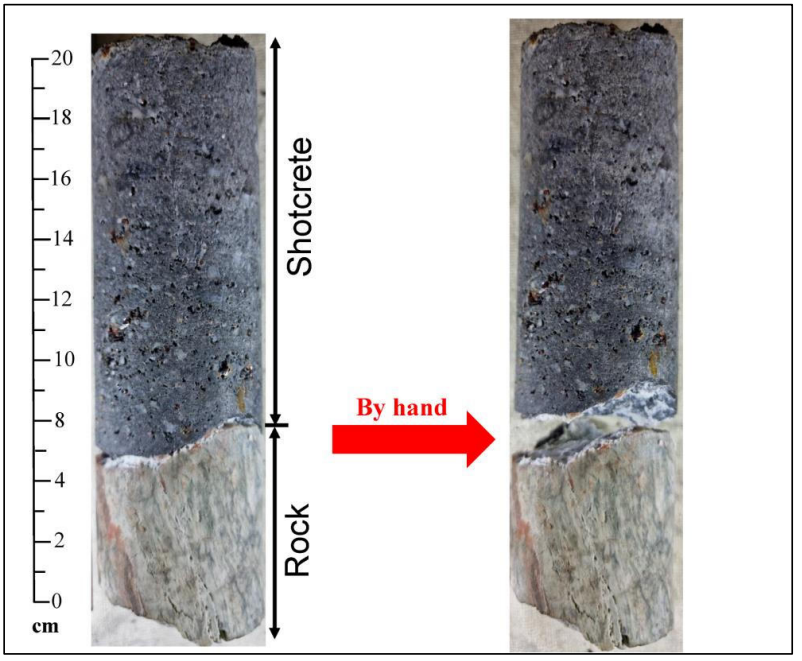


**Fig. 37:** Core 22 in the Hitra tunnel (also shown in Fig. 33d) split between rock and shotcrete by hand.

Fig. 37 indicates that when the thaumasite forms at the boundary between shotcrete and rock, the bond strength between them might become negligible.

Finally, the physical consequences of thaumasite attack are shown in Fig. 38.

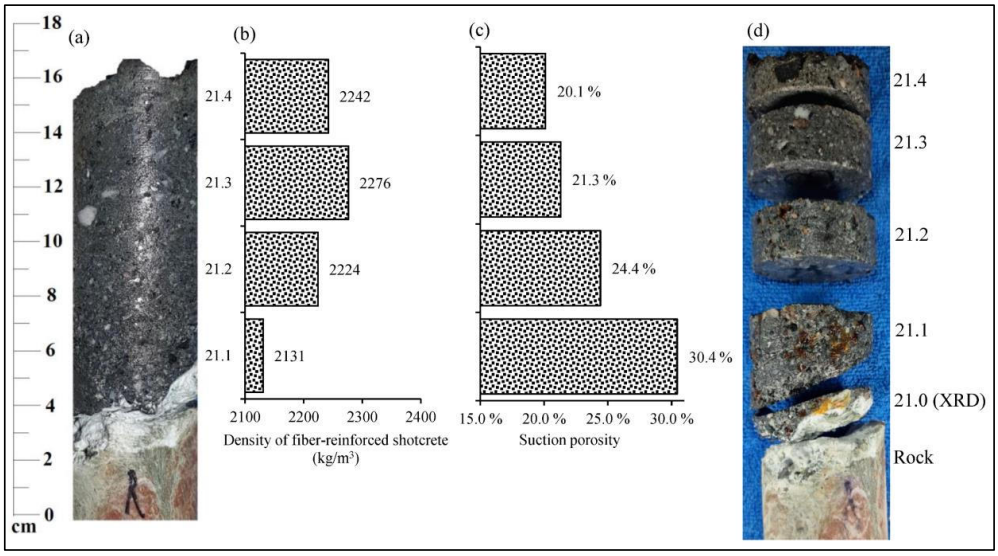


**Fig. 38:** Physical tests in core 21 where thaumasite attack was found at the contact with the rock extracted from the Hitra tunnel at chainage 3+090. (a) Core 21 (also shown in Fig. 33c), (b) shotcrete density, (c) suction porosity, (d) corresponding sample images. Note that the XRD result of sample 21.0 (shown in Fig. 38d) is given in Fig. 35.

Out of the 102 suction porosity tests carried in this research in 4 different tunnels, the sample 21.1 (Fig. 38c) adjacent to thaumasite sulfate attack gave the highest value equal to 30.4%.

## 3.4 Magnesium attack

Magnesium enrichment was found in the Nordkapp and Frøya subsea tunnels in connection with sulfur enrichment. However, the sulfur and magnesium enrichments areas do not overlap. In one case, magnesium was found in the carbonation zone of the shotcrete layer approximately 1 cm away from the shotcrete surface exposed to the traffic room. This was found in the Nordkapp tunnel and the results are available in paper 2 [19]. In the other case, magnesium enrichment was found in a shotcrete joint in the Frøya tunnel. Fig. 39 shows the three shotcrete cores extracted in the Frøya tunnel.

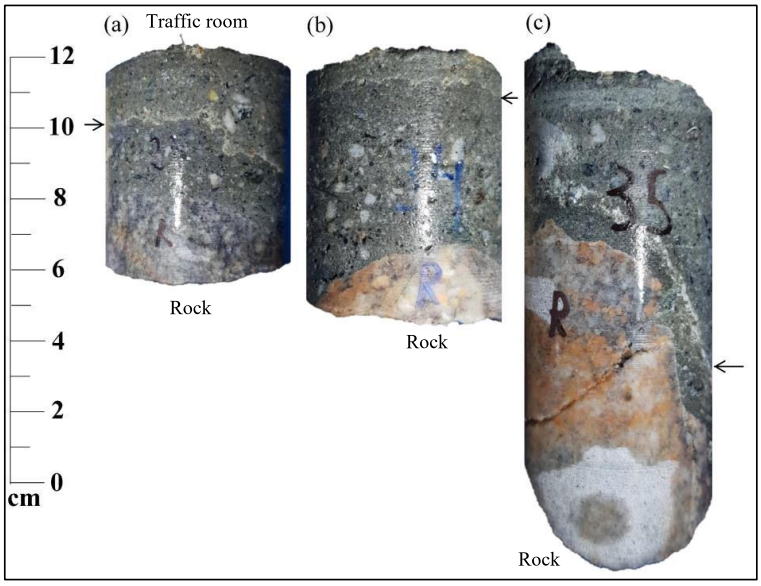


**Fig, 39:** Shotcrete cores extracted in the Frøya tunnel exposed to saline groundwater at chainage 5+480. (a) Core 33, (b) core 34, and (c) core 35.

Fig. 39 shows some white stains in the shotcrete layer highlighted with arrows. In core 35, shown in Fig. 39c, μ-XRF analysis was performed. Results are given in Fig. 40.

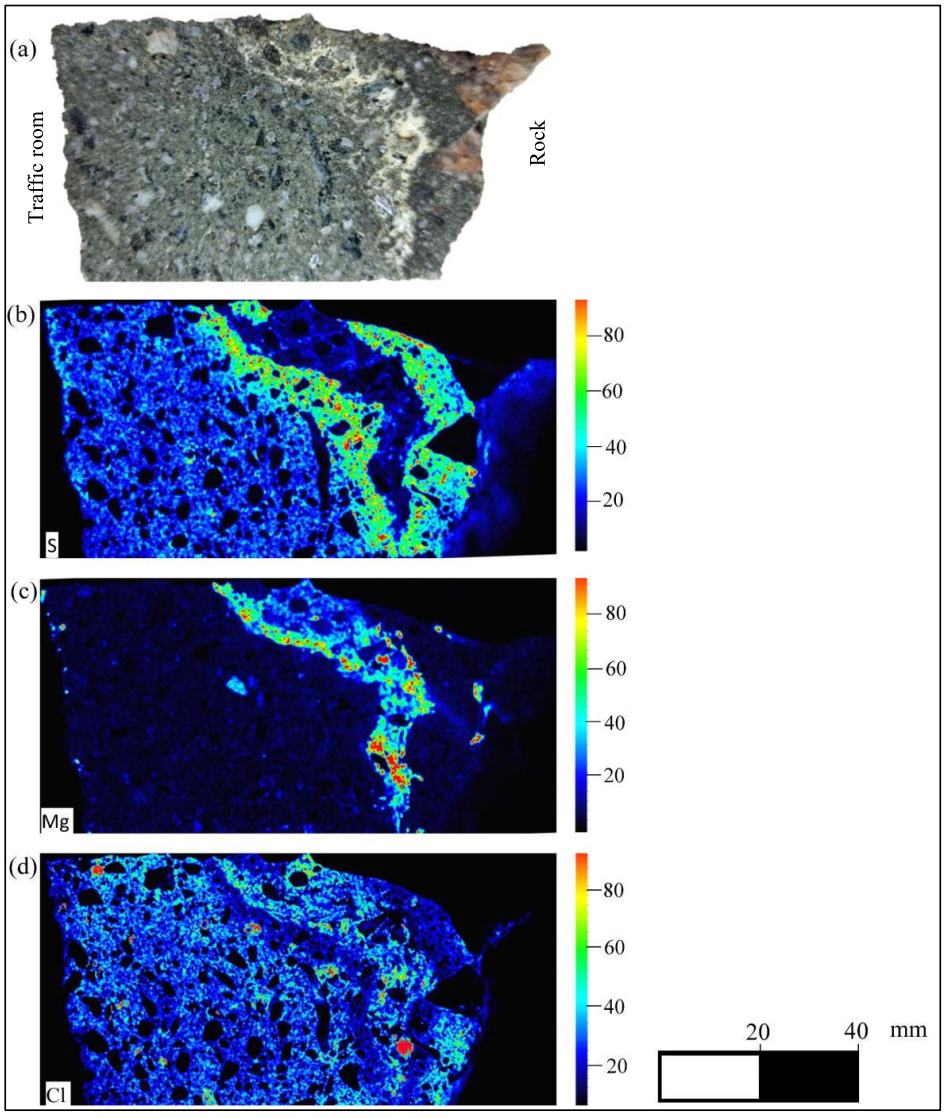


**Fig. 40:** μ-XRF results in core 35 extracted from the Frøya tunnel at chainage 5+480 exposed to saline groundwater. (a) One half of the shotcrete core split lengthwise, (b) sulfur map, (c) magnesium map, and (d) chloride map.

Fig. 40c clearly shows that the white stains observed in the shotcrete joints in Fig. 40a is rich in magnesium. Adjacent to this zone, there is a sulfur-rich zone. The severity of these white stains rich in magnesium was quantified in terms of density and suction porosity. The results are given in Fig. 41.

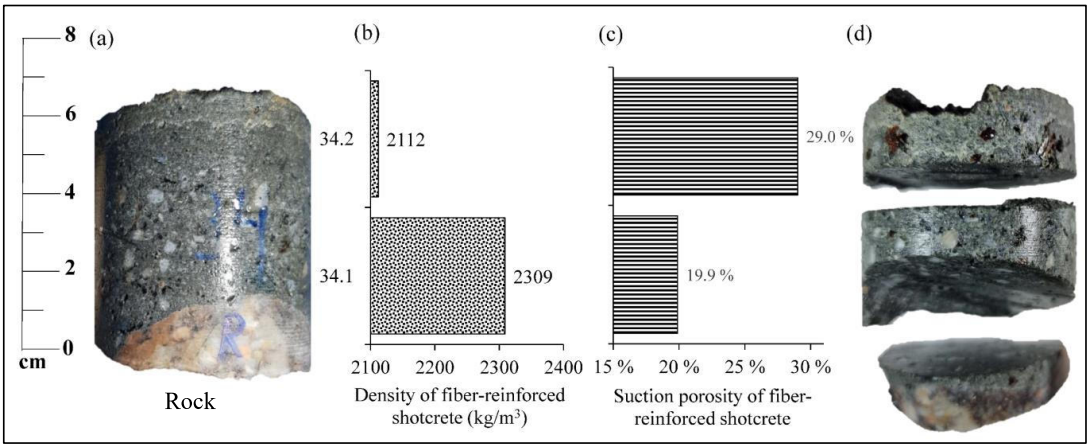


**Fig. 41:** Core 34 obtained from the Frøya tunnel at chainage 5+480. (a) Whole shotcrete core (also shown in Fig. 39b), (b) density of steel fiber-reinforced shotcrete, (c) suction porosity results, and (d) picture of samples holding shotcrete joints at the end of suction porosity test.

As shown in Fig. 41, the magnesium attack is quite serious, with a sudden reduction in shotcrete density and a significant increase of suction porosity.

## 3.5 Corrosion of steel fibers

In Fig. 11 of paper 2 [19], it was shown that the corrosion of steel fibers is limited to the carbonation depth. In the non-carbonated zone of the shotcrete, visible corrosion has not been observed despite of high chloride content in some shotcrete cores extracted from subsea tunnels.

# Chapter 4

## 4 Prognosis of degradation kinetics in steel fiber-reinforced shotcrete used in Norwegian road tunnels

### 4.1 Carbonation

Fig. 42 presents a summary of the carbonation depth measurements performed in the four tunnels inspected in this research. The carbonation depth measurements were obtained from the pH indicator results.

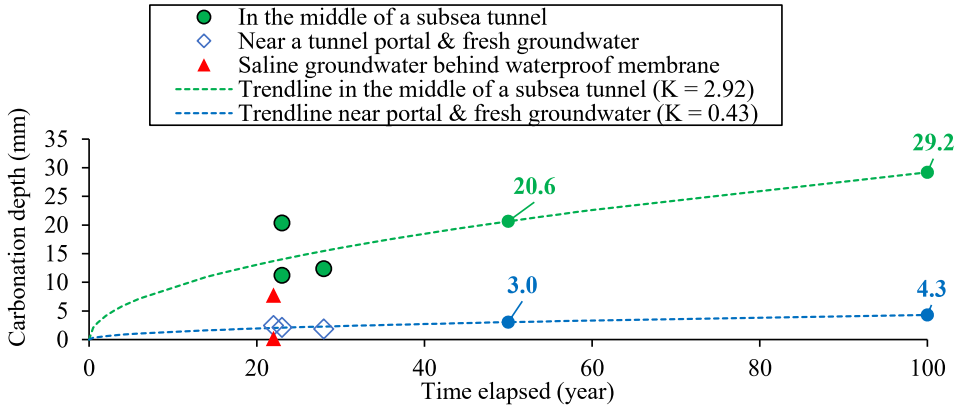


**Fig. 42:** Carbonation rate prognosis in Norwegian road tunnels

Fig. 42 represents the carbonation rate observed in the middle of subsea tunnels by green circles. These dots from the Nordkapp and Hitra tunnels present the highest carbonation depths. The corresponding proportionality factor $K_1$ (described in Eq. 12) obtained from the least squares method is 2.92. The average carbonation depth forecast after 50 years of exposure is 20.6 mm, and after 100 years of exposure is 29.2 mm.

Significantly lower carbonation depths were measured in shotcrete exposed to fresh groundwater in the Frøya, Hitra and Honningsvåg tunnels shown in blue rhombuses. This research did not perform long-term atmospheric measurements in the tunnels. However, the impression of a better visibility available and the fresh air near the portals compared to the case in the middle of the tunnels strongly suggest a different pollution level between them. The corresponding proportionality factor $K_2$ in this case is 0.43. The average carbonation depth forecast after 50 years of exposure is 3.0 mm, and for 100 years is 4.3 mm.

With regard to carbonation depth results in the middle of the Frøya tunnel, where a waterproof membrane was installed between the road users and the rock support (see paper 3, Fig 4), the results are dissimilar. Nevertheless, the two results available are always lower than carbonation depths in other subsea tunnels without the waterproof membrane. The high relative humidity created by the waterproof membrane in front of the rock support surface [93] is probably the reason why a faster carbonation rate in the Frøya tunnel is prevented.

Based on the obtained proportionality factors ($K_1$ $and$ $K_2$) below 6 mm /$\sqrt{year}$ for carbonation, the shotcrete samples studied for carbonation in this research are considered of good quality with a low porosity according to [56].

## 4.2 Corrosion of steel fibers

The conclusion in Section 3.5 is that corrosion of steel fibers is limited to the carbonation depth. Thus, it is inferred that the corrosion of steel fibers will follow the same corrosion kinetics as carbonation.

## 4.3 Leaching interacting with carbonation, chlorides and sulfur ingress

Based on the observations described in Section 3.2, a prognosis is shown in Fig. 43 for 50 and 100 years of exposure time in the investigated locations where leaching was identified.

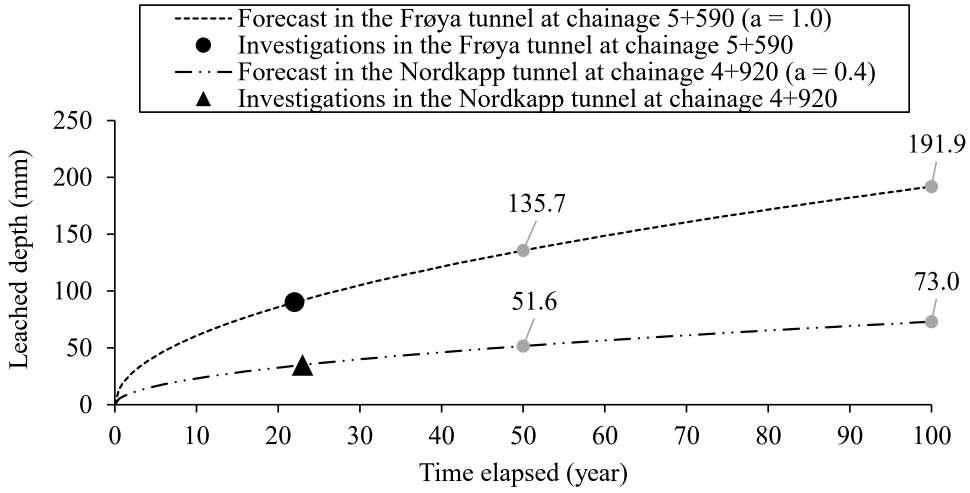


**Fig. 43:** Leached depth forecast in the Frøya tunnel at chainage 5+590 and in the Nordkapp tunnel at chainage 4+920 based on investigation results after 22 and 23 years respectively.

As depicted from Fig. 43, the equivalent proportionality factor $a$ (described in Eq. 13) for the shotcrete in the Frøya tunnel is 1.0, while for the shotcrete in the Nordkapp tunnel this is 0.4. These proportionality factors exceed the value mentioned in Section 2.6.2 equal to 0.14 for the cement paste with a low water-cement ratio (0.4) exposed to deionized water.

The difference in leaching observed between the Frøya and the Nordkapp tunnels does not seem obvious. In principle, these two tunnels had similar shotcrete specifications, the investigated locations in the tunnels had similar elevations below sea level, and the shotcrete surface from where drilling started was wet in both cases. One possible explanation could be the traffic density and the pollution involved. The traffic density is ten times higher in the Frøya tunnel than in the Nordkapp tunnel [94]. Another possible difference foreseen is that in the Frøya tunnel, the core drillings were performed just next to a concrete lining stretch where probably a weakness zone lay nearby. This fact increases the likelihood of a higher hydraulic gradient in the shotcrete layer as weakness zones facilitates the hydraulic pathway towards the traffic room [95].

## 4.4 Sulfate and magnesium attack

Sulfate and magnesium attack was randomly observed in singularities of the shotcrete core. That is to say, at the boundary of two adjacent shotcrete layers (shotcrete joints) and at the contact with the rock. Even though a prognosis about the degradation in the future is not performed in these cases, some suggestions are given in Section 5.7 to control and prevent these degradations from occurring.

# Chapter 5

## 5 Discussion

### 5.1 Sampling for UCS tests in shotcrete used as rock support

In paper 2 [19], the influence of shorter shotcrete samples than the traditional h/D of 2.0 for UCS tests was discussed. Specifically, the main conclusion from Fig. 25 [19] is that the traditional h/D equal to 2.0 only averages the UCS results without indicating a different trend in comparison to samples with a h/D equal to 1.0. On the other hand, samples with a h/D equal to 1.0 provide more sensitive results in case of local degradation with the possibility of having several UCS samples along the same shotcrete core. In addition, it is important to emphasize that a sample for a UCS test needs flat surfaces at both ends to be performed. This requirement wastes shotcrete material at both ends of the shotcrete core, allowing UCS tests to be performed only in thick shotcrete layers. In summary, with shorter UCS samples, there is more flexibility to perform UCS tests in shotcrete. In the just-mentioned Fig. 25 (paper 2), the sample diameter was in all cases in the order of 55 mm, being the shotcrete samples from the Nordkapp and Honningsvåg tunnels.

In the specific case of the Frøya and Hitra tunnels, some shotcrete cores were obtained from a larger core bit diameter of 92 mm in order to see if the results were sensitive to a change in diameter. The resulting shotcrete core diameter was approximately 84 mm. Fig. 44 presents the results of 19 UCS tests, where six of them were performed with the larger diameter of 84 mm.

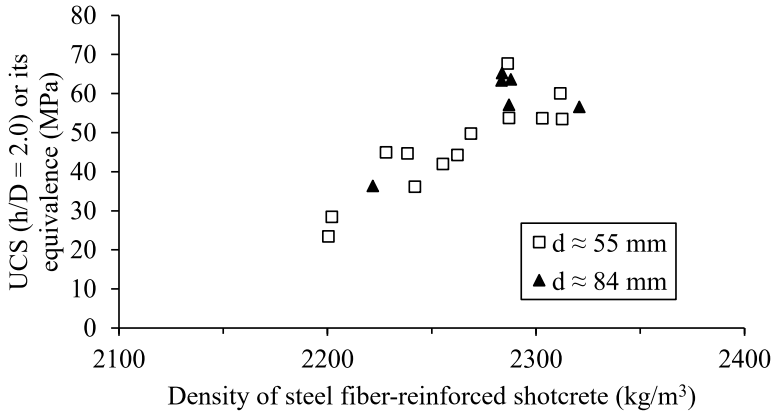


**Fig. 44:** UCS strength results over density in steel fiber-reinforced shotcrete installed in the Hitra and Frøya tunnels. A distinction is made between cylindrical concrete samples of 55 and 84 mm in diameter.

Fig. 44 indicates that differences in diameter between 55 mm and 84 mm of cylindrical shotcrete samples make no difference in UCS test results.

## 5.2 The role of alkali-free accelerator in shotcrete

In this research, the two subsea tunnels inspected where alkali-free accelerator was used in the shotcrete (Nordkapp and Frøya) showed noticeable leaching in the outermost 3.5-9 cm of the shotcrete layer towards the traffic room with evident mechanical strength loss (Figs. 26-29).

On the other hand, this research only found minor or no indications of leaching towards the traffic room when water-glass accelerator was used in shotcrete exposed to saline groundwater. Specifically, 16 shotcrete cores extracted from the Hitra subsea tunnel and 6 cores extracted from the Nordkapp subsea tunnel showed little or no leaching levels when water-glass accelerator was used. The results obtained in this research suggest that the sulfur contained in the alkali-free accelerator may be a factor promoting the leaching.

When alkali-free accelerators are used, it is expected that more ettringite will be present and evenly distributed in the shotcrete [96]. However, ettringite enrichment was identified at the boundary of two adjacent shotcrete layers (shotcrete joints). Coincidently or not, this noticeably happened in shotcrete where an alkali-free accelerator was used.

## 5.3 Sulfur dioxide emitted by vehicles as an additional source of sulfur

Sulfates in saline groundwater and aluminum sulfates in alkali-free accelerators have already been described in the literature. Less attention has been paid on the potential role of sulfur dioxide emitted by vehicles.

It is interesting to highlight that most of the cores analyzed in this research through μ-XRF near the shotcrete surface exposed to the traffic room gave some degree of sulfur ingress from the traffic room with a decay in content further into the shotcrete layer. In subsea tunnels, the sulfur ingress from the traffic room could be explained by seepage of groundwater that crosses the shotcrete layer through an easier pathway at a high point in the tunnel. Once on the shotcrete surface, the groundwater runs off by gravity. What is interesting in this research is the sulfur content in the shotcrete layer was also observed near the traffic room in shotcrete exposed to fresh groundwater. Fig. 45 gives two examples where the shotcrete was exposed to fresh groundwater and experienced sulfur ingress from the traffic room.

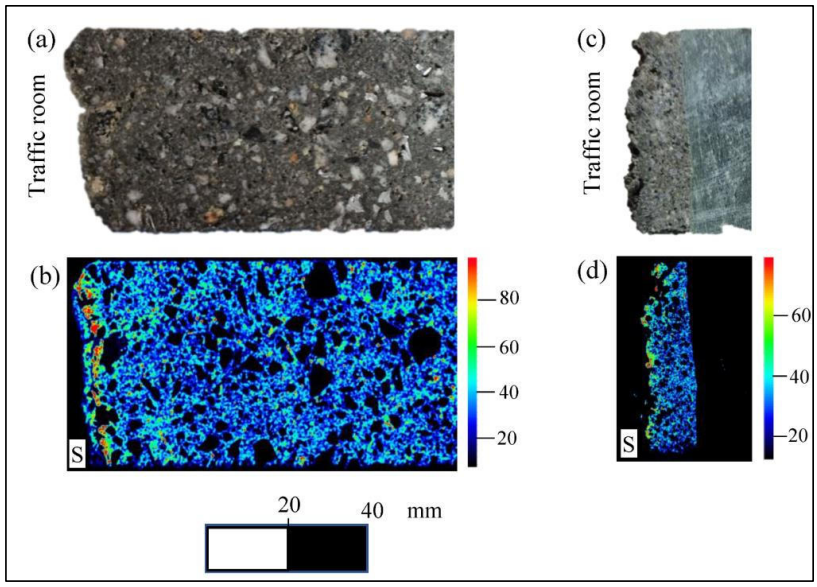


**Fig. 45:** Sulfur ingress in the shotcrete layer from the traffic room in a tunnel location exposed to fresh groundwater. (a) One half of the shotcrete core split lengthwise in the Frøya tunnel near the north portal, (b) sulfur map through μ-XRF related to Fig. 45a, (c) one half of the shotcrete core split lengthwise in the Hitra tunnel near north-west portal, and (d) sulfur map through μ-XRF related to Fig. 45c.

Fig. 45b and Fig. 45d show a higher intensity of sulfur near the traffic room (at the far left of the sulfur map). It is evident from these figures that the penetration depth of sulfur is not significant, but the result might be influenced by the probably low atmospheric pollution near the tunnel portals.

## 5.4 Corrosion of steel fibers in shotcrete installed in subsea tunnels

With regard to the corrosion of steel fibers in shotcrete, this research reinforces the literature stating that their corrosion is limited to the carbonation depth.

## 5.5 Alkali-silica reaction

Alkali silica reaction was not investigated in this research. This degradation is caused by reactive silica in aggregates with alkalis in the pore solution of cement paste [97]. This reaction will form an alkali-silica gel that can swell if water is present, eventually cracking the concrete. Then, the content of alkalis in the cement paste, the alkalinity of the pore fluid and the relative humidity (availability of water) play an important role in the long-term risk for alkali silica reaction. Previous field investigations in Norwegian road tunnels concluded that this degradation mechanism has not been a serious one [62,80]. One possible factor is the systematic use of silica fume in sprayed concrete for more than 40 years in Norway (see Fig. 11), reducing the pH in the pore solution, and therefore, reducing the risk of alkali-silica reaction. Another possible explanation is the limited maximum aggregate size used in shotcrete to prevent blockage of the hose and nozzle during spraying and

reduce the rebound rate loss after spraying, not exceeding 16 mm in diameter in the 1980's and 1990s [18,22]. As the expansion of the alkali-silica gel is proportional to the initial volume size of the aggregate, it implies that the smaller the aggregate, the more restricted is the expansion.

In the only case where SEM/EDS was performed in this research in the Nordkapp tunnel, the aggregates did not appear to be cracked.

## 5.6 Durability enhancement in rock bolts

The major tool to extend the lifespan of rock bolts is to prevent water seepage. A list of possible problems related to the flow of groundwater are, among others, the following:

- Wash-out the cement mortar during its plastic stage, leaving voids once it has hardened.
- Bring permanently aggressive ions to the rock bolts.
- Remove corrosion products on the steel surface or hot-dip galvanizing surface.
- Reduce the epoxy coating thickness
- Reduce the electrical resistivity of the epoxy coating

A water inflow of 300 l/min/km has traditionally been the limit in Norwegian subsea tunnels. This threshold value aims to minimize the cost of grouting during construction and pumping out the water during operation [98]. However, to the best of my knowledge the durability of rock support has not been considered in this assessment. In urban areas, systematic pre-grouting works ahead of the tunnel face have been performed to achieve water inflows lower than 100 l/min/km [99]. Thus, it seems feasible to further reduce the water inflow in the tunnels for the sake of rock support durability.

## 5.7 Durability enhancement in steel fiber-reinforced shotcrete

### 5.7.1 Prevent shotcrete joints

Shotcrete joints are a weakness zone in the shotcrete layer. Furthermore, they are more susceptible to chemical attack. Along the different shotcrete cores investigated, the following conditions/degradations were observed in shotcrete joints:

- Carbonation (Fig. 7 in paper 3)
- Magnesium attack (Fig. 40 in this thesis)
- Ettringite enrichment (Fig. 10b in paper 2 [19], probably causing sulfate attack)
- Highest suction porosity and lowest shotcrete density in the core (Figs. 21-23 in paper 2 [19])

Even in shotcrete exposed to fresh groundwater, shotcrete joints affect locally the physical properties and mechanical behavior of the shotcrete layer. Figs. 46-47 show physical and mechanical results from the Honningsvåg tunnel.

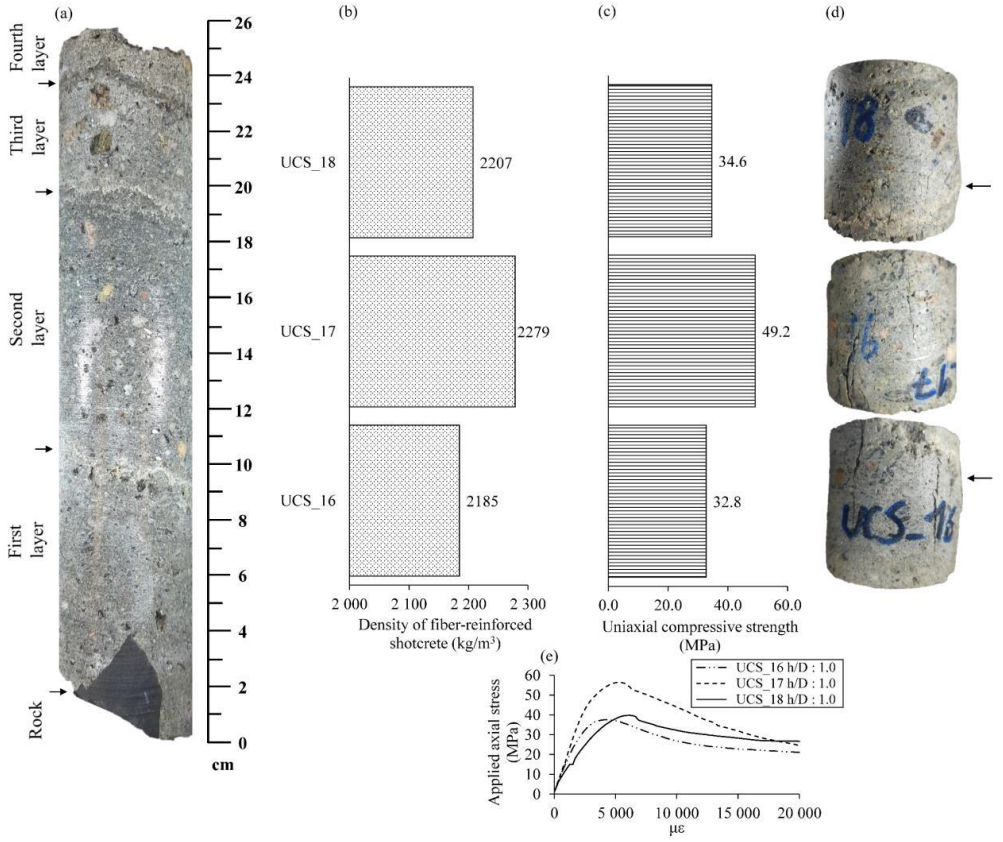


**Fig. 46:** Core obtained from the Honningsvåg road tunnel at chainage 0+560 exposed to fresh groundwater: (a) Whole shotcrete core, (b) shotcrete density, (c) equivalent uniaxial compressive test results (height-to-diameter ratio = 2.0), (d) shotcrete sample images after being tested, and (e) stress-strain curve.

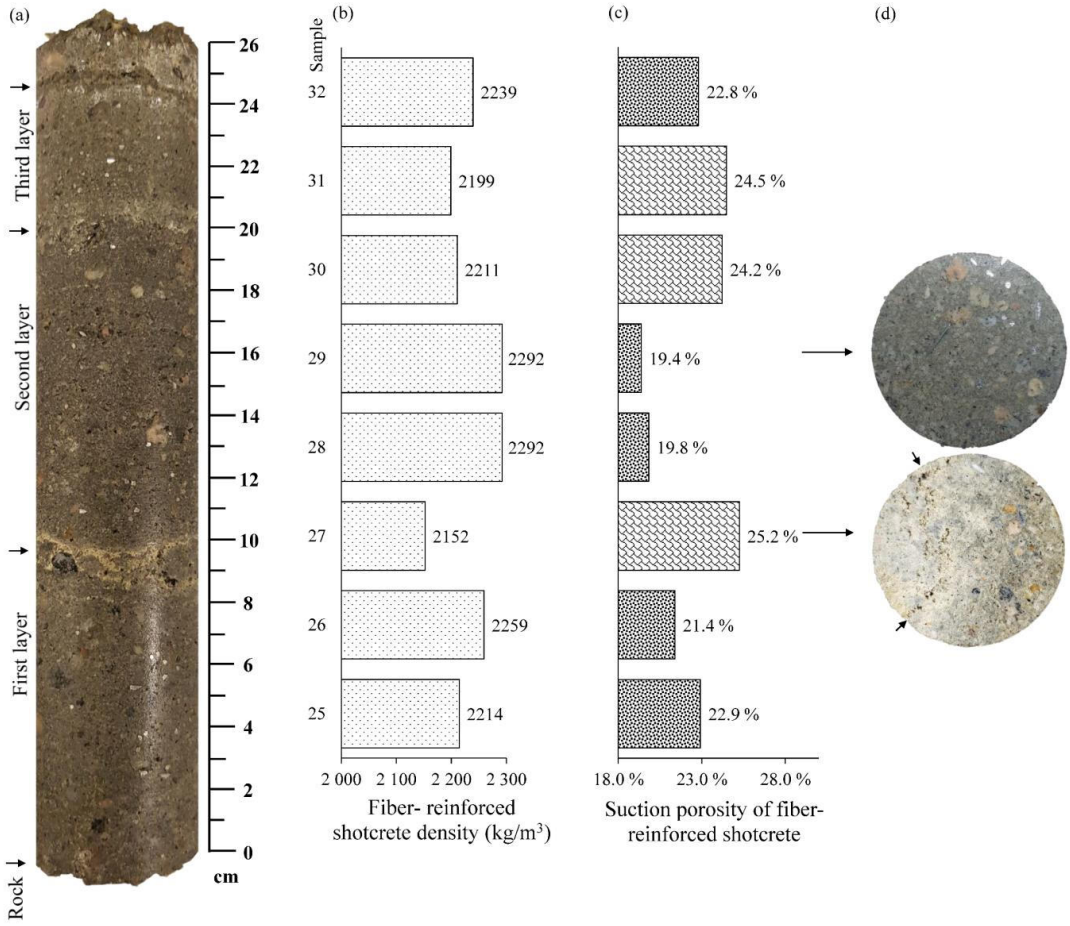


**Fig. 47:** Core obtained from the Honningsvåg tunnel at chainage 0+560 (neighboring core to the one shown in Fig. 46): (a) Whole shotcrete core, (b) shotcrete density, (c) suction porosity results, and (d) picture of the samples with the most extreme porosity values in the core.

Fig. 46 shows a reduction in compressive strength when a shotcrete joint is present in the sample. Fig. 47 shows an increase in suction porosity and a reduction in shotcrete density for those samples holding a shotcrete joint.

Nevertheless, it is not envisaged serious degradation in shotcrete joints when the shotcrete is exposed to fresh groundwater.

Whenever possible, spraying shotcrete in consecutive layers should always be prevented. Current regulations in Norwegian road tunnels state a minimum shotcrete thickness of 8 cm. Based on what was observed, it seems reasonable that this thickness is achieved in one operation.

### 5.7.2 Quality control in shotcrete near the contact with the rock

Regarding the weakness zone of the shotcrete layer at the contact with the rock, it is interesting to highlight Fig. 34, where thaumasite was formed. This mineral needs external sulfates and carbonates entering the shotcrete to form, and coincidently the suction porosity near the rock in this case was extremely high (Fig. 38c).

In saline groundwater, μ-XRF allows to visualize the eventual chloride ingress in the shotcrete layer from the rock side. Fig. 48 compares the eventual chloride ingress in the shotcrete layer from the rock side with suction porosity near the rock.

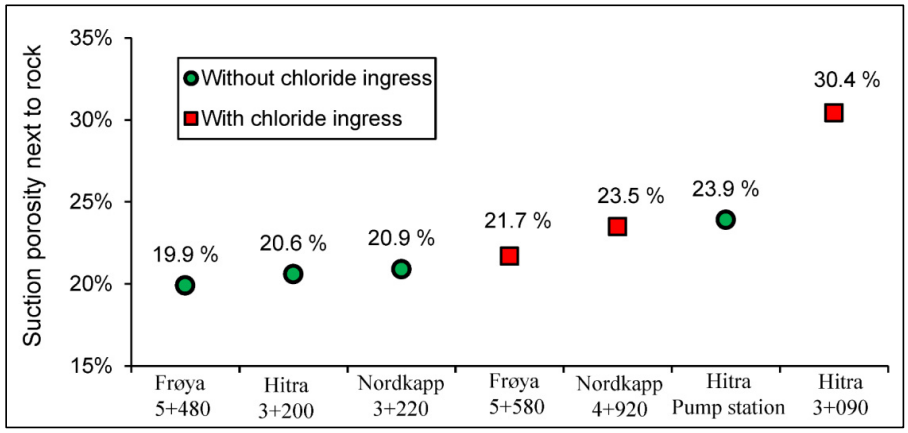


**Fig. 48:** Occurrence of chloride ingress in the shotcrete layer from the rock compared to shotcrete suction porosity near the rock in seven different locations lying in the three subsea tunnels inspected.

Fig. 48 shows in general that lower suction porosity values near the rock prevent chloride ingress in the shotcrete layer, while higher suction porosities do not prevent this ingress. However, there is a result from the shotcrete installed near the pump station in the Hitra tunnel, where the shotcrete suction porosity was relatively high and there was no chloride ingress. Figs. 49-51 show further results from this location.

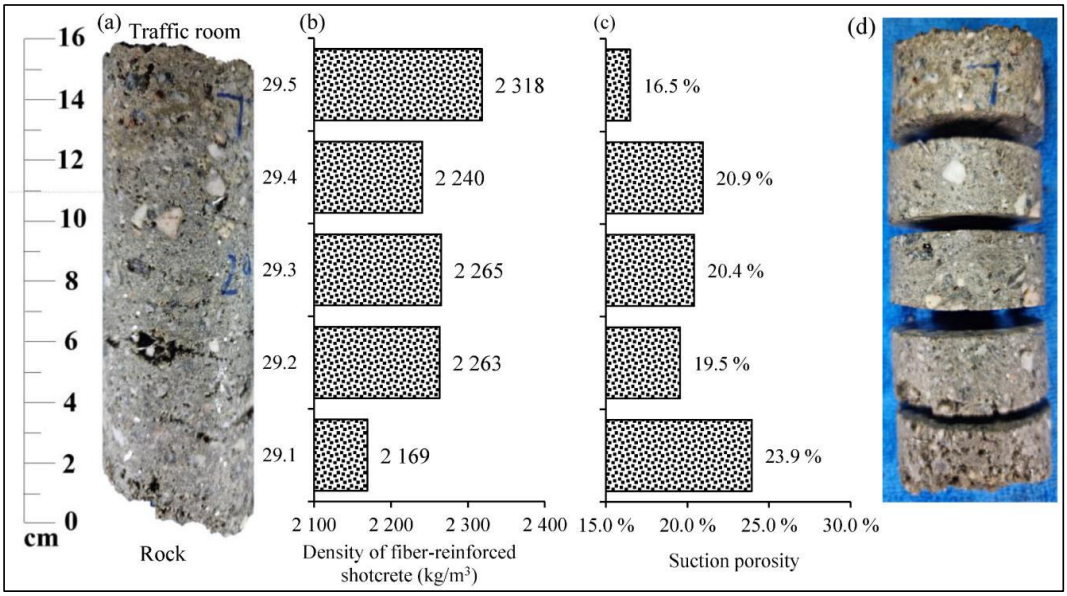


**Fig. 49:** Physical tests in core extracted near the pump station in the Hitra tunnel. (a) Real image of the Core, (b) shotcrete density profile, (c) suction porosity profile, and (d) corresponding sample images.

In Fig. 49, the closest sample to the rock (sample 29.1), gave a high local suction porosity and a low shotcrete density. A closer look at this sample is given in Fig. 50


**Fig. 50:** Bottom of sample 29.1 shown in Fig. 49 facing to the rock

Fig. 50 shows a porous shotcrete. It is important to highlight that sample 29.1 is a local case of high suction porosity and low density in the core. A possible explanation for this condition could be that when shotcrete is sprayed in the tunnel from top to bottom, rebound shotcrete from a higher point in the tunnel might fall onto exposed rock, turning into debris when shotcrete is sprayed on top [100].

On the other hand, Fig. 51 shows chemical results obtained from μ-XRF analysis performed in a neighboring core to the one shown in Fig. 49.

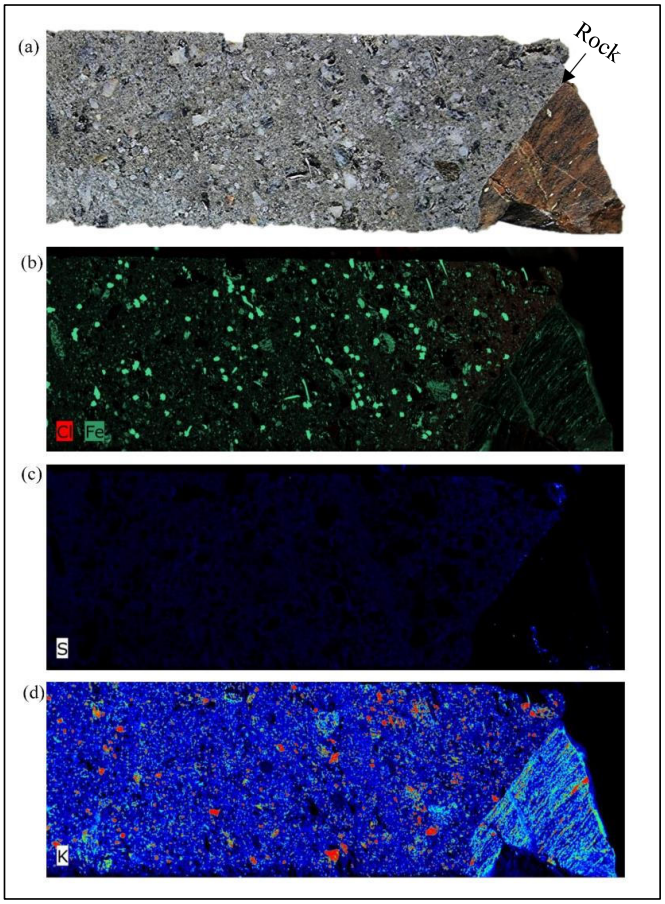


**Fig. 51:** μ-XRF results in a core extracted from the pump station in the Hitra tunnel. (a) Real image of the core, (b) chlorine and iron maps, (c) sulfur map, and (d) potassium map.

Fig. 51b and Fig. 51c show no chlorine and sulfur ingress respectively in the shotcrete layer from the rock side. Note as well that sulfur or chlorine elements are not visualized coming from rock discontinuities as shown in Fig. 34 for example. Fig. 51 emphasizes that the permeability of the rock mass can prevent aggressive groundwater from reaching the shotcrete layer.

Thus, Fig. 48 appears to provide consistent results and the limit for chloride ingress will only occur if the suction porosity of the shotcrete exceeds approximately 21%.

The back-up results in Fig. 48 from the Nordkapp tunnel are given in paper 2 [19]. The results in the Hitra tunnel at chainage 3+090 are given in Fig. 34a and Fig. 38c. The rest of the back-up results are given in Figs. 52-56.

In one of the cores extracted from Hitra tunnel at chainage 3+200, μ-XRF analysis was performed. The results are shown in Fig. 52.

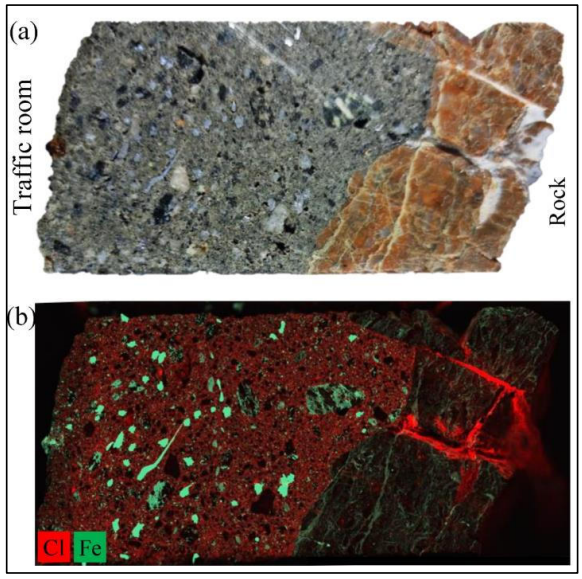


**Fig. 52:** μ-XRF result in core extracted from the Hitra tunnel at chainage 3+200. (a) Real image, and (b) chlorine and iron maps.

The interpretation from Fig. 52 is that there is no chloride ingress from the rock side, despite of the attack from the rock discontinuities. In Fig. 53, a profile of suction porosity and shotcrete density were performed in a core also extracted from the Hitra tunnel at chainage 3+200.

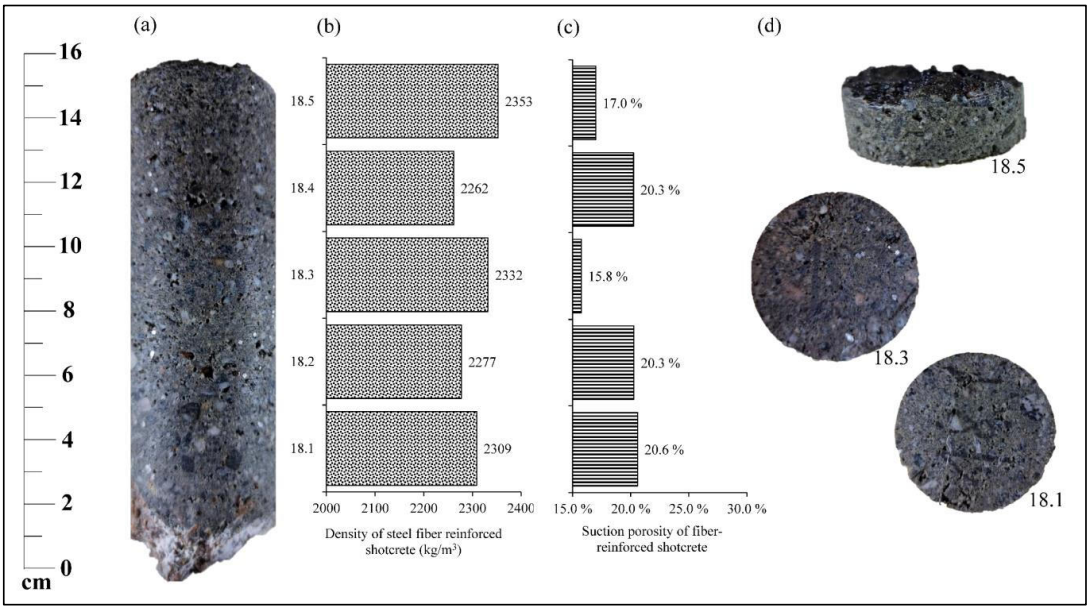


**Fig. 53:** Physical tests in a core extracted from the Hitra tunnel at chainage 3+200. (a) Real image of the core, (b) shotcrete density profile, (c) suction porosity profile, and (d) some of the sample images.

In the core shown in Fig. 53, the shotcrete suction porosity is general low, and near the rock is 20.6%.

In one of the cores extracted in the Frøya tunnel at chainage 5+580, μ-XRF analysis was performed. The results are shown in Fig. 54.

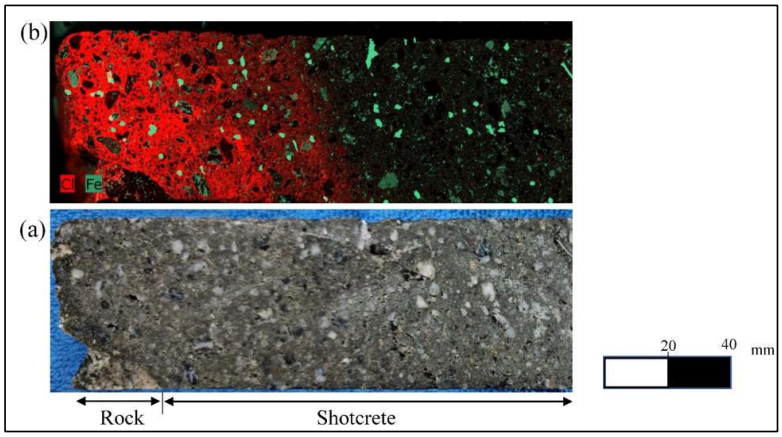


**Fig. 54:** μ-XRF result in core extracted from the Frøya tunnel at chainage 5+580. (a) Real image, and (b) chlorine and iron maps.

The interpretation from Fig. 54b is that there is chloride ingress from the rock side in about 6 cm. In Fig. 55, a profile of suction porosity and shotcrete density were performed in a core next to the one shown in Fig. 54.

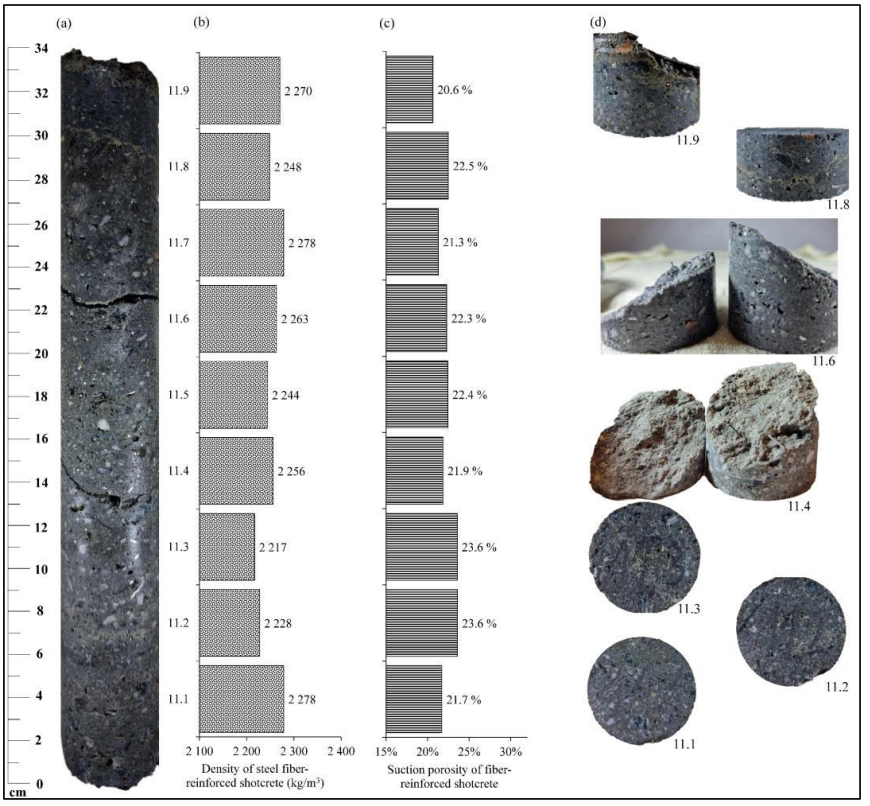


**Fig. 55:** Physical tests in a core extracted from the Frøya tunnel at chainage 5+580. (a) Real image of the Core, (b) shotcrete density profile, (c) suction porosity profile, and (d) some of the sample images.

Fig. 55 shows that suction porosity near the rock in the Frøya tunnel at chainage 5+580 is 21.7%.

In one of the cores extracted in the Frøya tunnel at chainage 5+480, μ-XRF analysis was performed. The results are shown in Fig. 56.

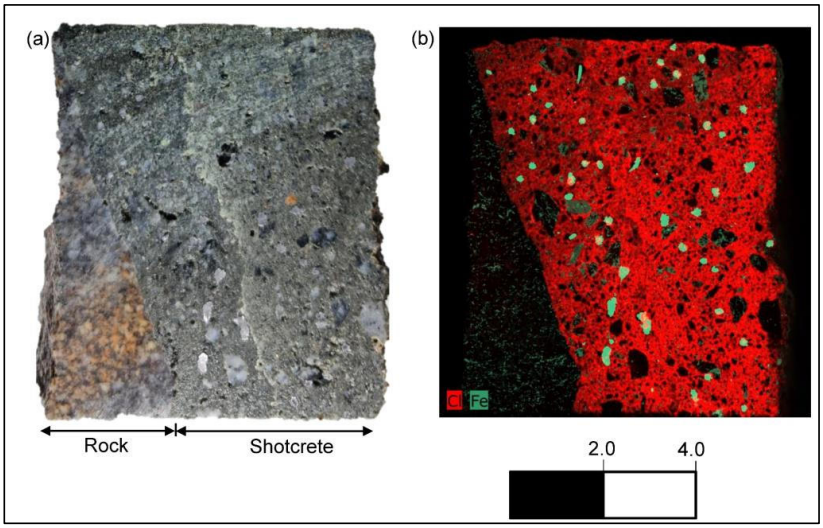


**Fig. 56:** μ-XRF result in core extracted from the Frøya tunnel at chainage 5+480. (a) Real image also shown in Fig. 39a, and (b) chlorine and iron maps.

The interpretation of Fig. 56b, is that chloride is not entering from the rock side, but rather from the traffic room.

The corresponding shotcrete suction porosity near the rock is given in Fig. 41c. The suction porosity value near the rock is 19.9%.

## 5.8 Useful life and tolerable degradation

Since 2016, the useful life of the permanent rock support in Norwegian road tunnel regulations is 100 years regardless of the environmental conditions [33]. With respect to rock bolts, for a diameter of 20 mm steel rebar coated with the duplex protection system, the expected reduction in cross-sectional area would be, on average 8% in acidic environment (100 years of exposure time) and 46% in saline environment (95 years of exposure time). The latter value seems high if the model code for service life design in reinforced concrete is considered [101]. In this reference, allowable loss of cross-sectional area in the rebar due to corrosion varies between 5% and 25%. By interpreting this reference, a 15% in loss of cross-sectional area seems to be the suggested value for rock bolts (anchorage zone with confinement). By considering this criterion, an exposure time of 100 years seems difficult to achieve in subsea tunnels.

In subsea tunnels, the degradation of steel fiber-reinforced shotcrete observed in the field has been evident in some cases after 22-23 years. Fig. 57 shows the comparison between suction porosity and shotcrete density tests performed in the Hitra and Frøya tunnels (70 dataset).

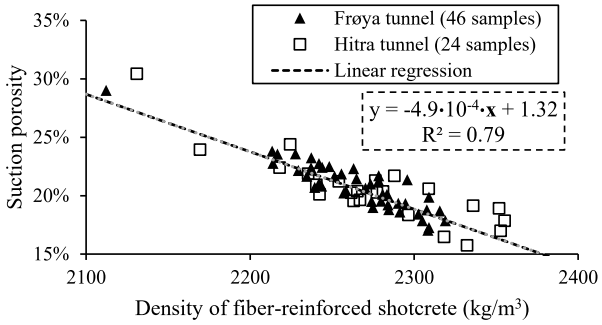


**Fig. 57:** Correlation between suction porosity and shotcrete density in the Hitra and Frøya tunnels.

The highest suction porosities in Fig. 57 correspond to chemical attack in singularities of the shotcrete layer. In particular, the suction porosity value of 30.4% is related to thaumasite sulfate attack in the Hitra tunnel (shown in Fig.38c), while the suction porosity value of 29% is related to magnesium attack in the Frøya tunnel (shown in Fig. 41c).

In paper 2 [19], Fig. 24b, the same comparison is given for cores extracted in the Nordkapp tunnel. In that case, the data set is 22, and the high suction porosity values of 28% and 28.6% in the Nordkapp tunnel (where alkali-free accelerator was used) are related to shotcrete joints with ettringite enrichment.

Other suction porosity values exceeding 25.5% are not found in the remaining 88 samples obtained from the Frøya, Hitra and Nordkapp subsea tunnels, The equivalent density for 25.5% suction porosity in the Hitra and Frøya tunnels based on Fig. 57 would be approximately 2170 kg/m$^3$, while in the Nordkapp tunnel based on Fig. 24b in paper 2 [19], would be a density in the order of 2140 kg/m$^3$.

In turn, this equivalent density could be converted into an equivalent compressive strength. Fig. 58 shows the comparison between shotcrete density and uniaxial compressive strength results in the Hitra and Frøya tunnels.

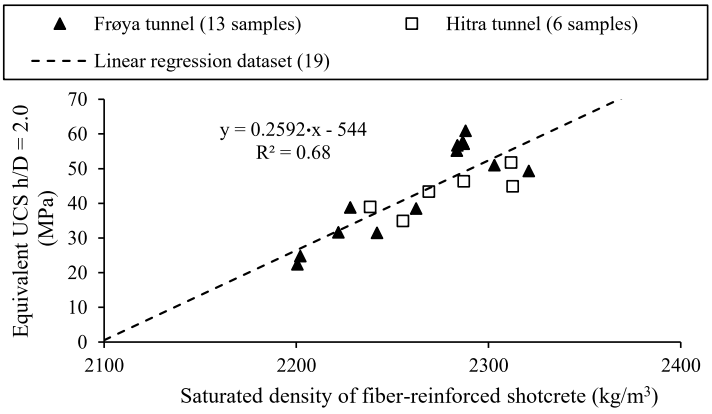


**Fig. 58:** Correlation between UCS test results and shotcrete density in the Frøya and Hitra tunnels.

If the equivalent density of 2170 kg/m$^3$ (from the suction porosity value of 25.5%) is applied to Fig. 58, the equivalent compressive strength would be 18.5 MPa. The same can be estimated in the Nordkapp tunnel, where Fig. 19b in paper 2 provides the relation between compressive strength and shotcrete density in that tunnel. If the equivalent density of 2140 kg/m$^3$ is applied to Fig. 19b in paper 2, the resulting compressive strength for a suction porosity of 25.5% would be 20.6 MPa in the Nordkapp tunnel.

The original requirement in the 1990s for shotcrete was C45 for subsea tunnels (see Fig. 11). The equivalent C45 strength required for cylindrical cores extracted from the field was 28.8 MPa according to Norwegian guidelines at that time [18]. This means that a shotcrete suction porosity of 25.5% indicates a strength reduction of 30-36% in relation to the original requirements and up to 60-70% reduction compared to non-degraded shotcrete found in the field after 23 years of exposure. Thus, a suction porosity value of 25.5% in the shotcrete layer could be considered as a threshold value of serious degradation. However, with this suction porosity value, leaching could have not been detected in the Frøya tunnel. A lower threshold value in suction porosity in the order of 22.5% could be considered to include leaching. However, shotcrete joints or debris during shotcrete application could be confused with shotcrete degradation.

Finally, it is important to mention that the shotcrete technology in the 1990s, when the investigated tunnels were constructed, did not have to fulfill a useful life of 100 years and it is not the same technology as the one used today. The major differences between the shotcrete used in the 1990s and the one used today are the introduction of blended cement (with approximately 20% fly ash) instead of pure Portland cement, and the introduction of a more stringent water-cement ratio below 0.4 in aggressive environments.

# 6 Conclusions

This thesis has provided insights on the topic of durability of rock bolts and steel fiber-reinforced shotcrete installed in Norwegian road tunnels.

In the case of rock bolts, there has been an evolution regarding the corrosion protection elements for the steel rebar from an uncoated rebar fully grouted with cement more than 50 years ago to an epoxy coating on top of the hot-dip galvanizing (duplex system) fully grouted with cement approximately 30 years ago.

Regarding uncoated carbon steel, a probability distribution was deduced for 25, 50 and 100 years of exposure based on the good correlation found between the extreme corrosivity level described in international standards for the corrosivity of atmospheres and the collected corrosion rates in carbon steel installed in Nordic underground structures.

The contribution in lifespan extension given by cement grout to a rock bolt was disregarded in this research.

In acidic environments, the contribution of hot-dip galvanizing was also disregarded. In saline environment, the lifespan extension given by hot-dip galvanizing is approximately 30 years, but the scatter is large.

When it comes to the duplex system exposed to a saline environment, the predicted middle value of the loss of cross-sectional area is much higher than in an acidic environment. However, mechanical damage in the epoxy coating would probably cause a higher corrosion rate in an acidic environment.

Flowing groundwater with a high content of dissolved oxygen can also be an aggressive environment for rock bolts, which is not always emphasized in the literature. Nevertheless, pre-grouting works ahead of the tunnel face can be performed during construction to ensure that this environment does not occur.

The constituents in shotcrete have also evolved in Norway. The steel fiber-reinforced shotcrete with the addition of silica fume has been systematically used for more than 40 years. Field and laboratory investigations performed in this research focused on:

- The condition of the singularities of the shotcrete layer (shotcrete layer at the contact with the rock, shotcrete joints and shotcrete surface exposed to the traffic room).
- The technological change approximately 25 years ago in the accelerator type used in the shotcrete from water-glass to alkali-free accelerator, where the main concern was the incorporation of sulfur content in the latter case.
- The condition differences in the shotcrete exposed to fresh and saline groundwater.

In total, four Norwegian road tunnels constructed in the 1990s were inspected. Three of them were subsea tunnels and the remaining tunnel is onshore. The most serious degradations were found in singularities of the shotcrete layer, that is to say, at its contact with the rock, between two adjacent shotcrete layers and the shotcrete surface exposed to the traffic room.

Thaumasite sulfate attack was found in the shotcrete layer at the contact with the rock in several neighboring cores in the Hitra subsea tunnel. In these cores, there was an evident degraded layer of about two centimeters, but suction porosity and density results indicate that the degraded zone compromises approximately half of the shotcrete layer.

A comparison between chloride ingress in the shotcrete layer from the traffic room and shotcrete suction porosity near the rock indicates that the upper bound to prevent chloride ingress is at approximately 21% in suction porosity. This suction porosity value could become a threshold value as quality control during construction.

Carbonation and magnesium attacks in the Frøya tunnel and ettringite enrichment in the Nordkapp tunnel were found in shotcrete joints. In addition, the portlandite content in shotcrete joints was in all cases lower than in the adjacent shotcrete. Current regulations in Norwegian road tunnels state a minimum shotcrete thickness of 8 cm. Based on what was observed, it seems reasonable that this thickness is achieved in one operation.

In the two subsea tunnels where an alkali-free accelerator was used in the shotcrete (Nordkapp and Frøya), evident leaching towards the traffic room was observed near the shotcrete surface. The sulfates from the saline groundwater, the sulfur dioxide from the traffic room and the aluminum sulfate in the alkali-free accelerator seem to be responsible in the dissolution process observed of the cement paste. This is probably interacting with leaching caused by the hydraulic pressure gradient towards the traffic room, and carbon dioxide and chloride ingress. In practice, this degradation observed in both tunnels led to a compressive strength reduction in the outermost 10 cm of the shotcrete layer between 36% and 69% in comparison to the strength in the same core near the rock. On the other hand, shotcrete leaching towards the traffic room was not noticeably observed when the water-glass accelerator was used.

In fresh groundwater, it is foreseen that both rock bolts and shotcrete should experience only very limited degradation. However, in case of improper handling during construction, it is envisaged that rock bolts are more sensitive than shotcrete.

In Norwegian subsea road tunnels constructed in the 1990s, it is predicted that the condition of shotcrete could become worse than in rock bolts. In this regard, the estimated lifespan extension of a rock bolt coated with the duplex protection system installed in subsea tunnels is, on average, 45 years. In principle, during this time period, the steel rebar will still be uncorroded. In contrast, in half that time, the condition of the shotcrete investigated in this research has in several cases become seriously degraded.

# 7 Further work

This research only provides a probability distribution for carbon steel in Nordic underground structures. The probability distribution of the corrosivity level when the rock bolt is coated with the duplex protection system is another relevant input that is not addressed in this research. Investigations performed in rock bolts during the rehabilitation of road tunnels could provide a substantial amount of information as long as the blasting of rock mass near the tunnel contour is significant. If this is the case, the information could be processed statistically. Without causing large interventions in existing subsea road tunnels, the corrosivity level behind blisters observed in rock bolt plates coated with the duplex system could also be investigated statistically. In addition, overcoring of rock bolts should be performed in areas where rock mass displacement has occurred to see if the grout has cracked and investigate the corrosivity level undergone.

Apart from subsea tunnels, in Norway tunnels excavated in alum-shale rock mass could also provide a sulfur-rich environment for the shotcrete where it could undergo severe degradation. The condition of the shotcrete layer, including its contact with the rock, the contact between consecutive shotcrete layers and the level of leaching experienced towards the traffic room should be investigated. Particular interest would be to determine the role of the alkali-free accelerator in this environment.

Pre-grouting works ahead of the tunnel face have traditionally been executed to control the water inflow during tunnel construction in Norway. Further investigations regarding the optimum pre-grouting efforts, including the durability of rock support and other elements needed in the tunnel, should be explored.

# 8 References


[1] H. Baji, C.Q. Li, S. Scicluna, J. Dauth, Risk-cost optimised maintenance strategy for tunnel structures, Tunn. Undergr. Sp. Technol. 69 (2017) 72–84. https://doi.org/10.1016/j.tust.2017.06.008.

[2] Y. Yuan, Y. Bai, J. Liu, Assessment service state of tunnel structure, Tunn. Undergr. Sp. Technol. 27 (2012) 72–85. https://doi.org/10.1016/j.tust.2011.07.002.

[3] E.K. Sund, What is the Cost of Eliminating the Maintenance Backlog on National Roads?. Report No. 75. Norwegian Public Roads Administration, 2012.

[4] J.A. Pritchard, J. Preston, Understanding the contribution of tunnels to the overall energy consumption of and carbon emissions from a railway, Transp. Res. Part D Transp. Environ. (2018) 551–563. https://doi.org/10.1016/J.TRD.2018.09.010.

[5] L. Huang, R.A. Bohne, A. Bruland, P.D. Jakobsen, J. Lohne, Environmental impact of drill and blast tunnelling: Life cycle assessment, J. Clean. Prod. 86 (2015) 110–117. https://doi.org/10.1016/j.jclepro.2014.08.083.

[6] C. Ahn, H. Xie, S. Lee, S. Abourizk, F. Peña-Mora, Carbon Footprints Analysis for Tunnel Construction Processes in the Preplanning Phase Using Collaborative Simulation. Construction Research Congress 2010 : Innovation for Reshaping Construction Practice, 2010.

[7] L. Huang, R.A. Bohne, A. Bruland, P.D. Jakobsen, J. Lohne, Life cycle assessment of Norwegian road tunnel, Int. J. Life Cycle Assess. 20 (2015) 174–184. https://doi.org/10.1007/s11367-014-0823-1.

[8] R. Rodríguez, F. Pérez, Carbon foot print evaluation in tunneling construction using conventional methods, Tunn. Undergr. Sp. Technol. 108 (2021). https://doi.org/10.1016/j.tust.2020.103704.

[9] E. Broch, E. Grøv, K.I. Davik, The inner lining system in Norwegian traffic tunnels, Tunn. Undergr. Sp. Technol. 17 (2002) 305–314. https://doi.org/10.1016/S0886-7798(02)00026-3.

[10] L. Huang, P.D. Jakobsen, R.A. Bohne, Y. Liu, A. Bruland, C.J. Manquehual, The environmental impact of rock support for road tunnels: The experience of Norway, Sci. Total Environ. 712 (2020) 136421. https://doi.org/10.1016/j.scitotenv.2019.136421.

[11] NFF, The Principles of Norwegian Tunnelling. Norwegian Tunnelling Society. Publication No. 26., 2017.

[12] E. Broch, A.M. Myrvang, G. Stjern, Support of Large Rock Caverns in Norway, Tunn. Undergr. Sp. Technol. 11 (1996) 11–19. https://doi.org/10.1016/0886-7798(96)00046-6.

[13] O.T. Blindheim, E. Grøv, B. Nilsen, Nordic sub sea tunnel projects, Tunn. Undergr. Sp. Technol. 20 (2005) 570–580. https://doi.org/10.1016/j.tust.2005.08.003.

[14] NPRA, The National Road Database, 2019.

[15] Y.C. Ou, Y.T.T. Susanto, H. Roh, Tensile behavior of naturally and artificially corroded steel bars, Constr. Build. Mater. 103 (2016) 93–104. https://doi.org/10.1016/j.conbuildmat.2015.10.075.

[16] S.T. Lee, D.G. Kim, H.S. Jung, Sulfate attack of cement matrix containing inorganic alkali-free accelerator, KSCE J. Civ. Eng. 13 (2009) 49–54. https://doi.org/10.1007/s12205-009-0049-0.

[17] NS-EN 12390-1, Testing hardened concrete Part 1: Shape, dimensions and other requirements for specimens and moulds, 2012.

[18] NB, Sprayed Concrete for Rock Support, in: Nor. Concr. Assoc. Publ. No. 7, 1993.

[19] C. Javier Manquehual, P. Drevland Jakobsen, K. Gunnar Holter, K. De Weerdt, T. Danner, A. Bruland, Comparison of the condition of steel fiber-reinforced shotcrete with water-glass and alkali-free activators after more than 20 years of service in a subsea road tunnel, Constr. Build. Mater. 328 (2022)

127090. https://doi.org/10.1016/j.conbuildmat.2022.127090.
[20] NPRA, Rock bolt handbook 215. Norwegian Public Roads Administration (in Norwegian), 1999.
[21] E. Grimstad, B. Pedersen, Long time effect on resin end-anchored and cement grouted rock bolts. Preliminary experiences., in: Annu. Conf. Nor. Tunn. Soc. 1986. (In Norwegian), 1986.
[22] NPRA, Handbook 025: Standard Code of Process 1: Roadworks. Norwegian Public Roads Administration, Main Process 7: Completion and special works (in Norwegian)., 1981.
[23] NPRA, Handbook 021: Road Tunnels. Norwegian Public Roads Administration (in Norwegian)., 1992.
[24] NPRA, Handbook 025: Standard Code of Process 1: Road contracts, in: 2007.
[25] NPRA, Handbook R761 Standard Code of Process 1: Road Contracts. Norwegian Public Roads Administration, Main Process 3: Tunnels (in Norwegian), 2012.
[26] NPRA, Handbook R761 Standard Code of Process 1: Road Contracts. Norwegian Public Roads Administration, Main Process 3: Tunnels (in Norwegian)., 2018.
[27] Norwegian Standardization Association, Norwegian Building Standardization Council Description texts for building and construction Oslo (in Norwegian), 1976.
[28] NB, Guidelines for Sprayed Concrete, 1971.
[29] O. Woldmo, The history of wet mix sprayed concrete from a Norwegian perspective, in: Fifth Int. Symp. Sprayed Concr. - Mod. Use Wet Mix Sprayed Concr. Undergr. Support. Lillehammer, Norway., 2008.
[30] G. Tjugum, Injection, sprayed concrete and grout for rock bolts. Are we updated and take advantage of the possibilities?. Annual conference of the Norwegian Tunnelling Society, (in Norwegian), 1997.
[31] NPRA, Handbook 021: Road tunnels. Norwegian Public Roads Administration. (In Norwegian)., 2002.
[32] NPRA, Handbook 021: Road Tunnels, in: Nor. Public Roads Adm. (In Norwegian), 2010.
[33] NPRA, Handbook N500: Road Tunnels. Norwegian Public Roads Administration (in Norwegian)., 2016. https://www.vegvesen.no/_attachment/61913.
[34] C.J. Manquehual, P.D. Jakobsen, A. Bruland, Corrosion Level of Rock Bolts Exposed to Aggressive Environments in Nordic Road Tunnels, Rock Mech. Rock Eng. 54 (2021) 5903–5920. https://doi.org/10.1007/s00603-021-02547-3.
[35] ISO 8044:2015(E/F), Corrosion of metals and alloys. Basic terms and definitions, n.d.
[36] E. Bardal, Corrosion and Protection, Springer, London, 2004. https://doi.org/https://doi.org/10.1007/b97510.
[37] Z. Yu, J. Hu, H. Meng, A Review of Recent Developments in Coating Systems for Hot-Dip Galvanized Steel, Front. Mater. 7 (2020) 1–19. https://doi.org/10.3389/fmats.2020.00074.
[38] Z. Panossian, N.L. de Almeida, R.M.F. de Sousa, G. de S. Pimenta, L.B.S. Marques, Corrosion of carbon steel pipes and tanks by concentrated sulfuric acid: A review, Corros. Sci. 58 (2012) 1–11. https://doi.org/10.1016/j.corsci.2012.01.025.
[39] S. Wang, D. Liu, N. Du, Q. Zhao, J. Xiao, Cathodic reactions involved in the corrosion of X80 steel in acidic soil simulated solution, Int. J. Electrochem. Sci. 11 (2016) 8797–8809. https://doi.org/10.20964/2016.10.08.
[40] Noranda, Designing Zinc Castings for Corrosion Resistance, Toronto, 1993.
[41] U. HH, Corrosion and Corrosion Control. 2nd, Ed. New York: John Wiley & Sons, 1971.
[42] P. Pokorný, P. Tej, M. Kouřil, Evaluation of the impact of corrosion of hot-dip galvanized reinforcement on bond strength with concrete – A review, Constr. Build. Mater. 132 (2017) 271–289. https://doi.org/10.1016/j.conbuildmat.2016.11.096.
[43] J.M. Roy, R. Preston, R.P. Bewick, Classification of Aqueous Corrosion in Underground Mines, Rock

Mech. Rock Eng. 49 (2016) 3387–3391. https://doi.org/10.1007/s00603-016-0926-z.

[44] NS-EN-ISO-9223, Corrosion of metals and alloys. Corrosivity of atmospheres. Classification, determination and estimation. Standard Norge., 2012.

[45] V.B. Møller, K. Dam-Johansen, S.M. Frankær, S. Kiil, Acid-resistant organic coatings for the chemical industry: a review, J. Coatings Technol. Res. 14 (2017) 279–306. https://doi.org/10.1007/s11998-016-9905-2.

[46] A.A. Sagüés, K. Lau, R.G. Powers, R.J. Kessler, Corrosion of epoxy-coated rebar in marine bridges - Part 1: A 30-year perspective, Corrosion. 66 (2010) 0650011–06500113.

[47] P.A. Sørensen, S. Kiil, K. Dam-Johansen, C.E. Weinell, Anticorrosive coatings: A review, J. Coatings Technol. Res. 6 (2009) 135–176. https://doi.org/10.1007/s11998-008-9144-2.

[48] N.A. i. A. Rahman, M.C. Ismail, Z. Man, The effect of hydrogen diffusivities on PANI-modified epoxy coating under potentiostatic charging, ARPN J. Eng. Appl. Sci. 11 (2016) 4214–4220.

[49] M. Kutz, Handbook of Environmental Degradation of Materials (Third edition), 2018.

[50] R.C. Hassell, Corrosion of Rock Reinforcement in Underground Excavations. PhD thesis, Western Australian School of Mines Department of Mining Engineering and Surveying Corrosion of Rock Reinforcement in Underground Excavations, 2008.

[51] C.C. Li, Principles of rockbolting design, J. Rock Mech. Geotech. Eng. 9 (2017) 396–414. https://doi.org/10.1016/j.jrmge.2017.04.002.

[52] P. Hagelia, Durability development for sprayed concrete as rock support in different tunnel environments. Norwegian Public Roads Administration. Report No. 566., 2018.

[53] E.C. Dos Santos, J.C. De Mendonça Silva, H.A. Duarte, Pyrite Oxidation Mechanism by Oxygen in Aqueous Medium, J. Phys. Chem. C. 120 (2016) 2760–2768. https://doi.org/10.1021/acs.jpcc.5b10949.

[54] Y. Wang, G. Cheng, W. Wu, Q. Qiao, Y. Li, X. Li, Effect of pH and chloride on the micro-mechanism of pitting corrosion for high strength pipeline steel in aerated NaCl solutions, Appl. Surf. Sci. 349 (2015) 746–756. https://doi.org/10.1016/j.apsusc.2015.05.053.

[55] H. Parangusan, J. Bhadra, N. Al-Thani, A review of passivity breakdown on metal surfaces: influence of chloride- and sulfide-ion concentrations, temperature, and pH, Emergent Mater. 4 (2021) 1187–1203. https://doi.org/10.1007/s42247-021-00194-6.

[56] L. Bertolini, B. Elsener, P. Pedeferri, E. Redaelli, R.B. Polder, Corrosion of Steel in Concrete: Prevention, Diagnosis, Repair, 2nd Edition, 2014.

[57] C.M. Hansson, The impact of corrosion on society, Metall. Mater. Trans. A Phys. Metall. Mater. Sci. 42 (2011) 2952–2962. https://doi.org/10.1007/s11661-011-0703-2.

[58] O.Ø. Knudsen, A. Forsgren, Corrosion control through organic coatings, Group, CRC Press. Taylor & Francis, 2017.

[59] K. Tarka, Corrosion of painted galvanized steel pretreated with Zr-based thin films, (2015).

[60] R.D. Granata, NACE Annual Corrosion Conference ", Paper No. 382., 1991.

[61] A. Ongstad, Useful life of rock bolts. Norwegian Public Roads Administration. Major Research and Development Project: Modern Road tunnels 2008-2011. Report No. 164., 2012.

[62] P. Hagelia, Deterioration mechanisms and durability of sprayed concrete in Norwegian tunnels. NFF Publication No. 17: Underground openings – operations, maintenance and repair, 2008.

[63] Y. Xu, Q. Zhang, Q. Zhou, S. Gao, B. Wang, X. Wang, Y. Huang, Flow accelerated corrosion and erosion−corrosion behavior of marine carbon steel in natural seawater, Npj Mater. Degrad. 5 (2021) 1–13. https://doi.org/10.1038/s41529-021-00205-1.

[64] E. Villaescusa, R. Hassell, A. Thompson, Corrosion of rock reinforcement in underground excavations,

in: Miner. Energy Res. Inst. West. Aust. Rep. No. 263., 2007.

[65] R. Thomas, Hot-dip galvanizing. Nordic Galvanizing Association, Oslo (In Norwegian)., 1978.

[66] Q. Zhou, Y. Wang, G.P. Bierwagen, Flow accelerated degradation of organic clear coat: The effect of fluid shear, Electrochim. Acta. 142 (2014) 25–33. https://doi.org/10.1016/j.electacta.2014.07.082.

[67] O. Bozorg-Haddad, M. Delpasand, H.A. Loáiciga, Water quality, hygiene, and health, Econ. Polit. Soc. Issues Water Resour. (2021). https://doi.org/https://doi.org/10.1016/B978-0-323-90567-1.00008-5.

[68] B. Kløve, H.M.L. Kvitsand, T. Pitkänen, M.J. Gunnarsdottir, S. Gaut, S.M. Gardarsson, P.M. Rossi, I. Miettinen, Overview of groundwater sources and water-supply systems, and associated microbial pollution, in Finland, Norway and Iceland, Hydrogeol. J. 25 (2017) 1033–1044. https://doi.org/10.1007/s10040-017-1552-x.

[69] A. Seither, P.E. Eide, T. Berg, B. Frengstad, The inorganic drinking water quality of some groundwater works and regulated wells in Norway. Geological Survey of Norway, NGU., 2012.

[70] H.R. Kim, T. Noguchi, H. Nagai, Evaluation of mechanical performance of corroded reinforcement considering the surface shape, J. Struct. Constr. Eng. 73 (2008) 181–188. https://doi.org/10.3130/aijs.73.181.

[71] NS-EN ISO 9223, Corrosion of metals and alloys. Corrosivity of atmospheres. Classification, determination and estimation, 2012., (2012).

[72] J.F.H. Eijnsbergen, Duplex Systems: Hot-dip galvanizing plus painting. Elsevier Science B.V., 1994.

[73] T. Van Gerven, G. Cornelis, E. Vandoren, C. Vandecasteele, Effects of carbonation and leaching on porosity in cement-bound waste, Waste Manag. 27 (2007) 977–985. https://doi.org/10.1016/j.wasman.2006.05.008.

[74] F.P. Glasser, J. Marchand, E. Samson, Durability of concrete - Degradation phenomena involving detrimental chemical reactions, Cem. Concr. Res. 38 (2008) 226–246. https://doi.org/10.1016/j.cemconres.2007.09.015.

[75] I. Galan, A. Baldermann, W. Kusterle, M. Dietzel, F. Mittermayr, Durability of shotcrete for underground support– Review and update, Constr. Build. Mater. 202 (2019) 465–493. https://doi.org/10.1016/j.conbuildmat.2018.12.151.

[76] V.B. Duong, R. Sahamitmongkol, S. Tangtermsirikul, Effect of leaching on carbonation resistance and steel corrosion of cement-based materials, Constr. Build. Mater. 40 (2013) 1066–1075. https://doi.org/10.1016/j.conbuildmat.2012.11.042.

[77] R. Ličbinský, J. Huzlík, A. Frýbort, J. Jedlička, K. Kreislová, Specific Air Pollution in Road Tunnels, Trans. Transp. Sci. 6 (2013) 107–116. https://doi.org/10.2478/v10158-012-0037-9.

[78] W. Müllauer, R.E. Beddoe, D. Heinz, Effect of carbonation, chloride and external sulphates on the leaching behaviour of major and trace elements from concrete, Cem. Concr. Compos. 34 (2012) 618–626. https://doi.org/10.1016/j.cemconcomp.2012.02.002.

[79] X.N. Li, X.B. Zuo, Y.X. Zou, Modeling and simulation on coupled chloride and calcium diffusion in concrete, Constr. Build. Mater. 271 (2021) 121557. https://doi.org/10.1016/j.conbuildmat.2020.121557.

[80] P. Hagelia, Durability of sprayed concrete for rock support. A tale from the tunnels. 8th International symposium on sprayed concrete - Modern use of wet mix sprayed concrete for underground support, Trondheim, Norway, 11-14 June, in: 8th Int. Symp. Sprayed Concr. - Mod. Use Wet Mix Sprayed Concr. Undergr. Support. Trondheim, Norway, 11-14 June 2018., 2018: pp. 167–182.

[81] NS-EN 206, Concrete: Specification, performance, production and conformity, 2017. NS-EN 206:2013+A1:2016+NA:2017, 2017.

[82] F.R. Steindl, I. Galan, A. Baldermann, M. Sakoparnig, L. Briendl, J. Juhart, M. Thumann, M. Dietzel,

R. Röck, W. Kusterle, F. Mittermayr, Sulfate durability and leaching behaviour of dry- and wet-mix shotcrete mixes, Cem. Concr. Res. 137 (2020) 106180. https://doi.org/10.1016/j.cemconres.2020.106180.

[83] E.K. Melara, P.O. Trentin, E. Pereira, R.A. Medeiros-Junior, Contribution to the service-life modeling of concrete exposed to sulfate attack by the inclusion of electrical resistivity data, Constr. Build. Mater. 322 (2022) 126490. https://doi.org/10.1016/j.conbuildmat.2022.126490.

[84] R. Myrdal, Chemical reflections on accelerators for sprayed concrete: Past, present and future challenges, in: 6th Int. Symp. Sprayed Concr. Tromsø, Norway, Sept. 12-15, 2011, 2011.

[85] C. Paglia, F. Wombacher, H. Böhni, The influence of alkali-free and alkaline shotcrete accelerators within cement systems: Influence of the temperature on the sulfate attack mechanisms and damage, Cem. Concr. Res. 33 (2003) 387–395. https://doi.org/10.1016/S0008-8846(02)00967-5.

[86] R.P. Salvador, D.A.S. Rambo, R.M. Bueno, S.R. Lima, A.D. Figueiredo, Influence of accelerator type and dosage on the durability of wet-mixed sprayed concrete against external sulfate attack, Constr. Build. Mater. 239 (2020) 117883. https://doi.org/10.1016/j.conbuildmat.2019.117883.

[87] V. Marcos-Meson, A. Michel, A. Solgaard, G. Fischer, C. Edvardsen, T.L. Skovhus, Corrosion resistance of steel fibre reinforced concrete - A literature review, Cem. Concr. Res. 103 (2018) 1–20. https://doi.org/10.1016/j.cemconres.2017.05.016.

[88] M. Sun, C. Sun, P. Zhang, N. Liu, Y. Li, J. Duan, B. Hou, Influence of carbonation on chloride binding of mortars made with simulated marine sand, Constr. Build. Mater. 303 (2021). https://doi.org/https://doi.org/10.1016/j.conbuildmat.2021.124455.

[89] A. V. Saetta, B.A. Schrefler, R. V. Vitaliani, The carbonation of concrete and the mechanism of moisture, heat and carbon dioxide flow through porous materials, Cem. Concr. Res. 23 (1993) 761–772. https://doi.org/10.1016/0008-8846(93)90030-D.

[90] S. Kamali, B. Gérard, M. Moranville, Modelling the leaching kinetics of cement-based materials - Influence of materials and environment, Cem. Concr. Compos. 25 (2003) 451–458. https://doi.org/10.1016/S0958-9465(02)00085-9.

[91] C. Le Bellego, I.S.A. Oxand, D.C. Montigny-sur-loing, Various Environments, 3 (2002) 632–640.

[92] M. Mainguy, C. Tognazzi, J.M. Torrenti, F. Adenot, Modelling of leaching in pure cement paste and mortar, Cem. Concr. Res. 30 (2000) 83–90. https://doi.org/10.1016/S0008-8846(99)00208-2.

[93] O.Ø. Knudsen, Corrosion protection in tunnels. Norwegian Public Roads Administration. Report No. 410. (In Norwegian)., 2015.

[94] C. Manquehual, J. Johansen, P.D. Jakobsen, B. Nilsen, Operation & Maintenance Costs of Subsea Road Tunnels in Norway, in: ITA-AITES World Tunn. Congr. - WTC2020, 2020: pp. 1569–1575.

[95] K.K. Panthi, B. Nilsen, Significance of grouting for controlling leakage in water tunnels - A case from Nepal, Undergr. Sp. Use Anal. Past Lessons Futur. - Proc. 31st ITA-AITES World Tunn. Congr. 2 (2005) 931–937. https://doi.org/10.1201/noe0415374521.ch138.

[96] R.P. Salvador, S.H.P. Cavalaro, I. Segura, A.D. Figueiredo, J. Pérez, Early age hydration of cement pastes with alkaline and alkali-free accelerators for sprayed concrete, Constr. Build. Mater. 111 (2016) 386–398. https://doi.org/10.1016/j.conbuildmat.2016.02.101.

[97] W. Wang, T. Noguchi, I. Maruyama, Mechanism understanding of alkali-silica reaction in alkali-activated materials system, Cem. Concr. Res. (2022). https://doi.org/10.1016/J.CEMCONRES.2022.106768.

[98] B. Nilsen, Characteristics of water ingress in Norwegian subsea tunnels, Rock Mech. Rock Eng. 47 (2014) 933–945. https://doi.org/10.1007/s00603-012-0300-8.

[99] NFF, Rock mass grouting. Norwegian Tunnelling Society, 2011.

[100] ASA Underground Committee, Position Statement #1, Spraying Shotcrete Overhead in Underground Applications, Am. Shotcrete Assoc. (2019) 1–5.

[101] fib, Model Code for Service Life Design. International Federation for Structural Concrete., 2006.

## Appendix A Laboratory research planning of shotcrete cores

**Nordkapp and Honningsvåg tunnels – October 2020**

**Nordkapp tunnel - saline groundwater - PK 3+220 (shotcrete with water-glass accelerator)**

| Core | diameter mm | UCS | µ-XRF | XRD | Suction porosity | Thymolphthalein |
|---|---|---|---|---|---|---|
| 1 | 55 | | | | 4 | |
| 2 | 55 | | 1 | | 4 | |
| 3 | 55 | | 1 | | | |
| 4 | 55 | 1 | | 1 | | |
| 5 | 55 | 1 | | | | 1 |
| 6 | 55 | 1 | | | | |

**Nordkapp tunnel - saline groundwater - PK 4+920 (shotcrete with alkali-free accelerator)**

| Core | diameter mm | UCS | µ-XRF | XRD | Suction porosity | Thymolphthalein |
|---|---|---|---|---|---|---|
| 7 | 55 | | | | 6 | |
| 8 | 55 | 3 | | 1 | | |
| 9 | 55 | 2 | | | | 1 |
| 10 | 55 | 1 | | 2 | | |
| 11 | 55 | 2 | | | | |
| 12 | 55 | | | | 8 | |
| 13 | 55 | 3 | | 1 | | |
| 14 | 55 | | Tip towards rock in parallel to core 2<br>Tip towards traffic room in parallel to core 3 | | | |

**Honningsvåg tunnel - fresh groundwater - PK 0+560**

| Core | diameter mm | UCS | µ-XRF | XRD | Suction porosity | Thymolphthalein |
|---|---|---|---|---|---|---|
| 15 | 55 | | | | 8 | |
| 16 | 55 | 3 | | | | |
| 17 | 55 | | | | 2 | 1 |

## Hitra and Frøya tunnels – August/September 2021

| Frøya tunnel - fresh groundwater - PK 8+070 | | | | | | |
|---|---|---|---|---|---|---|
| Core | diameter mm | UCS | µ-XRF | XRD | Suction porosity | Thymolphthalein |
| 4 | 55 | | Run in parallel to core 12 | (Shotcrete joint)<br>(Tip towards shotcrete surface) | | |
| 5 | 84 | | | | 12 | |
| 6 | 84 | h/D = 2.0<br>h/D = 1.5 | | | | 1 |
| 7 | 84 | | | | 6 | |
| 8 | 84 | h/D = 1.0<br>h/D = 1.0 | | | | |

| Frøya tunnel - saline groundwater - PK: 5+590 | | | | | | |
|---|---|---|---|---|---|---|
| Core | diameter mm | UCS | µ-XRF | XRD | Suction porosity | Thymolphthalein |
| 1 | 55 | h/D = 1.5<br>h/D = 1.5 | | (2) (tip towards shotcrete surface and adjacent to it) | | |
| 2 | 55 | | Run in parallel to core 12 | | | 1 |
| 3 | 55 | | | No test performed | | |
| 9 | 84 | | 1 | | 7 | |
| 10 | 84 | h/D = 1<br>h/D = 1 | | Tip towards shotcrete surface | | |

| Frøya tunnel - saline groundwater - PK: 5+580 | | | | | | |
|---|---|---|---|---|---|---|
| Core | diameter mm | UCS | µ-XRF | XRD | Suction porosity | Thymolphthalein |
| 11 | 55 | | | | 9 | |
| 12 | 55 | | Run in parallel to cores 2,4 | 6 | | |
| 36 | 55 | (4) h/D = 1 | | Tip towards rock | In shotcrete with crack | 1 |
| 37 | 55 | | | No test performed | | |
| 38 | 84 | | 1 | | 7 | |
| 39 | 84 | | | No test performed | | |

**Frøya tunnel - saline groundwater - PK: 5+480**

| Core | | UCS | µ-XRF | XRD | Suction porosity | Thymolphthalein |
|---|---|---|---|---|---|---|
| 33 | 84 | | 1 | | 2 | |
| 34 | 55 | | | | 2 | |
| 35 | 55 | | 1 | | | |

**Hitra tunnel - saline Groundwater PK: 3+200**

| Core | diameter mm | UCS | µ-XRF | XRD | Suction porosity | Thymolphthalein |
|---|---|---|---|---|---|---|
| 13 | 55 | | | | 2 | |
| 14 | 55 | (1) h/D = 1 | | | | |
| 15 | 55 | (1) h/D = 1 | | | | |
| 16 | 55 | | Run in parallel to core 19 | 4 | | |
| 17 | 55 | | | | | |
| 18 | 55 | | | | 5 | |

**Hitra tunnel - saline groundwater PK: 3+090**

| Core | diameter mm | UCS | µ-XRF | XRD | Suction porosity | Thymolphthalein |
|---|---|---|---|---|---|---|
| 19 | 55 | | Run in parallel to core 16 | 4 | | |
| 20 | 55 | | | | 4 | |
| 21 | 55 | | | | 4 | |
| 22 | 55 | h/D = 1<br>h/D = 1 | | (Tip towards rock)<br>(Tip towards shotcrete surface) | | |
| 23 | 55 | | Run in parallel to core 30 | | | |
| 24 | 55 | | | | 2 | |

**Hitra tunnel - saline groundwater Pump station**

| Core | diameter mm | UCS | µ-XRF | XRD | Suction porosity | Thymolphthalein |
|---|---|---|---|---|---|---|
| 29 | 55 | | | | 5 | |
| 30 | 55 | | Run in parallel to core 23 | | | |
| 31 | 55 | h/D = 1 | | Tip towards shotcrete surface | | |
| 32 | 55 | h/D = 1<br>h/D = 1 | | | | 1 |

| Hitra tunnel - fresh groundwater PK: 5+200 | | | | | | |
|---|---|---|---|---|---|---|
| Core | diameter mm | UCS | μ-XRF | XRD | Suction porosity | Thymolphthalein |
| 25 | 55 | | | | 1 | |
| 26 | 55 | | | | | 1 |
| 27 | 55 | | | | 1 | |
| 28 | 55 | | 1 | | | |

## Appendix B Shotcrete density and uniaxial compressive strength results

**Nordkapp tunnel - saline groundwater - PK 3+220 (shotcrete with water-glass accelerator)**

| | | Diameter | h/D | UCS | $UCS_{EQUIV}$ h/D = 2.0 | Shotcrete density |
|---|---|---|---|---|---|---|
| Core | Label | mm | - | MPa | MPa | kg/m$^3$ |
| 4 | UCS_12 | 55 | 1.0 | 62.8 | 55.3 | 2250 |
| 5 | UCS_1 | 55 | 1.0 | 56.0 | 47.4 | 2237 |
| 6 | UCS_2 | 55 | 1.0 | 67.9 | 58.0 | 2312 |

**Nordkapp tunnel - saline groundwater - PK 4+920 (shotcrete with alkali-free accelerator)**

| | | Diameter | h/D | UCS | $UCS_{EQUIV}$ h/D = 2.0 | Shotcrete density |
|---|---|---|---|---|---|---|
| Core | Label | mm | - | MPa | MPa | kg/m$^3$ |
| 8 | UCS_13 | 55 | 1.0 | 39.7 | 34.8 | 2199 |
| 8 | UCS_14 | 55 | 0.93 | 33.3 | 27.9 | 2200 |
| 8 | UCS_15 | 55 | 1.0 | 30.7 | 27.0 | 2172 |
| 9 | Ed_1 | 55 | 2.0 | 31.1 | 31.1 | 2202 |
| 9 | Ed_2 | 55 | 2.0 | 30.9 | 30.9 | 2182 |
| 10 | Ed_3 | 55 | 2.0 | 25.5 | 25.5 | 2163 |
| 11 | Ed_4 | 55 | 2.0 | 15.1 | 15.1 | 2156 |
| 11 | Ed_5 | 55 | 2.0 | 28.9 | 28.9 | 2213 |
| 13 | UCS_3 | 55 | 1.0 | 46.7 | 40.4 | 2247 |
| 13 | UCS_4 | 55 | 1.0 | 23.8 | 20.2 | 2123 |
| 13 | UCS_5 | 55 | 1.0 | 14.8 | 12.6 | 2082 |

**Honningsvåg tunnel - fresh groundwater - PK 0+560**

| | | Diameter | h/D | UCS | $UCS_{EQUIV}$ h/D = 2.0 | Shotcrete density |
|---|---|---|---|---|---|---|
| Core | Label | mm | - | MPa | MPa | kg/m$^3$ |
| 16 | UCS_16 | 55 | 1.0 | 37.5 | 32.9 | 2185 |
| 16 | UCS_17 | 55 | 1.0 | 56.4 | 49.2 | 2279 |
| 16 | UCS_18 | 55 | 1.0 | 39.8 | 34.6 | 2207 |

**Frøya tunnel - fresh groundwater - PK 8+070**

| | | Diameter | h/D | UCS | $UCS_{EQUIV}$ h/D = 2.0 | Shotcrete density |
|---|---|---|---|---|---|---|
| Core | Label | mm | - | MPa | MPa | kg/m$^3$ |
| 6 | 6.1 | 84 | 1.5 | 63.7 | 60.9 | 2287 |
| 6 | 6.2 | 84 | 2.0 | 57.2 | 57.2 | 2287 |
| 8 | 8.1 | 84 | 1.0 | 63.4 | 55.3 | 2284 |
| 8 | 8.2 | 84 | 1.0 | 65.3 | 56.7 | 2284 |

| Frøya tunnel - saline groundwater - PK: 5+590 | | | | | | |
|---|---|---|---|---|---|---|
| | | Diameter | h/D | UCS | $UCS_{EQUIV}$ h/D = 2.0 | Shotcrete density |
| Core | Label | mm | - | MPa | MPa | kg/m$^3$ |
| 1 | 1.1 | 55 | 1.5 | 53.7 | 51.1 | 2303 |
| 1 | 1.2 | 55 | 1.5 | 23.5 | 22.5 | 2200 |
| 10 | 10.1 | 84 | 1.0 | 56.6 | 49.3 | 2321 |
| 10 | 10.2 | 84 | 1.0 | 36.4 | 31.7 | 2222 |

| Frøya tunnel - saline groundwater - PK: 5+580 | | | | | | |
|---|---|---|---|---|---|---|
| | | Diameter | h/D | UCS | $UCS_{EQUIV}$ h/D = 2.0 | Shotcrete density |
| Core | Label | mm | - | MPa | MPa | kg/m$^3$ |
| 36 | 36.1 | 55 | 1.0 | 36.2 | 31.5 | 2242 |
| 36 | 36.2 | 55 | 1.0 | 28.5 | 24.8 | 2202 |
| 36 | 36.3 | 55 | 1.0 | 44.3 | 38.5 | 2262 |
| 36 | 36.4 | 55 | 1.0 | 67.7 | 57.8 | 2286 |

| Hitra tunnel - saline Groundwater PK: 3+200 | | | | | | |
|---|---|---|---|---|---|---|
| | | Diameter | h/D | UCS | $UCS_{EQUIV}$ h/D = 2.0 | Shotcrete density |
| Core | Label | mm | - | MPa | MPa | kg/m$^3$ |
| 14 | 14.1 | 55 | 1.0 | 60.1 | 51.8 | 2312 |
| 15 | 15.1 | 55 | 1.0 | 53.8 | 46.4 | 2287 |

| Hitra tunnel - saline groundwater PK: 3+090 | | | | | | |
|---|---|---|---|---|---|---|
| | | Diameter | h/D | UCS | $UCS_{EQUIV}$ h/D = 2.0 | Shotcrete density |
| Core | Label | mm | - | MPa | MPa | kg/m$^3$ |
| 22 | 22.1 | 55 | 0.91 | 42.0 | 34.9 | 2255 |
| 22 | 22.2 | 55 | 0.93 | 53.5 | 45.0 | 2312 |

| Hitra tunnel - saline groundwater - Pump station | | | | | | |
|---|---|---|---|---|---|---|
| | | Diameter | h/D | UCS | $UCS_{EQUIV}$ h/D = 2.0 | Shotcrete density |
| Core | Label | mm | - | MPa | MPa | kg/m$^3$ |
| 31 | 31.1 | 55 | 1.0 | 45.0 | 38.8 | 2228 |
| 32 | 32.1 | 55 | 1.0 | 49.8 | 43.4 | 2269 |
| 32 | 32.2 | 55 | 1.0 | 44.7 | 39.0 | 2238 |

## Appendix C Shotcrete density and suction porosity results

| Nordkapp tunnel - saline groundwater - PK 3+220 (shotcrete with water-glass accelerator) | | | |
|---|---|---|---|
| Core | Label | Shotcrete density kg/m$^3$ | Suction porosity % |
| 1 | 1 | 2250 | 20.9 % |
| 1 | 2 | 2254 | 21.5 % |
| 1 | 3 | 2217 | 22.2 % |
| 1 | 33 | 2243 | 21.4 % |
| 2 | 5 | 2263 | 20.1 % |
| 2 | 6 | 2285 | 19.7 % |
| 2 | 7 | 2244 | 21.7 % |
| 2 | 8 | 2247 | 19.6 % |

| Nordkapp tunnel - saline groundwater - PK 4+920 (shotcrete with alkali-free accelerator) | | | |
|---|---|---|---|
| Core | Label | Shotcrete density kg/m$^3$ | Suction porosity % |
| 7 | 8 | 2246 | 21.0 % |
| 7 | 9 | 2222 | 22.4 % |
| 7 | 10 | 2264 | 19.9 % |
| 7 | 11 | 2217 | 23.7 % |
| 7 | 12 | 2191 | 24.1 % |
| 7 | 13 | 2219 | 22.2 % |
| 12 | 14 | 2206 | 23.5 % |
| 12 | 15 | 2266 | 19.0 % |
| 12 | 16 | 2225 | 19.8 % |
| 12 | 17 | 2112 | 28.0 % |
| 12 | 18 | 2220 | 22.2 % |
| 12 | 19 | 2189 | 23.2 % |
| 12 | 20 | 2019 | 28.6 % |
| 12 | 21 | 2183 | 22.4 % |

| Honningsvåg tunnel - fresh groundwater - PK 0+560 | | | |
|---|---|---|---|
| Core | Label | Shotcrete density kg/m$^3$ | Suction porosity % |
| 15 | 25 | 2214 | 22.9 % |
| 15 | 26 | 2259 | 21.4 % |
| 15 | 27 | 2152 | 25.2 % |
| 15 | 28 | 2292 | 19.8 % |
| 15 | 29 | 2292 | 19.4 % |
| 15 | 30 | 2211 | 24.2 % |
| 15 | 31 | 2199 | 24.5 % |
| 15 | 32 | 2239 | 22.8 % |
| 17 | 34 | 2232 | 22.7 % |
| 17 | 35 | 2184 | 24.6 % |

| Frøya tunnel - fresh groundwater - PK 8+070 | | | |
|---|---|---|---|
| Core | Label | Shotcrete density kg/m$^3$ | Suction porosity % |
| 5 | 5.1 | 2284 | 19.2 % |
| 5 | 5.2 | 2257 | 20.2 % |
| 5 | 5.3 | 2319 | 17.9 % |
| 5 | 5.4 | 2305 | 17.9 % |
| 5 | 5.5 | 2275 | 19.0 % |
| 5 | 5.6 | 2308 | 17.0 % |
| 5 | 5.7 | 2274 | 19.5 % |
| 5 | 5.8 | 2291 | 18.6 % |
| 5 | 5.9 | 2284 | 18.8 % |
| 5 | 5.1 | 2303 | 18.4 % |
| 5 | 5.11 | 2284 | 20.0 % |
| 5 | 5.12 | 2251 | 21.7 % |
| 7 | 7.1 | 2239 | 20.7 % |
| 7 | 7.2 | 2258 | 20.4 % |
| 7 | 7.3 | 2283 | 20.1 % |
| 7 | 7.4 | 2316 | 18.7 % |
| 7 | 7.5 | 2308 | 18.8 % |
| 7 | 7.6 | 2273 | 21.0 % |

| Frøya tunnel - saline groundwater - PK: 5+590 | | | |
|---|---|---|---|
| Core | Label | Shotcrete density kg/m$^3$ | Suction porosity % |
| 9 | 9.1 | 2290 | 19.4 % |
| 9 | 9.2 | 2281 | 20.1 % |
| 9 | 9.3 | 2295 | 19.3 % |
| 9 | 9.4 | 2265 | 21.5 % |
| 9 | 9.5 | 2214 | 22.8 % |
| 9 | 9.6 | 2237 | 22.4 % |
| 9 | 9.7 | 2242 | 22.7 % |

| Frøya tunnel - saline groundwater - PK: 5+580 | | | |
|---|---|---|---|
| Core | Label | Shotcrete density kg/m$^3$ | Suction porosity % |
| 11 | 11.1 | 2278 | 21.7 % |
| 11 | 11.2 | 2228 | 23.6 % |
| 11 | 11.3 | 2217 | 23.6 % |
| 11 | 11.4 | 2256 | 21.9 % |
| 11 | 11.5 | 2244 | 22.4 % |
| 11 | 11.6 | 2263 | 22.3 % |
| 11 | 11.7 | 2278 | 21.3 % |
| 11 | 11.8 | 2248 | 22.5 % |
| 11 | 11.9 | 2270 | 20.6 % |
| 36 | 36.1 | 2296 | 21.4 % |
| 38 | 38.1 | 2237 | 22.2 % |
| 38 | 38.2 | 2229 | 22.2 % |
| 38 | 38.3 | 2242 | 21.1 % |
| 38 | 38.4 | 2280 | 19.5 % |
| 38 | 38.5 | 2235 | 21.7 % |
| 38 | 38.6 | 2309 | 17.3 % |
| 38 | 38.7 | 2244 | 20.8 % |

| Frøya tunnel - saline groundwater - PK: 5+480 | | | |
|---|---|---|---|
| Core | Label | Shotcrete density kg/m$^3$ | Suction porosity % |
| 33 | 33.1 | 2213 | 23.8 % |
| 33 | 33.2 | 2237 | 23.2 % |
| 34 | 34.1 | 2309 | 19.9 % |
| 34 | 34.2 | 2112 | 29.0 % |

| Hitra tunnel - saline Groundwater PK: 3+200 | | | |
|---|---|---|---|
| Core | Label | Shotcrete density kg/m$^3$ | Suction porosity % |
| 13 | 13.1 | 2281 | 20.4 % |
| 13 | 13.2 | 2267 | 19.7 % |
| 18 | 18.1 | 2309 | 20.6 % |
| 18 | 18.2 | 2277 | 20.3 % |
| 18 | 18.3 | 2332 | 15.8 % |
| 18 | 18.4 | 2262 | 20.3 % |
| 18 | 18.5 | 2353 | 17.0 % |

| Hitra tunnel - saline groundwater PK: 3+090 | | | |
|---|---|---|---|
| Core | Label | Shotcrete density kg/m$^3$ | Suction porosity % |
| 20 | 20.1 | 2352 | 18.9 % |
| 20 | 20.2 | 2355 | 17.9 % |
| 20 | 20.3 | 2336 | 19.1 % |
| 20 | 20.4 | 2296 | 18.4 % |
| 21 | 21.1 | 2131 | 30.4 % |
| 21 | 21.2 | 2224 | 24.4 % |
| 21 | 21.3 | 2276 | 21.3 % |
| 21 | 21.4 | 2242 | 20.1 % |
| 24 | 24.1 | 2218 | 22.4 % |
| 24 | 24.2 | 2288 | 21.7 % |

| Hitra tunnel - fresh groundwater - PK: 5+200 | | | |
|---|---|---|---|
| Core | Label | Shotcrete density kg/m$^3$ | Suction porosity % |
| 25 | 25.1 | 2254 | 21.2 % |
| 27 | 27.1 | 2235 | 21.9 % |

| Hitra tunnel - saline groundwater - Pump station | | | |
|---|---|---|---|
| Core | Label | Shotcrete density kg/m$^3$ | Suction porosity % |
| 29 | 29.1 | 2169 | 23.9 % |
| 29 | 29.2 | 2263 | 19.5 % |
| 29 | 29.3 | 2265 | 20.4 % |
| 29 | 29.4 | 2240 | 20.9 % |
| 29 | 29.5 | 2318 | 16.5 % |

**PAPER I**

**Title:** Corrosion Level of Rock Bolts Exposed to Aggressive Environments in Nordic Road Tunnels (2021)

**Authors:**
Manquehual, Cristobal Javier
Jakobsen, Pål Drevland
Bruland, Amund

**Published in:**
Rock Mechanics and Rock Engineering journal Volume 54, 5903-5920 (2021)

Rock Mechanics and Rock Engineering (2021) 54:5903–5920
https://doi.org/10.1007/s00603-021-02547-3

ORIGINAL PAPER

# Corrosion Level of Rock Bolts Exposed to Aggressive Environments in Nordic Road Tunnels

**Cristobal Javier Manquehual**[1] · **Pål Drevland Jakobsen**[1] · **Amund Bruland**[1]

Received: 12 February 2021 / Accepted: 14 June 2021 / Published online: 30 June 2021


## Abstract

For road tunnels in most Nordic countries, temporary rock support installed during tunnel excavation usually becomes a part of the permanent rock support. Rock bolts are the most common rock support measure in road tunnels excavated in hard rock, and their conditions over the period of tunnel operation play a significant role in the safety of these tunnels. The rock bolt types and aggressive environmental conditions considered in this research are focused on those used and observed in Norwegian and Swedish road tunnels. Findings elsewhere in similar environments are included to highlight the different kinetics of degradation. Based on the collected data, the corrosion levels in these road tunnels are comparable to those in the most polluted industrial areas. Aggressive groundwater conditions for rock bolts include a groundwater pH below four (which can be caused by sulfuric acid formation due to the oxidation of the mineral pyrite in the rock), marine groundwater, and flowing groundwater with a high concentration of dissolved oxygen. Furthermore, chloride-bearing deicing salts commonly used on roads located in cold climate regions during winter can promote corrosion in rock bolts from the tunnel room. For these environments, this research proposes a lognormal probability function to quantify the expected steel corrosion level for 25, 50, and 100 years of exposure time. The corrosion protection given by cement grouting, hot-dip galvanizing and epoxy coating are also addressed to explore their contributions to the lifespan extension of rock bolts in acidic and chloride-rich environments.

**Keywords** Rock bolt · Rock support tunnel · Durability · Corrosion · Probability of failure

## List of Symbols

| | |
|---|---|
| $b$ | Empirical constant related to the penetration rate of an acidic solution in cement grout (mm/year$^{0.5}$) |
| $b_e$ | Environmental transfer, which considers the influence of $T_{real}$ on the apparent diffusion coefficient (K) |
| $C(x_c, t)$ | Chloride content in grout mortar by weight of cement at depth $x_c$ and elapsed time $t$ (wt% cement) |
| $C_s$ | Initial chloride loading concentration at the rock–grout interface (wt% cement) |
| $d$ | Degradation depth in the grout mortar by acidic solution attack (mm) |
| $D_{app}\ (t,T_{real})$ | Apparent coefficient of chloride diffusion through the grout mortar after elapsed times $t$ and $T_{real}$ (m$^2$/s) |
| $D_{app\_28}$ | Theoretical coefficient of chloride diffusion after 28 days |
| $D_{paint}$ | Years of protection by direct application of the epoxy coating on carbon steel |
| $D_{zinc}$ | Years of protection by hot-dip galvanizing on carbon steel |
| $i$ | Ranking position of an observed value once the set sample has been sorted from the lowest to the highest values |
| $K$ | Synergistic factor for carbon steel protection by the duplex protection system of hot-dip galvanizing and epoxy coating |
| $k$ | Corrosion rate of metals in the first year (μm/year) |
| $n$ | Metal-environment time exponent parameter for corrosion rate |
| $N$ | Sample size of random observations |

✉ Cristobal Javier Manquehual
cristobal.j.manquehual@ntnu.no

[1] Department of Civil and Environmental Engineering, Norwegian University of Science and Technology, Høgskoleringen 7A, 7034 Trondheim, Norway

| | |
|---|---|
| $N(\mu; \sigma)$ | Normal distribution with mean μ and standard deviation σ |
| $t$ | Time elapsed (year) |
| $t_o$ | Reference time for the known value of the apparent coefficient of chloride diffusion; as the reference chloride diffusion is taken after 28 days, $t_o$ is 0.077 (year) |
| $T_{real}$ | Representative long-term cement grout temperature (°C) |
| $w/c$ | Water-cement ratio in grout mortar |
| $x_c$ | Distance from the borehole contour to the rock bolt surface (annulus grout thickness) (mm) |
| $\alpha$ | Aging exponent of the apparent chloride diffusion coefficient |

## 1 Introduction

Rock bolts can be used in underground structures as rock support for several purposes. In hard rock with low to moderate in situ stresses, rock bolts hold loose blocks and contribute to increasing the rock mass stiffness (Bobet 2009). In hard rock with high in situ stresses, rock bolts prevent failed rock from disintegrating if they are able to absorb the kinetic energy of the ejected rock (Li 2017a). In highly stressed soft rock, rock bolts deform with the rock mass until an equilibrium is reached and deformation ceases (Li 2017a). Regardless of the reason for utilizing rock bolts in underground structures, they are usually made of carbon steel and are therefore susceptible to corrosion. This chemical process causes steel to lose its cross-sectional area and form corrosion products on its surface due to interactions with the environment. Consequently, corrosion can reduce the strength capacity of rock bolts and diminish the bond strength with the surrounding material over time (Xia et al. 2013; Dorion and Hadjigeorgiou 2014). The rate at which this rock bolt corrosion proceeds depends on the chemical composition of the steel, the type of anchorage system, the type of corrosion protection, the quality control during installation, the environmental conditions where they are exposed and any increase in stress demand caused by the rock mass over time (Hadjigeorgiou et al. 2020).

The consequence of corrosion on rock bolts with a higher probability of failure over time can be visualized in Fig. 1. This figure shows the general principles of the probabilistic limit-state approach for the durability design of structures according to the standard ISO 13823 2008. In this approach,

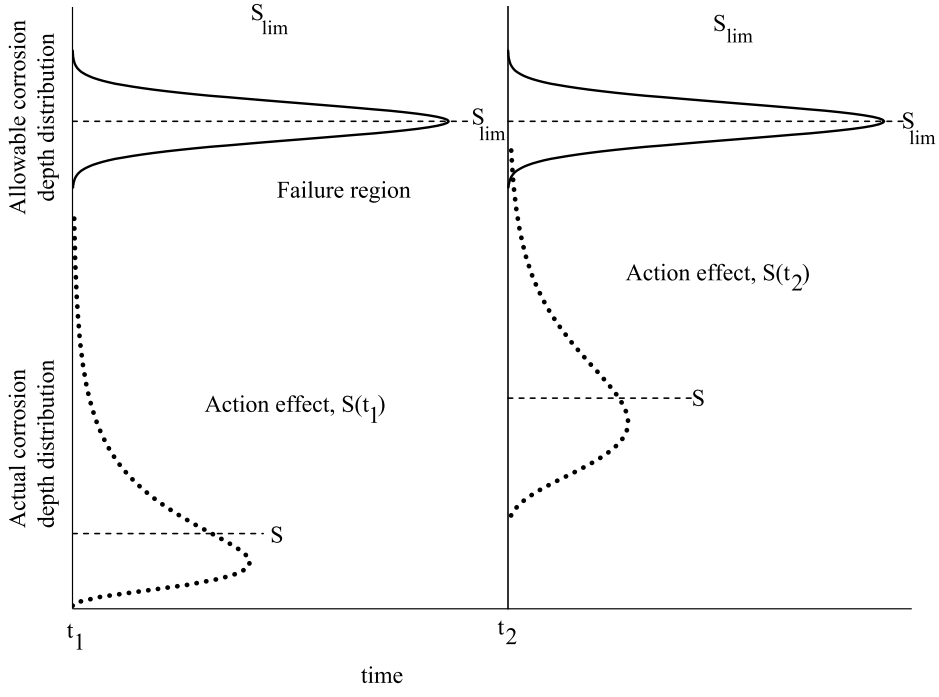


**Fig. 1** Probabilistic limit-state approach for predicting the useful life applied to rock bolt corrosion. Modified from standard ISO 13823 (2008)

an appropriate probability distribution is assigned to both the allowable corrosion depth $S_{lim}$ and the action effect $S$ for a specific exposure time. In this context, corrosion increases the probability of failure once the probability distribution curve of the action effect increases to such a level that it starts to overlap with the allowable corrosion depth curve. This failure region, highlighted as the shaded area in Fig. 1, is related to the probability of failure. For simplicity, Fig. 1 does not show changes in the allowable depth distribution over time. However, time-dependent geohazards, such as swelling or squeezing, aggravate the situation with an increasing load exerted by the rock mass over time (Stille and Palmström 2018).

The role of rock bolts as rock support in road tunnels is critical in not only Norway, but also Sweden, Finland, Iceland and the Faroe Islands. These tunnels, in comparison to those in many other countries, do not consider in principle a thick inner lining of cast-in-place concrete. If water and frost protection are needed, an inner lining detached from the rock support is installed. This slender inner lining is held by fixation bolts anchored directly to the rock mass (Broch et al. 2002). Figure 2 aims to show this layout solution with an inner lining of precast concrete segments typically used in Norwegian road tunnels with high traffic volume. In addition, some environmental parameters are indicated in the same figure.

Figure 2 shows the key role of temporary (and permanent) rock support in the safety of road tunnels with this layout. It also describes some atmospheric and aqueous environmental parameters that may affect the longevity of rock bolts. In current Norwegian regulations, the useful life of permanent rock support must be 100 years regardless of the actual

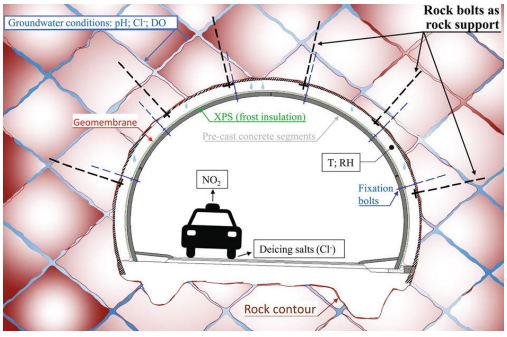


**Fig. 2** Pre-accepted solution in Norwegian road tunnels with an inner lining modified from NPRA (2016a). The following atmospheric parameters are also included: temperature (T), relative humidity (RH) and nitrogen dioxide ($NO_2$). In groundwater: pH, chloride content ($Cl^-$) and dissolved oxygen concentration (DO)

environmental conditions (NPRA 2016a). As a comparison, in Sweden, the Swedish Transport Administration (2016) stipulates a useful life requirement of 120 years for rock support systems.

The determination of the useful life of rock bolts by a probabilistic modeling requires a probability distribution for the action effect $S$, a probability distribution for the allowable corrosion depth $S_{lim}$ and a target probability of failure. The basis of the structural design in the European standard EN 1990:2002 differentiates the structures by reliability classes according to the consequences of failure. In this ranking, the consequences classes CC1, CC2 and CC3 represent low, medium, and high failure consequences respectively and are linked to the reliability classes RC1, RC2 and RC3. Later, the model code for service life design (fib 2006) specified reference values of the probability of failure for the different reliability classes. In particular, for the ultimate limit state in reliability class RC2, a failure probability value on the order of $10^{-5}$ is recommended, while for reliability class RC3, a failure probability value on the order of $10^{-6}$ is recommended. More recently, Stille and Palmström (2018) suggested placing low to medium traffic tunnels within consequence class CC2, and heavy traffic tunnels in consequence class CC3. Then, it is possible to say that the available literature provides target failure probabilities.

In regard to modeling the action effect of corrosion in rock bolts, the situation is different. Although there has been research presented on rock bolt conditions in the field and the kinetics of degradation studies in the laboratory, there has been insufficient progress in the literature to systematize the different findings and quantitatively improve the long-term design of rock bolts.

Classification systems aiming to rank the corrosion level of rock bolts in underground structures by identifying key environmental parameters have been proposed (Li 2000; Roy et al. 2016). However, there is no link between these classification systems and expected useful lives of various types of rock bolts.

On the other hand, reference values of the useful lives of different types of rock bolts have been given in the literature (Helfrich 1989; Pells and Bertuzzi 1999). However, the characterization of the environment in which these useful lives can be achieved is not specified.

This paper first describes the aggressive environments observed in Nordic road tunnels and synthesizes the corrosion level of carbon steel in these environments. Thereafter, the resulting description of the kinetics of steel corrosion is compared with international standards to contextualize the corrosion observed. In addition, this paper aims to derive a probabilistic distribution for the action effect $S$ caused by corrosion on rock bolts in aggressive environments based on the observed kinetics. Finally, an assessment is performed for the corrosion protection of rock bolts given by cement grouting, hot-dip galvanizing,

and epoxy coating in different aggressive environments to elucidate their contribution.

### 1.1 Evolution of Specifications Aimed at Improving the Durability of Rock Bolts in Norway

Cement grouted rebar bolts were introduced before the 1970s in road tunnels (Grimstad and Pedersen 1986). Practitioners in the early 1970s already agreed that rock bolts should be embedded in cement mortar (see Fig. 3a) to be considered part of the permanent rock support (KFF 1973). At that time, the rebars used were uncoated, and generally, they were installed far behind the tunnel face and not tensioned. This means that they were passive rock bolts, being the working load immediately after installation negligible. Thus, their full-strength capacity was available for long-term support.

Galvanized bolts have been used for corrosion protection in Norway since 1970 (Martinussen 2008). In the first Standard Code of Process (NPRA 1981), each rebar bolt was required to be fully grouted and galvanized (80 µm thickness). However, concerns about the eventual corrosion of zinc under the alkaline environment provided by cement mortar motivated further changes in technical specifications. The recommendations by the Norwegian road authority in the northern region to the first national handbook stated that fully grouted bolts with hot-dip galvanized coatings can be used as permanent supports as long as either the mortar held soluble chromates or bolts were passivated with chromate compounds (NPRA Northland 1990). However, some years later, the Norwegian Labor Inspection Authority set requirements for a low content of soluble chromates to reduce allergies of workers (NPRA 1999).

The duplex protection system of hot-dip galvanizing and the epoxy coating was added as a requirement in 1992 for all rock bolts installed in very corrosive environments (NPRA 1992). Today, its use has been extended to all rock bolts installed in road tunnels, regardless of the actual environmental conditions. Notably, in recent years, the minimum average thickness of epoxy coatings has increased. Between 2012 and 2018, the thickness specifications of epoxy coatings increased from 60 µm to 85 µm (NPRA 2012, 2018). In addition, quality control measures have been introduced in the current regulations, where no single measurement shall

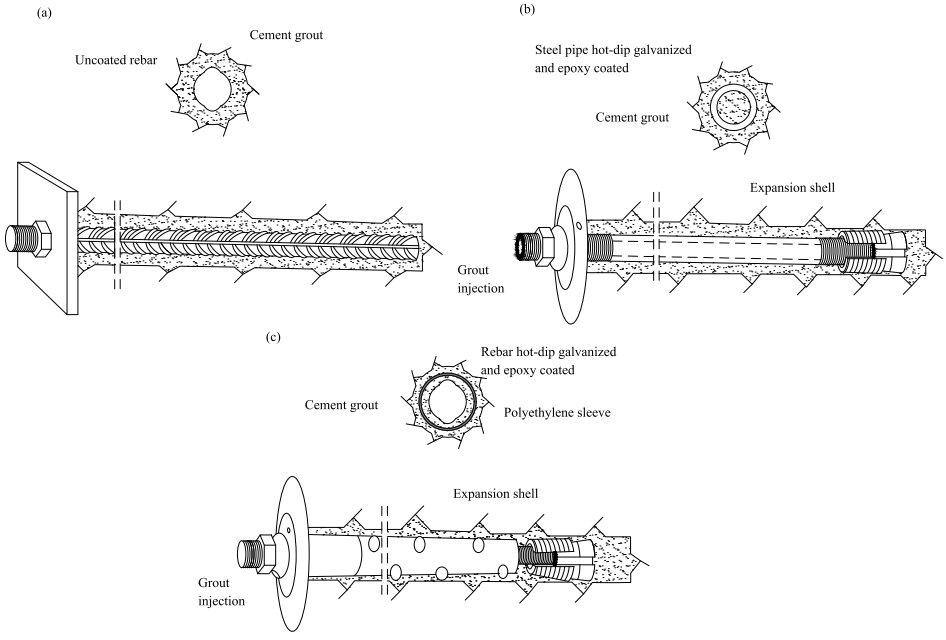


**Fig. 3** Some rock bolts used as permanent rock supports in Norwegian road tunnels. **a** Uncoated rebar cement grouted in the Haukeli road tunnel constructed between 1968 and 1969. The rebar is 20 mm in diameter and 2.4 m long (Pedersen and Hafsaas 1991). **b** Pipe bolt used in Byfjord and Mastrafjord subsea road tunnels constructed between 1989 and 1992. The 3-m-long rock bolt, steel pipe and accessories are hot-dip galvanized and epoxy coated (Espedal and Nærum 1992). **c** CT-Bolt used in the Frøya subsea road tunnel constructed between 1998 and 2000. The 3-m-long rock bolt, rebar and accessories are hot-dip galvanized and epoxy coated (Holmøy et al. 2009)

be thinner than 20 µm (NPRA 2018). Figure 3b, c show two types of rock bolts with a duplex protection system. These rock bolts are used as temporary and permanent rock supports. They are usually installed close to the tunnel face and tensioned to 30–50 kN with the expansion shell placed at the distal end of the rock bolt (NPRA 1999). At a later stage, they are postgrouted. Taking into account that the ultimate tensile strength of pipe bolts (Fig. 3b) is on the order of 130 kN, while that for a CT bolt (Fig. 3c) is 150 kN, the initial working stresses in these rock bolts are in the range of 20–40% with respect to their ultimate tensile strength. Furthermore, these rock bolts will undergo additional loads if installed near the tunnel face due to the remaining stresses in the rock mass that are not released until the tunnel face has advanced further ahead. Thus, the pre-tensioning and the installation near the tunnel face make pipe and CT rock bolts lose a fraction of their long-term strength capacity. In turn, this loss limits the allowable corrosion that they can undergo.

## 2 Aggressive Environmental Conditions

Several approaches have been proposed in the literature regarding the selection of relevant environmental parameters to explain the corrosion level in metals, such as the German standard DIN 50 929 part 3 (1985). There are also specific efforts to identify key environmental parameters affecting the corrosion of rock bolts (Li 2000; Roy et al. 2016). These three references coincide in the following water properties as relevant:

- pH
- Salinity (according to either the $Cl^-$ and $SO_4^{2-}$ content, electrical resistivity, or total dissolved solids in groundwater)
- Concentration of dissolved oxygen

Regarding the pH in groundwater, the three just-mentioned references agree that a pH of water below four is an important water property to promote corrosion. In Norway, such a low pH level has been measured in tunnels excavated in alum shale rock (NPRA 2016b). This rock contains the mineral pyrite ($FeS_2$), which under the presence of oxygen and water, it oxidizes creating sulfuric acid. Water samples in tunnels excavated in alum shale have measured pH values between two and three, and sulfate ion concentrations between 300 and 3000 mg/l (Hagelia 2018).

A high chloride content has been identified in the groundwater of subsea tunnels. The results of 40 water samples from different subsea tunnels indicate that the chloride concentration range is between 1000 mg/l and 50,200 mg/l, with an average close to 19,000 mg/l (Hagelia 2008). With this concentration level, subsea tunnels fall into the highest salinity level in all the rankings mentioned.

The occurrence of high concentrations of dissolved oxygen is expected in Nordic underground structures due to a general low groundwater temperature (< 7 °C) (Kløve et al. 2017). Although dissolved oxygen content in groundwater generally decreases with depth, high concentrations can be found at deep depths if the aquifer is permeable and connected to a brook (Seither et al. 2012). Thus, Nordic underground structures with permeable rock and low overburden are susceptible to have groundwater with high concentrations of dissolved oxygen.

### 2.1 Specific Atmospheric Environmental Conditions in Road Tunnels

Chlorides contained in deicing salts for roads are usually used in cold climate regions. The effect of traffic volume on chloride dispersion in road tunnels has been described in durability studies of sprayed concrete used for rock support. Studies on the measurement of salt deposition on the outer surface of sprayed concrete layers show that high salt concentrations have been systematically found on tunnel walls within the first ~ 2 m from the road level (Davik 1997). Above 2 m, chloride ion deposition remains high only in road tunnels with high traffic volume (Hagelia 2018).

With regard to relative humidity, Knudsen (2015) highlights the humid environment observed in Norwegian road tunnels, especially behind water and frost protection linings, where it can be close to 100%.

High concentrations of pollutants, particularly emitted by vehicles, exist in road tunnels (NILU 1990; Indrehus and Vassbotn 2001). $NO_2$ gas has been described as a moderate atmospheric corrosive agent for steel (iron) and zinc (Castaño et al. 2007; Leygraf et al. 2016). Research in road tunnels in Sweden has downgraded the influence of $NO_2$ gas on corrosion (Andersson and Sandberg 2003). This is because pollutants are ubiquitous in the air, yet significant differences in corrosion rate have been observed in the sides of flat metal sheets along the roads; the corrosion rate is much higher for the metal sheets facing the traffic.

Figure 4 shows the case of a rock bolt whose accessories and the protruding end of the rebar are corroded.

## 3 Probability Distribution of the Actual Corrosion Depth in Steel

Both uniform and localized (pitting) corrosion have been described in rock bolts installed in underground structures. Figure 5 summarizes the highest corrosion levels of carbon steel reported in nine underground structures in Nordic countries. Further details about these underground structures are

described in Table 1. Figure 5 shows 11 corrosion observations because in two underground structures, corrosion measurements took place in two different years. The collected data come from mainly rebars with grout defects and rock bolt ends protruding from the tunnel contour. Apart from examples from Norwegian and Swedish road tunnels, some other corrosion data from underground structures are given to complement the scarce long-term exposure data found in road tunnels.

International standards NS-EN ISO 9224 (2012) and NS-EN-ISO-9223 (2012) provide guiding values for the uniform corrosivity level that metals can undergo depending on the atmosphere to which they are exposed. In these international standards, the highest corrosivity category is the so-called extreme corrosivity level CX, which is related to the most polluted industrial areas. Eq. 1 provides the general corrosion rate prognosis in metals given in international standards as follows:

$$D = k \cdot t^{n} \ (\mu\text{m}). \tag{1}$$

In particular, for carbon steel exposed to the extreme corrosivity level CX, the parameter $k$ varies between 200 and 700 µm/year. The parameter $n$, which is usually less than 1, may be related to the inhibition of substrate corrosion by the growing oxide film on the surface over time. For carbon steel, the average value of parameter $n$ is 0.52. The use of these values in Eq. (1) are plotted in Fig. 5 to represent the most severe corrosivity category given in international standards as a comparison to the corrosion observed in Nordic underground structures.

The kinetics of pitting corrosion has been described in steel buried in soils by Romanoff (1957) and Melchers and Petersen (2018) via Eq. (1). For pitting corrosion, while the parameter $n$ varies between 0.44 and 0.58, the parameter $k$ varies between 732 and 843 µm/year.

Based on these reference values, the time-exponent parameter $n$ between uniform and localized corrosion is similar. With regard to the first-year corrosion rate $k$, pitting corrosion provides values similar to the upper bound of the extreme corrosivity level CX. The similarity in magnitude between uniform and localized corrosion has also been reported by Andersson and Sandberg (2003) during the

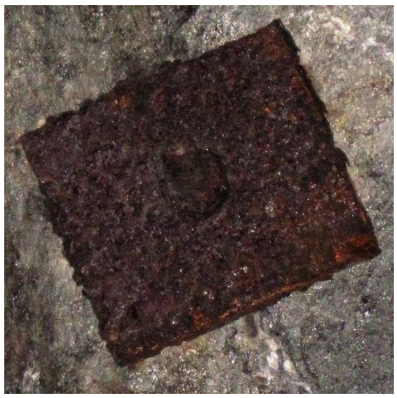

**Fig. 4** Fully grouted uncoated rebar with unprotected steel accessories in the Hamregjøl tunnel after 47 years in service (Ongstad 2012)

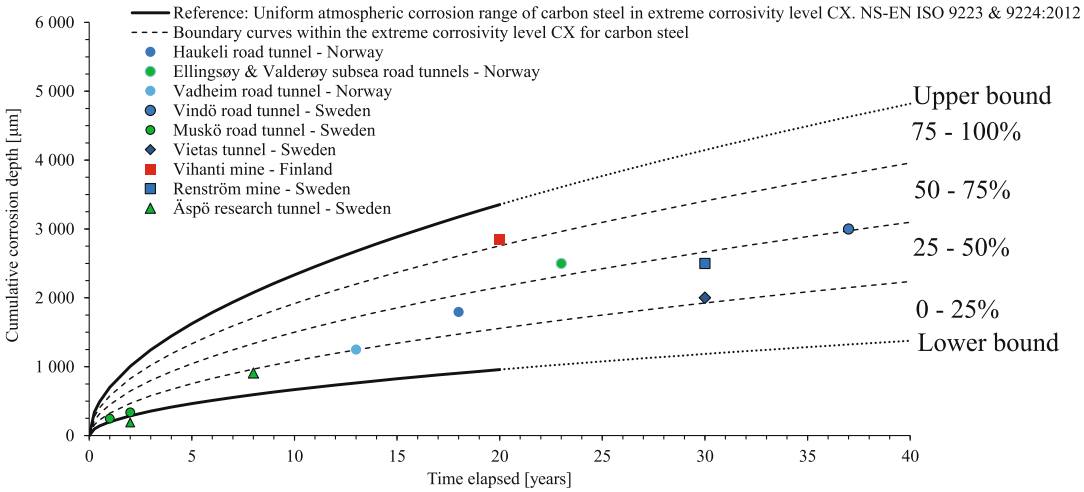


**Fig. 5** Long-term collection of corrosion progression on carbon steel in different underground structures. Blue and light blue dots reflect dripping/flowing water as the presumably predominant corrosion environment. Green dots represent chloride-rich groundwater. Red dot reflects a sulfide-rich environment with presumably low pH

**Table 1** Collected field investigations on carbon steel exposed to aggressive environments in underground structures

| Underground structure | Years of service before analysis | Investigation technique | Environmental conditions | Comment |
|---|---|---|---|---|
| Haukeli road tunnel, Norway. (Grimstad and Pedersen 1986) | 18 | Overcoring | Dripping groundwater conditions<br>pH ≈ 7.8<br>Chlorides ≈ 2.1 mg/l | Only 2 out of 19 rock bolts (≈ 10%) were not indeed fully encapsulated by mortar and underwent more severe corrosion |
| Vindö road tunnel, Sweden (Andersson and Sandberg 2003) | 37 | Rock bolt remainders after blasting during refurbishment | Local dripping groundwater<br>Chlorides ≈ 30 mg/l | Only 62 out of 1400 rock bolts (≈ 4%) showed measurable corrosion attack, occurring within 0.4 m from the bolt head |
| Äspö Research tunnel, Sweden (Sederholm and Reuterswärd 2013; Sederholm and Pahverk 2019) | 2 and 8 | Rock bolts placed in predrilled boreholes with their central stretch embedded in cement grout and both ends exposed | Chlorides > 5,000 mg/l<br>pH ≈ 7.2<br>Stagnant groundwater | Pitting corrosion observed toward tunnel room; no corrosion observed in central stretch embedded in cement grout |
| Vadheim road tunnel, Norway. (Grimstad and Pedersen 1986) | 13 | Overcoring | Presumably neither acidic nor saline groundwater | Pitting corrosion in uncoated bolt head protruding from the rock contour |
| Valderøy and Ellingsøy subsea road tunnels, Norway (Ongstad 2012) | 23 | Visual inspection | Marine groundwater<br>(Chloride rich) pH 6.0 | Corrosion on hot-dip galvanized bolt head and accessories |
| Muskö road tunnel, Sweden (Sederholm and Reuterswärd 2013) | 1 and 2 | Rock bolts left in predrilled boreholes | Chlorides > 3,500 mg/l<br>pH ≈ 7.8<br>Stagnant water | Cast-in bolts with their both ends ungrouted |
| Vietas tunnel, Sweden (Li 2000) | 30 | Corrosion observation of steel rods | Dripping water<br>Dissolved oxygen ≈ 4 mg/l<br>pH ≈ 8<br>Conductivity ≈ 100 µS/cm | Steel rod exposed to dripping water |
| Vihanti mine, Finland (Sundholm and Forsen 1995) | 20 | Overcoring | Sulfide rich deposits with presumably very acidic groundwater | Corrosion occurred in steel rebars with grout defects, mainly near the bolt head (9 observations in 5 rock bolts) |
| Renström mine, Sweden (Li 2000) | 30 | Corrosion observation of steel mesh | Dripping water<br>Dissolved oxygen ≈ 2.4 mg/l<br>pH ≈ 8<br>Conductivity ≈ 1,350 µS/cm | |

refurbishment of the Swedish road tunnel Vindö. This indicates a general blunt metal-loss defect in carbon steel over time, allowing uniform and localized corrosion observations to be plotted in a single chart.

Figure 5 shows that 10 out of the 11 long-term corrosion observations on carbon steel are within the range established for the extreme corrosivity level CX. This is equivalent to an approximately 91% confidence level for the corrosion observations shown in Fig. 5. This trend arises in observations from different aggressive environments, underground structures, and exposure times. Thus, this research will use this band as the expected corrosion depth range on carbon steel for longer exposure times in underground structures. Then, it is assumed that the corrosion kinetics of the carbon steel given in Eq. (1) will persist in the long-term. In addition, a confidence level of 91% will be extrapolated for longer exposure times (this corresponds to a 9% significance level for longer exposure times).

The following step is to find a suitable probability distribution. In this regard, Fig. 5 shows that most of the observations are closer to the lower bound of the extreme corrosivity level CX. To quantify this observation, three subdivisions are introduced for this corrosivity level. These subdivisions are evenly spaced for a given exposure time. The aim is to create a histogram based on the intervals shown on the right-hand side of Fig. 5 to reflect the distribution of the corrosion observations. Figure 6 shows the resulting histogram, where zero represents the lower bound and one represents the upper bound defined in Fig. 5.

Figure 6 includes the 10 corrosion observations within the extreme corrosivity level CX. The results show a higher density towards the lower bound, where seven out of the 10 observations lie below the median or 50th percentile. This suggests that a lognormal probability function might fit the corrosion observations classified for the different intervals of the extreme corrosivity level CX. In fact, the international standard NS-EN-ISO-9223 (2012) states that the corrosion rates of metals usually follow a lognormal distribution.

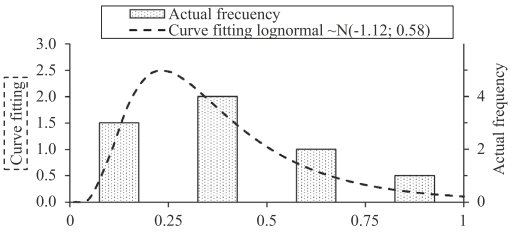


**Fig. 6** Frequency distribution for the different intervals defined in Fig. 5. In addition, a fitting curve following a lognormal distribution

The random variable to be statistically analyzed is the relative position of the cumulative corrosion depth (occurred for a certain time period) in relation to the lower and upper bounds given in Fig. 5 for the same period. The dataset varies between 0.03 and 0.79, where zero is the lower bound and one is the upper bound. One can verify whether a set of random observations $x_1, x_2, \ldots, x_N$ is lognormally distributed through a quantile–quantile plot. Once the data set has been sorted from lowest to highest, the quantile $f(x_i)$ value for a given observation $x_i$ corresponds to the fraction of observations in a data set whose values are below $x_i$. One method to calculate the corresponding quantile for each observation is through Eq. (2):

$$\frac{(i-0.5)}{N}. \tag{2}$$

Then, the lognormal quantile–quantile plot compares the inverse of the standard normal cumulative distribution of $f(x_i)$ on the horizontal axis with the natural logarithm of the corrosion observed $\ln(x_i)$ on the vertical axis. A straight trendline between these two data sets indicates a good representation of the lognormal distribution over the random observations. If this is the case, the slope of the straight trendline is the standard deviation of the lognormal distribution, while the intersection of the straight trendline with the vertical axis is the mean of the lognormal distribution. The results of the quantile–quantile plots are given in Fig. 7.

Since the sample size $N$ is 10 in Fig. 7a, each value along the horizontal axis becomes the inverse of the standard normal cumulative distributions of ten percentiles from 5 to 95% evenly spaced every 10%. Figure 7a considers the whole data set, and the statistical parameters obtained from the straight trendline can be used. However, for design purposes, it is convenient to prioritize a better calibration with the highest data values, since the latter values will control the design, as shown in Fig. 1. The principle behind this is that rock bolts with a higher corrosion rate will reach the allowable corrosion depth earlier. Therefore, Fig. 7b is introduced, and the resulting trendline gives a lognormal distribution of $\sim N(-1.12, 0.58)$. The comparison of this probability distribution with the original data set is shown in Fig. 6.

The last step to define a probability distribution for a given exposure time is to set how the 9% significance level is spread between the probability to get values above the upper bound and below the lower bound in Fig. 5. In this regard, the lognormal curve fitting shown in Fig. 6 gives a probability of 3% that the values will exceed one (where one represents the upper bound in Fig. 5); therefore, the resulting probability of obtaining values below the lower bound is 6%. These probability distributions above the upper bound and below the lower bound will be extrapolated to longer exposure times. The prognosis of actual corrosion depth in

steel at different exposure times in the described aggressive environments are given in Fig. 8.

The three exposure time curves given in Fig. 8 comply with a confidence level equal to 91% for the extreme corrosivity level CX band and the probability of exceeding its upper bound is 3%.

## 4 Useful Life Extension

Based on the aggressive environments identified in Sect. 2, particular emphasis is placed on the lifespan extension that cement grouting, hot-dip galvanizing, and epoxy coating can provide to rock bolts in chloride-rich and acidic groundwaters. The case of dissolved oxygen content is addressed in the discussion chapter.

### 4.1 Useful Life Extension by Cement Grouting

It is well known that carbon steel embedded in cement/mortar/concrete has long-term protection. One of the reasons is the high pH environment, which strongly reduces the corrosion rate of steel (establishing a stable oxide film on the steel surface). Another important factor is that cement becomes a physical barrier for corrosion-promoting agents such as oxygen, water and the aggressive ions and biota it may hold.

Passivated carbon steel at a pH value of approximately 13 gives a corrosion rate < 1 µm/year (Chitty et al. 2005). This is, of course, under ideal conditions with steel rebar embedded in nondegraded cement mortar and the absence of aggressive ions that can dissolve the oxide film on the steel surface. However, corrosive groundwater may promote a much faster corrosion rate.

#### 4.1.1 Chloride Resistance of Cement Mortar

Based on Fick's 2nd law of diffusion described by the International Federation for Structural Concrete (fib) (2006), which is given in Eq. (3), it is possible to roughly estimate the elapsed time until the onset of depassivation occurs at the bolt–grout interface due to chloride penetration in the cement mortar installed in chloride-rich groundwater.

$$C(x_c, t) = C_s\left[1 - \mathrm{erf}\left(\frac{x_c}{2 \times \sqrt{D_{app}(t,\ T_{real}) \times t}}\right)\right]. \quad (3)$$

A chloride concentration threshold value of 0.4% (wt% cement) is adopted for the start of depassivation at the bolt-grout interface following typical design values in the US and Europe for reinforced concrete (Angst et al. 2009). A $C_s$ value equal to 2.9% (wt% cement) is adopted from measured chloride profiles in uncracked sprayed concrete used for rock support in Norwegian subsea road tunnels (Hagelia 2018).

Considering a bolt borehole diameter of 45 mm and a rebar of 20 mm, the $x_c$ value is fixed to 12.5 mm.

The apparent coefficient of chloride diffusion through the grout mortar is given in Eq. (4) as follows:

$$D_{app}(t, T_{real}) = D_{app\_28}\left(\frac{t_o}{t}\right)^{\alpha} \cdot \exp\left(b_e\left(\frac{1}{293} - \frac{1}{273 + T_{real}}\right)\right). \quad (4)$$

The water cement ($w/c$) ratio for expandable cement mortar varies by supplier and user. Today, the $w/c$ ratio for expandable mortar in rock bolts is restricted to 0.44 (NPRA 2018). In this regard, it is assumed that the chloride diffusion coefficient at 28 days for this kind of mortar is well represented by CEM I Portland cement with a $w/c$ ratio between 0.4 and 0.45 following the normal

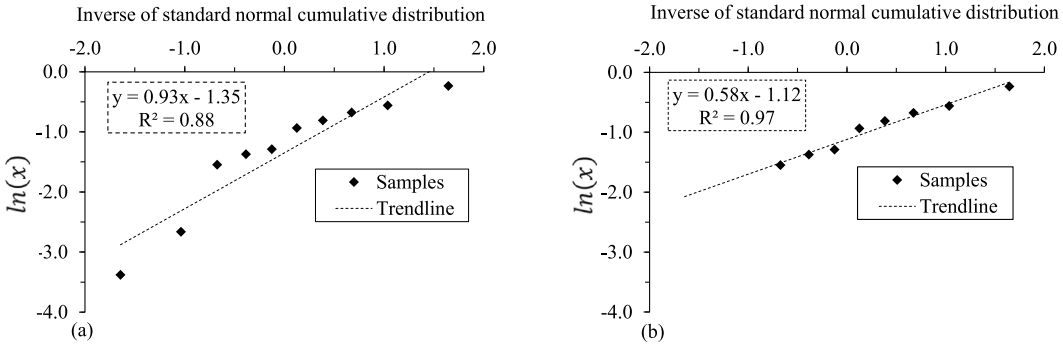


**Fig. 7** Lognormal quantile–quantile plot: **a** shows the trendline for the 10 observations plotted in Fig. 6, **b** shows a trendline for the highest 8 observed values

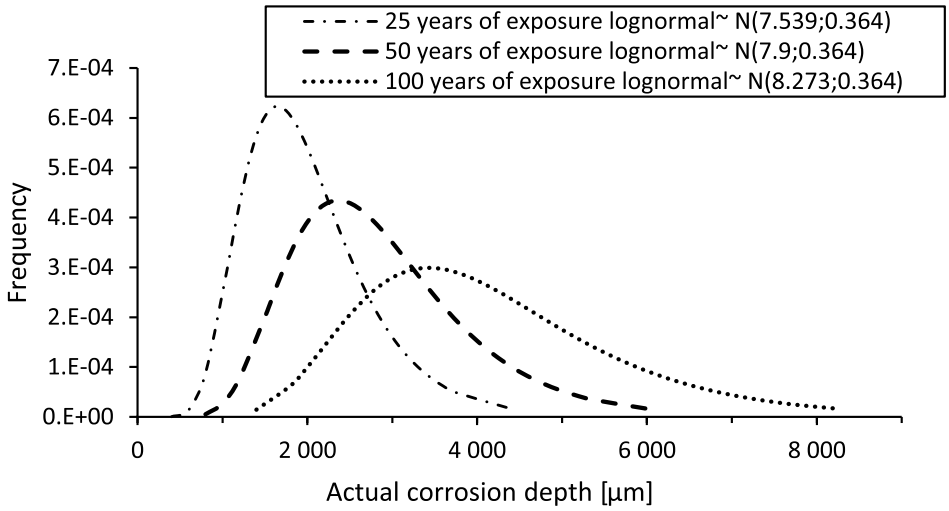


**Fig. 8** Probability distributions for the actual corrosion depth expected in carbon steel exposed to the aggressive environments described in this research for 25, 50, and 100 years

distributions of N ($8.9 \times 10^{-12}$ m$^2$/s; $1.78 \times 10^{-12}$ m$^2$/s) and ($10 \times 10^{-12}$ m$^2$/s; $2 \times 10^{-12}$ m$^2$/s) respectively, following fib (2006).

An $\alpha$ value equal to 0.3 is adopted according to fib (2006) for CEM I. The environmental transfer variable $b_e$ usually varies between 3300 and 5500 K. A value of 4800 K is adopted, as suggested by fib (2006). The temperature $T_{real}$ of cement mortar varies with geographical location, tunnel length, ventilation type, traffic volume, frost protection applied, etc. Based on a random selection of Norwegian literature about the temperature conditions in tunnels (Luke 2013; Holter and Geving 2016) a temperature $T_{real}$ equal to 7 °C was chosen. The results are given in Fig. 9.

In Fig. 9, the circles represent the predicted time for corrosion initiation. The range shown for each *w*/*c* ratio corresponds to one standard deviation from the mean of the expected chloride diffusivity value

Based on this figure, the expected useful life extension of mortar in chloride-rich groundwater is less than one year, even for a *w*/*c* ratio of 0.4. After this period, the steel starts to corrode. Then, for practical purposes, the corrosion protection of cement grout against chloride penetration is considered negligible.

#### 4.1.2 Sulfuric Acid Resistance of Cement Mortar

The pore solution in mortar has a high pH, protecting the bolt rebar. However, under acid attack, the low pH front inside the mortar will reach the bolt surface at some stage. The degraded zone in the mortar also undergoes a decalcification process (Grandclerc et al. 2018). The evolution of the dissolved calcium content in hardened cement paste was studied in samples immersed in a sulfuric acid solution. Pavlík (1994) suggests Eq. (5) for the kinetics of concrete degradation for a given concentration of an acid:

$$d = b \cdot \sqrt{t}. \tag{5}$$

A comparison of the degradation kinetics of ordinary Portland cement (OPC) mortar/concrete samples under sulfuric acid attack measured in the laboratory exposed to stagnant water (samples submerged in sulfuric acid) and flowing water (circulating acidic water in the laboratory) is given in Fig. 10.

In stagnant water, the degradation kinetics are proportional to the square root of time, as described in Eq. (5), and the degradation kinetics in flowing water are approximately linear with time. It is important to highlight as well that the sulfuric acid concentration in both cases is quite high, resulting in extremely acidic solutions (pH 1). In the same type of mortar shown in Fig. 10, Kawai et al. (2005) observed negligible degradation kinetics after 90 days with a lower sulfuric acid concentration (0.06 mol/l) and a less acidic solution (pH 2). By considering an annulus grout thickness $x_c$ equal to 12.5 mm, Fig. 10 indicates that the grout thickness may protect the rebar under flowing groundwater for only 3–5 months. In the case of stagnant acidic water, the projected lifespan extension is more than 13 years.

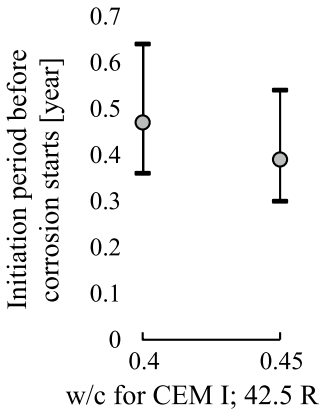


**Fig. 9** Time elapsed before a critical chloride concentration reaches the grout/steel interface

## 4.2 Useful Life Extension by Hot-Dip Galvanizing

In the literature, several benefits of using hot-dip galvanizing for steel corrosion protection are described. A summary is given as follows:

- The zinc coating acts as a barrier to oxygen and moisture, which are reactants needed for steel corrosion (Darwin et al. 2009).
- Zinc provides cathodic protection. Zinc has a lower electrochemical potential than carbon steel in the galvanic series; therefore, zinc is more active, working as a sacrificial anode (Darwin et al. 2009).
- Zinc undergoes a lower corrosion rate than iron for the same environmental condition in an approximate ratio of 1–10, respectively (NS-EN ISO 9223 2012).
- Zinc has a higher average critical chloride content for the onset of depassivation by galvanic coating in comparison to unprotected steel (Darwin et al. 2009; Pernicova et al. 2017).

The standard NS-EN ISO 9224 (2012) describes long-term uniform corrosion of zinc with Eq. (1). However, the statistical parameter $n$ is 0.813, which is close to 1. Hence, all the corrosion rate results for zinc found in the literature will be analyzed by considering a linear behavior with time.

### 4.2.1 Chloride Resistance Provided by Hot-Dip Galvanizing

Table 2 shows the results of several corrosion rate studies of hot-dip galvanized steel. Measurements were collected in the following areas:

- Flat sheet specimens made of hot-dip galvanized steel located along tunnel walls near the road level (the Söderled & Kvarnholm tunnels, Sweden)
- Hot-dip galvanized rebars left in predrilled boreholes (the Muskö and Äspö tunnels in Sweden and the Vardø tunnel in Norway)

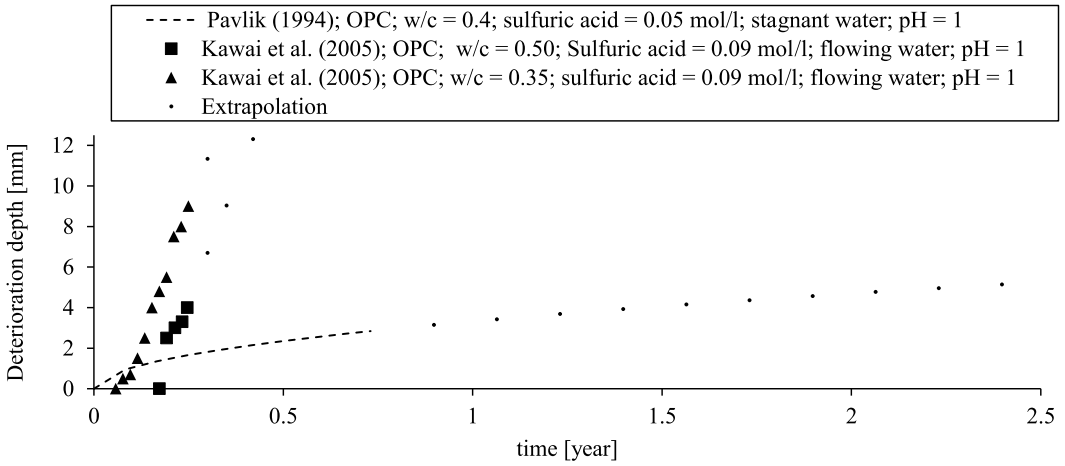


**Fig. 10** Kinetics of degradation in hardened cement paste triggered by sulfuric acid (Pavlík 1994; Kawai et al. 2005). Extrapolation dots represent deterioration depth projections not given by the original source

In addition, one case of hot-dip galvanized rebar submerged in oxygenated sea water in the laboratory is included.

The exposure to chloride given in Table 2 is due to either deicing salts, chloride-rich groundwater or sea water in the laboratory. The results in the Muskö and Äspö tunnels with chloride-rich groundwaters are provided twice. In one case, the results are related to ungrouted end rebar samples protruding from the rock contour, that is, exposed to atmospheric corrosion. Under these conditions, the corrosivity level of the rebar lies between the medium (C3) and high (C4). In the second case, the results come from the central stretch of the rebars that were grouted with cement mortar. In these conditions, the corrosivity level in both cases turned out to be extreme (CX). This is very likely due to the high pH environment triggered by the cement mortar with a very low *w*/*c* ratio of approximately 0.3. Then, the corrosion rate from the latter case should be considered with caution since the *w*/*c* ratio of the cement grout is not usually that low. As a lower bound, 9 years seems to be a more reasonable value for the lifespan extension given by hot-dip galvanizing in chloride-rich groundwater. As a reference, the average of the useful life extensions given in Table 2 is 35 years.

#### 4.2.2 Sulfuric Acid Resistance Provided by Hot-Dip Galvanizing

The comprehensive work carried out by Denison and Romanoff (1952) included the study of galvanized steel corrosion in samples buried in organic reducing acid soils. At one test site, the soil had a pH of 2.6. The exposure time of different samples in that soil varied between 2 and 13 years. Based on the weight loss of the galvanized steel, the equivalent corrosion rates exceeded 67 µm/year in all cases.

More recently, Satola and Aromaa (2004) reported corrosion rates of galvanized steel strands in pyritic rock masses. The reported groundwater pH was 2.6. The corrosion rate was on the order of 1000 µm/year. These results indicate that the contribution of hot-dip galvanizing to the lifespan extension of rock bolts is negligible in acidic environments.

### 4.3 Useful Life Extension by Duplex Protection System

In the duplex protection system, an epoxy coating is used as a topcoat after the steel is hot-dip galvanized. Organic coatings restrict the interaction of zinc with the environment. In turn, the zinc coating provides cathodic protection for the steel rebar.

Epoxy powder coating provides a good barrier against ions (Knudsen and Forsgren 2017). However, these coatings are not impermeable to oxygen and water (Sangaj and Malshe 2004). In addition, epoxy coatings are vulnerable to disbonding i.e., adhesion loss to the substrate, and aggressive ions can be transported under the disbonded coating. The exact mechanism behind the protection barrier provided by the epoxy coating to the metals is not fully understood (Sangaj and Malshe 2004). Organic coatings are a complex combination of binder, pigments, solvents, and other additives, which defines a unique epoxy resin network (Møller et al. 2017). Additionally, the epoxy coating can also undergo chemical degradation, changing its properties as a physical barrier against aggressive ions. Nevertheless, there are empirical proposals and observations that provide some insights into the corrosion protection given by epoxy coatings in chloride-rich and acidic environments.

#### 4.3.1 Chloride Resistance by the Duplex Protection System

Eijnsbergen (1994) has proposed Eq. (6) to estimate the useful life of the duplex system protection in years of outdoor exposure, considering a limit state of 5% rust on the carbon steel substrate as follows:

$$D_{\text{duplex}} = K \times \left(D_{\text{zinc}} + D_{\text{paint}}\right). \tag{6}$$

For a hot-dip galvanized coating with an average thickness of 85 µm, Eijnsbergen (1994) indicates that $D_{\text{zinc}}$ is approximately 30 years in the marine atmosphere. This is approximately the same as the average lifespan extension given in Table 2 for the same zinc thickness. However, a lower bound of 9 years, as discussed in Sect. 4.2.1, is possible.

With regard to $D_{\text{paint}}$ in Eq. (6), an epoxy coating thickness of 85 µm provides a protection of 3 years in a marine atmosphere. The factor $K$ varies between 1.5 and 2.3, and the lower bound is the proper value for the most aggressive environments.

Notably, the corresponding limit state in Eq. (6) corresponds to 5% rust on the carbon steel. This is equivalent to a corrosion depth of 500 µm around a rebar 20 mm in diameter. This corrosion depth in carbon steel may happen in 18 years, considering the duplex protection system with 85-µm-thick coating layers, and a synergistic factor $K$ equal to 1.5.

Figure 5 indicates that a corrosion depth of 500 µm in uncoated carbon steel can be achieved after approximately 4 years of exposure in marine environments. Hence, a rough estimate of the minimum lifespan extension by the duplex protection system is 14 years. This is considered the lower bound of lifespan extension by the duplex protection system.

**Table 2** Reported corrosion rates of hot-dip galvanized steel and their corresponding useful life extensions

| Place | Measured corrosion rate (μm/year) | Comments | Environmental conditions | Exposure time (year) | Corrosivity level NS-EN ISO 9223 (2012) | Useful life extension 85 μm zinc layer (year) |
|---|---|---|---|---|---|---|
| Söderled road tunnel—Sweden (Andersson and Sandberg 2003) | 1–10 | Flat sheet specimens made of hot-dip galvanized steel left on tunnel walls near the road level until 4 m above (lowest measured corrosion rate for backside of sheet specimen; highest rate for sheet specimens facing the roadway) | High traffic volume, creating dirt with high chloride content due to de-icing salt | 2 | From medium to Extreme; C3 to CX | 9–85 |
| Kvarnholm road tunnel—Sweden (Andersson and Sandberg 2003) | 0.6–2 | Flat sheet specimens made of hot-dip galvanized steel left on tunnel walls near the road level until 4 m above (lowest measured corrosion rate for backside of sheet specimen; highest rate for sheet specimens facing the roadway) | Low traffic volume, creating a low amount of dirt with low chloride content level (deicing salt) | 2 | Medium; C3 | 43–142 |
| Lab-Norway (Lange 2012) | 10 | Hot-dip galvanized rock bolts submerged | Oxygenated (8 mg/l) sea water | 0.25 | Extreme; CX | 9 |
| Both the Muskö road tunnel and the Äspö research tunnel-Sweden (Sederholm and Reuterswärd 2013; Sederholm and Pahverk 2019) | 1.6–3.2 | Ungrouted galvanized rebar samples protruding the rock surface | Chloride-rich groundwater | 2 and 8 years of exposure | From medium to high; C3 to C4 | 26–53 |
| Both Muskö road tunnel and Äspö research tunnel-Sweden (Sederholm and Reuterswärd 2013; Sederholm and Pahverk 2019) | 12.1–21.1 | Central stretch of cement grouted galvanized rebars placed inside predrilled boreholes; $w/c \approx 0.3$ (mortar) | Chloride-rich groundwater and high pH | 2 and 8 years of exposure | Extreme; CX | 4–7 |
| Vardø subsea road tunnel-Norway (Klemetsrud 2016) | ≈ 4 | Hot-dip galvanized rebars inserted into predrilled boreholes | Saline groundwater | 11 | High; C4 | 21 |

#### 4.3.2 Acid Resistance Provided by the Duplex Protection System

If the organic coating is damaged in an acidic environment, the zinc coating is exposed, and there will not be any additional protection for the surrounding epoxy coating (Knudsen and Forsgren 2017). Nevertheless, it has been reported that undamaged organic coatings can provide excellent resistance against acids (Møller et al. 2017). Khodair et al. (2019) measured the corrosion rate of mild steel with and without epoxy coating in acidic and saline environments as shown in Fig. 11.

Figure 11 clearly shows the contribution of the epoxy coating to the reduction in the corrosion rate in acidic environments. The high corrosion level observed, particularly for those measurements with exposed steel, is related to the short exposure time of only 5 h, during which time the oxide film starts to form. The performance of the epoxy-coated steel in saline and acidic solutions is also shown in Fig. 11. While the corrosion rate reduction of the epoxy-coated steel in the acidic environments is approximately 96% on average, the efficiency of the epoxy-coated steel in saline solutions is only 62%.

Popović et al. (2005) tested the corrosion behavior of mild steel with and without epoxy coating using electrochemical impedance spectroscopy (EIS) in 0.1 mol/l sulfuric acid solution. Based on the corrosion current density determined in each sample, the equivalent corrosion rate is 1150 µm/year for the exposed steel, while 149 µm/year is the equivalent corrosion rate for the epoxy-coated steel after 500 h of exposure. That is, an 87% improvement in corrosion rate reduction was achieved with the epoxy coating. This result is consistent with Fig. 11 for epoxy coating protection in acidic environments.

#### 4.3.3 Some Experience with the Duplex Protection System

Blistering of the epoxy coating in bolt accessories has been reported in subsea tunnels (Ongstad 2012). An illustration is given in Fig. 12. In some cases, steel corrosion was found behind the powder coating.

It is well known that epoxy coatings are is very sensitive to damage during handling and transportation (Manning 1996; Sagüés et al. 2010). A report described the setup of bolt corrosion research in the Oslofjord tunnel (Klemetsrud 2016), which considered painted galvanized steel bolts, observed unintended scratches and impurities in the epoxy coating after normal handling and before the test started. Research in the Muskö and Äspö tunnels also included the follow-up of epoxy-coated and hot-dip galvanized bolts. Intentional damage to the coating triggered adhesion loss of the epoxy coating after 8 years in some samples (Sederholm and Pahverk 2019). Nevertheless, duplex system coatings without preexisting damage to the rebars showed no deterioration after the same time period in the context of a chloride-rich environment.

## 5 Discussion

The parameter flowing groundwater conditions appears to be more relevant than previously considered in the classification of aqueous corrosive environments. Remarkable examples are Vietas, Haukeli, and Renström tunnels in Fig. 5, where corrosion rates meet the extreme corrosivity level CX without the groundwater having a low pH or a high salinity. In these tunnels, the steel was exposed to dripping groundwater. In this regard, the uniform corrosion rates on steel caused by flowing groundwater in some Australian mines studied by Villaescusa et al. (2007) gives corrosion rates that can be categorized as extreme corrosivity level CX. The requirement to reach this corrosivity level in these mines is flowing groundwater with a dissolved oxygen content exceeding 3 mg/l. It is important to highlight as well that the fastest kinetics of degradation in mortar immersed in sulfuric acid shown in Fig. 10 is related to flowing water. In hot-dip galvanizing, it is claimed that only 0.5 m/s is enough to remove the oxide film deposited on the zinc surface (Thomas 1978). Running water can also cause grout defects by damaging the cement grout in its plastic stage (NPRA 1999). Thus, the parameter flowing groundwater conditions is a key variable that should explicitly be mentioned in any proposed

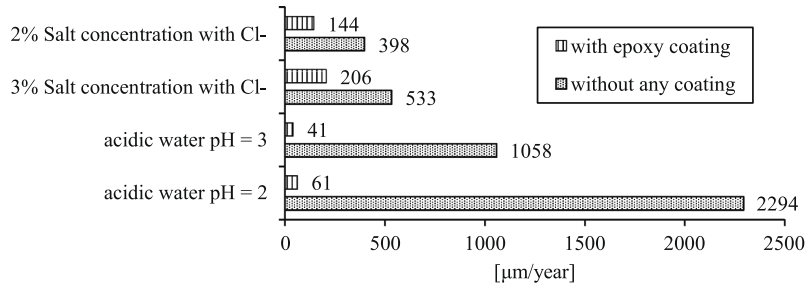


**Fig. 11** Corrosion rates of mild steel immersed in different aqueous solutions for five hours at 30 °C with and without epoxy coating (Khodair et al. 2019)

**Fig. 12** Blisters observed in the rock bolt plate in the Oslofjord subsea road tunnel after 10 years of exposure (Ongstad 2012)

classification system regarding the corrosivity level of rock bolts. Nevertheless, it is important to highlight that the variability of flowing groundwater can be restricted with pregrouting works ahead of the tunnel face.

For a given exposure time, Fig. 8 gives a probability distribution for the expected corrosion depth in steel exposed to aggressive environments. From a design point of view, an important inquiry to be addressed is how often these grout defects will coincide with the peak working stresses in the rock bolt. In wet tunnel stretches with aggressive groundwater and rock mass deformation, corrosion will very likely take place where the highest axial stresses are induced along the rock bolt, for the following reasons:

- In hard rock, groundwater flows through mainly discontinuities (Coli and Pinzani 2014).
- In hard rock, deformation is controlled by the rock mass discontinuities, which might eventually crack the cement grout as an extension of the discontinuity (Sandberg and Lagerblad 2002).
- In fully grouted rock bolts, the peak axial stress occurs in the grout defects (Li 2017b).

Hence, it is considered adequate to use the probability distributions given in Fig. 8 for cement grouted rebars installed in aggressive environments if rock mass deformation is expected. One can extend the use of Fig. 8 if grout defects by other means are foreseen in aggressive environments. Finally, Fig. 8 can also be applied for uncoated steel rebars fully grouted with cement in chloride-rich environments, even without grout defects, since the protection provided by cement mortar for the steel rebar is negligible in this environment.

For the rock bolts used today (with the duplex protection system and postgrouted), to derive a probability distribution for the long-term corrosion depth in the steel rebar or steel tube is more challenging. There is a complex interaction between the different protection elements, the steel and the different environments. In addition, the field experience is more limited than the case of cement grouted rebars. Nevertheless, the collected experiences in Sect. 4 indicate that epoxy coating and cement grouting protect better the steel rebar in acidic than in chloride-rich environments. On the other hand, hot-dip galvanizing provides higher protection in chloride-rich than in acidic environments. However, for the zinc thickness of 85 μm considered, it is inferred that the joint performance of the epoxy coating, hot-dip galvanizing, and cement grouting is better in acidic than in chloride-rich environments. Thus, a ranking from the most to the least unfavorable condition can be established for the rock bolts used today:

1. Chloride-rich environment with grout defects.
2. Chloride-rich environment without grout defects.
3. Acidic environment with grout defects.
4. Acidic environment without grout defects.

Apart from creating grout defects, deformable rock mass increases the risk of failure by inducing loads to the rock bolts. Considering that the type of rock bolts used these days are usually pretensioned and installed near the tunnel face, the extra load exerted by the rock mass limits further the allowable corrosion depth in these rock bolts. Overall, the rock bolts used today installed in subsea tunnels with expected deformation of the rock mass are of particular concern.

## 6 Conclusions

For rock bolts, the aggressive groundwater conditions identified in Nordic road tunnels are as follows:

1. Subsea tunnels with marine groundwater.
2. Groundwater with a pH below four (because of sulfuric acid formation due to the oxidation of the pyrite mineral in the rock).
3. Flowing groundwater conditions with a high concentration of dissolved oxygen.

In addition, deicing salts provide aggressive atmospheric conditions within the tunnel room. Any of these

environments might lead to the highest corrosivity level established in international standards, which is comparable to the most polluted industrial areas. Regarding the conditions described, the parameter representing the flowing groundwater conditions has not been consistently described in the literature properly and has even been overlooked in some references.

For 25, 50, and 100 years of exposure time, a probability distribution is derived for the stochastic corrosivity level of exposed steel in the described aggressive environments, taking advantage of the good fit between the corrosion observed in underground structures and the extreme corrosivity level CX described in international standards. This is considered a valuable input for the durability design of rock bolts.

The analysis on corrosion protection given by the duplex protection system and cement grouting for the rock bolts used these days indicates that those installed in subsea tunnels with deformable rock mass are of particular concern to achieve a useful life of 100 years.

**Funding** Open access funding provided by NTNU Norwegian University of Science and Technology (incl St. Olavs Hospital - Trondheim University Hospital).

## Compliance with Ethical Standards

**Conflict of interest** The authors declare that they have no conflict of interest.

**Consent for publication** All authors read and approved the final manuscript.



## References

Andersson P, Sandberg B (2003) The corrosive environment in road tunnels and investigation of rock bolts from Vindö tunnel. In: Swedish Rock Engineering research, SveBeFo. Annual Rock Mechanics meeting, Stockholm

Angst U, Elsener B, Larsen CK, Vennesland Ø (2009) Critical chloride content in reinforced concrete—a review. Cem Concr Res 39:1122–1138. https://doi.org/10.1016/j.cemconres.2009.08.006

Bobet A (2009) Elastic solution for deep tunnels. Application to excavation damage zone and rockbolt support. Rock Mech Rock Eng 42:147–174. https://doi.org/10.1007/s00603-007-0140-0

Broch E, Grøv E, Davik KI (2002) The inner lining system in Norwegian traffic tunnels. Tunn Undergr Sp Technol 17:305–314. https://doi.org/10.1016/S0886-7798(02)00026-3

Castaño JG, de la Fuente D, Morcillo M (2007) A laboratory study of the effect of $NO_2$ on the atmospheric corrosion of zinc. Atmos Environ 41:8681–8696. https://doi.org/10.1016/j.atmosenv.2007.07.022

Chitty WJ, Dillmann P, L'Hostis V, Lombard C (2005) Long-term corrosion resistance of metallic reinforcements in concrete—a study of corrosion mechanisms based on archaeological artefacts. Corros Sci 47:1555–1581. https://doi.org/10.1016/j.corsci.2004.07.032

Coli M, Pinzani A (2014) Tunnelling and hydrogeological issues: a short review of the current state of the art. Rock Mech Rock Eng 47:839–851. https://doi.org/10.1007/s00603-012-0319-x

Darwin D, Browning J, O'Reilly M et al (2009) Critical chloride corrosion threshold of galvanized reinforcing bars. ACI Mater J 106:176–183. https://doi.org/10.14359/56465

Davik KI (1997) Proper use of sprayed concrete in tunnels. Final report. In: Norwegian Public Roads Administration **(In Norwegian)**

Denison IA, Romanoff M (1952) Corrosion of Galvanized Steel in Soils. J Res Natl Bur Stand (1934)

DIN 50 929 part 3 (1985) DIN 50 929 part 3. Probability of corrosion of metalic materials when subject to corrosion from the outside—buried and underwater pipelines and structural components

Dorion JF, Hadjigeorgiou J (2014) Corrosion considerations in design and operation of rock support systems. Trans Inst Min Metall Sect A Min Technol 123:59–68. https://doi.org/10.1179/1743286313Y.0000000054

Eijnsbergen JFH (1994) Duplex Systems: Hot-dip galvanizing plus painting. Elsevier Science B.V.

EN 1990:2002 (2002) Eurocode: basis of structural design

Espedal TG, Nærum G (1992) The Rennfast Link at the Western coast of Norway with world's longest an deepest sub sea road tunnel. In: Subsea Tunnelling. Norwegian Tunnelling Society Publication 08.

fib (2006) Model code for service life design. International federation for structural concrete

Grandclerc A, Dangla P, Gueguen-Minerbe M, Chaussadent T (2018) Modelling of the sulfuric acid attack on different types of cementitious materials. Cem Concr Res 105:126–133. https://doi.org/10.1016/j.cemconres.2018.01.014

Grimstad E, Pedersen B (1986) Long time effect on resin end-anchored and cement grouted rock bolts. Preliminary experiences. In: Annual conference of the Norwegian Tunnelling Society, 1986 **(in Norwegian)**

Hadjigeorgiou J, Savguira Y, Thorpe SJ (2020) Impact of steel properties on the corrosion of expandable rock bolts. Rock Mech Rock Eng 53:705–721. https://doi.org/10.1007/s00603-019-01939-w

Hagelia P (2008) Deterioration mechanisms and durability of sprayed concrete in Norwegian tunnels. NFF Publication No. 17: underground openings—operations, maintenance and repair

Hagelia P (2018) Durability development for sprayed concrete as rock support in different tunnel environments. Norwegian Public Roads Administration. Report No. 566

Hassell RC, Kinsela B, Villaescusa E (2004) Corrosion assessment of ground support systems. In: Villaescusa E, Potvin Y (eds) Fifth international symposium on ground support, ground support in mining and underground construction, 28–30 September, Perth, Australia. Balkema, Rotterdam, pp 529–544

Helfrich HK (1989) The durability of rockbolts. Follow-up of rockbolts, belonging to different type and age, at the sandstone mine of Kvarntorp, central Sweden. Annual rock mechanics meeting in Stockolm

Holmøy KH, Lien JE, Palmstrøm A (2009) The Frøya tunnel—going subsea on the brink of the continental shelf. In: NFF Publication No. 18: Subsea Tunnels

Holter KG, Geving S (2016) Moisture transport through sprayed concrete tunnel linings. Springer, Vienna

Indrehus O, Vassbotn P (2001) CO and NO2 pollution in a long two-way traffic road tunnel: investigation of NO2/NOx ratio and modelling of NO2 concentration. J Environ Monit 3:221–225. https://doi.org/10.1039/b009493p

ISO 13823 (2008) General principles on the design of structures for durability

Kawai K, Yamaji S, Shinmi T (2005) Concrete deterioration caused by sulfuric acid attack. Durab Build Mater 20:5–9

KFF (1973) Practical handbook in rock bolting. Royal Norwegian Council for Scientific and Industrial Research. Office for Rock Blasting Technique **(in Norwegian)**

Khodair ZT, Khadom AA, Jasim HA (2019) Corrosion protection of mild steel in different aqueous media via epoxy/nanomaterial coating: preparation, characterization and mathematical views. J Mater Res Technol 8:424–435. https://doi.org/10.1016/j.jmrt.2018.03.003

Klemetsrud K (2016) Corrosion test on rock bolts in the Oslo-fjord tunnel. Norwegian Public Roads Administration. Report No. 466 **(in Norwegian)**

Kløve B, Kvitsand HML, Pitkänen T et al (2017) Aperçu des ressources en eau souterraine et des systèmes d'approvisionnement en eau, et pollution microbienne associée, en Finlande, Norvège et Islande. Hydrogeol J 25:1033–1044. https://doi.org/10.1007/s10040-017-1552-x

Knudsen OØ (2015) Corrosion protection in tunnels. Norwegian Public Roads Administration. Report No. 410 **(in Norwegian)**

Knudsen OØ, Forsgren A (2017) Corrosion control through organic coatings. Taylor & Francis Group, New York

Lange T (2012) Bolts for rock support—laboratory tests of corrosion protection. Norwegian Public Roads Administration. Report No. 97 **(in Norwegian)**

Leygraf C, Wallinder IO, Tidblad J, Graedel T (2016) Atmospheric corrosion, 2nd edn. Wiley, New York

Li CC (2000) Durability of rock bolts—verification of two classification systems with regard to the corrosivity of environments. In: Swedish Rock Engineering research, SveBeFo.Report 46

Li CC (2017a) Principles of rockbolting design. J Rock Mech Geotech Eng 9:396–414. https://doi.org/10.1016/j.jrmge.2017.04.002

Li CC (2017b) Rockbolting: principles and applications

Luke J (2013) Survey of environmental conditions in tunnels. The Hell tunnel, the Ekeberg tunnel and the Smestad tunnel

Manning DG (1996) Corrosion performance of epoxy-coated reinforcing steel: North American experience. Constr Build Mater 10:349–365. https://doi.org/10.1016/0950-0618(95)00028-3

Martinussen A (2008) Degradation of earlier reinforcement and support. In: NFF Publication No. 17: Underground openings—operations, maintenance and repair, pp 35–37

Melchers RE, Petersen RB (2018) A reinterpretation of the Romanoff NBS data for corrosion of steels in soils. Corros Eng Sci Technol 53:131–140. https://doi.org/10.1080/1478422X.2017.1417072

Møller VB, Dam-Johansen K, Frankær SM, Kiil S (2017) Acid-resistant organic coatings for the chemical industry: a review. J Coat Technol Res 14:279–306. https://doi.org/10.1007/s11998-016-9905-2

NILU (1990) Tromsøysundet Tunnel: asessment of air pollution. Norwegian Institute for Air Research

NPRA Northland (1990) Norms about road tunnels. Recommendations to the handbook 021

NPRA (1981) Handbook 025: Standard Code of Process 1: Roadworks. Norwegian Public Roads Administration, Main Process 7: completion and special works **(in Norwegian)**

NPRA (1992) Handbook 021: Road Tunnels. Norwegian Public Roads Administration **(in Norwegian)**

NPRA (1999) Rock bolt handbook 215. Norwegian Public Roads Administration **(in Norwegian)**

NPRA (2012) Handbook R761 Standard Code of Process 1: road contracts. Norwegian Public Roads Administration, Main Process 3: Tunnels (in Norwegian).

NPRA (2016a) Handbook N500: road tunnels. Norwegian Public Roads Administration **(in Norwegian)**

NPRA (2016b) Environmental loads in road tunnels. Norwegian Public Roads Administration. Report No. 577 **(in Norwegian)**

NPRA (2016c) Best practice for tunnel lining. Norwegian Public Roads Administration. Report No. 510 **(in Norwegian)**

NPRA (2018) Handbook R761 Standard Code of Process 1: road contracts. Norwegian Public Roads Administration, Main Process 3: Tunnels **(in Norwegian)**

NS-EN ISO 9223 (2012) Corrosion of metals and alloys. Corrosivity of atmospheres. Classification, determination and estimation, 2012

NS-EN ISO 9224 (2012) Corrosion of metals and alloys. Corrosivity of atmospheres. Guiding values for the corrosivity categories. Standard Norge

NS-EN-ISO-9223 (2012) Corrosion of metals and alloys. Corrosivity of atmospheres. Classification, determination and estimation. Standard Norge

Ongstad A (2012) Useful life of rock bolts. Norwegian Public Roads Administration. Major research and development project: modern road tunnels 2008–2011. Report No. 164

Pavlík V (1994) Corrosion of hardened cement paste by acetic and nitric acids part I: calculation of corrosion depth. Cem Concr Res 24:551–562. https://doi.org/10.1016/0008-8846(94)90144-9

Pedersen KB, Hafsaas G (1991) Overcoring and quality control of rock bolts. In: Annual conference of theNorwegian Tunnelling Society (in Norwegian)

Pells P, Bertuzzi R (1999) Permanent rockbolts—the problems are in the detail. In: Tenth Australian tunnelling conference. Melbourne, Vic, 21–24 March 1999

Pernicova R, Dobias D, Pokorny P (2017) Problems connected with use of hot-dip galvanized reinforcement in concrete elements. Proced Eng 172:859–866. https://doi.org/10.1016/j.proeng.2017.02.086

Popović MM, Grgur BN, Mišković-Stanković VB (2005) Corrosion studies on electrochemically deposited PANI and PANI/epoxy coatings on mild steel in acid sulfate solution. Prog Org Coat 52:359–365. https://doi.org/10.1016/j.porgcoat.2004.05.009

Romanoff M (1957) Underground Corrosion. U.S. Department of Commerce. National Bureau of Standards. Circular 579

Roy JM, Preston R, Bewick RP (2016) Classification of aqueous corrosion in underground mines. Rock Mech Rock Eng 49:3387–3391. https://doi.org/10.1007/s00603-016-0926-z

Sagüés AA, Lau K, Powers RG, Kessler RJ (2010) Corrosion of epoxy-coated rebar in marine bridges—Part 1: a 30-year perspective. Corrosion 66:0650011–06500113

Sandberg B, Lagerblad B (2002) Durability of cement grouted rock bolts. Swedish Rock Engineering research, SveBeFo

Sangaj NS, Malshe VC (2004) Permeability of polymers in protective organic coatings. Prog Org Coat 50:28–39. https://doi.org/10.1016/j.porgcoat.2003.09.015

Satola I, Aromaa J (2004) The corrosion of rock bolts and cable bolts. In: Ground support in mining and underground construction—Villaescusa & Potvin

Sederholm B, Pahverk H (2019) Corrosion testing of different types rock bolts in tunnels—long time exposure. In: Befo. Report 193 **(in Swedish)**

Sederholm B, Reuterswärd P (2013) Corrosion testing of different types of rock bolts. In: Befo. Rock Engineering Research Foundation. Report 127 **(in Swedish)**

Seither A, Eide PE, Berg T, Frengstad B (2012) The inorganic drinking water quality of some groundwater works and regulated wells in Norway. Geological Survey of Norway, NGU

Stille H, Palmström A (2018) Practical use of the concept of geotechnical categories in rock engineering. Tunn Undergr Sp Technol 79:1–11. https://doi.org/10.1016/j.tust.2018.04.035

Sundholm S, Forsen O (1995) Corrosion tests on cement grouted bolt. In: Annual conference of the Swedish Rock Engineering Research, SvebeFo

Swedish Transport Administration (2016) Tunnel construction requirements. Trafikverket **(in Swedish)**

Thomas R (1978) Hot-dip galvanizing. Nordic Galvanizing Association, Oslo **(in Norwegian)**

Villaescusa E, Hassell R, Thompson A (2007) Corrosion of rock reinforcement in underground excavations. Minerals and Energy Research Institute of Western Australia. Report No. 263

Xia N, Liang RY, Payer J, Patnaik A (2013) Probabilistic modelling of the bond deterioration of fully-grouted rock bolts subject to spatiotemporally stochastic corrosion. Struct Infrastruct Eng 9:1161–1176. https://doi.org/10.1080/15732479.2012.670649

**PAPER II**

**Title:** Comparison of the condition of steel fiber-reinforced shotcrete with water-glass and alkali-free activators after more than 20 years of service in a subsea road tunnel (2022)

**Authors:**
Manquehual, Cristobal Javier
Jakobsen, Pål Drevland
Holter, Karl Gunnar
De Weerdt, Klaartje
Danner, Tobias
Bruland, Amund

**Published in:**
Construction and Building Materials journal Volume 328, 18 April 2022

Construction and Building Materials 328 (2022) 127090

Contents lists available at ScienceDirect

Construction and Building Materials

journal homepage: www.elsevier.com/locate/conbuildmat

# Comparison of the condition of steel fiber-reinforced shotcrete with water-glass and alkali-free activators after more than 20 years of service in a subsea road tunnel

Cristobal Javier Manquehual [a,*], Pål Drevland Jakobsen [a], Karl Gunnar Holter [b], Klaartje De Weerdt [c], Tobias Danner [d], Amund Bruland [a]

[a] Department of Civil and Environmental Engineering, Norwegian University of Science and Technology (NTNU), Trondheim, Norway
[b] Norwegian Geotechnical Institute (NGI), Oslo, Norway
[c] Department of Structural Engineering, Norwegian University of Science and Technology (NTNU), Trondheim, Norway
[d] SINTEF Community, Architecture, Materials and Structures, Trondheim, Norway

ARTICLE INFO

*Keywords:*
XRD
μ-XRF
Sprayed concrete
Sulfur
Leaching
Chloride

ABSTRACT

The in-service condition of steel fiber-reinforced shotcrete installed more than 20 years ago as single-shell rock support lining in the Nordkapp subsea road tunnel was investigated. The novelty of this study is the comparison of shotcrete with water–glass and alkali-free activators in a saline groundwater environment. The lowest shotcrete density was obtained at joints between two adjacent shotcrete layers. In the case of alkali-free accelerator, ettringite enrichment was observed in these joints. Leaching appeared to be the main degradation mechanism in the outermost 10–15 cm towards the traffic room.

## 1. Introduction

Shotcrete is the standard method for permanent rock support in hard rock tunnels in Norway in combination of rock bolts [1]. The durability of shotcrete as a rock support element in these tunnels is crucial, as an inner lining of cast-in-place concrete is not usually installed, unless the geological conditions are extremely poor. A similar approach has been adopted in road tunnels constructed in Sweden and Finland [2].

The wet-mix shotcrete method was introduced for the first time in Norway in the early 1970s, but it took around a decade to be extensively used after it underwent several technological improvements. Among its innovations in the 1970s, one can highlight the shotcrete application using robots, the introduction of steel fibers in replacement of traditional wire meshes, the use of silica fume as an additive and the introduction of plasticizers in the mix [3]. Since the mid-1980 s, the steel fiber reinforced micro-silica wet-mix shotcrete method has completely dominated the shotcrete consumption in underground works in Norway [4]. Nowadays, the wet-mix spraying is the dominant method worldwide when it comes to spraying concrete [5].

A set accelerating agent is added to shotcrete in order to increase the hydration rate of the cement, achieving a higher early strength in the concrete sprayed and shortening its setting time [6]. Until mid-1990s, water soluble sodium silicate, also known as water–glass, was the most common accelerator in wet-mix shotcrete in Norway [7]. The fast hardening reaction of this accelerator is achieved by its content of silica reacting with the dissolved calcium ions ($Ca^{+2}$) in the fresh concrete, resulting in precipitation of calcium silicate hydrate compounds [8].

A non-alkaline shotcrete set accelerating admixture is defined according to NS-EN 934–5:2007 [9] by an alkali content (measured as $Na_2O$ equivalent) less than 1% by mass of the admixture. Aluminum sulfate in liquid form is commonly used as the main component in alkali-free accelerators [6,10]. Ettringite is the main reaction product formed once the alkali-free accelerator is added [6].

In Norwegian subsea road tunnels, alkali-free accelerators were for the first time used in the Nordkapp tunnel. The Nordkapp tunnel was part of the Fatima project, a road connection between the island of Magerøya and the mainland of Norway. The location of the Nordkapp tunnel is shown in Fig. 1.

Nordkapp is a single-tube tunnel with two lanes, one in each direction. It has a total length of 6.8 km and a cross section of 44 $m^2$ [11]. The average daily traffic is 454 vehicles [12]. The tunnel construction started in May 1995 from its both ends. From the mainland side, it was

* Corresponding author.
*E-mail address:* cristobal.j.manquehual@ntnu.no (C. Javier Manquehual).

https://doi.org/10.1016/j.conbuildmat.2022.127090
Received 24 November 2021; Received in revised form 4 March 2022; Accepted 5 March 2022
Available online 9 March 2022

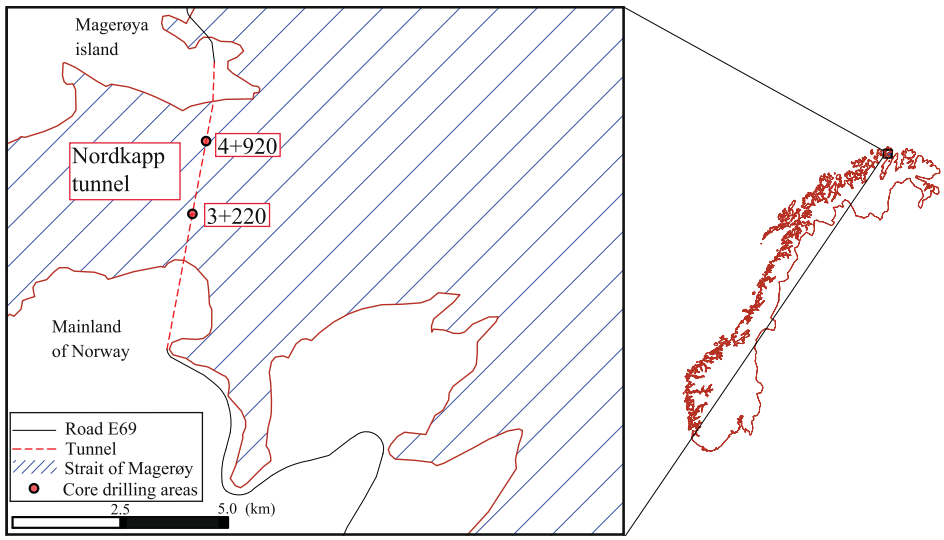


**Fig. 1.** Location of the Nordkapp tunnel and niches investigated in this study.

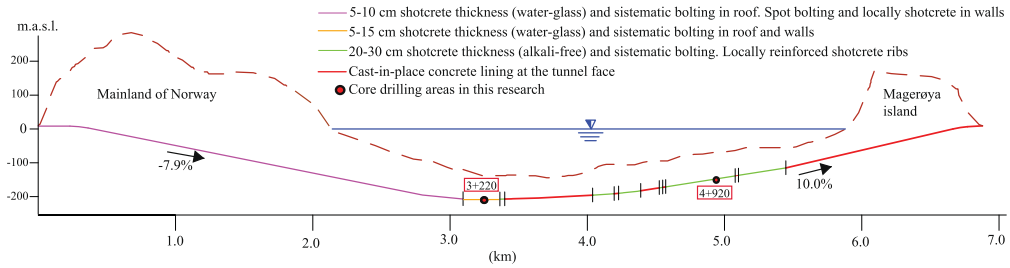


**Fig. 2.** Longitudinal profile of the Nordkapp tunnel with the final rock support distribution over chainage. (Modified from an unpublished as-built geological report prepared by the Norwegian Public Roads Administration).

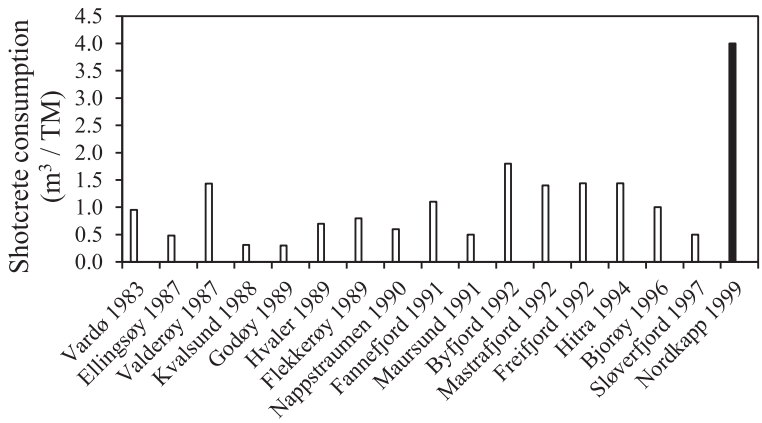


**Fig. 3.** Comparison of steel fiber-reinforced shotcrete consumption as rock support per tunnel meter (TM) in the Nordkapp tunnel with all the previous subsea road tunnels commissioned in Norway. Modified from [13].

**Table 1**
Wet-mix design in shotcrete with alkali-free accelerator used in the Nordkapp tunnel [11].

| | | |
|---|---|---|
| Aggregate 0–8 mm | 1450 | kg/m$^3$ |
| Cement CEM I RR | 520 | kg/m$^3$ |
| Silica fume | 26 | kg/m$^3$ |
| Alkali-free liquid accelerator | 33 | kg/m$^3$ |
| Plasticizer | 5 | kg/m$^3$ |
| Superplasticizer | 5 | kg/m$^3$ |
| Stabilisator | 2.5 | kg/m$^3$ |
| Internal curing | 5 | kg/m$^3$ |
| Steel fibers | 40 | kg/m$^3$ |
| w/c | 0.45 | |

experienced good rock mass conditions for almost 3400 m. Shotcrete with water–glass based accelerator was used in thicknesses between 5 and 10 cm in the first 3050 m and between 5 and 15 cm in the following 350 m (See Fig. 2). On the other hand, the excavation from the island side presented geological difficulties from the very beginning which required systematic cast-in-place concrete lining at the tunnel face [11]. These different geological conditions encountered from each tunnel face led to different excavation progresses. In September 1996, the excavation progress from the mainland had reached 3400 m, while that from the island side had only achieved 600 m. Since the mainland side started to cope with the same geological difficulties as the island side, cast-in-place concrete lining started to be used from both sides at the tunnel face. This prompted the search for alternatives in order to speed up the excavation rate. Several in-situ investigations trying to find the optimal composition of wet-mix shotcrete with alkali-free accelerator discovered that it was possible to spray concrete in thick layers thanks to the high early strength development achieved. Full scale application of alkali-free accelerator started in June 1997 from both sides, where the tunnel face from the mainland side had progressed 4050 m and the one from the island side had achieved 1200 m. This technological change in the shotcrete led to prevent the use of cast-in-place concrete lining in many stretches of poor rock mass conditions for the remaining 1550 m to be excavated [11]. The tunnel breakthrough occurred in January 1998, 4.5 km away from the mainland side. Fig. 2 shows the final rock support installed over chainage for the Nordkapp tunnel.

In Fig. 2, the tunnel stretch between 3.4 and 3.42 km also shows the application of shotcrete with alkali-free accelerator. This was probably an extra shotcrete layer applied after the tunnel breakthrough to reinforce the transition between cast-in-place concrete lining and shotcrete.

Fig. 3 compares the consumption of shotcrete in the Nordkapp tunnel with the consumption of other Norwegian subsea road tunnels previously commissioned.

A shotcrete mix design used in the Nordkapp tunnel is given in Table 1.

The wet-mix design of the shotcrete with the water–glass accelerator was probably the same as Table 1, except for the accelerator type. This statement is based on other Norwegian subsea road tunnels constructed in those years for the same owner as the Nordkapp tunnel [14]. However, an accelerator dose of 33 kg/m$^3$ (approximately 6.3% by weight of cement) per cubic meter of shotcrete seems a bit high for the common Norwegian practice in those years with the water–glass accelerator. For instance, the dose of water–glass accelerator in the shotcrete used in the Freifjord subsea tunnel, completed in 1992, was 5.2% by weight of cement. In the case of the Byfjord and Mastrafjord subsea tunnels, finished during the same year, the dose was 4.7% by weight of cement in

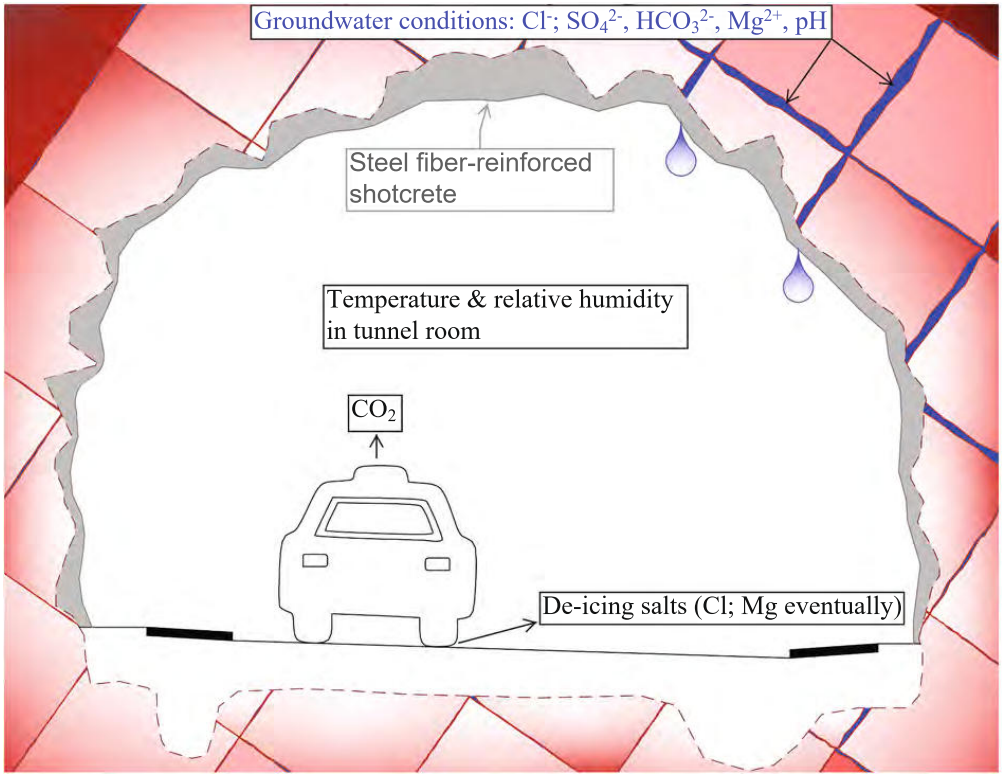


**Fig. 4.** Potential sources of aggressive elements for steel fiber-reinforced shotcrete installed in road tunnels without any inner lining.

**Table 2**
Extent of field work in each niche and some key features of their shotcrete and environmental conditions.

| Zone | 1 | 2 |
|---|---|---|
| Tunnel | Nordkapp | Nordkapp |
| Chainage | 3 + 220 | 4 + 920 |
| Shotcrete core label | 1–6 | 7–14 |
| Total shotcrete thickness (cm) | 9–11 | 25–32 |
| Number of shotcrete layers | 2 | 3 or 4 |
| Type of accelerator | Water glass | alkali-free |
| Comments during drilling | 1 core (No. 4) broke at the contact with the rock. 5 cores recovered rock. | 2 cores (No. 8 and 9) broke at the contact with the rock. 2 cores (No. 7 and 10) broke at shotcrete joints. 4 cores (No. 11–14) recovered rock |
| Groundwater pH[(1)(2)] | 7.3 | 7.8 |
| Electrical conductivity of groundwater EC (mS/cm) [(1)(3)] | 47.3 (saline) | 48 (saline) |
| Estimated [$Cl^-$] (mg/l)[(4)] | 15,460 | 15,688 |

(1) Dripping groundwater coming from the tunnel roof was collected after percolating the shotcrete layer.
(2) The measurement of pH was carried out by Laquatwin pH33, Horiba.
(3) The measurement of groundwater conductivity was carried out by Laquatwin-EC-33, Horiba.
(4) Estimation of the chloride concentration [$Cl^-$] (mmol/l) = 9.22·EC (mS/cm) [32].

both cases [14].

Steel fiber-reinforced shotcrete installed in tunnels as rock support is in direct contact with groundwater as long as the groundwater level is above the tunnel alignment [15]. Groundwater might percolate the shotcrete layer if there is a hydraulic gradient available from its contact with the rock to the traffic room. The magnitude of this gradient between both ends of the shotcrete layer in subsea tunnels depends on the height difference between the sea water level and the depth of the specific place in the tunnel, the permeability of the rock mass, the tunnel lining design and the atmospheric conditions in the traffic room. This gradient might be a relevant driving force for the movement of ions towards the traffic room in the shotcrete under study [16,17]. Then, shotcrete is susceptible to leaching [18], triggering eventually a reduction of mechanical strength, an increase in porosity [19] and a reduction of alkali metals (such as potassium) [20]. Leaching might be accentuated in tunnels which do not include an inner lining attached to the rock support, leaving the shotcrete layer alone to restrain percolation.

If groundwater holds sulfate ions, as may be the case in marine groundwater, it can trigger sulfate attack of the cement paste in the concrete. This attack promotes the formation of ettringite, gypsum and thaumasite [19]. In the latter compound, carbonate ions are needed in addition to sulfate ions for its formation. While the degradation mechanism of ettringite is related to expansion caused by the formation of voluminous water-rich ettringite crystals, the chemical deterioration causing the formation of thaumasite is related to a general disintegration of the cement paste due to the replacement of calcium-silicate-hydrate or in short C-S-H with thaumasite which has very poor cementing properties [19]. The formation of gypsum may lead to expansion and cracking in the cement paste [18]. Potentially, sulfate attack could also come from the constituents in the wet-mix. This might be the case for the aluminium sulfate compound in alkali-free accelerators, becoming shotcrete susceptible to internal sulphate attack [8,21]. Recent investigations in concrete have described the interaction between sulfate attack and leaching, indicating that the dissolution of hydrated cement phases caused by leaching facilitates the formation of secondary expansive minerals under an external source of sulfate [18,22]. Moreover, magnesium ions also available in seawater, might be aggressive for the concrete. As a result of magnesium attack, portlandite and C-S-H can be replaced by respectively brucite and M−S−H, which have inferior cementing properties [19].

Marine groundwater might also have chloride ions, which can attack the steel fibers. In ordinary Portland cement, free chlorides entering into the pore solution of the concrete can either react with hydration products, forming Friedel's salt for example, can be physically adsorbed on C-S-H hydrated cement due to its large surface area or remain as free chlorides in the pore solution [23,24].

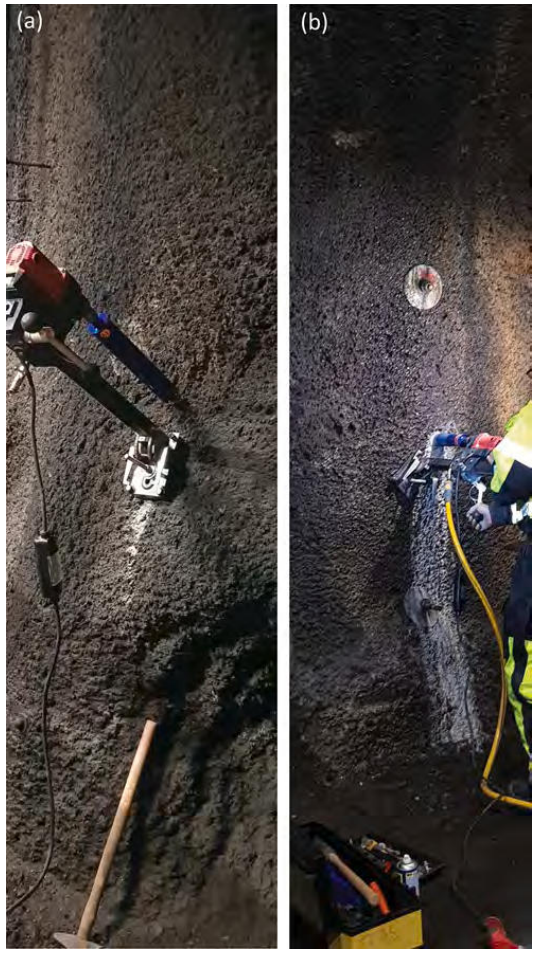


**Fig. 5.** Core drilling in: (a) Zone 1 located in the Nordkapp tunnel at chainage 3 + 220, and (b) zone 2 placed in the Nordkapp tunnel at chainage 4 + 920.

**Table 3**
Operating parameters for the μ-XRF surface mapping.

| Parameter | Value |
|---|---|
| Step width | 50 μm |
| Time per pixel | 2 ms |
| Beam voltage | 50 kV |
| Tube current | 600 μA |
| Dead time | 20% |
| chamber pressure | Vacuum, 20 mbar |
| Elemental filter | No filter |

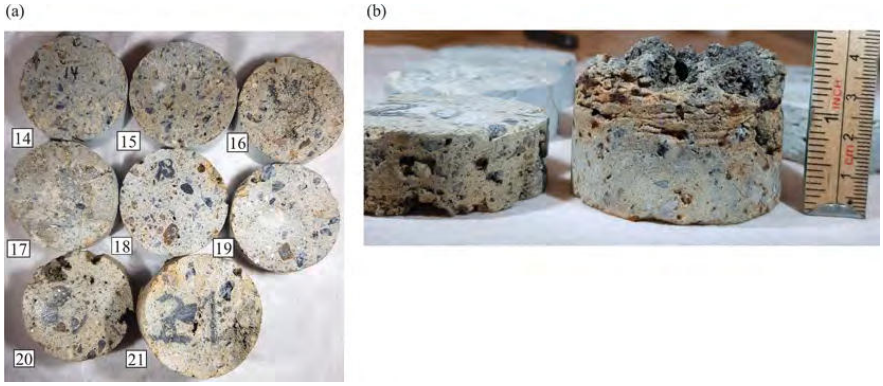


**Fig. 6.** Example of shotcrete samples for suction porosity test after the core has been sliced obtained from core 12 (zone 2 in Table 2).(a) Top view, and (b) in perspective.

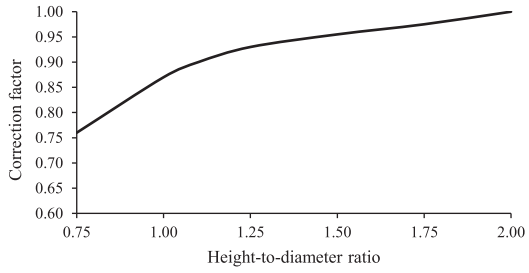


**Fig. 7.** Correction factor adopted for UCS test samples with a height-to diameter ratio lower than two, following Norwegian standard NS 3420:1986 [41].

Another consequence related to the absence of an inner lining in a tunnel is the exposure of shotcrete to the traffic environment. Carbon dioxide available in the air reacts through solution with the calcium rich phases such as portlandite and C-S-H, and results in the precipitation of calcite and alkali rich silica gel. This leads to a reduction in the pH of the pore solution [19]. The reduction of the pH favors the corrosion of steel fibers. Alike, the lack of an inner lining leaves the shotcrete layer exposed to de-icing salts, such as NaCl, $MgCl_2$ or $CaCl_2$, commonly used in roads located in cold winter climates. Its chloride content might also promote the corrosion of steel fibers.

Fig. 4 shows some environmental factors that might affect the durability of shotcrete installed in road tunnels.

The goal of the test program in the Nordkapp tunnel is to compare the in-service condition of shotcrete where water–glass and alkali-free accelerators were used in different stretches of this tunnel. Unlike the comparison of concrete with different accelerators in the laboratory [6,25,26], the comparison of shotcrete in the field incorporates construction variables such as the condition of joints between two adjacent shotcrete layers and the boundary between shotcrete and rock. Moreover, the environment of comparison is unique, combining the pollution of road tunnels with the saline groundwater of subsea tunnels. Finally, few other projects in the world provide the possibility to study shotcrete with alkali-free based accelerator installed more than 20 years ago.

After the introduction of alkali-free accelerators in shotcrete in the mid-1990s, its use has become widespread, and not only in Norway. Apart from the possibility to apply shotcrete in thicker layers, the literature highlights its low pH, reducing the risk of alkali-silica reaction in concrete [27]. In general, accelerators tend to reduce the long-term strength in comparison to concrete without this additive. In this regard, it is reported that concrete strength loss is minimal when alkali-free accelerator is used. In contrast, water–glass accelerator can reduce the long-term compressive strength between 20% and 50% [21,28,29]. Moreover, safer conditions for workers are claimed when using alkali-free accelerator instead of water–glass accelerator since the latter is highly caustic [10,27]. However, some authors have warned of the inconvenience of using alkali-free accelerators in concrete exposed to sulfur-rich environments [8,30,31].

In the tunnel under study, leaching was investigated by creating profiles along the cores of suction porosity, shotcrete density, Uniaxial Compressive Strength (UCS) and potassium content by Micro-x-ray fluorescence (μ-XRF). Eventual sulfur, chlorine and magnesium enrichments in specific areas of the different cores were also investigated by μ-XRF. The identification of deleterious minerals was undertaken by powder X-ray diffraction (XRD). In addition to concrete density, suction porosity and XRD tests, carbonation was investigated with Thymolphthalein pH indicator. Finally, iron mapping along the cores were undertaken through the μ-XRF technique to facilitate the identification of corroded and uncorroded steel fibers in the real images.

## 2. Experimental procedures in the field and laboratory

Since the tunnel was in operation when it was inspected, the cores were extracted from niches (emergency lay-bys in the tunnel). The inspection occurred on October 28, 2020. In the field, 14 shotcrete cores were drilled in total.

### 2.1. In the field

In order to apply different investigation techniques to the cores, the chosen places for core extraction are areas where a thick shotcrete layer was expected. Shotcrete where water–glass based accelerator was used in thicknesses larger than 10 cm is only found in the Nordkapp tunnel between chainages 3+050 and 3+400 (See Fig. 2). Then, one of the core drilling locations is at chainage 3+220 in the Nordkapp tunnel (see Figs. 1-2), called zone 1 in Table 2. The shotcrete surface on this zone appeared dry with dripping water nearby (See Fig. 5a).

The second niche chosen in the Nordkapp tunnel is at chainage 4 + 920. In this niche, alkali-free accelerator was used in the concrete sprayed. The shotcrete surface where the drillings occurred was wet and there was dripping water nearby (See Fig. 5b). This is zone 2 in Table 2.

The core drill machine used in both niches is the Hakken SPJ-122Hi with a diamond core bit of 62 mm as external diameter. The resulting shotcrete core diameter is 55.8 ± 0.2 mm. Table 2 summarizes the main characteristics of the shotcrete core extracted and the exposure

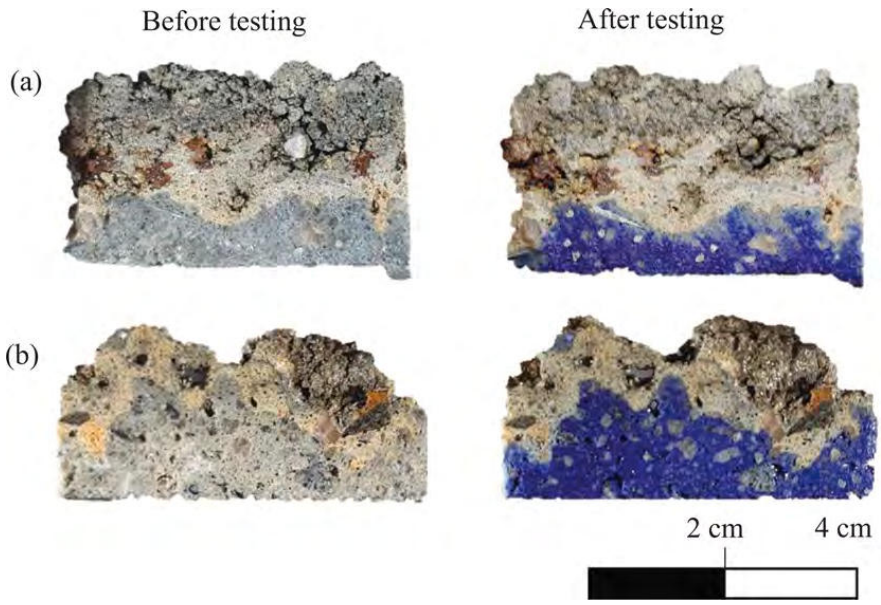


**Fig. 8.** Extent of carbonation in shotcrete samples exposed to the traffic room estimated by pH indicator Thymolphthalein: (a) core 5 (zone 1), and (b) core 9 (zone 2).

environment.

The electrical conductivity (EC) measured in Table 2 confirms the presence of saline groundwater in the two spots under study [33]. The estimated chloride concentrations, based on EC results, are coherent with water samples from other subsea tunnels in Norway [34]. In this reference, detail chemical analyses were undertaken in several Norwegian road tunnels. In particular, saline groundwater from subsea tunnels with similar chloride concentrations had sulfate ion content varying between 410 and 2,740 mg/l, magnesium ion content between 158 and 1420 mg/l and bicarbonates between 23 and 161 mg/l. According to the standard NS-EN 206:2013 [35], these ranges lie between slightly and moderately aggressive chemical environments for concrete.

At approximately 3:00 pm on the day of the inspection, the temperature and relative humidity in the tunnel at chainage 4+920 were 5° C and 69% respectively. As a reference, outside the tunnel, the temperature and relative humidity were −3° C and 90%. These atmospheric parameters were recorded with the instrument Reed R6020.

In the field, after core extraction, samples were marked, photographed, wrapped with stretch plastic film to prevent corrosion of steel fibers and further carbonation. On top of the plastic film, bubble wrap is used for transportation. The marking includes the number assigned to the core (see shotcrete core label in Table 2) and the orientation, being (T) the far-end towards the traffic room, and (R) the opposite end towards the rock.

### 2.2. *In the laboratory*

The procedures implemented for the different laboratory tests are described as follows.

#### 2.2.1. *pH indicator*

Thymolphthalein was used to study the extent of the carbonation depth at the outermost part of the shotcrete cores exposed to the traffic room. This pH indicator sprayed on fresh surfaces of concrete gives a blueish color when the pH of the pore solution exceeds 10.5 [36]. Otherwise, it is colorless. This colorless area is related to the carbonation zone. In this research, the fresh shotcrete surface was achieved by splitting longitudinally the cores in halves with water-cooled saw just before spraying the pH indicator. The solution sprayed on the shotcrete surface consists of 1 g of Thymolphthalein dissolved in 30 ml of deionized water and 70 ml of ethanol.

The shotcrete cores 5 (zone 1) and 9 (zone 2) are analyzed with this pH indicator. The results are presented with images from the sprayed cores.

#### 2.2.2. *μ-XRF scanning*

The 2D spatial distribution of sulfur, magnesium and chlorine along a shotcrete core is determined using μ-XRF analysis. The instrument used was an M4 Tornado from Bruker. The maps show the X-ray intensity related to the chosen chemical measured in counts per second (CPS) [37]. All maps are normalized individually to the highest intensity within the picture. This implies that this technique allows direct comparison in terms of intensities (element content) of two or more samples if scanned together. As no calibration was performed, the analysis does not provide absolute concentrations of a specific element.

Cores 2, 3 and 14 are fully split lengthwise in two halves to obtain a fresh, flat surfaces. They have a length of approx. 9 cm, 11 cm and 27 cm respectively. Therefore, the shotcrete samples for μ-XRF scanning are rectangles of 55.8 mm wide (diameter of the shotcrete core) by the length of the shotcrete core. Prior to the μ-XRF scanning, the relevant surface is dried by an air compressor. No polishing is undertaken on the flat surface to be scanned. Thereafter, the whole sample is inserted in the chamber of the M4 Tornado. However, the scanning area of the instrument is only a rectangle of 160 mm × 190 mm. This size allows to compare two different shotcrete samples put in parallel. However, longitudinally the scanning of core 14 is trimmed to the scan range of the instrument.

Apart from detecting the distribution of potential aggressive elements along the shotcrete cores, iron is also mapped along the cores to facilitate the identification of steel fibers, with or without signs of corrosion.

Finally, leaching was also studied with the M4 Tornado. A decrease

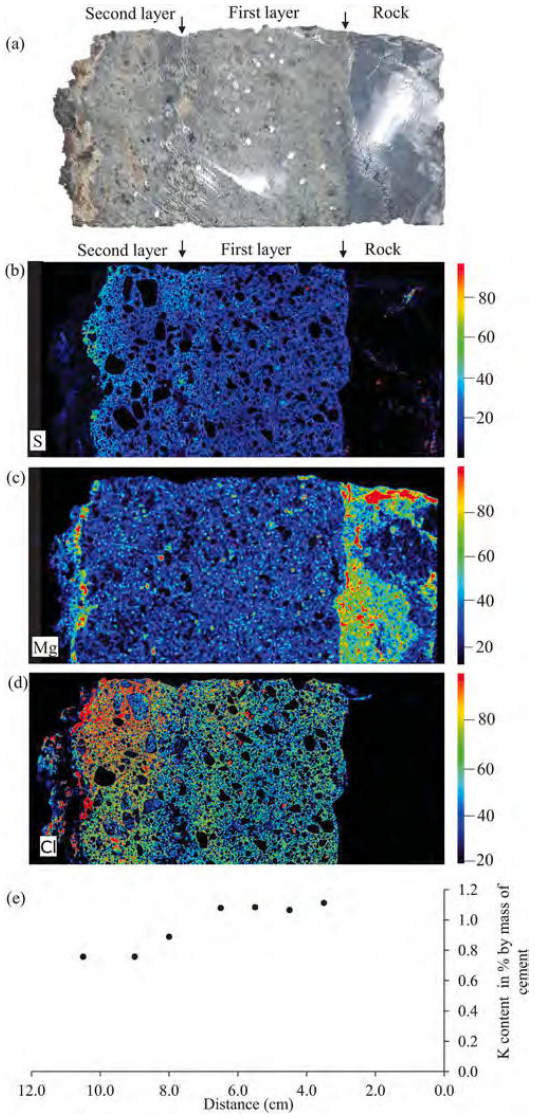


**Fig. 9.** μ-XRF analysis in core 3 (See Table 2): (a) One half of the shotcrete core split lengthwise, (b) sulfur mapping along the core, (c) magnesium mapping along the core, (d) chlorine mapping along the core and (e) profile of potassium content along the core in mass percent of cement.

in potassium content in the pore solution towards the traffic room is an indication of this deterioration process. The M4 Tornado software allows distinguishing different phases (e.g., aggregate and cement paste) by dividing the whole scanned area into smaller areas of similar chemical composition. Once a phase is defined, it is possible to retrieve its spectra. In particular, calcium is adopted to obtain the cement paste phase in a concrete sample [20]. By choosing this element to distinguish the cement paste from the aggregates, the potassium content in the cement paste is determined semi-quantitatively with the software. A profile of potassium content present in the cement paste is achieved after a discretization of the whole surface area of the shotcrete sample into smaller mapping areas, retrieving in each of these areas the corresponding spectra of the cement paste. From these spectra, averaged potassium content is obtained for each smaller mapping area [38]. From the same spectra, relative concentrations of chlorine by mass of cement are also given.

The M4 Tornado is equipped with a silver X-ray tube and two SDD detectors. The X-ray beam is focused by polycapillary lenses to a spot size of 20 μm. The operating parameters used for surface mapping are given in Table 3:

In the case of mapping smaller areas for spectra extraction, the operating parameters are the same except from the step width of 25 μm and the time per pixel of 5 ms to increase the signal statistics.

### 2.2.3. XRD

X-ray powder diffraction analysis was used qualitatively to identify the different minerals present in some shotcrete samples. Mineral phases were identified with the PDF-4 + 2021 database from the International Centre for Diffraction data. In addition, phase quantification via Rietveld analysis was performed with the software Topas from Bruker. Among the minerals to be searched are calcite as an indication of carbonation, thaumasite, gypsum and ettringite as an indication of sulfate attack, along with brucite as an indication of magnesium attack. The instrument used is the D8 Advance from Bruker. After slicing the core to obtain bulk shotcrete samples for XRD test, the samples are crushed in a fly press rock crusher to about 2 mm. At this stage, samples are split in groups of about 25 g. The crushing continues in a disc mill to reach a particle size of about 50 μm. Samples are then crushed in a McCrone micronizing mill to about 10 μm in ethanol. The following operating parameters are used: step size 0.01°, time per step 0.6 s, rotation 60 rpm, radiation 1.79 Å (Co-Kα) with a generator voltage and current of 40 kV and 40 mA respectively.

### 2.2.4. Suction porosity

According to the SINTEF procedure KS 70110 [39], suction porosity in a concrete sample is estimated as follows:.

1. Drying at 105 °C until constant weight loss (0.01% within an hour).
2. Cooling for two hours at room temperature before measuring the weight ($W_1$).
3. Immersion in water for seven days.
4. Measuring the weight of the sample ($W_2$).
5. Measuring the apparent weight of the sample immersed in water ($W_2^{'}$).

The samples for this test are disc-shaped, where the sample diameter coincides with the core diameter. When it comes to disc thickness, the shotcrete cores used for suction porosity analysis were sliced each 20 mm in the longitudinal direction following [39]. The sample size exception is for the ones exposed to the traffic room with an uneven surface on one side. These latter samples have in all cases a larger volume than the disc-shaped ones.

Eq. (1) describes the determination of suction porosity $p_s$ as follows:.

$$p_s = \frac{W_2 - W_1}{W_2 - W_2^{'}} \tag{1}$$

The balance used in the lab is the Mettler PC4400 with a fine weighing range of 400 g and a readability of 0.01 g.

In total, 22 suction porosity tests are executed from the cores 1 and 2 (zone 1), and cores 7 and 12 (zone 2). One has to bear in mind that, in the longitudinal direction, approximately 5 mm of sample material are lost each time the core is sliced (thickness of the saw blade).

Fig. 6 shows samples 14–21 in core 12 before being tested.

### 2.2.5. Uniaxial compressive strength with axial strain measurements

In total, 14 UCS tests are executed in the Triaxial Testing Systems GCTS RTRX-140CL9. In order to get a profile of UCS test results in a

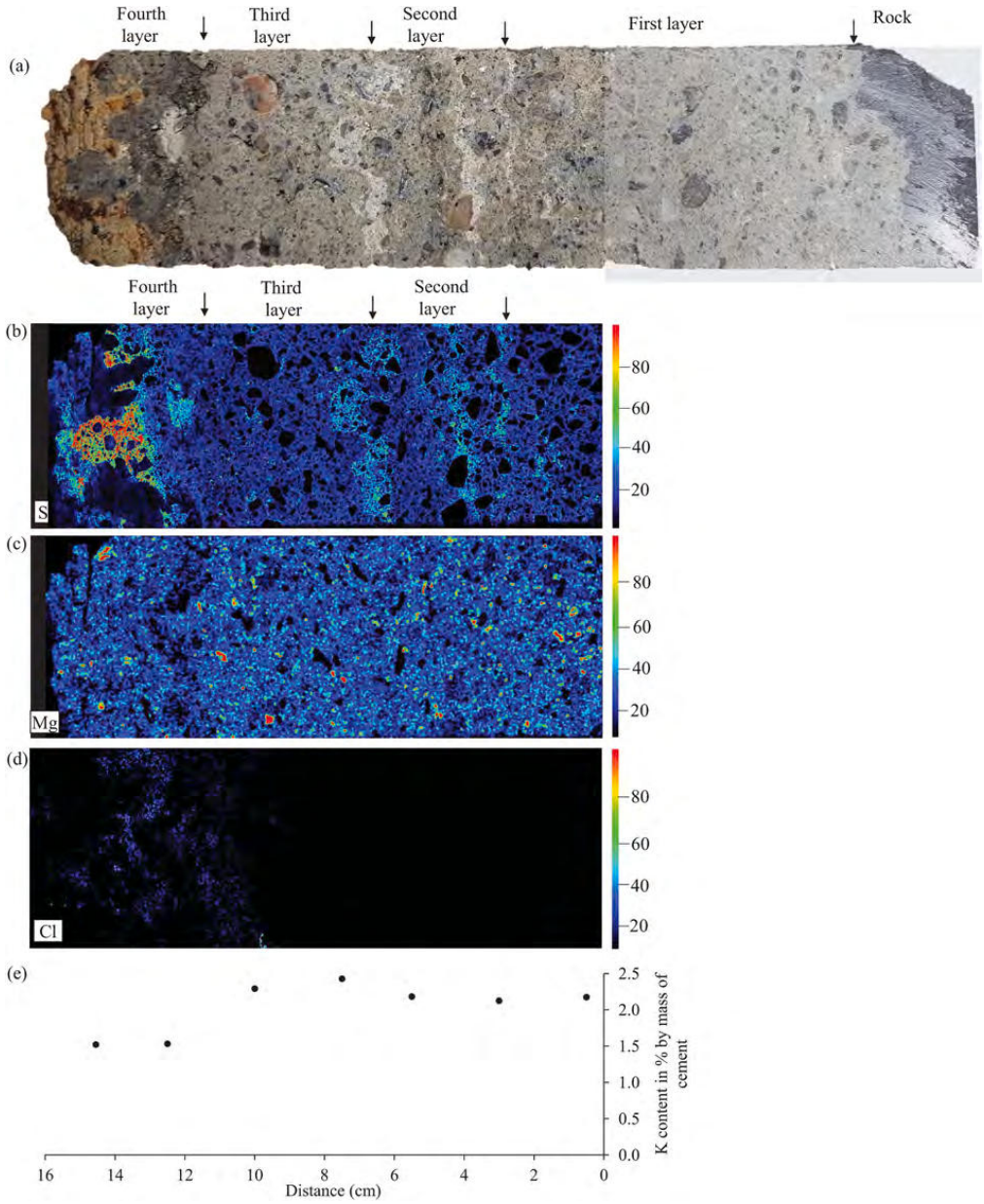


**Fig. 10.** μ-XRF analysis in core 14: (a) One half of the shotcrete core split lengthwise, (b) sulfur mapping along the core, (c) magnesium mapping along the core, (d) chlorine mapping along the core and (e) profile of potassium content along the core in mass percent of cement.

single shotcrete core, shorter samples were adopted. While five sample tests are undertaken for a height-to-diameter ratio (h/D) of two, fulfilling standard NS-EN 12390–1:2012 [40], the remaining nine samples have a nominal height-to-diameter ratio of one. In order to homologate all the UCS test results, a correction factor was applied for those shorter samples as shown in Fig. 7:

The diameter of the samples for the UCS test is fixed by the drilled core diameter. Vertical strain measurements are included in the execution of the UCS tests to visualize eventually differences in the post-peak behavior between different samples. For this reason, the loading procedure chosen is strain controlled instead of the usual constant load rate. According to standard NS-EN 12390–3:2019 [42], the latter rate for the compressive strength of hardened concrete should be 0.6 ± 0.2 MPa/s. By an adjustable strain rate applied for each sample calibrated with low magnitude stress cycles, most of the tests are within the load rate range stated in standard [42] before the samples reach the peak

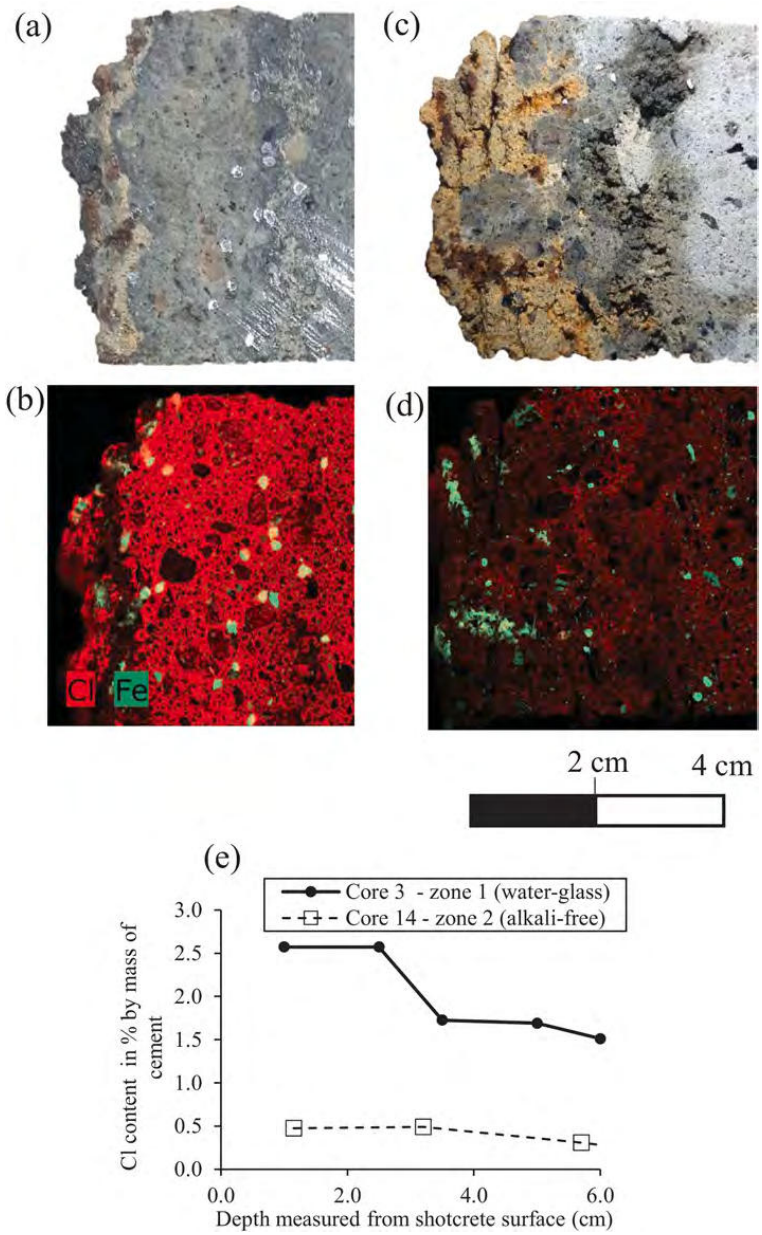


**Fig. 11.** Closeup for cores 3 and 14 near the traffic room. (a) Core 3 image near the traffic room, (b) chlorine and iron mappings in core 3, (c) core 14 image near the traffic room, (d) chlorine and iron mappings in core 14, and (e) profiles of Cl concentration near the shotcrete surface in both cores.

load. The type of sensor used for the vertical strain measurement is the LVDT SR-DF-C375-100 with a theoretical accuracy of 0.001 mm. Any correction factor was applied to the stress–strain curve results.

The shotcrete samples were sliced, ground and immersed in water for seven days before testing.

*2.2.6. Shotcrete density*

The bulk density of shotcrete samples described in this research is connected to the weight gained by the samples after they have been immersed in water for at least seven days ($W_2$), following the SINTEF procedure [39]. The balance used for the weight measurement is the same as in the suction porosity test.

In the case of samples used for the suction porosity test, their volume is determined by the buoyancy method as described in Eq. (2).

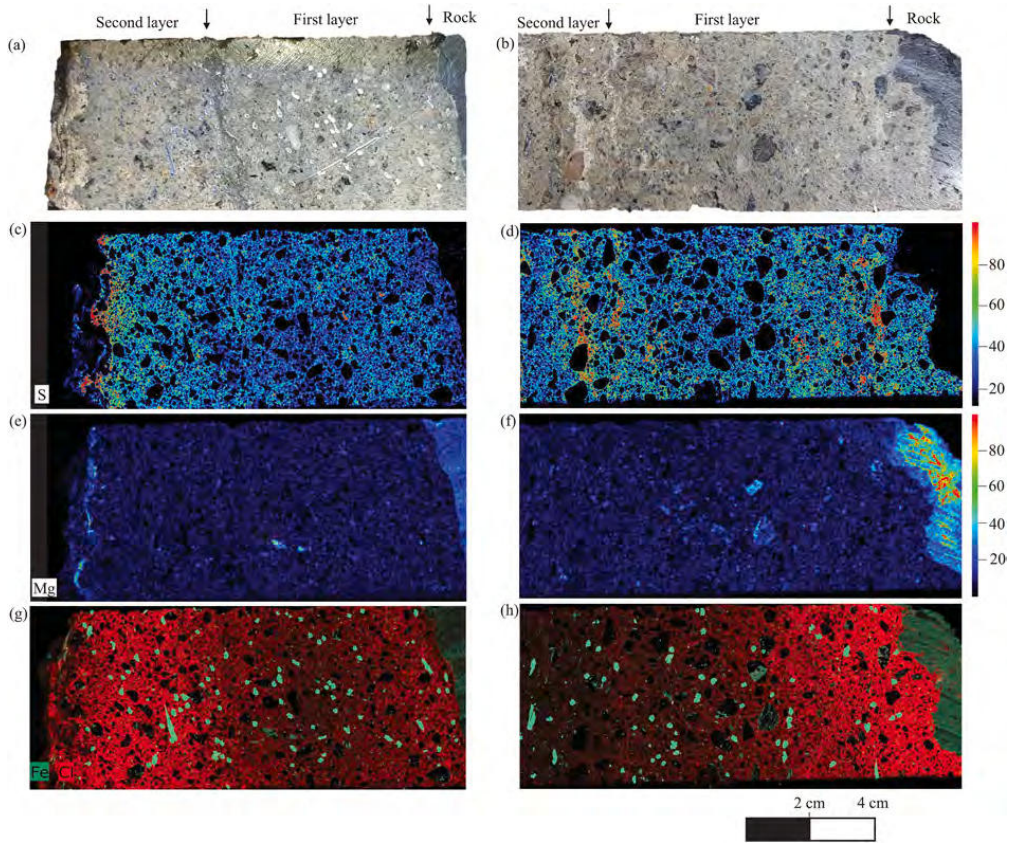


**Fig. 12.** μ-XRF analysis in cores 2 (on the left) and 14 (on the right) scanned in the same run: (a, b) Real image of one half of the shotcrete core split lengthwise, (c, d) sulfur mapping, (e, f) magnesium mapping, and (g, h) chlorine-iron mapping.

$$V = \frac{W_2 - W_2^{'}}{\rho_w} \quad (2)$$

Where $\rho_w$ is the density of water considered to be 1000 kg/m$^3$. On the other hand, the volume of the cylindrical samples used for the UCS test is determined by a digital caliper following the standards suggested by the ISRM [43]. Eq. (3) shows the formula used:.

$$V = \frac{\pi * d^2}{4} * L \quad (3)$$

Where $d$ and $L$ are the averaged diameter and length dimensions respectively of a shotcrete sample after it has been sliced and ground.

## 3. Results

### 3.1. pH indicator

Shotcrete samples from two different cores were tested with the pH indicator Thymolphthalein. The samples chosen for this test belong to the core-end exposed to the traffic room. Fig. 8 shows shotcrete samples from cores 5 and 9 before and after Thymolphthalein is sprayed on them.

Fig. 8 shows that the carbonation depth in zone 1 is slightly higher than in zone 2, exceeding two cm in the first case after approximately 23 years of exposure. It is important to highlight that Fig. 8 suggests that there is no need to spray a pH indicator to determine the carbonation zone since this area stands out for a brownish color, contrasting the gray color of the cement paste. Finally, thanks to the blueish background given by the thymolphthalein in Fig. 8a on the right, some steel fibers can be identified without any sign of corrosion in the uncarbonated zone.

### 3.2. μ-XRF scanning

Figs. 9-10 show the results of μ-XRF analysis in core 3 (extracted from zone 1) and core 14 (extracted from zone 2) respectively. In the latter case, the μ-XRF scanning is trimmed since the length of the core exceeds the scan range of the machine. The scan length adopted is approximately 16 cm, long enough to include all the shotcrete joints of this core. The rest of core 14 is shown in Fig. 12. Figs. 9-10 are comparable since they were scanned in the same run.

Fig. 9b and Fig. 10b show a higher sulfur content in the cement paste near the traffic room, suggesting that the main source of sulfur comes from the traffic room. However, it is important to highlight that there is a sudden drop in sulfur compounds at the carbonation zone in both cases. Fig. 10b also illustrates sulfur enrichment in shotcrete joints. To a minor extent, Fig. 9b shows sulfur enrichment as well in the shotcrete joint.

With regard to magnesium content along the cores, Fig. 10c does not give any indication of magnesium attack. On the other hand, Fig. 9c shows magnesium enrichment in the cement paste at the far-end of core 3 near the traffic room. If Fig. 9c and Fig. 9d are analyzed together, one

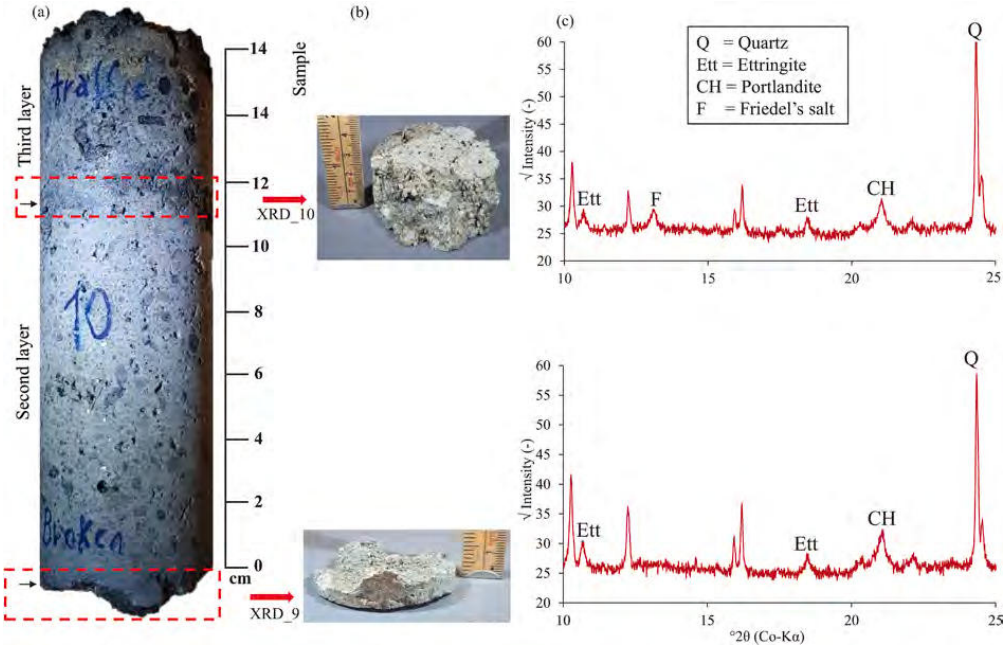


**Fig. 13.** XRD analyses in shotcrete joints belonging to core 10 from the Nordkapp tunnel where alkali-free accelerator was used. (a) whole shotcrete core, (b) bulk shotcrete joint sample, and (c) XRD results with the square root of the counts in Y-axis.

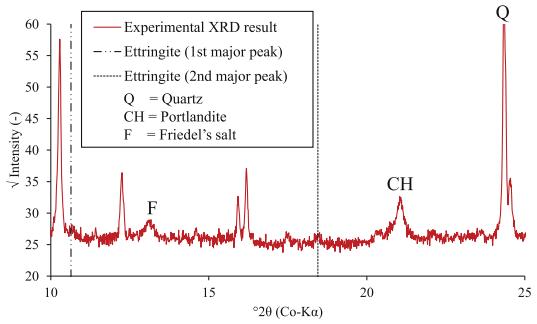


**Fig. 14.** XRD analysis in bulk shotcrete near the rock obtained from core 13 in the Nordkapp tunnel where alkali-free accelerator was used.

can see that chlorine and magnesium do not overlap.

Regarding the origin of chlorine, Fig. 9d indicates that it comes from the traffic room. This is not surprising due to the use of de-icing salts on the route where the Nordkapp tunnel lies. However, Fig. 10d shows very limited chloride ingress in core 14 from the traffic room.

Fig. 11 focuses on the condition of the steel fibers in the shotcrete layer near the traffic room in cores 3 and 14. Apart from the real images near the traffic room in both cores, the iron mapping through μ-XRF is included in this figure to identify corroded and uncorroded steel fibers along with the corresponding chlorine concentration.

Fig. 8 has already described the link between the brownish color near the traffic room and the carbonation zone affected by a lower pH. The additional information provided by Fig. 11 is the connection between some dark reddish spots in the carbonation zone (Fig. 11a and Fig. 11c) and their iron content (Fig. 11b and Fig. 11d respectively). All of the

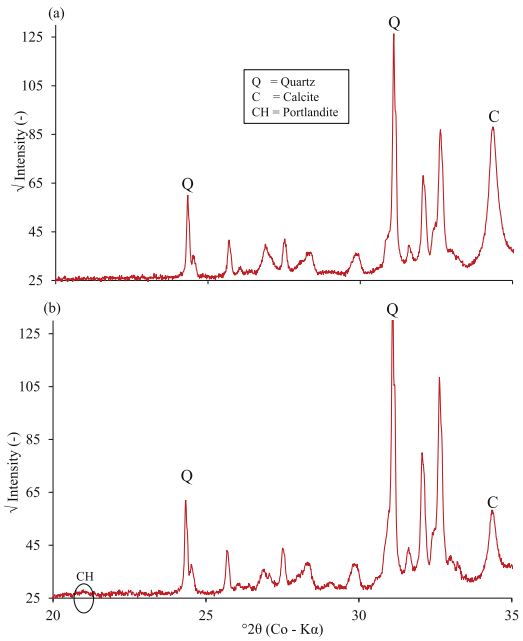


**Fig. 15.** XRD analyses in shotcrete samples exposed to the traffic room in: (a) Core 4 (zone 1), and (b) core 8 (zone 2).

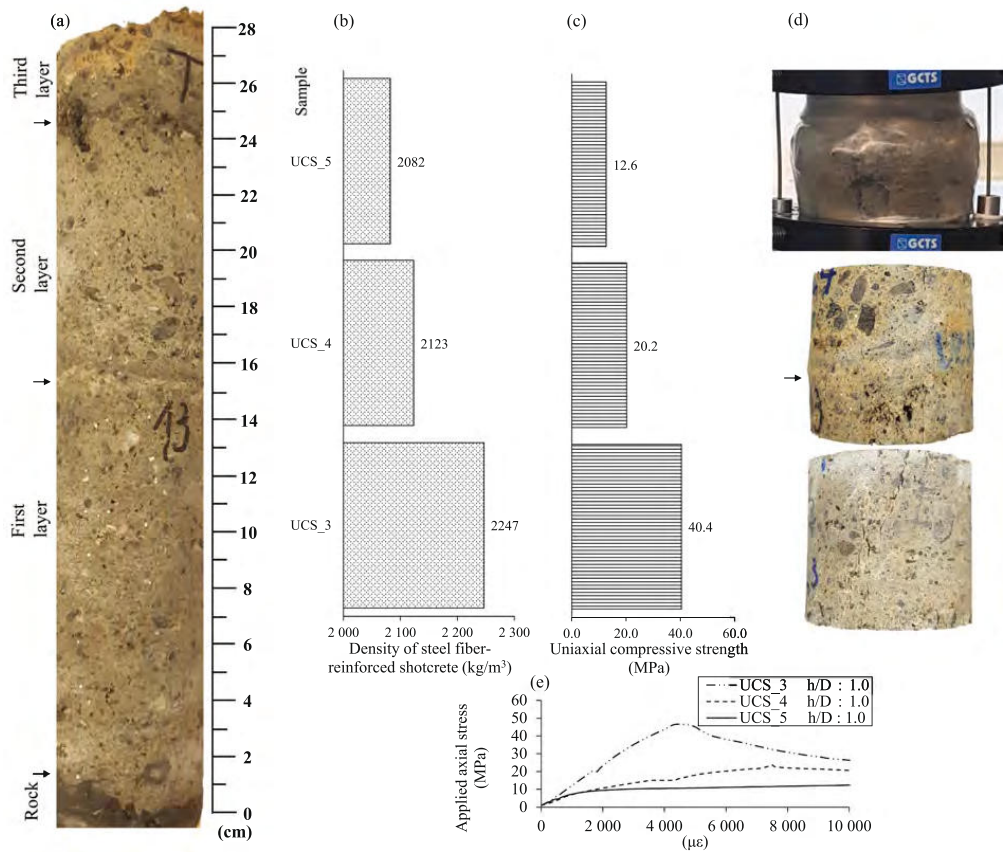


**Fig. 16.** Core 13 from Nordkapp subsea road tunnel where alkali-free accelerator was used: (a) Whole shotcrete core, (b) density of steel fiber-reinforced shotcrete, (c) equivalent uniaxial compressive test results after applying the correction factors given in Fig. 7, (d) shotcrete sample images after being tested for UCS strength, and (e) stress–strain curve during UCS test with axial deformation.

above strongly suggests that the dark reddish stains are iron oxides, a common corrosion product of steel. Furthermore, note that these dark reddish spots are only identified in the carbonation zone. On the other hand, in the uncarbonated zone steel fibers do not show any sign of corrosion product.

Fig. 9e and Fig. 10e show a similar trend with a reduction in potassium content towards the tunnel room, indicating that alkali-metals in the pore solution are being leached out from the shotcrete layer following the flow direction driven by the hydraulic gradient.

Fig. 12 shows the comparison between the opposite end of core 14 (towards the rock) and core 2.

Alike Fig. 9d, Fig. 12g also illustrates chlorine ingress from the traffic room. These two figures belong to zone 1. What is interesting in both figures is the lower chlorine content in the cement paste near the rock compared to the rest of the shotcrete layer, which suggests that there is no chloride ingress from the rock side. On the other hand, core 14 shows chlorine ingress from the rock (Fig. 12h).

Regarding sulfur intensities comparison between the cores 2, 3 and 14 analyzed through μ-XRF, it is important to mention that the shotcrete joint between the first and second layer in core 14 was mapped twice. The first mapping of this joint was shown in Fig. 10b, which was undertaken in parallel to core 3. The second mapping is shown in Fig. 12d which was simultaneously mapped with core 2. The color difference for the same shotcrete joint in Fig. 10b and Fig. 12d is due to the highest intensity found when mapped. In the first mapping, the highest intensity occurred near the shotcrete surface in core 14 (see Fig. 9b and Fig. 10b as a whole), while in the second mapping similar intensities were found in both the shotcrete joint itself and in core 2 near the shotcrete surface (Fig. 12d and Fig. 12c). Thus, taking as reference this shotcrete joint, it is concluded that the highest sulfur intensity between cores 2, 3 and 14 happened in core 14 (zone 2) near the shotcrete surface adjacent to the carbonation zone.

### 3.3. XRD

XRD analyses were executed in 12 samples. Emphasis was placed on the core-end towards the traffic room and shotcrete joints. Fig. 13 shows two shotcrete joints belonging to a core extracted from zone 2 where the shotcrete holds alkali-free accelerator.

It is important to highlight that the bulk samples shown in Fig. 13b include aggregates and cement paste. The main peaks with high intensities from the aggregates generally overshadow the intensities of the cement paste. That is why the range of the x-axis in Fig. 13c is only between 10° and 25° and the square root of the intensities were plotted in the Y-axis. The XRD results shown in Fig. 13c detected ettringite in these shotcrete joints. This agrees with Fig. 10b and 12d, where sulfur enrichment was detected in shotcrete joints from a core in the same tunnel zone (zone 2) using μ-XRF.

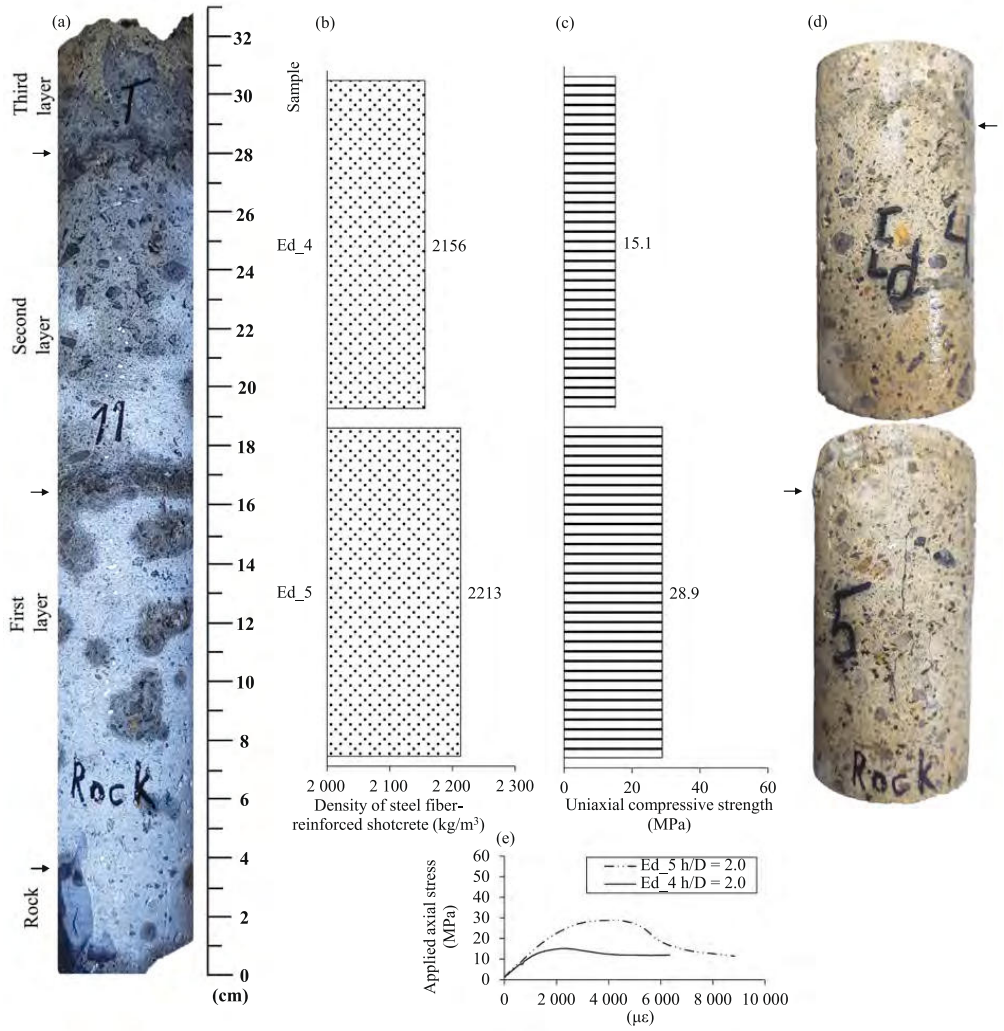


**Fig. 17.** Core 11 obtained from zone 2 where alkali-free accelerator was used: (a) Whole shotcrete core, (b) density of steel fiber-reinforced shotcrete, (c) uniaxial compressive test results, (d) shotcrete sample images after being tested for UCS strength, and (e) stress–strain curve during UCS test with axial deformation.

When alkali-free accelerator is used, ettringite is expected to be found evenly distributed in the core, and not only in shotcrete joints. An example of a XRD pattern from bulk shotcrete near the rock in the same tunnel zone is showed in Fig. 14. The specimen was obtained from a sample that previously had been used for a UCS test (UCS_3 shown in Fig. 16).

In comparison to the XRD diffraction patterns in Fig. 13, Fig. 14 shows a lower intensity peak for ettringite. In fact, Rietveld analysis performed with the software Topas normalized to 100% crystalline content yields 0.58 % for ettringite in the sample shown in Fig. 14. As a comparison, the Rietveld analyses for the quantification of ettringite in Fig. 13 give 1.66% in sample XRD_10 and 1.08% in sample XRD_9. These results are consistent with the sulfur enrichment detected with μ-XRF and indicate that ettringite enrichment occurs in shotcrete joints where alkali-free accelerator was used.

Friedel's salt mineral was detected between the second and third shotcrete layer of core 10 shown in Fig. 13 (sample XRD_10). Since this shotcrete joint is close to the shotcrete surface, the chlorine element in this mineral came very likely from de-icing salts. In the other shotcrete joint analyzed in this core (sample XRD_9), Friedel's salt was not identified. This second shotcrete joint is approximately in the middle of the total shotcrete layer and probably chloride ingress has not yet reached that far (See Fig. 12h, which is a core located approximately 25 cm apart from core 10 with the absence of chlorine between the first and second shotcrete layer).

Fig. 15 shows a comparison of XRD results in shotcrete samples exposed to the traffic room.

Fig. 15 shows that calcite has formed in the shotcrete exposed to the traffic room. More in detail, Fig. 16b shows that XRD analysis in core 8 (zone 2) still detects portlandite minerals near the shotcrete surface exposed to the traffic room, while the XRD result in core 4 (zone 1) represented in Fig. 16a does not identify portlandite. On the other hand, the latter figure shows a higher intensity for calcite in comparison to Fig. 16b.

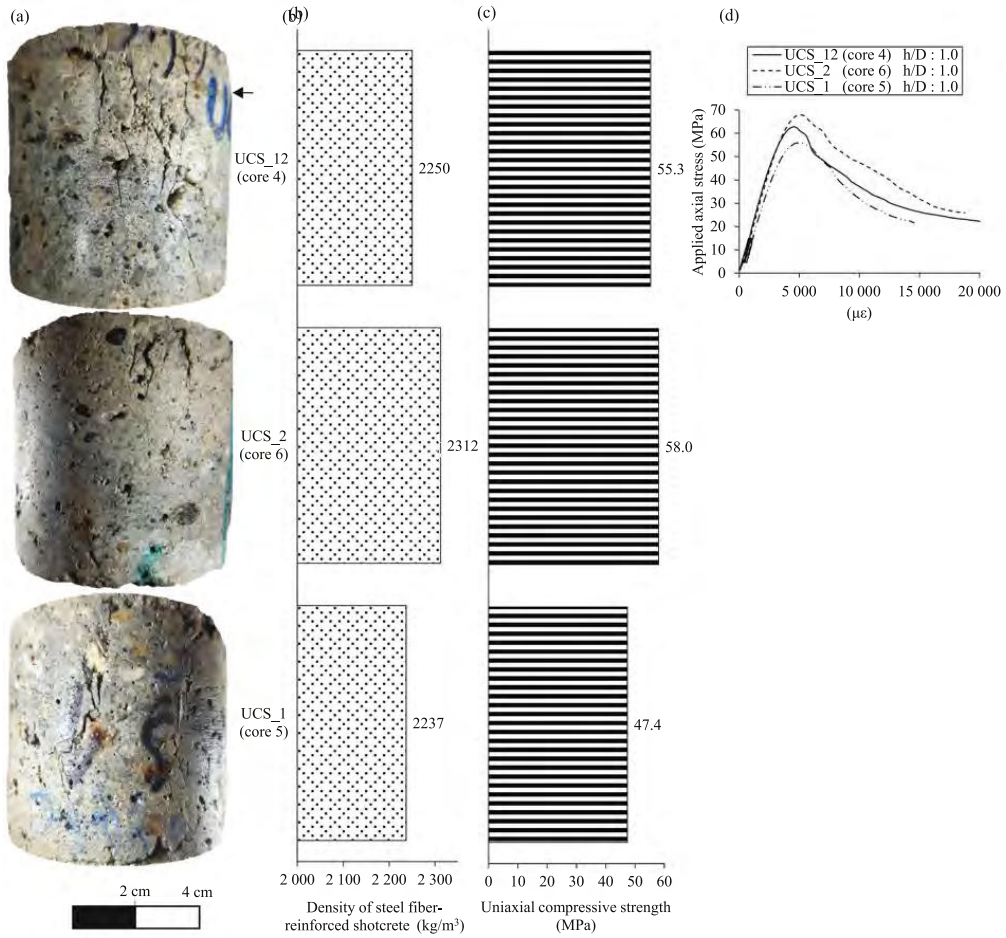


**Fig. 18.** Three UCS test results obtained from zone 1 where water glass accelerator was used: (a) Shotcrete sample images after being tested for UCS strength, (b) density of steel fiber-reinforced shotcrete, (c) equivalent uniaxial compressive test results after applying the correction factors given in Fig. 7, and (d) stress–strain curve during UCS test with axial deformation.

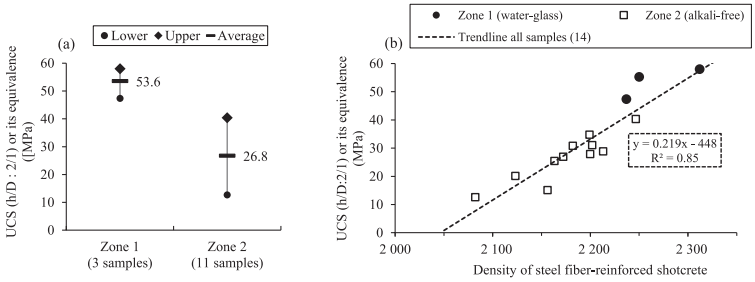


**Fig. 19.** Statistical analysis related to UCS test results: (a) UCS test results grouped by the tunnel zones where shotcrete cores were extracted, and (b) correlation between UCS test results and shotcrete density broken down for each zone.

Ettringite is only stable when the pH is greater than 10.7 [44]. Then, it is not surprising that the carbonated shotcrete samples exposed to the traffic room shown in Fig. 15 did not detect ettringite, since the carbonation area has a pH below 10.5, as demonstrated by the pH indicator. In agreement with this observation, Fig. 9b and 10b show a sudden reduction in sulfur content in the carbonation zone.

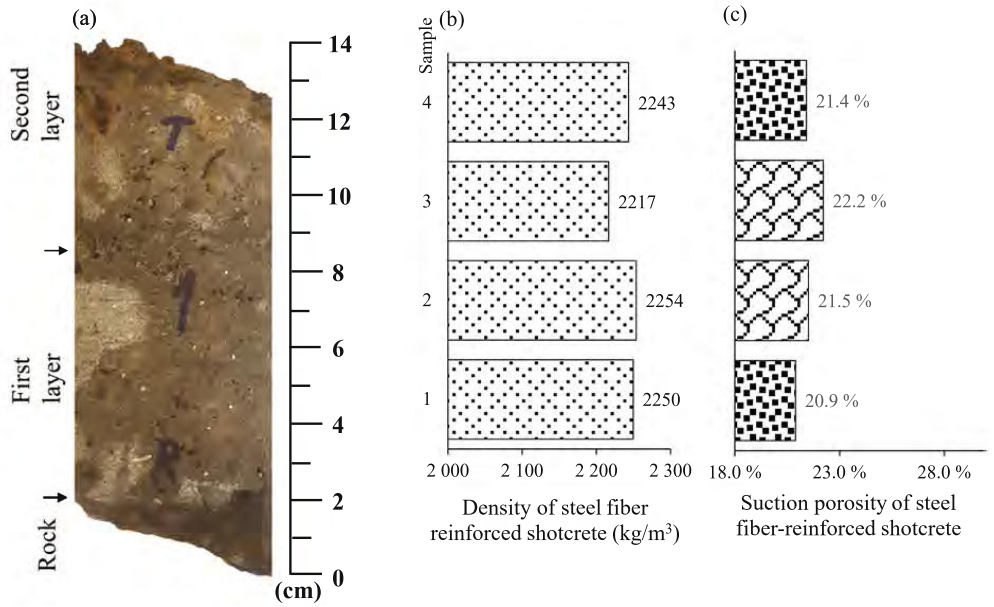


**Fig. 20.** Core 1 obtained from the Nordkapp tunnel where water–glass accelerator was used: (a) Whole shotcrete core, (b) density of steel fiber-reinforced shotcrete, (c) suction porosity results.

At the carbonation zone, it is reported that Friedel's salt dissolves [24]. Fig. 15 supports this statement where Friedel's salt was not identified in any of the two spectra.

### 3.4. UCS and density

Since shotcrete samples were weighed before the execution of the UCS tests, it is possible to visualize the relation between the UCS test and shotcrete density results along the cores. Fig. 16 shows the results in core 13 (zone 2 in Table 2).

Fig. 16 clearly shows a decay of.UCS strength towards the traffic room. As a reference, the valid regulations for subsea tunnels in 1996 in Norway required a minimum characteristic compressive strength of a 15 cm cube at 28 days equal to 45 MPa or C45 [45] following the European standards. For strength class C45, the Norwegian guidelines for shotcrete at that time suggested a minimum in-situ strength from extracted core cylinders after 28 days of 28.8 MPa [46]. Then, it is possible to say that sample UCS_3 in Fig. 16 still complies with the original regulations. On the other hand, the strength of sample UCS_5 shows a reduction to approximately 40% of the original compressive strength required.

Fig. 16 also shows that shotcrete density diminishes towards the traffic room in approximately the same proportion as the compressive strength. The stress–strain curve shown in Fig. 16e also indicates a change from a strain-softening behavior near the rock to an elastic–plastic behavior near the traffic room. In other words, it shows a gradual reduction in the difference between peak and residual values towards the traffic room.

The arrows in Fig. 16a indicate the boundary between two consecutive shotcrete layers. The middle and upper shotcrete samples in Fig. 16 (samples UCS_4 and UCS_5) hold one of these shotcrete joints. Specifically in sample UCS_4, the image after the execution of this UCS test indicates that the shotcrete joint had an influence on the failure mode undergone in this sample. In the case of sample UCS_5, a more extensive degradation is observed which involves the whole sample.

The UCS test results from a core in the same zone (Core 11) is shown in Fig. 17.

Unlike the shotcrete samples shown in Fig. 16, the samples in Fig. 17 have a height-to-diameter ratio equal to two, allowing to determine the UCS strength result without any correction factor. Despite this difference, Fig. 17 shows the same trend as described in Fig. 16 for the UCS test and shotcrete density results.

Due to the thinner total shotcrete thickness in zone 1, a profile of UCS test results along a core in this tunnel zone is not possible to be elaborated. Nevertheless, results of UCS tests from three different cores are shown in Fig. 18.

Fig. 18 shows high shotcrete density values and high UCS strength results in zone 1. This is also the case for sample UCS_12 which held a shotcrete joint. In addition, stress–strain curves show evident differences between peak and residual values. Finally, a statistical comparison of UCS test results between zones 1 and 2 is given in Fig. 19.

Fig. 19a shows that zone 1 has no indication of degradation since it shows high UCS strength values with little scattering. On the other hand, zone 2 shows lower UCS strength values with high scattering.

Fig. 19b incorporates shotcrete density results measured just before the execution of the 14 shotcrete samples tested for UCS strength. This figure clearly illustrates that the highest two UCS test and shotcrete density results correspond to zone 1 and the lowest ten UCS test and shotcrete density results belong to zone 2. It is also important to highlight the good correlation between UCS and shotcrete density test results shown in Fig. 19b, even for extreme values. This is remarkable considering that only some of these samples are shotcrete-joint free and different failure modes took place along with different stress rate applied during testing (strain controlled tests).

### 3.5. Suction porosity and density

Figs. 20-21 show the results of suction porosity and density along two shotcrete cores extracted in zone 1.

In Fig. 20, samples 2–3 contain shotcrete joints. In Fig. 21, only

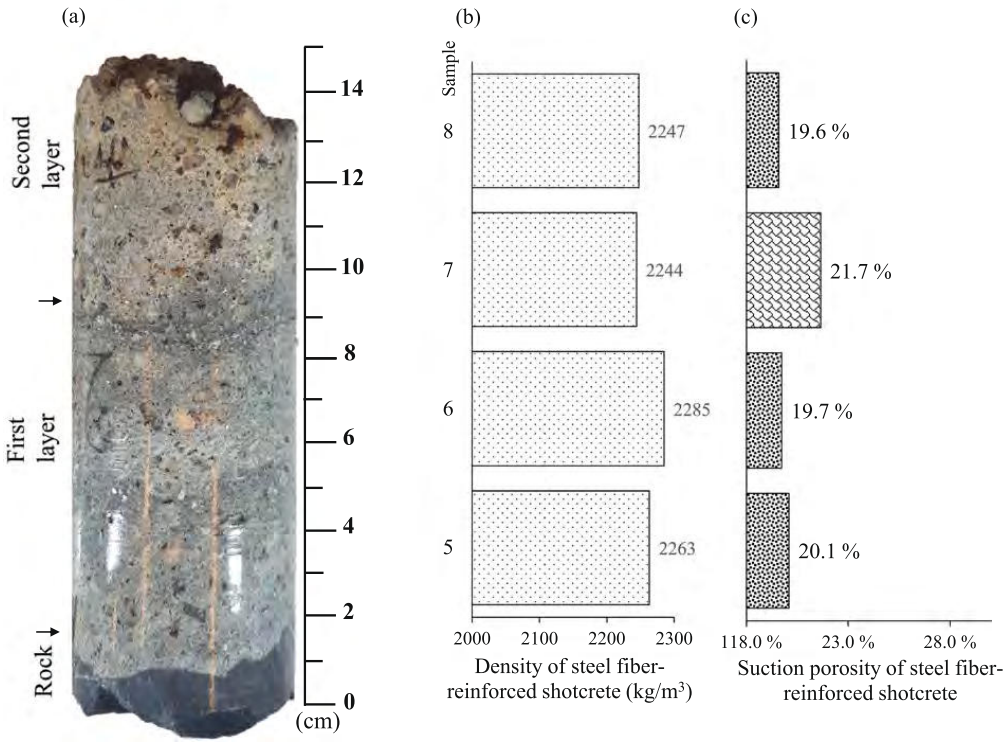


**Fig. 21.** Core 2 obtained from the Nordkapp tunnel where water–glass accelerator was used: (a) Whole shotcrete core, (b) density of steel fiber-reinforced shotcrete, (c) suction porosity of steel fiber-reinforced shotcrete.

sample 7 holds a shotcrete joint. Figs. 20 and 21 show that shotcrete samples holding shotcrete joints have the highest suction porosity and the lowest shotcrete density in the core.

Fig. 20 shows a slight trend of higher suction porosity towards the traffic room. The exception is the last sample exposed to the traffic room with a sudden decay in suction porosity. This latter observation is probably associated with the formation of calcite in the carbonation zone.

Fig. 22 shows the results of suction porosity and shotcrete density in core 12 (Zone 2).

Fig. 22 shows a clear trend of higher suction porosity and lower shotcrete density towards the traffic room. Alike Figs. 20-21, the samples holding shotcrete joints in Fig. 22 (samples 17 and 20) have the highest suction porosity and lowest density values in the core. In addition, Fig. 22 also indicates carbonation at the far end of the core exposed to the traffic room with a drop in suction porosity.

Fig. 23 shows the results of core 7 located in zone 2 as well.

Fig. 23 shows that the core broke at a shotcrete joint, despite the machine continued drilling for about 10 cm more. In addition, the core in Fig. 23 also gives the highest suction porosity and the lowest density values in the shotcrete joint. The trend in suction porosity and shotcrete density towards the traffic room are similar to Fig. 23. The only exception is sample 10 in Fig. 23 with a local higher density and lower suction porosity.

Finally, a statistical overview of suction porosity results and their relation to shotcrete density are given in Fig. 24 for both tunnel zones.

In comparison to zone 1 in Fig. 24a, zone 2 presents a higher average suction porosity value and a higher dispersion of the results. Both observations indicate that the level of degradation is higher in zone 2.

It is important to point out as well in Fig. 24b the good correlation between suction porosity and shotcrete density test results, even for the extreme values.

## 4. Discussion

### 4.1. Sampling and investigation methods

With regard to sample height for UCS tests, traditional concrete testing recommends a nominal h/D of 2 for cylinders [40]. This is a challenging requirement when it comes to shotcrete testing. First of all, the contact between the rock and shotcrete is uneven. The same happens on the shotcrete surface exposed to the traffic room. Then, to get a cylinder of shotcrete with flat surfaces on both ends, the core extracted from the field should have a clearance in length of several cm on top of the required height. In addition, about 5 mm is lost each time the sample is sliced (thickness of diamond saw). This is why, shorter samples with a h/D of 1 were executed in addition to some samples with a h/D of 2. As shown in Fig. 7, the ultimate axial stress obtained with these shorter samples is, in average, 15% higher than those longer ones with a h/D of 2. Alike Fig. 19b, Fig. 25 plots UCS strength results over shotcrete density. However, Fig. 25 groups the samples by h/D instead of the zone where they were extracted.

Fig. 25 illustrates that taller samples (h/D = 2.0) tend to average the results, but all the samples can be linked to the same trend line. When it comes to the analysis of degradation, a test which is more sensitive is valuable, and that is what a shorter sample can give in addition to the creation of profiles along the cores.

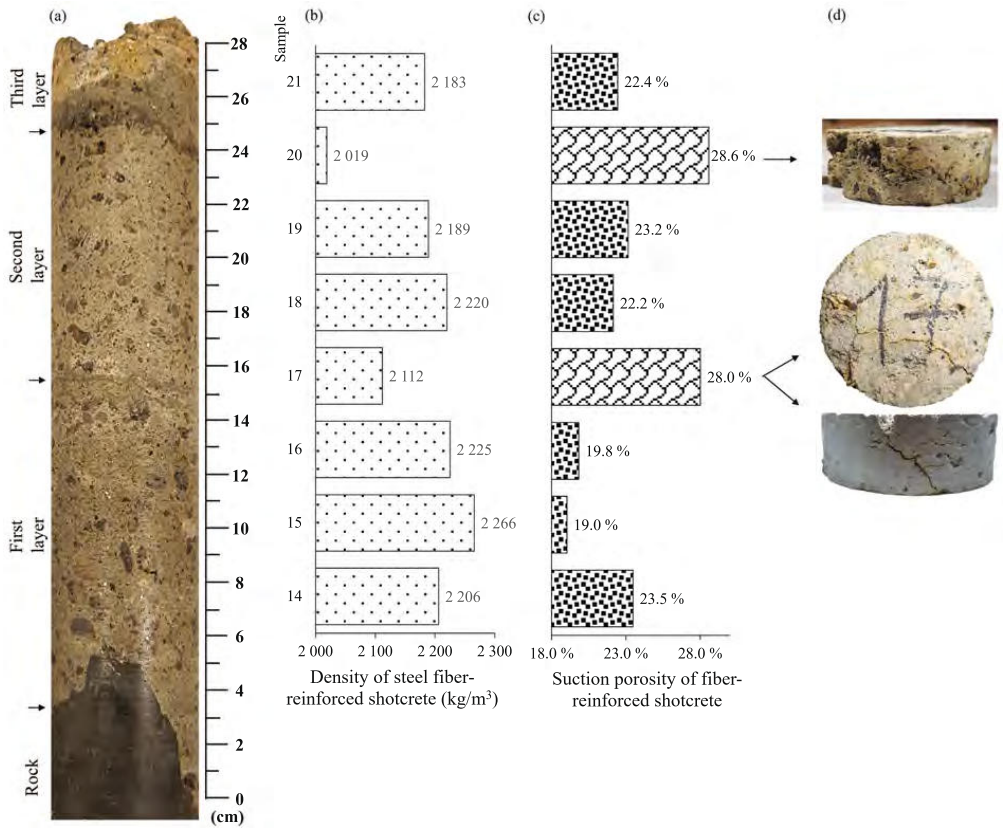


**Fig. 22.** Core 12 obtained from Nordkapp tunnel where alkali-free accelerator was used: (a) Whole shotcrete core, (b) density of steel fiber-reinforced shotcrete, (c) suction porosity results, and (d) picture of samples holding shotcrete joints at the end of suction porosity test.

### 4.2. Results

The zones investigated in the Nordkapp tunnel indicate that the in-situ condition of shotcrete with water–glass accelerator (zone 1) is better than the shotcrete installed in zone 2, where alkali-free accelerator was used. This is supported by higher UCS and shotcrete density results along with lower suction porosity values with limited scattering in all the just-mentioned parameters in zone 1.

The observation that the shotcrete with water–glass based accelerator results in a higher long-term strength compared to the one using alkali-free accelerator might be considered in contradiction with several studies reported in the literature. In some studies, however, the comparison of concrete strength with different accelerator types are judged to be unfair, using the highest accelerator dosages in concrete samples containing the water–glass accelerator [29,47]. In these two references, the doses of water–glass accelerator were 10% and 12% respectively, well above the Norwegian practice 25 years ago.

Other studies conclude that alkali-free accelerators are able to reach higher long-term mechanical strength for the shotcrete and reduce the susceptibility to sulfate attack in comparison to alkaline activators [6,25,26,48]. However, in these references, the alkaline accelerators are only represented by sodium aluminate solutions, not sodium silicates (water–glass). In particular, it is concluded that the aluminates are responsible for a higher amount of different aluminate hydrates, among others, monosulfoaluminate. The higher amount of monosulfoaluminate in this type of accelerator makes the concrete more susceptible to form ettringite under an external source of sulfate and inhibits further hydration of the alite at early stages of hydration.

A historic review of shotcrete as rock support in Norway in the mid-1990 s, where water–glass was the dominant accelerator type, concluded that a compressive strength close to 50 MPa from drilled cores after 28 days of curing was normal [49]. Furthermore, another research undertaken in Norway some years later between shotcrete using water–glass and alkali-free accelerators obtained no significant differences in UCS values after 28 days of curing, exceeding the samples 50 MPa regardless of the accelerator type [50]. The main finding of this research is not the satisfactory condition of the shotcrete with water–glass accelerator, but rather the physical and mechanical changes observed in the shotcrete layer where alkali-free accelerator was used.

The leaching severity in zone 2 is observed by:.

- A noticeable decay of density towards the traffic room shown in Figs. 16, 17 and 22
- A significant increase of suction porosity towards the traffic room in Figs. 22-23
- A clear reduction of UCS strength towards the traffic room shown in Figs. 16 and 17

Ettringite enrichment in shotcrete joints is also observed in the shotcrete where the alkali-free accelerator was used. The high suction porosity values measured in these shotcrete joints suggest that there might be a link between the ettringite formation in these joints and the

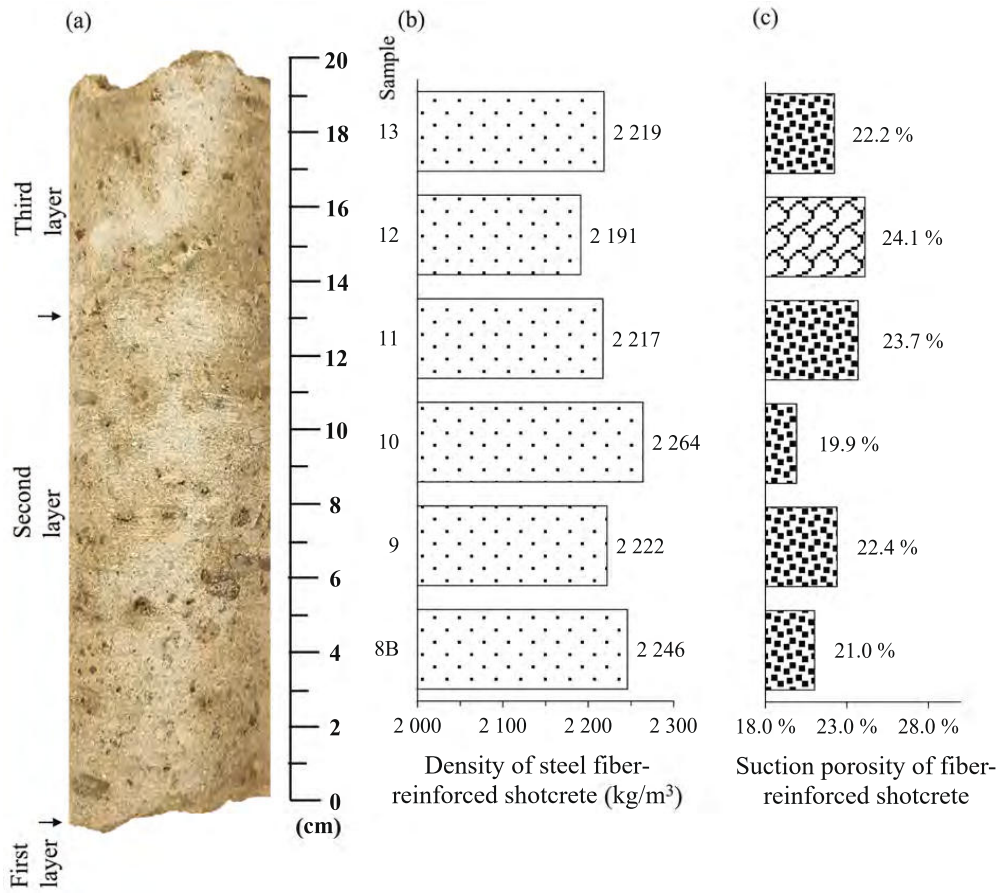


**Fig. 23.** Core 7 obtained from the Nordkapp tunnel where alkali-free accelerator was used: (a) Whole shotcrete core, (b) density of steel fiber-reinforced shotcrete, (c) suction porosity results.

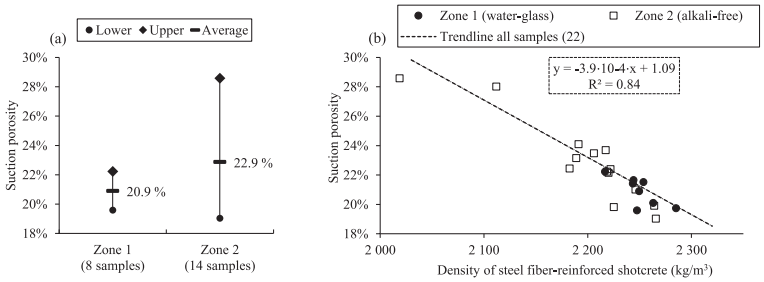


**Fig. 24.** Statistical analysis related to suction porosity test results: (a) suction porosity results grouped by the zones where shotcrete cores were extracted (See Table 2), and (b) correlation between suction porosity and shotcrete density broken down for the different zones.

eventual increase of suction porosity due to the expansion capacity of ettringite. In this regard, it is important to highlight that sample 17 in Fig. 22, cracked after a drying and wetting cycle for the suction porosity test. This was observed only in this sample out of 22 suction porosity samples. In agreement with these observations, Table 2 indicates that the only two cores which broke at shotcrete joints occurred in cores belonging to zone 2.

The shotcrete condition in zone 2 is poor with a shotcrete joint near the shotcrete surface. In the area of the shotcrete layer just next to the carbonation zone, apart from a higher suction porosity and lower shotcrete density detected, the highest sulfur concentration was observed. Within the carbonation zone, high sulfur concentrations are

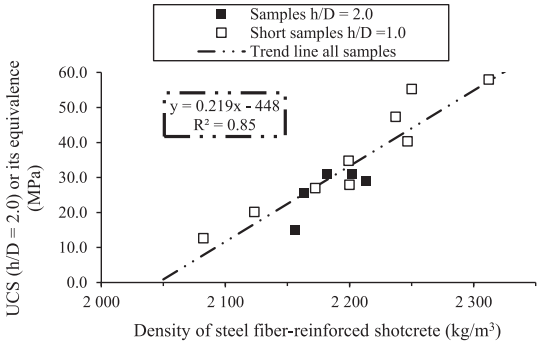


**Fig. 25.** UCS strength results over density of steel fiber-reinforced shotcrete after immersing the samples in water for seven days. Samples with height-to-diameter ratio of 1 were corrected by Fig. 7.

not expected since several sulfur containing minerals in the cement paste are not stable when the Ph less than 10.7 [44].

Regarding the distribution of sulfur concentration, it is important to mention that to a minor extent zone 1 also contained higher sulfur intensities near the shotcrete surface adjoining the carbonation zone (see Fig. 9b and Fig. 12c). This observation identified in both tunnel zones suggests that there is an extra source of sulfur coming from the traffic room. Thus, the shotcrete with alkali-free based accelerator installed in a subsea road tunnel has three potential sources of sulfur. From the accelerator itself, from the marine groundwater and from the traffic room. With regard to the latter case, air pollution analysis in traffic tunnels describes sulfur dioxide $SO_2$ as a common gas emitted by vehicles [51,52], which is soluble in water. This is the probable explanation for what was observed near the traffic room in the three cores where μ-XRF analysis was executed.

The sources of sulfur combined with a hydraulic gradient that might promote leaching can create an aggressive interaction for the shotcrete. The availability of Ca, Al and Si ions in the pore solution generated by the leaching of hydrated cement phases facilitate the formation of secondary expansive minerals under an external source of sulfate [18,22]. On the other hand, the higher is the porosity in the concrete caused by leaching, the easier is for aggressive ions to penetrate farther into the concrete. In turn, the cracking generated by sulfate attack can also promote further ingress of aggressive ions in the concrete and promote leaching.

Considering that a higher water-cement ratio leads to a higher suction porosity [53], there is an indication that during construction the water conditions between zones 1 and 2 were different based on the local suction porosity measured near the rock in these two zones. While suction porosity results near the rock in zone 1 were 20.1% and 20.9% (samples 1 and 5 in Figs. 20-21 respectively), the suction porosity measurement near the rock in zone 2 gave 23.5% (sample 14 in Fig. 22). In connection with these findings, there was no sulfur and chlorine ingress from the rock in zone 1 (Fig. 9b and Fig. 12c for sulfur and Fig. 9d and Fig. 12g for chlorine), while there was sulfur and chlorine ingress in zone 2 (Fig. 12d for sulfur and Fig. 12h for chlorine).

Magnesium was identified by μ-XRF analysis near the shotcrete surface exposed to the traffic room in cores 3 and 2 extracted from zone 1 (Fig. 9c and Fig. 12e respectively). None of the XRD analyses in the area identified brucite. The origin of the magnesium content coming from the traffic room is unknown. A possible source of magnesium could be $MgCl_2$ used as dicing salts. However, there is no evidence from the

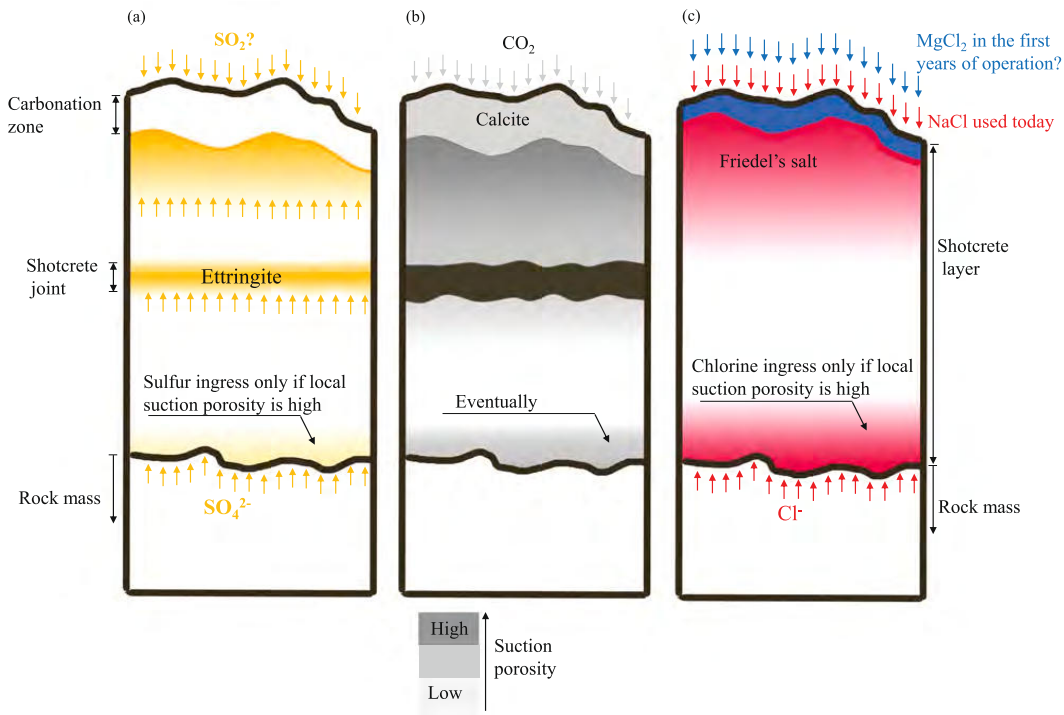


**Fig. 26.** Summary of observations in the Nordkapp subsea road tunnel. (a) Sulfur ingress and distribution along the core, (b) suction porosity distribution along the core, and (c) chlorine and magnesium ingresses.

road authorities in this regard and today only NaCl is being used for winter maintenance of the roads. The source could also come from saline groundwater running down the shotcrete surface, but this second hypothesis does not explain the lack of magnesium in zone 2 (Fig. 10c), where the shotcrete surface is wet.

In the cores extracted from the Nordkapp subsea road tunnel, a summary of what was observed is given in Fig. 26:

Fig. 26a mainly represents the shotcrete where alkali-free accelerator was used. Nevertheless, sulfur ingress from the traffic room and less evident sulfur enrichment in shotcrete joints are also observed in shotcrete where water–glass accelerator was used. Fig. 26b fairly represents all the shotcrete analyzed. Finally, Fig. 26c shows the ingress of chloride and magnesium ions in the cement paste coming from the traffic room, which was mainly observed in the shotcrete where water–glass was used.

In the carbonation area of the different shotcrete samples, corrosion of steel fibers is expected as the pH decreases and steel fibers depassivate. In addition, there is also chloride attack from the traffic room generated by de-icing salts which are dispersed all over the tunnel lining by the vehicles [54]. In the non-carbonated part, steel fibers are not visible corroded (Fig. 11). A possible explanation is that there is no macro-cell corrosion taking place in the fibers (no huge area difference between localized attack and the rest of the steel passivated) as it happens in rebars or rock bolts under a localized attack. Moreover, a recent experimental study concludes that the critical chloride concentration is higher in steel fiber than in steel rebar, being both embedded in concrete [55].

In the Nordkapp tunnel, there is no risk of frost deterioration since it has anti-freezing doors at both ends of the tunnel. These doors only open during winter when a vehicle approaches the tunnel.

## 5. Conclusions

The Nordkapp subsea road tunnel was investigated in order to explore the in-service condition of steel fiber-reinforced shotcrete used as permanent rock support without any inner lining after more than 20 years of operation. The inspection of this tunnel offers the opportunity to compare the shotcrete applied with both water–glass and alkali-free accelerator types exposed to saline groundwater. This tunnel is of particular interest because it was the first time alkali-free accelerator was used in Norwegian road tunnels.

Two phenomena are observed in the shotcrete analyzed regardless of the core location:.

1. Carbonation occurs at the shotcrete surface exposed to the traffic room detected by calcite deposition in XRD test, lower pH of the pore solution determined by the thymolphthalein pH indicator and a relative reduction in suction porosity. The carbonation depth exceeds 20 mm in specific spots of the Nordkapp tunnel after 23 years in service.
2. The highest suction porosity and the lowest shotcrete density was observed at the boundary of two consecutive layers (shotcrete joints) in a core. This research highlights these areas as weakness zones within the shotcrete core.

In the specific case of shotcrete with alkali-free based accelerator, indications of leaching was observed by:.

1. A significant increase in suction porosity accompanied by a reduction in shotcrete density towards the traffic room.
2. Noticeable strength reduction along the cores towards the traffic room shown by UCS test results down to 40% of the original strength required in one case in the last 10 cm.

Coincidently with these leaching indications, the highest sulfur concentration detected with μ-XRF occurred near the shotcrete surface, adjoining the carbonation zone, where the suction porosity is high.

Furthermore, in this shotcrete with alkali-free accelerator, indications of leaching and sulfate attack were also observed in shotcrete joints by:.

1. Ettringite enrichment found by XRD analyses and sulfur mapping with μ-XRF.
2. How weak these shotcrete joints showed to be during core extraction, being two cores broken (out of eight cores) in these joints, despite the fact that the drilling continued for approximately 10 more cm.
3. Visible cracks in a sample containing a shotcrete joint used for the suction porosity test after the drying and wetting cycle.

To a minor extent, slightly higher sulfur concentration and suction porosity values were also observed in the shotcrete with water–glass based activator near the shotcrete surface just next to the carbonation zone. Nevertheless, no detrimental mechanical consequences for the shotcrete were found.

Regardless of the accelerator type, a reduction in potassium content was observed in the cement paste towards the traffic room, indicating that alkali-metals are being leached out from the shotcrete layer. However, these profiles did not accurately fit with density and suction porosity profiles along the cores.

Corrosion of steel fibers was only observed within the carbonation area. In the uncarbonated area, steel fibers did not show visible signs of corrosion.

The results obtained from the field in this research highlight the need to study together the susceptibly of sulfate attack and leaching, i.e., to perform laboratory tests on shotcrete samples exposed to sulfate bearing solutions under a unilateral pressure. This research also emphasizes the need to monitor the concentration of different gases in road tunnels as environmental factors which influence the durability of materials. In shotcrete, particular emphasis should be placed on sulfur dioxide.

## 6. Declarations

This research did not receive any specific grant from funding agencies in the public, commercial, or not-for-profit sectors.

## 7. Consent for publication

All authors read and approved the revised manuscript.

*CRediT authorship contribution statement*

**Cristobal Javier Manquehual:** Conceptualization, Methodology, Data curation, Writing – original draft. **Pål Drevland Jakobsen:** Funding acquisition, Supervision, Writing – review & editing. **Karl Gunnar Holter:** Investigation, Writing – review & editing. **Klaartje De Weerdt:** Writing – review & editing, Validation. **Tobias Danner:** Conceptualization, Writing – review & editing. **Amund Bruland:** Project administration, Supervision.

## Declaration of Competing Interest

The authors declare that they have no known competing financial interests or personal relationships that could have appeared to influence the work reported in this paper.

## References

[1] E. Broch, E. Grøv, K.I. Davik, The inner lining system in Norwegian traffic tunnels, Tunn. Undergr. Sp. Technol. 17 (2002) 305–314, https://doi.org/10.1016/S0886-7798(02)00026-3.

[2] W. Aldrian, A. Thomas, N. Chittenden, K.G. Holter, Permanent Sprayed Concrete Linings, ITA Working Group n°12 and ITAtech (2020).

[3] O.A. Opsahl, Use of wet-process steel-fibrous shotcrete in tunnel linings, in: T. Tapir (Ed.), International Symposium on Low Cost Road Tunnels, Oslo 1984: pp. 305–315.

[4] R. Kompen, Sprayed concrete for concrete repair: Quality requirements and quality follow-up, Norwegian Public Roads Administration, Internal Report No. 1700 (In Norwegian), 1994.

[5] T.A. Melbye, R.H. Dimmock, Modern advances and applications of sprayed concrete, in: International Conference on Engineering Developments, Hobart, Tasmania, Aust. April, 2001. https://doi.org/10.1201/9781003078678-3.

[6] R.P. Salvador, S.H.P. Cavalaro, I. Segura, A.D. Figueiredo, J. Pérez, Early age hydration of cement pastes with alkaline and alkali-free accelerators for sprayed concrete, Constr. Build. Mater. 111 (2016) 386–398, https://doi.org/10.1016/j.conbuildmat.2016.02.101.

[7] NFF. Norwegian Tunnelling Technology, Publication No. 23, Norwegian Tunnelling Society, 2014.

[8] R. Myrdal, Chemical reflections on accelerators for sprayed concrete: Past present and future challenges, in: 6th International Symposium on Sprayed Concrete, Tromsø Norway, 12–15 Sept, 2011.

[9] NS-EN 934–5:2007, Admixtures for concrete, mortar and grout - Part 5: Admixtures for sprayed concrete. Definitions, requirements, conformity, marking and labelling, 2007.

[10] R. Myrdal, Accelerating admixtures for concrete: State of the art, in: Sintef Rep. No. SBF BK A07025, 2007: pp. 1–35. https://www.researchgate.net/publication/288883755_Accelerating_admixtures_for_concrete.

[11] I.D. Hovland, J.P. Holtmon, C. Hauck, FATIMA - Increased Tunnelling Results with Replacement of Fully Casted Lining at the North Cape Tunnel, in: Third International Symposium on Sprayed Concrete - Modern Use of Wet Mix Sprayed Concrete for Underground Support. Gol, Norway. Sept. 26-29, 1999.

[12] C. Manquehual, J. Johansen, P.D. Jakobsen, B. Nilsen, Operation & Maintenance Costs of Subsea Road Tunnels in Norway, in: ITA-AITES World Tunn. Congr. - WTC2020, 2020: pp. 1569–1575.

[13] K. Melby, E. Ovstedal, F.H. Amundsen, G. Ranes, Subsea road tunnels in Norway. Norwegian Public Roads Administration. Report No. 98, 2002.

[14] K.I. Davik, Proper use of sprayed concrete in tunnels. Norwegian Public Roads Administration, Chapter B, subsea tunnels, (In Norwegian), 1997.

[15] I. Galan, A. Baldermann, W. Kusterle, M. Dietzel, F. Mittermayr, Durability of shotcrete for underground support– Review and update, Constr. Build. Mater. 202 (2019) 465–493, https://doi.org/10.1016/j.conbuildmat.2018.12.151.

[16] K.G. Holter, S. Geving, Moisture Transport Through Sprayed Concrete Tunnel Linings, Rock Mech. Rock Eng. 49 (2016) 243–272, https://doi.org/10.1007/s00603-015-0730-1.

[17] K.G. Holter, Loads on sprayed waterproof tunnel linings in jointed hard rock: A study based on Norwegian cases, Rock Mech. Rock Eng. 47 (2014) 1003–1020, https://doi.org/10.1007/s00603-013-0498-0.

[18] F.R. Steindl, I. Galan, A. Baldermann, M. Sakoparnig, L. Briendl, J. Juhart, M. Thumann, M. Dietzel, R. Röck, W. Kusterle, F. Mittermayr, Sulfate durability and leaching behaviour of dry- and wet-mix shotcrete mixes, Cem. Concr. Res. 137 (2020), 106180, https://doi.org/10.1016/j.cemconres.2020.106180.

[19] F.P. Glasser, J. Marchand, E. Samson, Durability of concrete - Degradation phenomena involving detrimental chemical reactions, Cem. Concr. Res. 38 (2008) 226–246, https://doi.org/10.1016/j.cemconres.2007.09.015.

[20] G. Plusquellec, M.R. Geiker, J. Lindgård, K. De Weerdt, Determining the free alkali metal content in concrete – Case study of an ASR-affected dam, Cem. Concr. Res. 105 (2018) 111–125, https://doi.org/10.1016/j.cemconres.2018.01.003.

[21] Y. Wang, C. Shi, Y. Ma, Y. Xiao, Y. Liu, Accelerators for shotcrete – Chemical composition and their effects on hydration, microstructure and properties of cement-based materials, Constr. Build. Mater. 281 (2021), 122557, https://doi.org/10.1016/j.conbuildmat.2021.122557.

[22] R. Ragoug, O.O. Metalssi, F. Barberon, J.M. Torrenti, N. Roussel, L. Divet, J. B. d'Espinose de Lacaillerie, Durability of cement pastes exposed to external sulfate attack and leaching: Physical and chemical aspects, Cem. Concr. Res. 116 (2019) 134–145, https://doi.org/10.1016/j.cemconres.2018.11.006.

[23] K. De Weerdt, Chloride binding in concrete: recent investigations and recognised knowledge gaps: RILEM Robert L'Hermite Medal Paper, Mater Struct. Constr. 54 (2021) (2021) 1–16, https://doi.org/10.1617/s11527-021-01793-9.

[24] M. Sun C. Sun P. Zhang N. Liu Y. Li J. Duan B. Hou Influence of carbonation on chloride binding of mortars made with simulated marine sand Constr. Build. Mater. 303 2021 https://doi.org/https://doi.org/10.1016/j.conbuildmat.2021.124455.

[25] R.P. Salvador, S.H.P. Cavalaro, R. Monte, A.D. Figueiredo, Relation between chemical processes and mechanical properties of sprayed cementitious matrices containing accelerators, Cem. Concr. Compos. 79 (2017) 117–132, https://doi.org/10.1016/j.cemconcomp.2017.02.002.

[26] R.P. Salvador, D.A.S. Rambo, R.M. Bueno, S.R. Lima, A.D. Figueiredo, Influence of accelerator type and dosage on the durability of wet-mixed sprayed concrete against external sulfate attack, Constr. Build. Mater. 239 (2020), 117883, https://doi.org/10.1016/j.conbuildmat.2019.117883.

[27] G. Tjugum, B. Kristiansen, D.A. Juvik, G.O. Johannessen, The future approach of chemicals in practical production of resistant shotcrete with liquid accelerators without Na+ and K+ which enhance the risk of alkali-silica reaction, in: Second International Symposium on Sprayed Concrete - Modern Use of Wet Mix Sprayed Concrete for Underground Support. Gol, Norway. Sept. 23-26, Norwegian Concrete Association, 1996.

[28] C. Maltese, T. Cerulli, C. Pistolesi, D. Salvioni, E.D. Negro, R. Hansen, Alkali free and alkali rich accelerators for shotcrete: Effects on cement Hydration, in: Fourth International Symposium on Sprayed Concrete – Modern. Use of Wet Mixed Sprayed Concrete, Underground Support, 2002, pp. 238–252.

[29] J. Kim J. Ryu R.D. Hooton Evaluation of strength and set behavior of mortar containing shotcrete set accelerators Can. J. Civ. Eng. 35 2008 400 407 https://doi.org//10.1139/L07-115.

[30] S.T. Lee, D.G. Kim, H.S. Jung, Sulfate attack of cement matrix containing inorganic alkali-free accelerator, KSCE J. Civ. Eng. 13 (2009) 49–54, https://doi.org/10.1007/s12205-009-0049-0.

[31] C. Paglia, F. Wombacher, H. Böhni, The influence of alkali-free and alkaline shotcrete accelerators within cement systems: Influence of the temperature on the sulfate attack mechanisms and damage, Cem. Concr. Res. 33 (2003) 387–395, https://doi.org/10.1016/S0008-8846(02)00967-5.

[32] H. Peinado-Guevara, C. Green-Ruíz, J. Herrera-Barrientos, O. Escolero-Fuentes, O. Delgado-Rodríguez, S. Belmonte-Jiménez, M.L. de Guevara, Relationship between chloride concentration and electrical conductivity in groundwater and its estimation from vertical electrical soundings (VESs) in Guasave, Sinaloa, Mexico, Cienc. e Investig. Agrar. 39 (2012) 229–239, https://doi.org/10.4067/S0718-16202012000100020.

[33] Z. Zheng, Y. Fu, K. Liu, R. Xiao, X. Wang, H. Shi, Three-stage vertical distribution of seawater conductivity, Sci. Rep. 8 (2018) 1–10, https://doi.org/10.1038/s41598-018-27931-y.

[34] P. Hagelia, Deterioration mechanisms and durability of sprayed concrete in Norwegian tunnels. NFF Publication No. 17: Underground openings – operations, maintenance and repair., 2008.

[35] NS-EN 206:2013+A1:2016+NA:2017, Concrete: Specification, performance, production and conformity, 2017.

[36] A.B. Revert, K. De Weerdt, K. Hornbostel, M.R. Geiker, Carbonation Characterization of Mortar with Portland Cement and Fly Ash, Comparison of Techniques, Nord. Concr. Fed. 1/2016. Publ. No. 54. (2016).

[37] F.A. Wahid Characterising concrete using micro X-ray fluorescence (μXRF) Department of Civil and Environmental Engineering 2016 Imperial College London.

[38] J. Lindgård, T. Østnor, B. Fournier, Ø. Lindgård, T. Danner, G. Plusquellec, K., De Weerdt, Determining alkali leaching during accelerated ASR performance testing and in field exposed cubes using cold water extraction (CWE) and μxRF, in, MATEC Web Conf. (2018) 1–8, https://doi.org/10.1051/matecconf/201819903004.

[39] Sintef, Internal procedure No. KS 70110. Concrete testing. Capillary suction capacity and porosity, 1996.

[40] NS-EN 12390-1, Testing hardened concrete Part 1: Shape, dimensions and other requirements for specimens and moulds, 2012.

[41] NS 3420, Description texts for building and construction. Special print on concrete structures., Nor. Counc. Build. Stand. (In Norwegian). (1986).

[42] NS-EN 12390-3:, Testing hardened concrete Part 3: Compressive strength of test specimens, 2019.

[43] ISRM, International Society for Rock Mechanics and Rock Engineering. Suggested Methods for Determining Water Content, Porosity, Density, Absorption and Related Properties and Swelling and Slake-Durability Index Properties, 1977.

[44] A. Gabrisová, J. Havlica, S. Sahu, Stability of calcium sulphoaluminate hydrates in water solutions with various pH values, Cem. Concr. Res. 21 (1991) 1023–1027, https://doi.org/10.1016/0008-8846(91)90062-M.

[45] NPRA, Handbook 021: Road Tunnels. Norwegian Public Roads Administration (in Norwegian)., 1992.

[46] NB, Sprayed Concrete for Rock Support, in: Nor. Concr. Assoc. Publ. No. 7, 1993.

[47] H.G. Park, S.K. Sung, C.G. Park, J.P. Won, Influence of a C12A7 mineral-based accelerator on the strength and durability of shotcrete, Cem. Concr. Res. 38 (2008) 379–385, https://doi.org/10.1016/j.cemconres.2007.09.016.

[48] F. Winnefeld, J. Kaufmann, R. Loser, A. Leemann, Influence of shotcrete accelerators on the hydration of cement pastes and their impact on sulfate resistance, Constr. Build. Mater. 266 (2021), 120782, https://doi.org/10.1016/j.conbuildmat.2020.120782.

[49] A. Bakken, E. Holtermann, Steel fibre reinforced shotcrete for temporary and permanent rock support in tunnels, in: N. Gol, . Sept. (Eds.), 2nd International Symposium on Sprayed Concrete - Modern Use of Wet Mix Sprayed Concrete for Underground Support, 1996, pp. 23–26.

[50] I. Storås, B. Bakke, C. Hauck, K.I. Davik, Full-scale testing of alkali-free accelerators with special emphasis on working environment, safety and quality. Third International Symposium on Sprayed Concrete - Modern Use of Wet Mix Sprayed Concrete for Underground Support. Gol, Norway. Sept. 26-29, 1999.

[51] A. Kristensson, C. Johansson, R. Westerholm, E. Swietlicki, L. Gidhagen, U. Wideqvist, V. Vesely, Real-world traffic emission factors of gases and particles measured in a road tunnel in Stockholm, Sweden, Atmos. Environ. 38 (2004) 657–673, https://doi.org/10.1016/j.atmosenv.2003.10.030.

[52] R. De Fre, P. Bruynseraede, J.G. Kretzschmar, Air pollution measurements in traffic tunnels, Environ. Health Perspect. 102 (1994) 31–37, https://doi.org/10.1289/ehp.94102s431.

[53] J. Pae, Y. Zhang, L.H. Poh, J. Moon, Three-dimensional transport properties of mortar with a high water-to-cement ratio using X-ray computed tomography, Constr. Build. Mater. 281 (2021), 122608, https://doi.org/10.1016/j.conbuildmat.2021.122608.

[54] P. Hagelia, Durability development for sprayed concrete as rock support in different tunnel environments. Norwegian Public Roads Administration. Report No. 566., 2018.

[55] J.P. Hwang, M.S. Jung, M. Kim, K.Y. Ann, Corrosion risk of steel fibre in concrete, Constr. Build. Mater. 101 (2015) 239–245, https://doi.org/10.1016/j.conbuildmat.2015.10.072.

**PAPER III**

**Title:** Leaching in steel fiber-reinforced shotcrete installed in the Frøya subsea road tunnel

**Authors:**
Manquehual, Cristobal Javier
Jakobsen, Pål Drevland
Holter, Karl Gunnar
De Weerdt, Klaartje
Bruland, Amund

**Under review in:**
Cement and Concrete Research journal

**PAPER IV**

**Title:** Operation & Maintenance Costs of Subsea Road Tunnels in Norway (2020)

**Authors:**
Manquehual, Cristobal Javier
Johansen, Johnny
Jakobsen, Pål Drevland
Nilsen, Bjørn

**Published in:**
Proceedings of the ITA-AITES World Tunnel Congress, WTC 2020, Malaysia.

# Operation & Maintenance Costs of Subsea Road Tunnels in Norway

C. Manquehual[1] J. Johansen[2] P.D. Jakobsen[1] B. Nilsen[3]
[1]*Department of Civil & Environmental Engineering, NTNU, Trondheim, Norway*
[2]*ViaNova Plan og Trafikk AS*
[3]*Department of Geoscience and Petroleum, NTNU, Trondheim, Norway*
*E-mail*: cristobal.j.manquehual@ntnu.no

**ABSTRACT:** In Norway, there are currently more than 30 subsea road tunnels in operation. The Vardø Tunnel was the first one, finalized in 1983. In general, road tunnels require rock support for its stabilization along with other materials, equipment, consumptions and activities that affect the cost during their Operation and Maintenance (O&M). These resources aim to fulfil requirements related to water and frost protection, fire protection system, drainage system, ventilation system, lighting, air purification systems, etc. A subsea tunnel incorporates additional and unique features such as marine water leakages, a restricted access for maintenance of tunnels and a considerable elevation difference between their portals and the deepest point. The estimated annual O&M costs for existing subsea road tunnels in Norway analysed herein show that Traffic volume by AADT is alone a good predictor for such costs per tunnel meter with limited scattering.

**KEYWORDS:** Road tunnels, Subsea tunnels, Operation and Maintenance, Costs, Norway

## 1. INTRODUCTION

Data and experience obtained from operation, maintenance, rehabilitation and eventually upgrading of tunnels can be a source of data for Life Cycle Cost (LCC) estimations (Moretti, L., Cantisani,G., Di Mascio P., 2016). A thorough comprehension of LCC in road infrastructure may then lead to improve the use of limited resources by assessing new projects for their whole lifespan.

This research will focus on the costs for the Operation and Maintenance (O&M) of subsea road tunnels in Norway. The analysis of their costs may provide indications of the conditions of tunnels if they are analyzed over time. Moreover, it may provide feedbacks about the financial consequences of new standard regulations (Norwegian Public Roads Administration, 2012b). Finally, the thorough understanding of activities and equipment during O&M of subsea road tunnels may be the basis for their environmental footprint assessment (Huang, Bohne, Bruland, Jakobsen, & Lohne, 2015).

In Norway, there are currently 33 subsea road tunnels under operation (Table 1) and several more under construction.

The European standard NS-EN 13306:2017 (Standard Norge, 2017) defines operation as a combination of all technical, administrative and managerial actions, other than maintenance actions, that results in the item being in use. In turn, it defines Maintenance as: "the combination of all technical, administrative and managerial actions during the life cycle of an item intended to retain it in, or restore it to, a state in which it can perform the required function".

In this analysis, maintenance activities may involve the replacement of elements and equipment, but a distinction in comparison with rehabilitation and/or upgrading (which are not covered in this research) is made. In the first case, the replacement is done according to the original standards (when the tunnel was constructed) while in the former two cases, the replacement is done according to current regulations.

Operation and maintenance shall ensure that the level of safety in the tunnel is upheld by maintaining the assumed functional requirements and safety (Norwegian Public Roads Administration, 2004).

The O&M of roads in Norway are tendered to different contractors where the country is split in packages. These contracts usually last for three to five years. Within these packages, the contractor may have a set of tunnels to be operated and maintained (Norwegian Public Roads Administration, 2018a).

The Norwegian Public Roads Administration aims to monitor their policies and standard regulations in order to ensure that life cycle of tunnels and their equipments are in accordance with their strategies and the experience gained after commissioning is registered and applied in new projects (Norwegian Public Roads Administration, 2012b).

The O&M costs presented herein are derived from MOTIV. This is a program belonging to the Norwegian Public Roads Administration which yields cost estimates for the O&M of each tunnel. The model was created in order to properly allocate budget annually for the O&M of road traffic. These estimates are based on the different elements and their corresponding quantities that each tunnel has according to the Norwegian road database "Nasjonal vegdatabank NVDB" (Norwegian Public Road Administration, 2018b). On the other hand, unit prices given by Contractors during the bidding process for the different tasks and activities to be undertaken during O&M are inferred in the model from actual operating contracts. In this regard, it is important to mention that the degree of details and tasks assigned vary between contracts and therefore unit prices for each task are not directly obtained from such contracts.

Figure 1 describes the distribution of estimated annual O&M costs in road tunnels (not only subsea tunnels) belonging to the national network (Norwegian Public Roads Administration, 2012b).

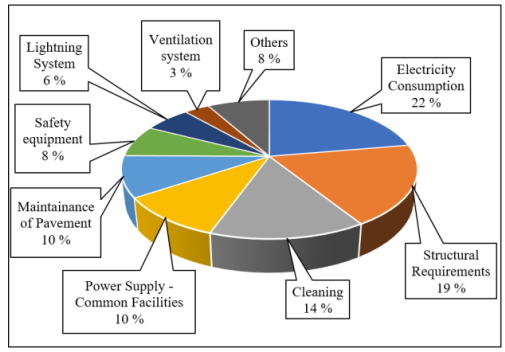


Figure 1: Annual O&M Cost distribution of National Road Tunnels in Norway – 2011, where 620 km were analyzed *(Norwegian Public Roads Administration, 2012b)*

Table 1: Summary of subsea road tunnels in Norway studied in this research

| | Subsea Tunnel: | Commisioning year | Tunnel Length [m] | Deepest point from sea water surface [m] | AADT - 2018 (Per Tunnel) | Amount of Frost $F_{10}$ estimated [h°C][1] | Number of Tubes | Number of Lanes per Tube[2] | Estimated Annual O&M Cost (2018) 1000 x USD/year |
|---|---|---|---|---|---|---|---|---|---|
| 1 | Vardø | **1983** | 2890 | 88 | 862 | **17 460** | 1 | 2 | 321 |
| 2 | Ellingsøy | 1987 | 3536 | 140 | 10 276 | 1 800 | 1 | 3 | 1 006 |
| 3 | Valderøy | 1987 | 4225 | 137 | 8 568 | 1 163 | 1 | 3 | 989 |
| 4 | Kvalsund | 1988 | 1647 | 56 | 1 009 | 6 600 | 1 | 2 | 190 |
| 5 | Godøy | 1989 | 3849 | 153 | 1 683 | 650 | 1 | 2 | 337 |
| 6 | Hvaler | 1989 | 3768 | 121 | 2 564 | 7 520 | 1 | 2 | 512 |
| 7 | Flekkerøy | 1989 | 2314 | 101 | 4 577 | 3 450 | 1 | 2 | 422 |
| 8 | Nappstraumen | 1990 | 1780 | 60 | 1 819 | 3 400 | 1 | 2 | 221 |
| 9 | Fannefjord | 1991 | 2747 | 100 | 4 056 | 1 680 | 1 | 2 | 613 |
| 10 | Maursund | 1991 | 2124 | 92 | 605 | 14 405 | 1 | 2 | 164 |
| 11 | Byfjord | 1992 | 5880 | 223 | 9 773 | 1 740 | 1 | 3 | 1 963 |
| 12 | Mastrafjord | 1992 | 4421 | 132 | 8 144 | 1 620 | 1 | 3 | 1 152 |
| 13 | Freifjord | 1992 | 5109 | 132 | 4 036 | 3 720 | 1 | 3 | 813 |
| 14 | Hitra | 1994 | 5650 | 264 | 1 776 | 3 330 | 1 | 3 | 690 |
| 15 | Tromsøysund | 1994 | 3436 | 101 | 10 902 | 6 600 | 2 | 2 | 1 220 |
| 16 | Bjorøy | 1996 | 2012 | 85 | 1 731 | 1 450 | 1 | 2 | 169 |
| 17 | Sløverfjord | 1997 | 3329 | 100 | 1 427 | 5 220 | 1 | 2 | 446 |
| 18 | Nordkapp | 1999 | 6875 | 212 | 454 | 10 710 | 1 | 2 | 589 |
| 19 | Oslofjord | 2000 | 7261 | 134 | 9 446 | 11 880 | 1 | 3 | **2 173** |
| 20 | Frøya | 2000 | 5301 | 164 | 1 969 | 1 875 | 1 | 2 | 592 |
| 21 | Ibestad | 2000 | 3418 | 125 | 570 | 11 340 | 1 | 2 | 255 |
| 22 | Bømlafjord | 2000 | 7913 | 260 | 5 294 | 1 253 | 1 | 3 | 1 614 |
| 23 | Skatestraum | 2002 | 1902 | 80 | 405 | 660 | 1 | 2 | 217 |
| 24 | Eiksund | 2007 | 7849 | **287** | 2 997 | 2 322 | 1 | 3 | 1 157 |
| 25 | Halsnøy | 2008 | 4170 | 135 | 1 120 | 1 960 | 1 | 2 | 346 |
| 26 | Atlanterhavs | 2009 | 5788 | 249 | 2 413 | 3 220 | 1 | 3 | 857 |
| 27 | Finnøy (Finnfast) | 2009 | 5806 | 150 | 1 222 | 1 720 | 1 | 2 | 539 |
| 28 | Skansen[4] | 2010 | 506 | 14 | 11 977 | 10 120 | 1 | 2 | 173 |
| 29 | Rya | 2010 | 2682 | 87 | 636 | 6 600 | 1 | 2 | 216 |
| 30 | Knappe (Nordåsstraumen)[3] | 2010/2015 | 6400 (2172) | 29 | (20 753) | 1 520 | 2 | 2 | (878) |
| 31 | Bjørvika[4] | 2 010 | 1 083 | 11 | **73 681** | 11 880 | **2** | **3** | 1 140 |
| 32 | Karmøy | 2 013 | **8 903** | 138 | 4 377 | 870 | 1 | 3 | 1 531 |
| 33 | Kvernsund | 2 018 | 3 264 | 125 | **300** | 9 400 | 1 | 2 | 299 |

[1] The variable Amount of Frost $F_{10}$ is calculated as the product between the accumulated time with the air temperature below zero Celsius degree in a year and the corresponding air temperature magnitude. The sub-index 10 represents the return period. This means that $F_{10}$ is the amount of frost which is statistically exceeded once every ten years (Norwegian Public Roads Administration, 2014). $F_{10}$ value is available for each municipality in Norway.

[2] Those tunnels stated as 3 lanes correspond to two-way traffic tunnels with one lane in each direction where an additional "overtaking lane" is added in the exit direction as long as they have a stretch steeper than 6% gradient and an AADT (foreseen in 20 more years) > 2500. (Norwegian Public Roads Administration, 2004)

[3] Knappetunnelen has a total length of 6.4 km and was constructed in two stages. The first stage finalized in 2010 and the second one in 2015. The tunnel stretches analyzed herein, which have some meters below the seabed, are 2.2 km long. The tunnel length, the traffic volume AADT and annual O&M cost used herein for this tunnel is given between parentheses.

[4] Concrete tunnel with rectangular cross section tube(s). (All other are rock tunnels).

As shown in Figure 1, the electricity consumption is the highest expense accounting for 22%. This cost represents the aggregate electricity consumption from lighting (during day, twilight and night), jet fans, pumps and some other needs and facilities in tunnels.

Structural Requirement costs, which accounts for 19% in Figure 1, represent the costs related to the inspection and eventual repair for rock support such as bolts, sprayed concrete, sprayed concrete ribs, cast concrete lining, etc., and removal of loose rock blocks (scaling) (Norwegian Public Roads Administration, 2013). In addition, this cost encompasses the inspection and eventual repair for water and frost protection elements (Norwegian Public Roads Administration, 2012c).

The solutions that have been applied for water and frost protection in existing Norwegian subsea road tunnels are (Norwegian Public Roads Administration, 2006); (Norwegian Public Road Administration 2018b):

- Corrugated steel plate in walls and roof.
- Tunnel Sealing, consisting of a waterproof membrane in walls and roof.
- A Polyethilene PE foam sheet covered by a layer of sprayed concrete with Polypropylene PP fibers in walls and roof.
- Pre-cast concrete elements (in walls or walls & roof) protected by an Extruded Polystyrene foam XPS sheet and a waterproof membrane. In case this solution is only applied on walls, the most common solution for the roof to create a thermal insulation vault is with a PE foam sheet covered by sprayed concrete with PP.
- Cast in place concrete lining with a waterproof membrane.

The third highest expense are cleaning costs. It encompasses not only the cleaning of the main tunnel's roof and walls, but also escape routes, niches, equipment, traffic signs, railings, etc. Tunnel cleaning shall secure the function and lifetime of the tunnel equipment, secure clean air in the tunnel (less dust whirled up by traffic) and contribute to a positive experience for road users by ensuring an aesthetically pleasing and safe tunnel.

Power supply and common facilities include the O&M of transformers, Power distribution board, earthing system, cable bridges, UPS (Uninterruptable Power Supply) etc. The activities include their cleaning, functional testing, visual inspection and thermography.

Maintenance of Pavement includes the resurface of pavement and to a lesser extent, the inspection of its smoothness, surface friction control, de-icing salt consumption, etc.

Safety equipments costs include the right O&M of fire-fighting extinguishers, emergency telephones, air quality monitoring equipments, etc.

The O&M of tunnel lighting includes the light fittings, conventional lightning equipment for entry zone and for the night, evacuation light fittings, replacement of fluorescent lamps, etc.

Ventilation system costs consider the O&M of jet fans in tunnels and shafts and the corresponding control system to ensure pollutant concentration under control at all times and managing the smoke under a fire.

Within the concept of "others" costs, it is included the O&M of pump, air cleaning system, drainage system, railings and cushions, curbs, dehumidification plant, event detection, etc. Except pumps, drainage system and curbs, most of these objects are only present in few tunnels.

## 2. METHODOLOGY FOR ANALYSIS

The variables to be analyzed in this research, which may influence the annual O&M cost of subsea road tunnels in Norway are:

- Tunnel Length
- Traffic volume AADT
- Traffic layout (Number of tubes & driving lanes)

Table 2 describes shortly these variables.

Table 2: Description of variables considered in this study

| Variable | Short Description |
|---|---|
| Tunnel Length | Longer tunnel means more infrastructure to be operated and maintained. |
| Traffic Volume AADT | The traffic volume is quantified by the Annual Average Daily Traffic AADT. This variable corresponds to the total annual traffic in a tunnel in both directions divided by 365. As shown in Figure 2, the traffic volume quantified as AADT is a key variable in defining tunnel categories, which in turn define safety measures and safety equipment in tunnels (longer than 500 m). |
| Traffic Layout | The number of tubes and driving lanes have consequences regarding safety issues such as layout of emergency lay-bys and turning niches as shown in Table 3. In addition, it is interrelated with traffic volume and the longitudinal slope (eventual extra overtaking lane for steep longitudinal slope stretches). |

As already mentioned, tunnel categories determine the requirements for safety measures and safety equipment in tunnels longer than 500 m. This applies, for example, to the number of tunnel tubes and their corresponding cross section area, the need for emergency lay-bys, turning niches and emergency exits. (Norwegian Public Roads Administration, 2016).

Figure 2 shows the different tunnel categories according to current regulations.

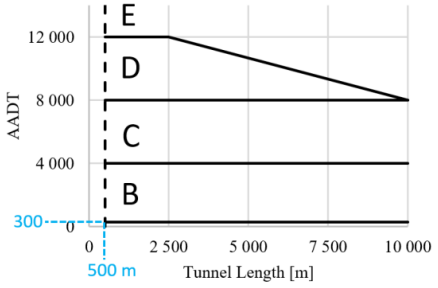


Figure 2: Tunnel categories based on current regulations (Norwegian Public Roads Administration, 2016).

There are two more tunnel categories not mentioned in Figure 2. One is class A for AADT < 300 AADT and the other one is class F for AADT > 50,000. In both cases, the stated boundaries of traffic volume are not dependent on tunnel length. In the same regulations, it states that tunnel category E and F shall have two tubes.

As an example, Table 3 gives the interval for emergency lay-bys and turning niches as a function of tunnel categories.

Table 3: Normal distance for emergency lay-bys and turning niches according to current regulations (Norwegian Public Roads Administration, 2016).

| Tunnel Category | Normal distance for emergency lay-bys [m] | Normal distance for turning point [m] | Comments |
|---|---|---|---|
| A | - | - | Meeting Points in single lane tunnels used by traffic in both directions. |
| B | 500 | 2000 | Turning points for tunnels longer than 4 km. |
| C | 375 | 1500 | Turning points for tunnels longer than 3 km. |
| D | 250 | 1000 | Turning points for tunnels longer than 2 km. |
| E | 500 | - | The specified distance applied for each tunnel tube (Twin tubes). |
| F | 250 | - | The specified distance applied for each tunnel tube (Twin tubes). |

## 3. RESULTS

### 3.1 Tunnel Length

Table 1 shows the estimated annual O&M costs for the 33 subsea road tunnels under operation in Norway. These values are plotted in Figure 3 as a function of tunnel length. This chart also gives the O&M costs "per tube", as the variable "tunnel length" in twin tube tunnels does not take into consideration the roughly double cost in comparison to a single tube tunnel for the same tunnel length.

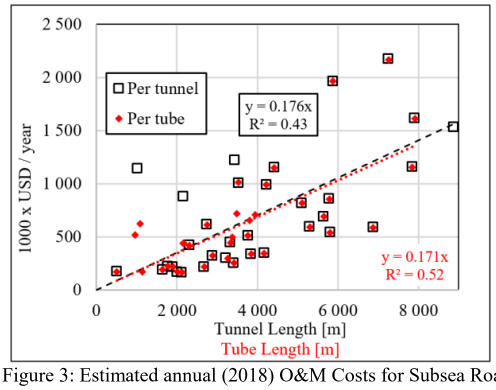


Figure 3: Estimated annual (2018) O&M Costs for Subsea Road Tunnels as a function of length.

When the tunnel has only one tube, the O&M cost "per tunnel length" and "per tube length" coincides as shown in Figure 3. In only four cases this match did not occur, three of them because they are twin tube tunnels (Tromsøysund, Knappe, and Bjørvika). The remaining case (Karmøy), has a branch approximately perpendicular to the main tunnel, i.e. the tunnel has three portals.

As expected, the linear regression for the O&M cost "per tube length" provides less scattering than "per tunnel length". This can be identified visually since empty squares are farther in relation to their trend line in contrast to the red diamonds in Figure 3, which are closer to its fitting line.

As shown by Figure 3, the O&M cost of subsea road tunnels in Norway increases with their lengths, but also the scattering is higher for longer tunnels.

### 3.2 Traffic Volume AADT

Figure 4 shows the 33 subsea tunnels studied in this research clustered by traffic volume AADT. The range for each cluster was selected taking into account the current regulations depicted in Figure 2.

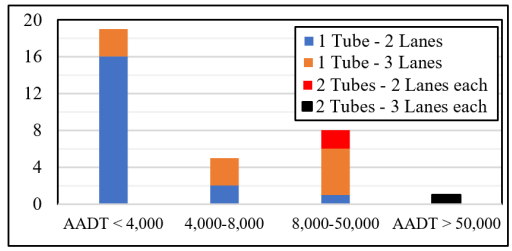


Figure 4: Distribution of subsea road tunnels in Norway (33) by traffic volume - 2018

As depicted in Figure 4, the majority of subsea road tunnels in Norway have been constructed for low traffic volumes (AADT < 4,000). It suggests that most of subsea tunnels would be class B if the current regulations were applied (Figure 2).

It is important to mention as well from Figure 4 that there is one tunnel with one tube and two driving lanes in the traffic volume range between 8,000 and 50,000 AADT. This is the Skansen tunnel, the shortest subsea road tunnel in Norway located in an urban area (City of Trondheim).

If the estimated annual O&M costs "per tunnel" displayed in Figure 3 is broken down by traffic volume AADT, different straight trend lines can be drawn for each cluster as shown in Figure 5:

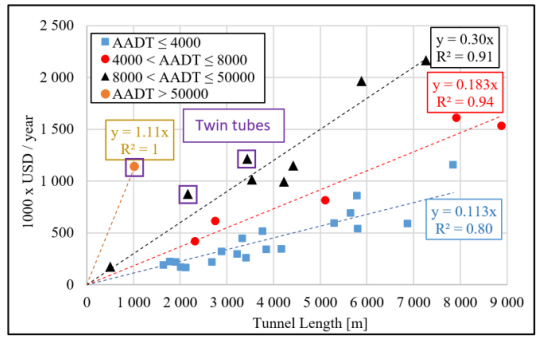


Figure 5: Estimated annual (2018) O&M costs for subsea road tunnels grouped by similar traffic volume as a function of tunnel length.

From Figure 5 it is possible to get an average O&M cost per traffic volume range. Table 4 summarizes the results:

Table 4: Estimated annual O&M cost in subsea road tunnels in Norway per traffic volume range.

| Traffic Volume range | O&M costs USD / year / TM | Number of data | Correlation coefficient |
|---|---|---|---|
| AADT ≤ 4000 | 113 | 19 | 0.80 |
| 4000 - 8000 | 183 | 5 | 0.94 |
| 8000 - 50000 | 300 | 8 | 0.91 |
| AADT > 50000 | 1100 | 1 | 1.00 |

Figure 5 also indicates that there is a directly proportional relation between the annual O&M cost per tunnel meter and traffic volume. One could then conclude that the higher is the traffic volume, the higher is the annual O&M cost per tunnel meter. However, if the analysis incorporates the variable unit of traffic volume into the same cost per tunnel meter, the conclusion is the opposite, being those tunnels with heavier traffic cheaper than those with lower traffic as shown in Figure 6.

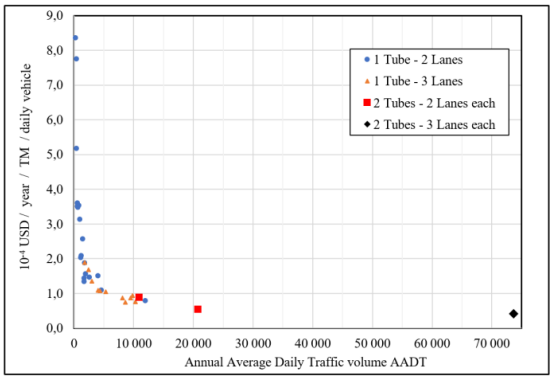


Figure 6: Estimated annual (2018) O&M Cost for subsea road tunnels per tunnel meter and per unit of traffic volume over traffic volume.

It is important to highlight in Figure 6 that the ratio between the annual O&M cost per tunnel meter and per unit of traffic volume for a traffic volume range between 500 AADT and 5000 AADT is roughly 8 times, while the ratio between tunnels conveying 5000 AADT and 50000 AADT is only 2 times.

To conclude on traffic volume, Figure 7 shows the correlation coefficient for both: Annual O&M cost per tunnel meter over traffic volume and annual O&M cost per tube meter over traffic volume.

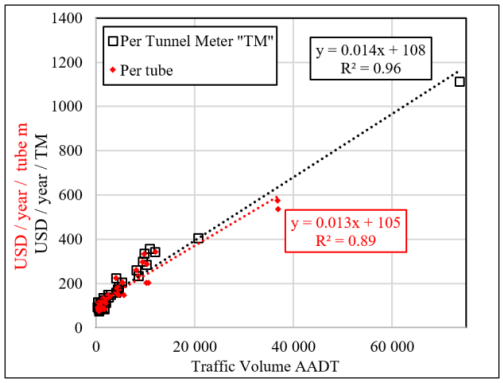


Figure 7: Estimated annual (2018) O&M Costs per tunnel meter /tube meter for subsea road tunnels as a function of traffic volume.

Figure 3 shows that there is a better correlation between O&M cost per tube over tube length than the same cost for each tunnel over tunnel length. However, Figure 7 exhibits less scattering between O&M cost per tunnel meter than per tube meter when they are both plotted over traffic volume. The difference in correlation coefficient in Figure 7 is not very large, since the results are influenced by all the tunnels with single tubes (where annual O&M cost per tunnel meter and per tunnel tube are the same).

### 3.3 Traffic layout

Figure 7 gives an indication about the influence of traffic layout on annual O&M cost. There is a very high correlation between annual O&M cost per tunnel meter over traffic volume without having broken down the tunnels by traffic layout. The next chart (Figure 8) gives the same figures disaggregated by traffic layout.

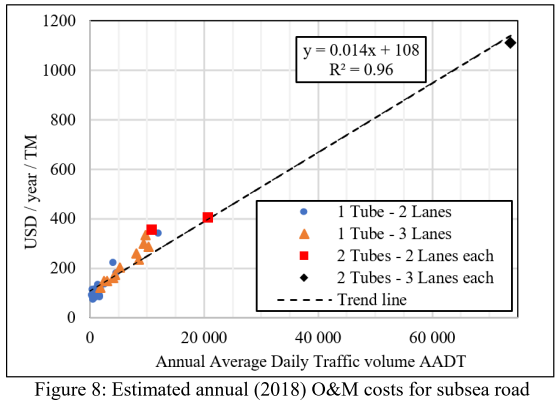


Figure 8: Estimated annual (2018) O&M costs for subsea road tunnels over traffic volume broken down by traffic layout.

It is important to note from Figure 8 the strong relation between traffic layout and traffic volume.

Figure 9 aims to show the simultaneous interaction between tunnel layout and traffic volume over annual O&M cost per tunnel meter.

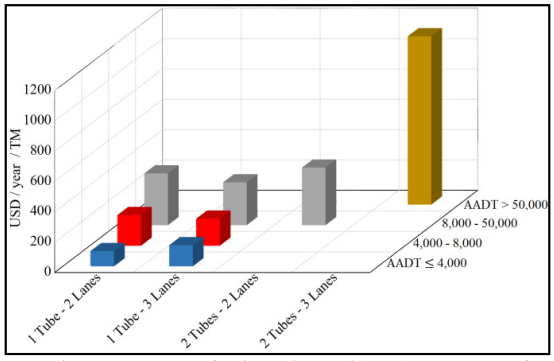


Figure 9: Average of estimated annual (2018) O&M Cost of subsea road tunnels for the respective traffic volume and traffic layout. (The grid is empty when there is no subsea tunnel in Norway with the specified traffic volume and traffic layout).

In Figure 9, it is important to mention that the representation of subsea tunnels is unequal. Figure 4 gives the actual number of subsea tunnels for each traffic layout-traffic volume combination. While sixteen subsea tunnels can be categorized as "1 Tube – 2 Lanes" with a traffic volume AADT ≤ 4,000, only one tunnel is available for the grid "2 Tubes – 3 Lanes" and "AADT > 50,000". Leaving this uneven representation aside, which may trigger bias in the conclusion, Figure 9 shows an unambiguous increase relation between traffic volume (AADT) and the annual O&M cost per tunnel meter. The same cannot be stated for traffic layout, where a larger number of driving lanes/tubes does not imply necessarily a higher O&M cost per tunnel meter.

## 4. DISCUSSION

All the estimated O&M costs shown in Table 1 come from the program MOTIV calculated for the year 2018. Some sources of errors and shortcomings are important to be mentioned:

- The consolidation of the raw data related to the bill of materials collected by the Norwegian road database (Norwegian Public Road Administration, 2018b) is still evolving. Besides, rehabilitation and upgrading of tunnels are constantly taking place. Then, quantities of equipment and new technology updates may not be registered or wrongly registered.
- Some cost features are not covered by the level of detail implemented in the model.
- The cost model is based on the presumption that the tunnels are built according to the regulations with no faults.

The above-mentioned limitations may influence the sensitivity of the annual O&M cost results. Nevertheless, they do not affect significantly the overall view of O&M costs per year since the program MOTIV has developed for more than one decade.

It is very likely that more detail information for each subsea tunnel may increase the annual O&M cost dispersion as particular issues not identified by idealization of cost items will appear, but on the other hand, the continuous upgrading of tunnels to a similar level of comfort and safety should dampen the scattering generated by this extra information.

As traffic volume AADT variable is explicitly stated in Norwegian regulations, it is not surprising its good correlation with the annual O&M cost per tunnel meter. Some other factors may intensify this good correlation such as existing guidelines for O&M Contracts in Norway (Norwegian Public Roads Administration, 2018a) and the upgrading of several subsea tunnels to a similar level of safety and comfort.

As shown in Figure 7, a better correlation is obtained with traffic volume when the O&M cost per unit length is classified per tunnel instead of per tube. This is not intuitive, as an analysis per tunnel does not reflect the roughly double cost of a twin tube tunnel compared to a single tube tunnel with the same tunnel length. Nevertheless, an extra tube entails a higher traffic volume, trading off the extra cost. In addition, the fact that the tubes in a twin tube tunnel do not have the same cost triggers more scattering in the analysis per tube.

The maximum depth below sea water level gives an idea of the maximum elevation difference within a tunnel as long as their portals are near the seashore, which is normally the case. O&M costs that may be linked to this variable are electricity consumption for pumping out water and removal of air pollutants. In subsea tunnels, one could expect a certain correlation between the deepest point measured from seawater surface and the tunnel length, as there are practical restrictions on the longitudinal slope. The longitudinal slope for road tunnels in Norway today is restricted to 5%. Some older subsea tunnels, however, have overcome a gradient of 10% and even more. (Norwegian Public Roads Administration, 2012a). Figure 10 shows the maximum depth below seawater over tunnel length for the 33 tunnels analysed.

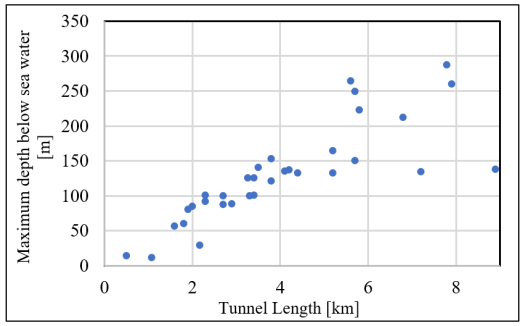


Figure 10: Relation between maximum depth below sea level and tunnel length in Norwegian subsea road tunnels (33).

An expectation from Figure 10 could be an increasing cost per tunnel meter for longer subsea tunnels if the variable "maximum depth below sea water" was relevant for the O&M costs. However, Figure 5 indicates that they are constant per unit length for each traffic volume range and therefore one may conclude that maximum depth below sea water is not relevant. This latter statement may be misleading, as inherent shortcomings from the model already mentioned may be affecting the sensitivity of the results. Nevertheless, it is a fact the systematic reduction of water leakage after commissioning in most of the subsea tunnels. (Norwegian Public Roads Administration, 2002). This may indicate that there is a certain self-sealing capacity of the rock mass. One possible explanation may be the filling of sediment in rock mass discontinuities washed out from the sea bottom (Nilsen, B., 2014).

In general, frost is an issue in road Norwegian tunnels near portal areas (Norwegian Public Roads Administration, 2004). Nevertheless, winter maintenance routines, which ensure a proper road surface at the entrance and approach zone, represent a very small part of total O&M costs in tunnels. Furthermore, subsea road tunnels in Norway are located near the coastline and therefore they are exposed to a mild cold climate compared to the rest of the country. Table 1 gives the amount of frost $F_{10}$ estimated for each tunnel, where in most of the cases this variable is less than 8000 h°C. The latter threshold value is the upper boundary for not protecting tunnels against frost according to current Norwegian regulations (Norwegian Public Roads Administration, 2016).

The long-term degradation of materials such as corrosion in bolts (Norwegian Public Roads Administration, 2015) and biodeterioration in concrete (Karacic, Wilen, Suarez, Hagelia, & Persson, 2018) are not visualized in these costs. Nevertheless, analysis on rehabilitation/upgrading costs in tunnels may provide findings regarding the costs related to these degradation mechanisms.

## 5. CONCLUSION

The 33 subsea road tunnels currently under operation in Norway were analyzed herein. The estimated O&M costs studied in this research come from the program MOTIV for the year 2018. The available results indicate that the influencing variables on the annual O&M cost of subsea road tunnels in Norway are:

- Tunnel Length
- Traffic volume

Traffic volume by AADT has shown to explain alone the annual O&M costs per tunnel meter with limited scattering (Figure 8).

From Figure 8, a straight trend line between O&M cost per tunnel meter in subsea road tunnels and Traffic volume is proposed:

$$USD/year/TM = 0.014*AADT + 108 \quad (R^2 = 96\%) \quad (1)$$

The good correlation between the estimated annual O&M costs of subsea road tunnels in Norway per tunnel meter and traffic volume is not coincidental as several requirements related to comfort and safety for road users are explicitly related to tunnel categories, which in turn depend on traffic volume.

The available O&M costs belong to subsea road tunnels, which have different ages (between 1983 and 2018) and therefore relate to different regulations and specifications during construction. Nevertheless, if O&M costs are grouped by a similar traffic volume, a constant O&M cost per tunnel meter can be inferred for each cluster (Figure 5).

Even though, the O&M cost per unit length increases with a higher traffic volume, the analysis of O&M cost per vehicle - kilometer suggests that tunnels with heavier traffic are in fact much cheaper than those constructed for a low traffic (Figure 6). The ratio is 8 times more expensive for the AADT range between 500 and 5,000 and a ratio of 2 times for the AADT range between 5,000 and 50,000.

Traffic layout, which describes the number of tubes and driving lanes in a tunnel (and therefore relates to its total cross section area), is strongly influenced by traffic volume (Figure 8). However, Figure 9 indicates that O&M cost per tunnel meter is not much sensitive to traffic layout, but conclusion may be bias by the underrepresentation of the existing twin tube subsea tunnels (Figure 4). To conclude on traffic layout, it is important to mention that the term “one tube with three lanes” used in this research does not imply that the whole subsea tunnel has actually three lanes, as an extra overtaking lane only apply on steep stretches (steeper than 6%) next to portal zones.

Available O&M costs indicate that the variable “Maximum depth below sea level” is not relevant, but there are several shortcomings in the model that may be misleading the conclusion.

Amount of frost, which only affects the entrance zone of tunnels, is not a relevant variable for the O&M cost of subsea tunnels. Two main factors are: 1- Subsea road tunnels are located near the shoreline and 2- they are relatively long (Only 5 out of 33 tunnels are shorter than 2 km).

Further studies on rehabilitation/upgrading costs may provide findings regarding degradation mechanisms in subsea road tunnels.

## 6. REFERENCES


Huang, L., Bohne, R., Bruland, A., Jakobsen, P., & Lohne, J. (2015). Life Cycle Assessment of Norwegian Road Tunnels. Int J Life Cycle Assess, 174-184.

Karacic, S., Wilen, B., Suarez, C., Hagelia, P., & Persson, F. (2018). Subsea Tunnel Reinforced sprayed concrete subjected to deterioration harbours distinct microbial communities. Biofouling, DOI: 10.1080/08927014.2018.1556259.

Moretti, L., Cantisani,G., Di Mascio P., (2016) Management of road tunnels : Construction, maintenance and lighting costs. Tunnelling and Underground Space Technology 51 84-89.

Nilsen, B. (2014). Characteristics of Water Ingress in Norwegian Subsea Tunnels. Rock Mech Rock Eng, 47:933-945.

Norwegian Public Roads Administration. (2002). Subsea Road Tunnels in Norway, Publication 98.

Norwegian Public Roads Administration. (2004). Road Tunnels Manual 021.(*In Norwegian*).

Norwegian Public Roads Administration. (2006). Water and Frost Protection in Tunnels. Handbook 163. (*In Norwegian*)

Norwegian Public Roads Administration. (2012a). Major Research and Development Project: Modern Road Tunnels 2008-2011. The Limits of our Knowledge about Tunneling - Lengths and Depths. Report 136. (*In Norwegian*).

Norwegian Public Roads Administration. (2012b). Operation and Maintenance of road tunnels - Main Costs, report 132. (*In Norwegian*).

Norwegian Public Roads Administration. (2012c). What is the cost of repairing the national roads? - Report 75. (*In Norwegian*)

Norwegian Public Roads Administration. (2013). Inspection of Rock Mass and rock support in Road Tunnels, Report 199. (*In Norwegian*).

Norwegian Public Roads Administration. (2014). Road Construction Handbook N200. (*In Norwegian*).

Norwegian Public Roads Administration. (2015). Corrosion Protection in tunnels, Report 410. (*In Norwegian*).

Norwegian Public Roads Administration. (2016). Handbook of Road Tunnels N500. (*In Norwegian*).

Norwegian Public Roads Administration. (2018a). Manual R763 - Documents for Operational Road Contracts. (*In Norwegian*).

Norwegian Public Road Administration (2018b) The National Road Database https://www.vegvesen.no/en/professional/roads/national-road-database

Standard Norge, E. (2017). NS-EN 13306:2017 Maintenance Terminology. Standard Norge.

ISBN 978-82-326-5976-0 (printed ver.)
ISBN 978-82-326-6243-2 (electronic ver.)
ISSN 1503-8181 (printed ver.)
ISSN 2703-8084 (online ver.)





NTNU

Norwegian University of
Science and Technology